On the neuronal processing of movement dynamics

by

Camillo Padoa-Schioppa

Laurea in Physics
University "La Sapienza" of Rome, 1996

Submitted to the Department of Brain and Cognitive Sciences
in partial fulfillment of the requirements for the degree of

Doctor of Philosophy in Cognitive Neuroscience

at the
Massachusetts Institute of Technology
June 2002
[February 2002]

Signature of Author .....
Camillo Padoa-Schioppa
January 18, 2002

Certified by .....
Emilio Bizzi, M.D.
Eugene McDermott Professor in the Brain Sciences and Human Behavior, MIT
Thesis Supervisor

Certified by .....
Nancy Kanwisher, Ph.D.
Professor of Cognitive Neuroscience, MIT
Thesis Supervisor

Accepted by .....
Earl Miller, Ph.D.
Class of 1956 Associate Professor, MIT
Chairman, Department Graduate Committee

To my farewell friends
and to my family

Acknowledgments

I am but last in a long list of scientists decisively indebted to the generosity of Emilio Bizzi, and to his grand personality. I am particularly grateful to Emilio for giving me the opportunity to join the Department as a student, for his liberal but precious advice, and for his example. Enjoying his mentorship is an invaluable good.

I also like to thank the other members of my thesis committee, Nancy Kanwisher, Earl Miller, and Peter Strick. I am fortunate and honored to have such a mindful and prestigious committee.

I cannot imagine this thesis coming together without the contribution of Ray Li. In the past few years, Ray has been at times a teacher, a ghost-advisor, and a good friend. I warmly thank him for all these reasons.

Recordings from PMd/v were carried out by Jun Xiao, and I thank him for that.

I also like to thank the members and affiliates of the Bizzi laboratory that created in these years a lively and stimulating scientific environment. I am particular thankful to Matt Tresch for important insights and helpful comments on my work. I also thank Philippe Saltiel, Andrea d'Avella, Brian Benda and Maureen Holden for numerous valuable discussions.

I am grateful to many others that provided helpful comments on the work presented here. In particular, I wish to thank Paul Cisek, John Kalaska, Sandro Mussa-Ivaldi, Reza Shadmehr, and Steve Wise.

Many others have been of great help, but none has more than Margo Cantor has. I thank her intelligent assistance in many and many occasions. In addition, I thank Sylvester Szczepanowski for his wonderful work, and the veterinarians and the personnel at the animal facility for their help. I also thank Charlotte Potak for her kind help.

I also like to thank Ed Tehovnik, Pablo Blazquez, Naotaka Fujii and Wael Asaad for technical suggestions.

Finally, I feel thankful towards the friends that have been around in these years, especially so for Emilia La Nave, Ioana Popescu, Amir Nashat, Cheryl Roberts. Thanks to all of them and to many others for greatly enriching my life. I also wish to thank my aunt Laura Pizer for make me feel as though home were only few blocks away.
Last but not least, I thank Lori Markson for her love, and for her comments on my writing.

Abstract

The thesis collects five essays on how neurons in four motor areas of the frontal lobe process the movement dynamics. In the experiments described, monkeys executed visually instructed reaching movements while holding the handle of a robotic arm. Motors attached to the robot allowed turning on and off perturbing forces that deviated the hand of the monkeys. After some exposure, the monkeys adapted to the perturbation. The experiments were designed to dissociate the activity related to the desired kinematics from that related to the dynamics. Furthermore, the experiments dissociated the activity related to motor performance (desired kinematics and dynamics) from that related to motor learning (learning a new dynamics). The thesis describes the following results.

1. *During motor execution*, the movement dynamics is processed across multiple areas. Specifically, dynamics-related activity is found in all areas projecting to the spinal cord under study, namely the primary motor cortex (M1), supplementary motor area (SMA), dorsal premotor (PMd), and ventral premotor area (PMv).
2. Dynamics-related activity is also present *during motor planning* in both PMd and SMA, but not in M1 and PMv. This suggests that the dynamics is processed "upstream" of M1. The activity of SMA reflects *during motor planning* a kinematics-to-dynamics transformation. Neuronal correlates of that transformation are observed both at the level of the population and for single cells.
3. Extensive neuronal plasticity is observed in these areas when monkeys learn a new dynamics. The activity of single neurons modifies as monkeys adapt to the force, and changes outlast the exposure to the perturbation. With respect to M1, comparison of the movement-related activity recorded prior to, during, and after exposure to the perturbing force reveals a double level of neuronal coding. As a population, neurons in M1 display changes that mirror the changes observed in the EMG of muscles. In a statistical sense, the population activity of M1 after re-adaptation is not distinguishable from that before exposure to the force. Thus, the population activity of M1 reflects *motor performance*. However, single neurons maintain –after re-adaptation –trace of the adaptation experience. Thus, the activity of M1 neurons also reflects *motor learning*.

Table of Contents

Chapter 1. Introduction

When we sit at the dinner table and reach for a glass of wine, our central nervous system (CNS) undertakes a sequence of mental operations. We must first interpret the signals that arrive to our retinas, localize the glass on the table, and make the decision to reach for the glass. Then we must design the trajectory that will take our hand to the glass, and compute the forces that will implement that trajectory. Finally, we must execute the movement. Conceptually, these operations can be grouped into three computational stages: (1) processing of the visual stimuli (including decision making), (2) processing of the movement kinematics (hand trajectory and the like), and (3) processing of the movement dynamics (the forces that implement the movement). In this scheme, the problem of motor control is for the CNS to process the kinematics and the dynamics of the movement. For neuroscientists, the problem is to understand how the CNS goes about it.

This thesis collects five essays on the neuronal processing of the movement dynamics. More precisely, on how five motor areas of the frontal lobe process the movement dynamics. The thesis develops three main themes. First, how does the CNS process the kinematics-to-dynamics transformation necessary for movements? Second, how does the activity of neurons modify when we learn to process a new dynamics? Third, how does the activity of different areas combine to control movements?

The kinematics-to-dynamics transformation (or KD transformation) is widely acknowledged a fundamental operation for motor control. Yet, few (if any) studies have previously investigated its neuronal underpinnings. Our work helps address questions such as the following: (1) Is the KD transformation processed while *planning* movements, or is it processed on-line? (2) Is it processed "upstream" of the primary motor cortex (M1), by the M1, or "downstream" of the M1 (or multiple of the above)? (3) Is the KD transformation processed through a cascade of subsequent sub-populations, or by single neurons? In the study presented in Chapter 2, we show that neurons in the SMA process the KD transformation *during motor planning*, at a time when the M1 is essentially silent. Moreover, we show that the neuronal correlates of the KD transformation can be observed also at the level of single neurons. These results have important implications for the cortical control of movements, some of which should become clearer in the following.

Computationally, processing the movement dynamics is rather challenging, and can be thought to be achieved through the use of "internal models" (i.e., internal models for the dynamics). In practice, internal models represent predictions that the CNS has

about the dynamic properties of the external world. Previous work in humans showed that new internal models can be acquired through experience, for instance when subjects adapt to external perturbing forces. The study presented in Chapter 3 describes the neuronal correlates of this learning process recorded in the primary motor cortex (M1) of non-human primates. We compared the activity of single M1 neurons recorded before, during, and after exposure to perturbing forces (which monkeys adapt to). In general, we found a variety of plastic changes in the activity of neurons. For instance, new neurons that are initially not task-related become committed to the task after learning (tune-in cells), as other neurons leave the pool (tune-out cells). In addition, neurons that are task-related before, during, and after the learning experience change their activity patterns as a result of that learning. For many cells, plastic changes outlast the exposure to the perturbation, and remain after the monkeys re-adapt to the non-perturbed conditions (memory cells).

Our study of M1 helps address –among others –the following specific question. How can plastic changes –underlying *motor learning* –coexist with the fact that M1 is necessary for *motor performance* (i.e., how can the same population of neurons learn a new internal model and not forget the old one)? We show that memory cells are of two groups, memory I cells and memory II cells. After re-adaptation to the non-perturbed conditions, the changes observed for the two groups balance each other. Thus, the activity of the population after learning (and re-adaptation) is statistically non-distinguishable from that before learning. Yet, single neurons maintain a trace of that learning experience, as their activity remains modified. Thus, our study provides a clear example of neuronal plasticity associated with motor learning, and also proposes an account how a network of actual neurons may acquire new memories.

In the traditional understanding, the "premotor" areas compute "early" sensorimotor processes and feed the primary motor cortex, which ultimately "executes" movements. More recently, however, it was found that direct projections to the spinal cord originate from numerous areas, including the dorsal and ventral premotor areas, the supplementary motor area, the dorsal and ventral cingulate motor areas, and the primary motor cortex. Although these projections partly differ from area to area, their existence suggests that the processing of "late" computational stages –in particular, the movement dynamics –might be rather widespread across areas. In a series of studies, we attacked this issue by recording in several "premotor" areas the neuronal activity related to the dynamics, and the neuronal plasticity associated with the acquisition of a new internal model. Our results are described in Chapter 4 for the supplementary motor area (SMA), and in Chapter 5 for the dorsal and ventral premotor areas (PMd and PMv). The findings can be summarized as follows. First, dynamics-related activity is widely present in all these areas. In particular, both SMA and PMd process the dynamics of the upcoming movement during motor planning, while all three areas do so during motor execution. Second, when monkeys acquire a new internal model for the dynamics, plastic changes occur in all these areas, but in different proportions. In particular, comparing the M1 with the SMA and the PMd, we see a "gradient" of plasticity: more in the M1, not-as-much in the SMA, and less in the PMd (which may appear paradoxical). The results for the PMv are more difficult to interpret, though plastic changes are definitely present.

Taken together, the results of Chapters 3-5 leave us with a complex picture of how the activity of different areas combines to control movements. On the one hand, they

argue against a strictly serial view, because different areas extensively overlap (e.g., they all process the dynamics during motor execution). On the other hand, they argue against a strictly parallel view, because significant differences are present between areas (e.g., only SMA and PMd do so also during motor planning). The study presented in Chapter 6 further develops the idea of overlapping but non-equivalent contributions. Here, we directly contrast the activity of neurons in the M1, SMA, PMd, PMv, and preSMA (or pre-supplementary motor area, a "supra-motor" area lacking direct projections to the cord). Specifically, by analyzing the timing of activation recorded in the five areas, we show that (1) all these areas are increasingly active over the course of the trial, and all reach their maximal activity during the movement, and that (2) these areas fall in a "logical" sequence, where preSMA, PMd, SMA, M1 appear in order (the PMv is more difficult to interpret). The emerging picture resembles that of subsequent, overlapping waves of increasing magnitude. Among other reasons, these results are interesting because they help "put on the map" the SMA, an area only recently re-discovered. Our data indicate that –of the areas under study –the SMA is the closest and just "upstream" of the primary motor cortex.

Stylistically, Chapters 2-6 are written as five independent papers. For this reason, they are partly redundant in the Methods sections, and refer to each other as they do to other papers. The legend is as follows: Chapter 2 (Padoa-Schioppa, Li and Bizzi, submitted); Chapter 3 (L., P.-S., and B., 2001); Chapter 4 (P.-S., L. and B., in preparation); Chapter 5 (Xiao, P.-S., and B., in preparation); Chapter 6 (P.-S. and B., in preparation).

Chapter 2. Planning movements: Kinematics-to-dynamics transformation in the supplementary motor area[1]

It is widely acknowledged that movements are planned at the level of the kinematics. However, the central nervous system must ultimately transform the kinematic plans into dynamics-related commands. How, when and where the kinematics-to-dynamics (KD) transformation is processed are fundamental and unanswered questions. We recorded from the supplementary motor area (SMA) of monkeys executing visually-instructed reaching movements. We specifically analyzed a delay period following the instruction but prior to the go signal (motor planning). During the delay, neurons in SMA progressively come to reflect the dynamics rather than the kinematics of the upcoming movement. This finding, obtained both for the population and for single cells, indicates that during motor planning neurons in SMA process the KD transformation.

[1] Elsewhere in the thesis, Chapter 2 is referred to as (Padoa-Schioppa, Li and Bizzi, submitted). Note that the next Chapter (Chapter 3) is here referred to as "previous work" (Li, Padoa-Schioppa and Bizzi, 2001).

Introduction

Reaching movements can be described at two different levels: kinematics and dynamics. The kinematics is the evolution in time of the joint angles and hand position. The dynamics is the set of forces exerted by the muscles. In Newtonian mechanics, the causal relationship is from the dynamics to the kinematics: muscle forces cause hand movements. The central nervous system, however, is faced with the inverse problem: given a desired hand trajectory (kinematics), how to generate appropriate muscle forces (dynamics). Thus, a central problem in motor control is that of transforming desired kinematics into suitable dynamics[1-4]. Previous work found a prominent activity in the SMA *during motor planning*[1,5,6]. Other work found that *during motor execution* neurons in SMA reflect the dynamics of the movement[7]. To investigate the neuronal correlates of the kinematics-to-dynamics (KD) transformation, we studied how –during planning – neurons in SMA[8-12] reflect the dynamics of the upcoming movement.

In our experiments, two monkeys held the handle of a robotic arm and executed reaching movements instructed by targets appearing on a computer monitor. A cursor on the monitor indicated the position of the hand. To study the neuronal activity related to motor planning, we introduced a delay of variable duration (0.5-1.5 s) between the presentation of the instruction (the *cue*) and the *go* signal (Figure 1a). In essence, the delay "stretches" the time during which the KD transformation takes place and "draws a line" between a phase of motor planning (prior to the *go* signal) and that of motor execution. The present results refer –unless otherwise specified –to the activity prior to the *go* signal.

The key feature of our experiments was the introduction of a mechanical perturbation resulting in a mismatch between the kinematics and the dynamics of the movement. The mechanical perturbation consisted of forces exerted upon the hand of the monkeys by motors attached to the robotic arm. In each session, the monkeys performed in a Baseline epoch (160 trials, no forces), followed by a Force epoch (160 trials). In the Force epoch, movements were initially deviated by the perturbing force. The monkeys, however, rapidly adapted and the kinematics converged to that observed in the Baseline (Figure 1b). In other words, the monkeys learned to transform the unaltered desired kinematics into a new dynamics[13,14] (Figure 1c-f). In the analysis, we compared the neuronal activity across the two epochs, disregarding the initial adaptation phase. Thus, we could distinguish the activity associated with the dynamics (activity modified by the perturbation) from the activity associated with the kinematics (activity not influenced by the perturbation). The forces used are described by "force fields" F=BV, where V is the instantaneous hand velocity and B is a rotation matrix B=[0 –b; b 0]. Depending on the sign of "b", F was clockwise (CK) or counterclockwise (CCK).

Results

Dynamics-related activity during motor planning

We recorded a total of 252 neurons in the SMA. For each trial, we considered the 500 msec preceding the *go* signal. Figure 2a illustrates the activity of a representative cell recorded in SMA with a CK force field. The cell is represented by a tuning curve, plotted in blue in polar coordinates. The preferred direction (Pd, in red) indicates the direction for

which the cell's activity would optimally contribute to the movement. The activity of the cell is very different in the two epochs. In the Baseline, the Pd of the cell is oriented towards 153°. In the Force epoch, however, the tuning curve changes and the Pd rotates CK by 36°. These changes indicate that the delay activity of the cell reflects the dynamics of the upcoming movement. Note that the visual instructions were identical in the two epochs. Likewise, the kinematics of the following movement were essentially the same in the two epochs. Thus, neither the processing of visual stimuli[15-17] nor the planning of the kinematics[18,19] can explain changes of neuronal activity across epochs. In addition, because the force field was proportional to the velocity (F=BV), no force was actually present during the delay (because V=0). Thus, changes of neuronal activity do not reflect "online" motor execution or changes in proprioceptive feedback. Instead, the changes of activity observed in the Force epoch reveal that during the delay neurons in SMA contribute to motor planning, and process the dynamics of the subsequent movement.

In the Force epoch, the Pd of the cell shown in Figure 2a shifts in the direction of the external force (CK). This phenomenon was consistent across the neuronal population. We defined the Pd only for directionally tuned cells, and 81/252 cells satisfied this criterion in both the Baseline and the Force epoch. As a population, neurons significantly shifted their Pd in the direction of the external force in the Force epoch compared to the Baseline (mean shift 11.1°, $p<0.013$, circular *t*test; Figure 2b). Most importantly, the shift of Pd observed for cells *during the delay* corresponded to an analogous shift of Pd observed for muscles *during the following movement* (mean shift 19.2°, $p<0.003$, *t*test) (Figure 1d,e). For muscles, the shift of Pd is imposed by the curl force fields[13,20]. For cells, the shift of Pd can be regarded as a fingerprint of the new dynamics[13]. The significant shift of Pd observed for the population of SMA during the delay (Figure 2b) indicates that during motor planning the population of SMA processes the dynamics of the upcoming movement. In a complementary analysis, we considered the delay activity of individual SMA cells. For 26/81 (22%) neurons we found a significant shift of Pd in the Force epoch compared to Baseline ($p<0.05$, see methods).

Shift of Pd and adaptation

We studied in more detail the correlation between the neuronal shift of Pd in SMA in the delay and the performance in the task. As the monkeys adapted to the perturbation in the Force epoch, trajectories were essentially straight, with some trial-by-trial variability in the initial direction of the trajectory. If the shift of Pd reflects the adaptation to the new dynamics, it should also directly correlate with the performance in the task. In particular, big shifts of Pd should correspond to well-adapted movements (goodADA), with small or no initial errors. To test this prediction, we computed the perpendicular displacement d of the actual trajectory from the straight line passing through the initial position and the center of the target. The displacement d was computed 150 msec after the onset of the movement. Thus, for each trial in the Force epoch d quantified the initial error. We then divided all the trials in two groups, according to d: goodADA ($d \leq \text{median}(d)$) and poorADA ($d \geq \text{median}(d)$). We obtained two tuning curves for the two groups of trials and we computed their Pd. As illustrated by the example in Figure 3, we found that goodADA trials had a greater shift of Pd than poorADA trials (ADA effect). The ADA effect was significant at the population level, as the goodADA Pd were significantly more shifted than the poorADA Pd ($p<0.02$, circular *t*test). Thus, the dynamics computed

during motor planning –as processed by neurons in the SMA –is reflected in the trajectory of the upcoming movement.

We also observe the correlation between the shift of Pd and the performance when we quantify the goodness of adaptation with an indicator related to the speed profile. Using a similar analysis as above, we divided all trials according to the correlation coefficient (CC), which captures the similarity between the actual speed profile and an ideal speed profile. Again, we find that large shifts of Pd correspond to well-adapted movements ($CC \geq \text{median}(CC)$), while small shifts of Pd correspond to poorly adapted movements ($CC \leq \text{median}(CC)$) . This effect is significant at the population level ($p<0.01$, circular *t*test).

Kinematics-to-dynamics transformation

To investigate the neuronal correlates of the KD transformation, we analyzed the time course of the shift of Pd *within* the delay. We aligned all the trials with the presentation of the *cue* and computed the Pd in sliding time windows of 300-msec width. We first considered the entire population. In Figure 4a-b, cells are aligned with the Pd in the Baseline at the end of the delay, and positive values indicate shifts in the direction of the external force. In the Baseline, the Pd are essentially constant throughout the delay (Figure 4, left)[21]. In the Force epoch, the Pd are initially aligned with the Baseline. During the delay, however, the Pd progressively shift towards the direction of the external force (Figure 4, right). A linear regression analysis indicates a slope of 26°/s ($p<10^{-9}$). Thus, neurons in SMA process the dynamics of the upcoming movement *increasingly* over the course of the delay.

We interpret the *progressive* shift of Pd as the neuronal correlate of the KD transformation. Neurons in SMA process the KD transformation both in the Baseline and in the Force epoch. The KD transformations computed in the two epochs differ from each other only for the "value" of the dynamics. In the Baseline, the kinematics and the dynamics are "aligned" and the population Pd is constant throughout the delay. In the Force epoch, there is a mismatch between the kinematics and the dynamics and as the KD transformation occurs the Pd gradually shift.

Progressive shifts of Pd are also observed at the level of single neurons. For all three cells shown in Figure 5, the Pd in the Force epoch (red color) progressively departs from the corresponding Pd in the Baseline (black color). It can be noticed that the Pd of single neurons is not constant throughout the delay[21] neither in the Baseline nor in the Force epoch. This "precession" of Pd observed for single cells, however, averages out when we consider the entire population in the Baseline (Figure 4a). We studied the progressive shift of Pd for single cells by computing –for each 300-msec time bin –the difference between the Pd in the Force epoch and the corresponding Pd in the Baseline. We then stated whether the shift of Pd was *progressive* using a linear regression analysis. We found that the slope of the regression line was significantly positive for 31% of the cells (10/32), indicating that the shift of Pd had occurred progressively during the delay. In contrast, the slope of the regression line was negative for only 6% of the cells (2/32). This result is extremely unlikely ($p<10^{-xx}$, multinomial test) if positive and negative slopes occur with equal probability (i.e., if the observed significantly positive slopes occur at random). We conclude that the KD transformation can be traced down to the activity of single SMA cells.

Shift of Pd and reaction time

The previous result is supported by the analysis of the shift of Pd in relation to the reaction time (RT) necessary for the monkey to initiate the movement after the *go* signal. As the KD transformation must be completed before the movement begins, the extent to which it occurs during the delay should anti-correlate with the RT (ref.[22]). To investigate the relation between shift of Pd and RT we divided the trials in two groups according to their RT: shortRT trials (RT ≤ median(RT)) and longRT trials (RT ≥ median(RT)). We then computed two separate Pds for the two groups of trials. Consistent with our prediction, we find a greater shift of Pd for shortRT trials than for longRT trials. For the cell illustrated in Figure 6a, when all the trials are considered (allRT, not shown), the Pd shifts by 19° in the Force compared to the Baseline. When the shortRT and longRT trials are computed separately, the shift is more pronounced for the shortRT (24°) than for the longRT (10°). This RT effect is consistent at the population level ($p<0.031$, circular bootstrap, Figure 6b), considering the cells with an allRT-shift of Pd above average (30 cells). Note, however, that we find no direct correlation between the RT and the displacement d (Table 1), suggesting that the degree of adaptation is independent of the extent to which the KD transformation occurs within the delay.

Other areas

We are currently recording from other cortical motor areas, including the primary motor cortex (M1; ref.[13]), and the dorsal and ventral premotor areas (PMd and PMv; Xiao, P.-S. and B., in preparation). Preliminary observations suggest that the phenomena described here are particularly prominent in SMA, but not unique to SMA. A total of 162 M1 cells, 142 PMd cells, and 143 PMv cells are currently available for analysis. Considering the delay activity, we observe a pronounced activation in the PMd (41/142 cells), where the shift of Pd reaches significance (mean shift 10.4°, $p<0.05$, circular *t*test). In contrast, we find little delay activity and no significant shift in M1 (16/162 cells; mean shift 4.9°, $p=0.4$, circular *t*test) and in PMv (17/143 cells; mean shift 3.1°, $p=0.8$, circular *t*test). Considering the movement-related activity, however, we find significant shifts of Pd in all four areas: PMd (43/142 cells; mean shift 11.8°, $p<0.02$, circular *t*test); SMA (128/252 cells; mean shift 16.0°, $p<10^{-5}$, circular *t*test); M1 (62/162 cells; mean shift 16.2°, $p<10^{-5}$, circular *t*test); and PMv (41/143 cells; mean shift 15.1°, $p<0.03$, circular *t*test). If confirmed, these results would indicate that the dynamics of the movement is represented in PMd and in SMA during planning, and in all four areas during execution.

Discussion

We have presented here two main results. First, the dynamics of the upcoming movement is reflected in the activity of neurons in SMA during the instructed delay, when the monkeys can only plan the movement. Second, over the course of the delay neurons in SMA *progressively* come to reflect the dynamics rather than the kinematics of the upcoming movement. Thus, neurons in SMA process the kinematics-to-dynamics (KD) transformation during motor planning. These results are supported by two independent measures of correlation. First, the dynamics computed during the instructed delay –as reflected in the activity of SMA neurons –correlates with the initial direction of the

upcoming movement (ADA effect). Second, the state of the KD transformation at the end of the delay –as reflected in the activity of SMA neurons –anti-correlates with the following reaction time (RT effect). Preliminary observations suggest that the phenomena described here for the SMA may be shared by the PMd.

One important concern is whether monkeys deal with the perturbing force by adopting a different strategy than that hypothesized here. In particular, a possible way to deal with a curl force field would be for the monkey to aim at a "virtual" target slightly shifted in the direction opposite to the force field compared to the actual target (the movement endpoint). In this case, the adaptation would consist in re-mapping the visual stimulus into a new desired target, similar to what presumably occurs when experimenters deliberately manipulate that mapping[23]. We can reject the virtual target hypothesis by comparing the trajectories predicted by that hypothesis –which can be computed using a simple mathematical model –with the trajectories actually recorded during the experiments. Assuming that in the Force epoch monkeys plan straight-line trajectories akin to that observed in the Baseline (where essentially mean(d)=0; see Table 1), the virtual target hypothesis predicts over-compensated movements. In other words, if the monkey really aimed at a visual target slightly displaced in the direction opposite to the external force, then its hand trajectory would start off directed towards that virtual target and gradually land over the actual target under the effect of the force field. In contrast, the hand trajectories actually recorded during the experiments are slightly under-compensated, as quantified by the displacement d (in the Force epoch, mean(d) = 1.5 mm; see Table 1). The virtual target hypothesis can therefore be excluded.

Another possible concern is whether adapted movements require an extra mental operation[24]. Specifically, in the Force epoch, monkeys could first transform the desired kinematics into the "old" dynamics (KD) and subsequently transform the old dynamics into the new dynamics (DD'). Then, the shift of Pd would reflect the DD' transformation, not the KD transformation. The analysis of the RT, however, argues against this hypothesis. If a DD' transformation occurs in the Force epoch, it either is or is not always completed within the delay. In the first case we should not find a RT effect. In the second case, the mean RT should be longer in the Force epoch than in the Baseline, contrary to our observations (see Table 1). We conclude that no extra operation is required for adapted movements and that the shift of Pd is the neuronal correlate of the KD transformation, unveiled by the new dynamics.

A motor area in the frontal medial wall was discovered and named "*SMA*" 50 years ago[25,26]. More recently, that "*SMA*" was divided into a rostral preSMA (or F6) and a caudal SMA-proper (or SMA, or F3) [8,11,12,27]. The present study was carried on the SMA-proper, here referred to as SMA. Among other differences, the preSMA and the SMA are distinguished by their anatomical projections, because SMA projects directly to the spinal cord and to M1[9,10] whereas preSMA lacks such projections. The undivided "*SMA*" was originally thought to harbor early sensorimotor processes and complex motor functions. Subsequent studies have however assigned these "high" functions to the preSMA[12,27-29]. Consequently, the functions of the newly defined SMA are still largely unexplored. Our data indicate that SMA processes the movement dynamics and participates in the KD transformation. In other words, they implicate SMA in a rather "late" computation, thus providing a physiological counterpart for the most recent anatomical maps.

Although our results contrast with the conclusions of a previous work by Alexander and Crutcher (A&C, ref.[1]), a closer examination of their data indicates rather converging findings. In their study, A&C trained monkeys in an assistive/null/resistive load task and found a significant effect loads in the delay for "only" 20% of SMA cells (ANOVA, $p<0.001$). They concluded that *"the near absence of preparatory loading effects ... suggests that directional preparatory activity ... may not play a significant role in coding for either the dynamics or the muscle activation patterns of pre-planned movements"*. The discrepancy between our conclusions and that of A&C is due to the different analysis and read-out criteria. From a statistical standpoint, the present conclusions (based on data passing a statistical test) are more sound than that of A&C (based on multiple failures to reject the null hypothesis). Moreover, A&C did not appreciate the fact that 20% of cells passing a statistical test with significance level of $p<0.001$ was an important presence, not a "near absence". In spite of the conclusions drawn by A&C, the only SMA cell shown in their paper (right side of Figure 9 in ref.[1]) has the characteristics described in the present article. The activity of the cell is directional (it is higher before extension than before flexion) and load-dependent (it is higher before opposed than before assisted movements). Moreover, inspection of the activity preceding opposed movements reveals a clear RT effect. Specifically, the RT effect can be seen comparing the delay activity in the top five trials (shortRT, higher activity) with that in the bottom five trials (longRT, lower activity). The RT effect is also evident in the only load-dependent SMA cell shown by A&C in the second paper of their series (Figure 3 in ref.[7]). In conclusion, the data of A&C –re-examined in the light of our results –support our conclusions.

Previous work found dynamics-related (or load-dependent) activity *during motor execution* in a number of cortical and sub-cortical motor areas, including the dorsal premotor area[30] (PMd), the supplementary motor area[7] (SMA), the primary motor cortex[31,32,7,13] (M1), the ventral premotor area[33] (PMv), the putamen[7], and the dentate and interpositus nuclei of the cerebellum[34]. In contrast, no dynamics-related activity was found in area 5 (ref.[35]). We therefore hypothesize that dynamics-related signals are present in all cortical areas that project directly to the spinal cord. Some of the projecting areas –notably the PMd and the SMA –also show prominent activation *during motor planning*[5,36,1]. These areas seem therefore natural candidates for processing the KD transformation. The present work focused on the SMA. We showed that SMA neurons reflect the dynamics of the upcoming movement increasingly over the course of the delay. The presence of a significant *trend* indicates that the activity of neurons in SMA reflects the KD transformation. At this time, limited data on other candidate areas are available for analysis. A preliminary assessment suggests that some of the phenomena described here may be not unique to the SMA. Further work is however needed to investigate the interplay of different areas in the processing of the KD transformation, which is –many authors have argued –a necessary and fundamental operation for motor control[1-4,14].

With respect to the cortical organization of motor control, our data imply one of the two following: the *input* received by M1 contains information on the dynamics[37-39] and/or different areas work in parallel to control the activation of muscles[8,9,40].

Methods

Behavioral task

Two male rhesus monkeys (*Macaca mulatta*), C and F, participated in the experiment and both performed with the right arm. The experimental setup and behavioral paradigm were essentially the same as described in ref.[13]. A center square appeared on the monitor and the monkey moved the cursor into the center square to initiate the trial. After 1 s, a peripheral target (*cue*) appeared randomly at one of eight locations around the clock. The monkey held the cursor within the center square for a random delay of 0.5 to 1.5s. The center square was then extinguished (*go* signal). The monkey had to move and acquire the peripheral target within 3s and to remain within the peripheral target for 1s to receive a juice reward. Movements were confined to a horizontal plane. The center square and peripheral targets were 16x16-mm squares (1.1° of visual angle) that appeared on a screen situated 75 cm in front of the monkey. The cursor was a 3x3-mm square (0.2° visual angle). Movements were 8 cm in length and the trajectories were confined within 60° on both sides of the line passing through the center square and peripheral target.

In each session, the monkeys performed in the Baseline and Force epochs, followed by a Washout epoch were the forces were removed. Each epoch included approximately 20 successful trials per direction. The present analysis focused exclusively on the Baseline and Force epochs. For the force fields, we used b=±0.06 N sec/m. Monkeys were trained in the non-perturbed reaching task and the force fields were only introduced during the recordings. For monkey C, sessions with the two force fields were run in blocks (27 and 28 sessions, respectively), starting with the CK force field. Monkey F was tested on the CCK force field only (40 sessions).

Recordings

The SMA was identified and distinguished from the preSMA through electrical microstimulation (monkey C) and histology (monkey F). For microstimulation, we used a train of 20 biphasic pulse pairs (width=0.1msec, duration=60 msec), at 330 Hz and 10-40 μ Amp. Before the recordings, we extensively stimulated the left medial wall and we obtained a map closely matching that in ref.[11]. We presently report on cells recorded in the arm region of SMA. For the histology, we marked the recording sites with electrolytic lesions (cathodal current, 20 μ A, 2 min). After euthanasy, the brain was photographed, sectioned (coronal plane, 28 μ m sections), and Nissl-stained. Recordings were located in the medial wall, caudal to the alignment with the genu of the arcuate sulcus. Microscopic inspection revealed that the recording region was poorly laminated, and lied within 6 mm rostral to tissue displaying a single line of giant pyramidal cells[8].

Hand trajectories were recorded at 100 Hz. Neuronal recordings followed standard procedures[13]. For the electromyographic activity (EMG), we manually implanted bipolar wires, in separate sessions. We recorded the EMG of the muscles Pectoralis, Deltoid, Biceps, Triceps and Brachioradialis (15 instances total). The EMG traces were rectified, integrated over the movement time, averaged across trials, and submitted to the same analysis as cells. NIH guidelines on the use of animals were followed throughout the experiment.

Data analysis

The correlation coefficient (CC) was defined as in ref.[13], and ranged in values between −1 and 1 (CC close to 1 for actual trajectories close to ideal). To compare movements with similar kinematics, we disregarded for each epoch the first four successful trials in each direction. Loose time constraints were imposed on the RT during the experiments. In the analysis, we excluded anticipatory movements (RT<200 msec) and outliers (RT>400 msec). The remaining trials were considered for further analysis. For each trial we defined the movement onset (*mo*) and movement end (*me*), with threshold-crossing criteria on the speed (4 cm/sec). We defined the initial position as the average position in the 50 msec preceding the *mo* and computed the displacement *d* 150 msec after the *mo*. Neurons were identified through manual clustering (Autocut3, DataWave Technology). For the activity "during motor execution" (or movement-related activity), we considered the activity from 200 msec before the *mo* to the *me*. This same movement-related time window was used for muscles.

The Pd was computed subject to the pre-condition of directional tuning (i.e., unimodal distribution of activity across directions) as revealed by the Rayleigh test ($p<0.01$, see ref.[41] p70). The Pd was defined as the direction of the vector average of the eight directional activation. For the population analyses, we "flipped" the data recorded with the CK force field to obtain positive values when the Pd shifted in the direction of the external force. The statistical analysis for the neuronal population followed standard methods of circular statistics, as described in ref.[41] p75 (circular bootstrap) and p76 (circular *t*test). Individual cells were analyzed with a procedure based on error propagation, as described in ref.[13]. The linear regression analysis was operated following ref.[42] p65-68.

We analyzed the ADA effect of all the cells in the pool (81 cells total), with the condition that both the goodADA and the poorADA tuning curves passed the directional-tuning test (Rayleigh test). This condition was satisfied by 75 cells for the *d*-based analysis, and by 70 cells for the CC-based analysis. The slope of the regression (Figures 4,5) was computed in the 300-800msec following the *cue*. With respect to single neurons (Figure 5), the slope analysis was restricted to cells whose Pd shift measured at the end of the delay was above average (36 cells total). We only considered the time bins such that the corresponding tuning curve passed the directional-tuning test (Rayleigh test) in both the Baseline and the Force epoch. To compute the slope, we also imposed the condition that at least three data points be present. A total of 32 cells satisfied this condition. The RT effect analysis (Figure 6) was restricted to cells with a Pd shift above average (36 cells). We also imposed that both the shortRT and longRT tuning curves passed the directional-tuning test (Rayleigh test). A total of 30 cells satisfied this condition.

For a control, we computed the population shift of Pd (Figure 2b) using a different criterion instead of the Rayleigh test as a pre-condition to compute the Pd. We tested the SMA population with the following pre-conditions: ANOVA ($p<0.05$ and $p<0.01$); cosine tuning ($R^2>0.7$); adjustable width cosine ($R^2>0.7$, see ref.[43]); bootstrap ($p<0.01$, see ref.[44]). All these tests except that based on the strict cosine tuning indicated a significant shift of Pd for the population.

Acknowledgements

We are thankful to Matt Tresch for fruitful discussions and to Steve Wise, Sandro Mussa-Ivaldi and Lori Markson for comments on the manuscript. We also thank Pablo Blazquez for help with the histology and Margo Cantor, Sylvester Szczepanowski and Eva Skokanova for technical assistance and animal care.

References

1. Alexander, G.E. & Crutcher, M.D. Preparation for movement: neural representations of intended direction in three motor areas of the monkey. *J. Neurophysiol.* **64,** 133-150 (1990).
2. Kalaska, J.F. & Crammond, D.J. Cerebral cortical mechanisms of reaching movements. *Science* **255,** 1517-1523 (1992).
3. Mussa-Ivaldi, F.A. & Bizzi, E. Motor learning through the combination of primitives. *Phil. Trans. R. Soc. Lond.* B **355,** 1755-1769 (2000).
4. Saltzman, E. Levels of sensorimotor representation. *J. Math. Psychol.* **20,** 91-163 (1979).
5. Kurata, K. & Wise, S.P. Premotor and supplementary motor cortex in rhesus monkeys: neuronal activity during externally- and internally-instructed motor tasks. *Exp. Brain Res.* **72,** 237-248 (1988).
6. Tanji, J. The supplementary motor area in the cerebral cortex. *Neurosci. Res.* **19,** 251-268 (1994).
7. Crutcher, M.D. & Alexander, G.E. Movement-related neuronal activity selectively coding either direction or muscle pattern in three motor areas of the monkey. *J. Neurophysiol.* **64,** 151-163 (1990).
8. Matelli, M., Luppino, G. & Rizzolatti, G. Architecture of superior and mesial area 6 and the adjacent cingulate cortex in the macaque monkey. *J. Comp. Neurol.* **311,** 445-462 (1991).
9. Dum, R.P. & Strick, P.L. The origin of corticospinal projections from the premotor areas in the frontal lobe. *J. Neurosci.* **11,** 667-689 (1991).
10. Wise, S.P. Corticospinal efferents of the supplementary sensorimotor area in relation to the primary motor cortex. *Adv. Neurol.* **70,** 57-69 (1996).
11. Luppino, G., Matelli, M., Camarda, R.M., Gallese, V. & Rizzolatti, G. Multiple representations of body movements in mesial area 6 and the adjacent cingulate cortex: an intracortical microstimulation study in the macaque monkey. *J. Comp. Neurol.* **311,** 463-482 (1991).
12. Matsuzaka, Y., Aizawa, H. & Tanji, J. A motor area rostral to the supplementary motor area (presupplementary motor area) in the monkey: neuronal activity during a learned motor task. *J. Neurophysiol.* **68,** 653-662 (1992).
13. Li, C-S.R., Padoa-Schioppa, C. & Bizzi, E. Neural correlates of motor performance and motor learning in the primary motor cortex of monkeys adapting to an external force field. *Neuron* **30,** 593-607 (2001).
14. Shadmehr, R. & Mussa-Ivaldi, F.A. Adaptive representation of dynamics during learning of a motor task. *J. Neurosci.* **14,** 3208-3224 (1994).
15. Andersen, R.A., Snyder, L.H., Li, C-S. & Stricanne, B. Coordinate transformations in the representation of spatial information. *Curr. Opin. Neurobiol.* **3,** 171-176 (1993).
16. Newsome, W.T. The King Solomon Lectures in Neuroethology. Deciding about motion: linking perception to action. *J. Comp. Physiol. [A]* **181,** 5-12 (1997).
17. Gold, J.I. & Shadlen, M.N. Representation of a perceptual decision in developing oculomotor commands. *Nature* **404,** 390-394 (2000).
18. Wise, S.P., di Pellegrino, G. & Boussaoud, D. Primate premotor cortex: dissociation of visuomotor from sensory signals. *J. Neurophysiol.* **68,** 969-972 (1992).

19. Shen, L. & Alexander, G.E. Neural correlates of a spatial sensory-to-motor transformation in primary motor cortex. *J Neurophysiol.* **77,** 1171-94 (1997).
20. Thoroughman, K.A & Shadmehr, R. Electromyographic correlates of learning an internal model of reaching movements. *J. Neurosci.* **19**, 8573-8588 (1999).
21. Johnson, M.T.V., Coltz, J.D., Hagen, M.C. & Ebner, T.J. Visuomotor processing as reflected in the directional discharge of premotor and primary motor cortex neurons. *J. Neurophysiol.* **81,** 875-894 (1999).
22. Riehle, A. & Requin, J. The predictive value for performance speed of preparatory changes in neuronal activity of the monkey motor and premotor cortex. *Behav. Brain Res.* **53,** 35-49. (1993).
23. Alexander, G.E. & Crutcher, M.D. Neural representation of the target (goal) of visually guided arm movements in three motor areas of the monkey. *J. Neurophysiol.* **64,** 164-178 (1990).
24. Cisek, P. & Scott, S.H. An alternative interpretation of population vector rotation in macaque motor cortex. *Neurosci. Lett.* **272,** 1-4 (1999).
25. Penfield, W. & Welch, K. The supplementary motor area of the cerebral cortex. *Arch. Neurol. Psychiatry* **66,** 289-317 (1951).
26. Woolsey, C.N., Settlage, P.H., Meyer, D.R., Sencer, W., Pinto Hamuly, T. & Travis, A.M. Patterns of localization in precentral and "supplementary" motor areas and their relation to the concept of premotor area. *Res. Publ. Assoc. Nerv. Ment. Dis.* **30,** 231-250 (1952).
27. Picard, N. & Strick, P.L. Motor areas of the medial wall: a review of their location and functional activation. *Cereb. Cortex* **6,** 342-353 (1996).
28. Shima, K. & Tanji, J. Neuronal activity in the supplementary and presupplementary motor areas for temporal organization of multiple movements. *J. Neurophysiol.* **84,** 2148-2160 (2000).
29. Hikosaka, O. *et al.* In: *The New Cognitive Neuroscience* (ed Gazzaniga, M.S.) 553-572 (MIT Press, Cambridge MA, 2000).
30. Werner, W., Bauswein, E. & Fromm, C. Static firing rates of premotor and primary motor cortical neurons associated with torque and joint position. *Exp. Brain Res.* **86,** 293-302 (1991).
31. Evarts, E.V. Relation of pyramidal tract activity to force exerted during voluntary movement. *J. Neurophysiol.* **31,** 14-27 (1968).
32. Kalaska, J.F., Cohen, D.A.D., Hyde, M.L. & Prud'homme, M. A comparison of movement direction-related versus load direction-related activity in the primate motor cortex, using a two-dimensional reaching task. *J. Neurosci.* **9,** 2080-2102 (1989).
33. Hepp-Reymond, M.C., Husler, E.J., Maier, M.A. & Qi, H.X. Force-related neuronal activity in two regions of the primate ventral premotor cortex. *Can. J. Physiol. Pharmacol.* **72,** 571-579 (1994).
34. Thach, W.T. Correlation of neural discharge with pattern and force of muscular activity, joint position, and direction of intended next movement in motor cortex and cerebellum. *J. Neurophysiol.* **41**, 654-676 (1978).
35. Kalaska, J.F., Cohen, D.A., Prud'homme, M. & Hyde, M.L. Parietal area 5 neuronal activity encodes movement kinematics, not movement dynamics. *Exp. Brain Res.* **80**, 351-364 (1990).

36. Wise, S.P., Boussaoud, D., Johnson, P.B. & Caminiti, R. Premotor and parietal cortex: corticocortical connectivity and combinatorial computations. *Annu. Rev. Neurosci.* **20**, 25-42 (1997).
37. Georgopoulos, A., Kalaska, J., Caminiti, R. & Massey, J. On the relations between the direction of two-dimensional arm movements and cell discharge in primate motor cortex. *J. Neurosci.* **2,** 1527-1537 (1982).
38. Moran, D.W. & Schwartz, A.B. Motor cortical representation of speed and direction during reaching. *J. Neurophysiol.* **82,** 2676-2692 (1999).
39. Todorov, E. Direct cortical control of muscle activation in voluntary arm movements: a model. *Nat. Neurosci.* **3,** 391-398 (2000).
40. Prut, Y. & Fetz, E.E. Primate spinal interneurons show pre-movement instructed delay activity. *Nature* **401,** 590-594 (1999).
41. Fisher, N.I. *Statistical analysis of circular data.* (Cambridge University Press, Cambridge, 1993).
42. Neter, J., Wasserman, W. & Kutner, M.H. *Applied linear statistical models.* (R. Irwing Inc., Homewood IL, 1985).
43. Battaglia-Mayer, A. *et al.* Early coding of reaching in the parietoccipital cortex. *J. Neurophysiol.* **83,** 2374-2391 (2000).
44. Crammond, D.J. & Kalaska, J.F. Differential relation of discharge in primary motor cortex and premotor cortex to movements versus actively maintained postures during a reaching task. *Exp. Brain Res.* **108,** 45-61 (1996).

Figure legends

Figure 1. *Methods.* **A.** Trial sequence (see methods for details). **B.** Representative trajectories (CK force field). **C.** Experimental paradigm. In the force epoch, the monkeys learn to compute a new dynamics to implement the desired kinematics. **D.** The CK force field plotted in velocity space. **E.** Effects of the adaptation on the activity of muscles. In the Force epoch, the force of muscles (green) and the external force field (red) sum (blue). Consequently, the Pd of all the muscles shifts in the direction of the external force. **F. Left:** Biceps, EMG traces. Movements towards 225° are aligned at the *go* signal. Notably, there is no EMG activity in the delay. **Right:** Tuning curve plotted in polar coordinates. In the Force epoch, the Pd (red) shifts in the direction of the external force (CCK).

Figure 2. *Shift of preferred direction.* **A.** Tuning curve of one cell. The dotted lines indicate the mean activity in the 0.5 s before the cue. **B.** Population. The histogram represents the shift of Pd between the Force epoch and the Baseline. Positive values on the x-axis indicate shifts in the direction of the external force. The "m" and "M" are the mean and median of the histogram, respectively. The population shows a significant shift ($p<0.013$, *t*test). The last 0.5 s before the *go* signal are considered here.

Figure 3. *ADA effect.* This cell was recorded with a CK force field. When at the end of the delay the Pd is more shifted, movements are well-adapted (goodADA). When the Pd is less shifted, movements are poorly adapted (poorADA). The last 0.5 s before the *go* signal are considered here.

Figure 4. *Time evolution of the Pd: population.* Trials are aligned with the cue (time=0) and the Pd is computed in 300-msec time windows (25-msec shift). On the y-axis, "zero" is the Pd in the Baseline at the end of the delay. Positive values indicate shifts of Pd towards the external force. In the Force epoch, the Pd progressively shifts. Vertical bars indicate standard deviations. Blue asterisks indicate data points significantly greater than zero ($p<0.01$, *t*test). We considered only the activity preceding the *go* signal. The large error bars early in the delay are due to the "precession" of Pd seen for single cells (Figure 5).

Figure 5. *KD transformation for single cells.* See text.

Figure 6. *RT effect.* **A.** RT effect, one neuron. When the Pd shifts more within the delay, the RT is shorter (shortRT). When the Pd shifts less, the RT is longer (longRT). This cell was recorded with a CK force field. The last 0.5 s before the *go* signal are considered here. **B.** RT effect, population. The x-axis is the shift of Pd for the shortRT trials. The y-axis is the shift of Pd for the longRT trials. Each point represents one cell, and the cell shown in **A.** is indicated in red. The population tends to lie below the diagonal line ($p<0.031$).

Table

Table 1.

	Baseline	Force epoch
Mean *d* : all ADA (mm)	-0.05 (± 2.2)	1.5 (± 2.2)
good ADA	-1.6 (± 2.4)	-0.4 (± 2.2)
poor ADA	1.5 (± 2.1)	3.4 (± 2.1)
Mean RT: all RT (msec)	284 (± 16)	283 (± 16)
short RT	258 (± 14)	257 (± 15)
long RT	308 (± 19)	309 (± 19)
Correlation (*d*, RT)	-0.01 (± 0.16)	0.01 (± 0.15)

Legend. For each session, we computed the mean *d* and mean RT for the different groups of trials. The data reported are averages across sessions (± SD). For the displacement *d*, positive values correspond to displacements in the same direction as the force field. The correlation is computed session by session and averaged across sessions.

Figures

Figure 1

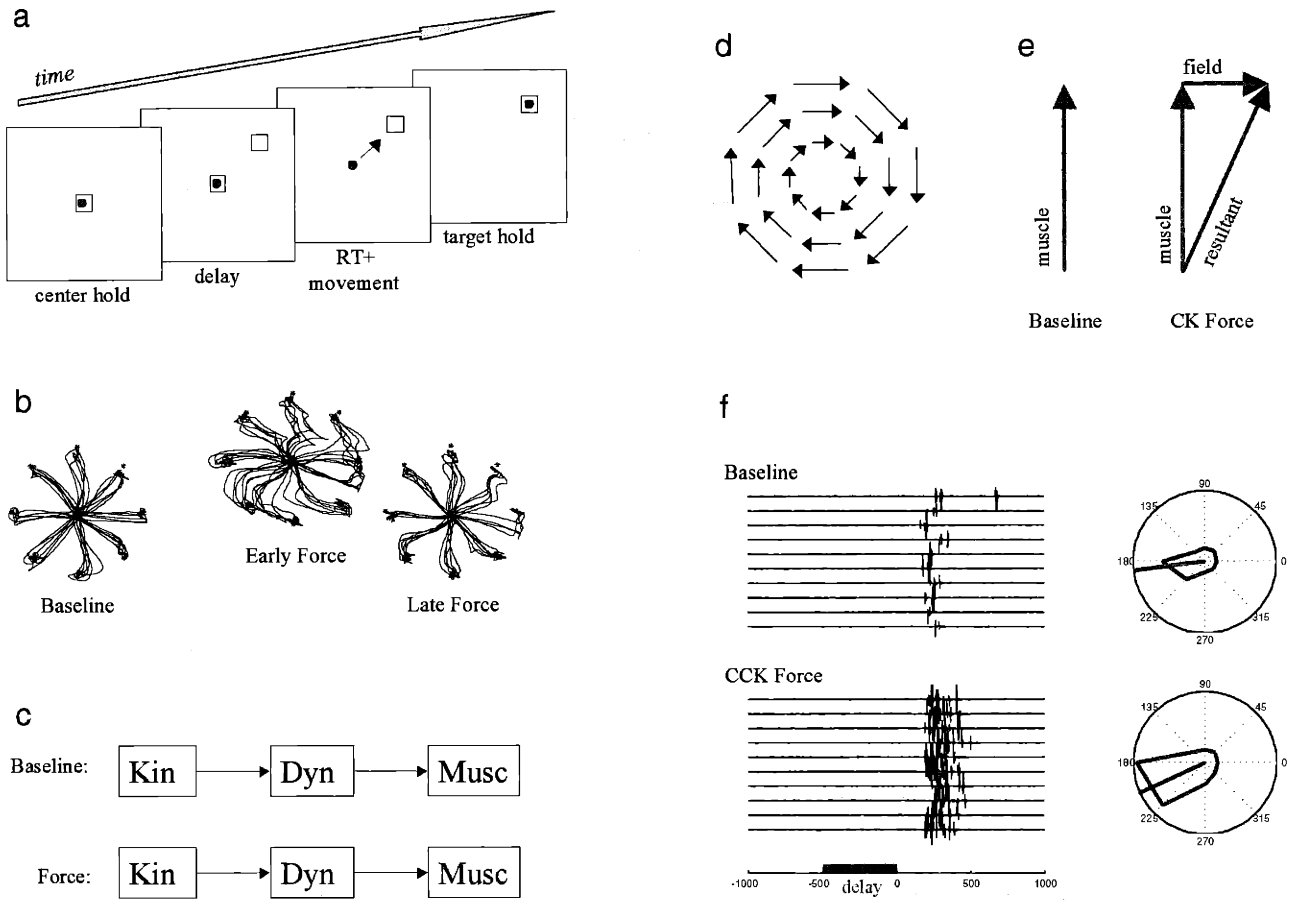

Figure 2

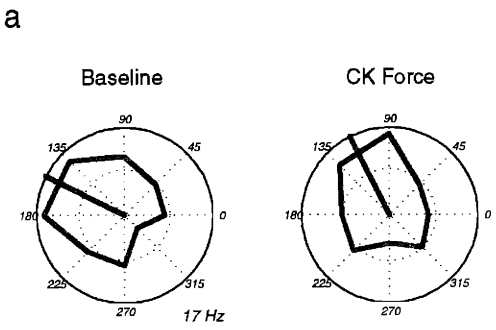
a
Baseline
CK Force
90
45
135
180
0
225
315
270
17 Hz
b
m=11.1
M=10.2
15
10
5
0
90
45
0
45
90

Figure 3

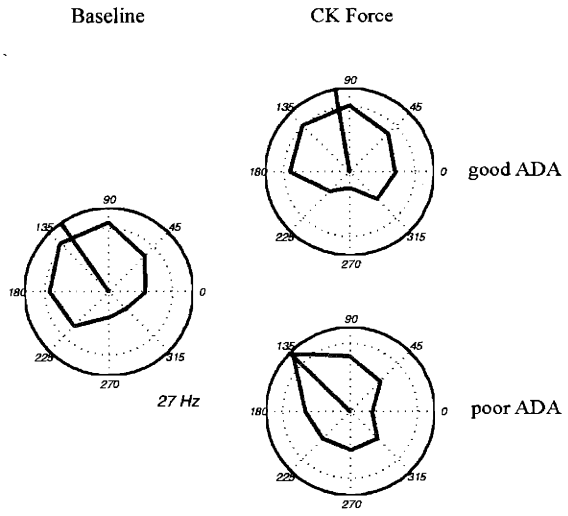
Baseline
CK Force
90
45
135
180
0
225
315
270
27 Hz
good ADA
poor ADA

Figure 4

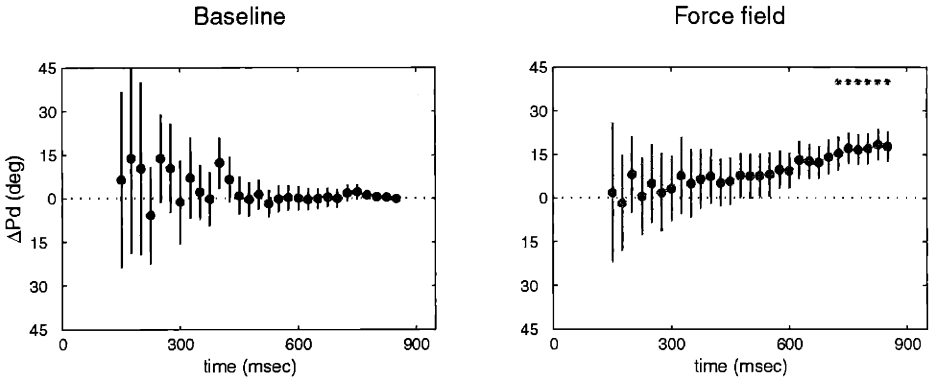
Baseline
Force field
ΔPd (deg)
45
30
15
0
15
30
45
0
300
600
900
time (msec)
******

Figure 5

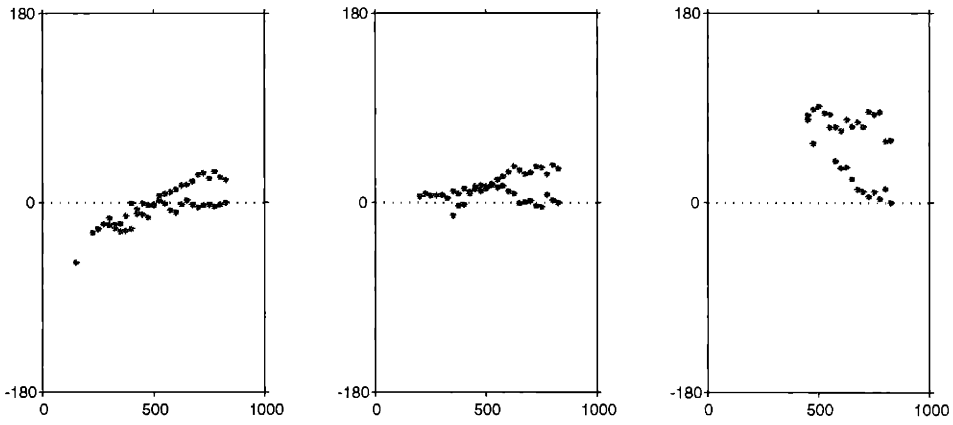

Figure 6

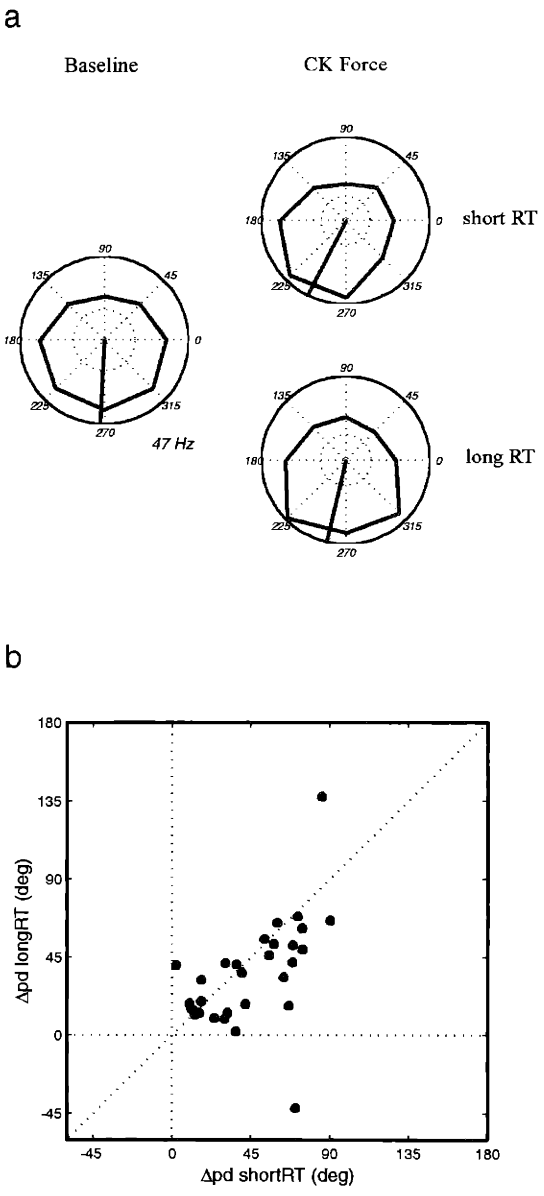
a
Baseline
CK Force
short RT
long RT
47 Hz
90
45
0
315
270
225
180
135
b
Δpd longRT (deg)
Δpd shortRT (deg)
180
135
90
45
0
-45

Chapter 3. Neuronal correlates of motor performance and motor learning in the primary motor cortex[1]

The primary motor cortex (M1) is known to control motor performance. Recent findings have also implicated M1 in motor learning, as neurons in this area show learning–related plasticity. In the present study, we analyzed the neuronal activity recorded in M1 in a force field-adaptation task. Our goal was to investigate the neuronal reorganization across behavioral epochs (before, during and after adaptation). Here we report two main findings. First, memory cells were present in two classes. Class I memory cells changed their activation following adaptation and maintained the new activation after removal of the perturbation. Class II memory cells, whose activation was not changed by the exposure to the force field, changed their activation following re-adaptation to the non-perturbed conditions. With respect to the changes of preferred direction (Pd), these two classes complemented each other after re-adaptation. Second, for the entire neuronal population the shift of Pd matched the shift observed for muscles. These results provide a framework whereby the activity of distinct neuronal sub-populations combines to subserve both functions of motor performance and motor learning.

[1] Reprinted from *Neuron* Vol. 30, 2001, pp 793-607, Li et al: "Neuronal correlates of motor performance and motor learning in the primary motor cortex," © 2001, with permission from Elsevier Science. Elsewhere in the thesis, Chapter 3 is referred to as (Li, Padoa-Schioppa and Bizzi, 2001).

Introduction

A wealth of evidence derived from studies with humans and non-human primates indicates that the sensory and motor areas of the cerebral cortex are plastic. For instance, experiments on primates showed that re-mapping occurs in the somatosensory cortex when sensory nerves from a body part are severed or deactivated by a local anesthetic (Faggin et al., 1997; Florence and Kaas, 1995; Manger et al., 1996; Borsook et al., 1998). After recovery, the cortical area deprived of the sensory input from the amputated part was activated by stimulation of an adjacent body part. Similar observations have been made when a lesion was selectively placed in a small, circumscribed cortical area (Xerri et al., 1998). Neuronal plasticity has also been demonstrated in studies employing electrical microstimulation and behavioral training. For instance, it was found that cortical representation increases in the primary auditory cortex for a frequency range that monkeys were trained to discriminate (Recanzone et al., 1993). Nudo and colleagues used intracortical microstimulation to map the representation of the distal forelimb zone of the primary motor cortex of monkeys (Nudo et al., 1996). Microstimulations were applied before and after training on two tasks that differentially engaged specific sets of digit and forelimb movements. When monkeys performed in a small-object retrieval task, in which they actively used their digits, the cortical representation of their digits increased. In contrast, when monkeys were trained on a key-turning task, which engaged the wrist/forearm, the corresponding cortical areas were found to be enlarged.

Further evidence for plasticity comes from functional imaging experiments with humans. Studies using magnetic source imaging revealed that the cortical representation of the left-hand digits of string players was larger than that of control subjects (Elbert et al., 1995). Training on a sequence of finger movements over a few weeks resulted in enlarged activation of the primary motor cortex when subjects performed the practiced sequence, compared to a novel, unpracticed sequence (Karni et al., 1995). Using transcranial magnetic stimulation (TMS), Pascual-Leone and colleagues found that both mental and physical practice led to an improvement in five-finger piano exercises. Such improvement was associated with the modulation of cortical motor output to the muscles utilized in the task (Pascual-Leone et al., 1994). More recently, Classen and colleagues used focal TMS of the motor cortex to elicit isolated limb movements (Classen et al., 1998). They found that continuous training on a particular direction of thumb movement for as little as 10 minutes could bias the direction of evoked movements, suggesting that training rapidly alters the cortical network subserving thumb movement. The authors speculated that this change could subserve a short-term memory for movement and might potentially be the first stage of skill acquisition.

Neuronal recordings from awake, behaving monkeys have also revealed plasticity at the single cell level in a number of learning tasks. For example, neurons in the primary motor cortex, the premotor cortex and the supplementary eye field exhibited learning-dependent activity changes in a visuomotor association task (Mitz et al., 1991; Chen and Wise, 1995; Wise et al., 1998). Nakamura and colleagues showed that a subset of medial frontal neurons were more active during performance of a new sequence compared to a learned sequence of movements, and suggested that these neurons might be involved in the acquisition of new sequential procedures (Nakamura et al., 1998). Previous studies on

the neural correlates of long-term memory had also revealed neuronal plasticity associated with perceptual learning (Sakai and Miyashita, 1991).

To our knowledge, however, no studies have explored changes in neuronal activity during learning that involved a change in movement dynamics. Psychophysical experiments conducted in our laboratory have demonstrated that human subjects adapt to a viscous force field imposed on their visually guided planar reaching movements (Shadmehr and Mussa-Ivaldi, 1994). The perturbation of the movement trajectories decreased and eventually disappeared as subjects adapted to these force fields. When the force field was removed, the movement trajectories curved in the direction opposite of that observed when the force field was first imposed. The existence of this aftereffect suggested that subjects developed an internal model of the dynamics of the motor environment as they adapted to the force field. In the current study, we extended the force field adaptation paradigm to monkeys. Our aim was to examine the change in neuronal activity in the primary motor cortex of monkeys as they adapt to a new dynamic environment.

We have previously reported that when monkeys engage in this adaptation paradigm, new cells (tune-in cells) are recruited as other cells leave the pool (tune-out cells) (Gandolfo et al., 2000). In the present study, we investigated the changes of the neuronal activity of the primary motor cortex (M1) with respect to the parameters characterizing their tuning curves. We found that two different classes of memory cells coexist and balance each other after exposure to the force field. When the entire population was considered, the changes of preferred direction across behavioral epochs observed for neurons matched the corresponding changes observed for muscles. This match was due to the concurrent presence of the two classes of memory cells.

Results

Adaptation to the force field

Two monkeys performed center-out visually instructed reaching movements. The monkeys held the manipulandum of a two-degree-of-freedom, lightweight, low-friction robot arm. The position of the manipulandum and the targets were displayed on a computer monitor placed in front of the monkey (Figure 1A). This setup was essentially identical to that previously used in human behavioral studies (Shadmehr and Mussa-Ivaldi, 1994). In the task, the monkeys performed delayed, visually instructed, reaching movements, as illustrated in Figure 1B. Each experimental session was divided into three behavioral epochs: (1) a Baseline epoch, in which the monkey performed the task without a force field; (2) a Force epoch, in which a force field was applied; and (3) a Washout epoch, in which the force field was removed. Typically the monkey performed 160 to 200 successful trials ("hits") in each epoch, which averaged to 20 to 25 "hits" for each of the eight movement directions. Each experiment lasted for approximately two hours. In each session, one of two curl, viscous force fields -- clockwise or counterclockwise -- was applied in the Force epoch (Figure 1C). These force fields imposed predictable changes on the muscular activity in the Force epoch (Figure 1D).

To characterize the "goodness" of movements, we derived the speed profile from each trajectory. We then computed a correlation coefficient (CC) measuring the similarity between the actual speed profile and an ideal speed profile (Shadmehr and Mussa-Ivaldi,

1994). The values of the CC range between –1 and 1, and are close to 1 when the actual speed profiles are close to ideal. The results of a representative experimental session are depicted in Figure 2. In the Baseline, when no force was present, the CC was high and the trajectories were straight. When a counterclockwise force field was introduced, the performance deteriorated (the CC dropped) and trajectories deviated in the direction of the force. As the monkey adapted to the perturbation, however, trajectories returned straight and the CC reached a steady state. During the late Force epoch, performance was essentially indistinguishable from the Baseline. When the force field was removed – in the Washout -- an "aftereffect" was observed, in which the trajectories deviated in a way that mirrored the change in the early Force. After a brief re-adaptation phase, the movement trajectories again became straight and the CC regained its original high values.

The activity of neurons in the primary motor cortex (M1) was recorded while monkeys performed during the Baseline, Force and Washout epochs. In the analysis presented in the following sections, we focused on the neuronal and muscular activity recorded in trials with similar kinematics. In other words, we only considered trials corresponding to the three bottom panels of Figure 2B and to the steady state regions of the correlation coefficient. Thus, we were able to dissociate the neural activity related to the kinematics from the activity related to the dynamics of movement. In the Force epoch, the kinematics were essentially the same as in the Baseline (i.e. the trajectories were straight and the speed profiles were close to ideal). However, the dynamics were different since the monkeys compensated for the external force field in the Force epoch but not in the Baseline. In addition, we were able to dissociate the motor performance from the effects of motor adaptation. In the Washout, the performance of the monkeys was essentially identical to the Baseline, both in terms of the kinematics and the dynamics of movement. Differences in activity between the Washout and the Baseline epochs were therefore attributed to the effects of adaptation. These considerations served as the bases for classifying neurons.

Neural plasticity in M1

A total of 162 neurons were considered for the present analysis. For each trial, we analyzed the neuronal activity from 200 msec before the onset of the movement to the end of the movement (movement-related activity). A tuning curve was constructed from the neuronal activity of the eight directions of movement. Three parameters were used to characterize each tuning curve. (1) The preferred direction (Pd) was defined as the direction of the vector sum of the vectors representing the activity for the each of the eight directions of movement. (2) The average firing frequency (Avf) was defined as the average of the neuronal firing rates in the eight movement directions. (3) The tuning width (Tw) was defined as the angle over which the activity was higher than half of the maximal activity (maximum of the tuning curve). The Pd and Tw were computed only for those neurons showing a significant non-uniform distribution of activity across the eight movement directions ($pR<0.05$, Rayleigh test). The neuronal activity in the Baseline, Force and Washout epochs were statistically compared in terms of the three parameters used to characterize the tuning curve. The comparison was made separately for each parameter.

Neurons whose activity remained invariant across the three behavioral epochs (*x-x-x*) were called kinematic cells, as their activity appeared to be correlated with the

kinematics of the movement. Neurons whose activity was modulated by the force field (*x-y-x*) were called dynamic cells. Some cells, modulated by the force field, retained their modulation in the Washout epoch such that their activity profile in the Washout was more similar to that in the Force than in the Baseline epoch (*x-y-y*). These neurons were named "memory" cells, as they appeared to maintain in the Washout a memory trace of the force field imposed in the Force epoch. We also found another class of cells whose activity was not modulated by the force but was modulated in the Washout (*x-x-y*). We classified the (*x-x-y*) cells as memory cells because their activity in the Washout was different from the Baseline. We named the (*x-y-y*) and (*x-x-y*) cells Class I and Class II memory cells, respectively. In some instances, cells were modulated by the force and again in the Washout (*x-y-z*).

Figures 3A-E show examples of kinematic, dynamic and memory cells. Since the preferred direction (Pd), average firing frequency (Avf) and tuning width (Tw) were used separately to characterize the neuronal activity, a cell could exhibit dynamic or memory properties in terms of any of the three parameters. The shifts of Pd are particularly interesting because they reflect the constraints imposed by the curl force fields. The Pd of the cell shown in Figure 3A remained essentially unchanged across the three behavioral epochs. This cell was thus classified as kinematic. Dynamic cells shifted their Pd in the Force epoch compared to the Baseline. This shift typically occurred in the direction of the applied force field (clockwise in the example shown in Figure 3B). In the Washout, the Pd of dynamic cells returned to their original values. Class I memory cells (*x-x-y*) shifted their Pd in the Force epoch. Their shifts also occurred in the direction of the external force field (Figure 3C). In the Washout, however, Class I memory cells maintained their newly acquired Pd. In contrast, Class II memory cells (*x-y-y*) did not change their Pd in the Force epoch, but shifted their Pd in the Washout. This shift typically occurred in the direction opposite to the previously experienced force field. For the cell shown in Figure 3D, which was recorded in a session where a clockwise force field had been introduced in the Force epoch, the shift of Pd occurred in the Washout in the counterclockwise

10^{-6}
direction.

Recording experiments were occasionally conducted without using the force field (7 cells total). In these sessions, the monkeys performed approximately 600 hits in the Baseline condition. 3/7 cells were directionally tuned in all three epochs and all of them were classified as kinematic according to the changes of Pd. Figure 3F shows one cell recorded in a control experiment. It can be seen that the tuning curve stays essentially stable throughout the session.

At the population level, we first analyzed the distribution of the preferred directions. The distribution for the three behavioral epochs is shown in Figure 4. Circular statistics performed to test for the homogeneity of the distribution revealed that the null hypothesis of homogeneity holds for all three epochs (V=1.279, Baseline; V=0.838, Force; V=1.236, Washout, $p>0.15$ in all cases, see Fisher, 1993). We then studied the shifts of Pd across epochs. As a population, the neurons showed a shift of Pd in the direction of the applied force field in the Force epoch compared to the Baseline (average change of Pd = 16.2 deg., std. dev. = 26 deg., $p<10^{-6}$, Figure 5A). As the monkey continued in the Washout epoch, the Pd shifted in the opposite direction (14.3 deg., std.

dev. = 32 deg., $p<0.0003$), such that there was no net change of Pd between the Washout and the Baseline ($p=0.9$). The fact that the changes of Pd between the Washout and the Baseline essentially averaged to zero reflects the presence of the two classes of memory cells. Furthermore, at the population level, the neuronal shifts of Pd across epochs matched the shifts of Pd recorded for single muscles (see next section).

We also studied the differences of average firing frequency (Avf) between the Force epoch and the Baseline for the neuronal population (Figure 5B). The Avf increased in the Force epoch compared to the Baseline, and the average increase was 19% (std. dev. = 65%, $p<0.001$). The Avf increased again by 12% (std. dev. = 51%, $p<0.004$) in the Washout, compared to the Force epoch.

Finally, we analyzed the changes of tuning width (Tw) across epochs. As a population, neurons did not show any significant change of Tw in the Force epoch or in the Washout (Figure 5C).

Figure 6 shows, for each parameter, the change in the Force epoch compared to the Baseline versus that in the Washout compared to the Force epoch. All neurons are shown and color-coded according to their category. Consider first the three plots 6Aa, 6Bb and 6Cc (diagonal plots), referring to the changes of Pd, Avf and Tw respectively. The kinematic cells (black) show no significant change in either x or y measures, and lie close to the origin of the axes. The dynamic cells (blue) show changes on both axes but in opposite directions, and thus lie on the diagonal crossing the second and fourth quadrant. The Class I memory cells (green) display modulation in the x but not in the y measure and therefore lie close to the x-axis. The Class II memory cells (red), displaying a modulation in the y but not in the x measure, lie on the y-axis. Note that there do not appear to be clear-cut boundaries between the different categories of neurons, which were classified according to statistical measures. The percentages of cells in each category, for the three parameters studied, are reported in Table 1.

The other, off-diagonal, plots of Figure 6 illustrate the relations between changes of different parameters. Consider for instance plot 6Ab. The position of each cell in the plot refers to the changes of Pd (axes: Pd), while the color refers to the changes of Avf (color: Avf). The conventions for colors are the same as in the diagonal plots. It can be seen that, unlike in the diagonal plots, there is no systematic relationship between the color and the position on the axes. In other words, the classifications performed according to the Pd and the Avf appear to be independent. The same conclusion holds when considering plot 6Ba, where the position on the axes refers to the changes of Avf (axes: Avf) and the color refers to the changes of Pd (color: Pd). The remaining plots illustrate the relations between changes of Pd and changes of Tw (plots 6Ac, 6Ca) and between changes of Avf and changes of Tw (plots 6Bc, 6Cb). Again, the classifications based upon different parameters do not appear to be directly related.

Finally, when multiple parameters were considered at the same time, most neurons showed some change across epochs (61/64 considering Pd and Avf; 21/25 considering Pd and Tw; 24/25 considering Avf and Tw; 25/25 considering Pd, Avf and Tw).

Electromyographic activity: theoretical predictions and experimental results

The Electromyographic activity (EMG) was rectified and integrated over the same movement-related time window used for cells (from 200 msec before movement onset up

to the end of movement). We represented the activity of each muscle with a tuning curve and defined a preferred direction. The curl fields used in the adaptation paradigm provided an isotropic (rotation-invariant) perturbation, in that the external force was always orthogonal to the movement for all eight directions. This choice imposed a constraint on the change in muscle activity following adaptation to the force field (Figure 1D). Briefly, when monkeys performed in the Force epoch, the external force summed with the force exerted by the muscles on the hand. As a result, the preferred direction of the muscles rotated in the direction of the external force field. Because the perturbation was isotropic, the rotation occurred for all muscles in the same direction -- clockwise or counterclockwise depending on the force field used -- irrespective of their initial preferred direction[2].

These predictions were experimentally confirmed. For muscles, the directional tuning of the EMG activity changed in the direction of the applied force in the Force epoch and returned to the baseline in the Washout epoch. Figure 7 shows the EMG data collected from four muscles recorded with a clockwise force field. The data are plotted separately for each muscle sampled and for each behavioral epoch. We observed that the preferred direction of all four muscles rotated in the direction of the force in the Force epoch, and rotated back in the Washout. On average, the Pd of muscles shifted by 18.8 degrees (median 21.4 deg) in the Force epoch compared to the Baseline, and shifted back by -21.7 degrees (median -21.7 deg) in the Washout compared to the Force epoch. The classification of muscles is reported in Table 2.

Discussion

Single cell plasticity and population changes in the primary motor cortex

If the primary motor cortex ultimately controls the movement through its projections to the sub-cortical structures and the spinal cord, then its overall output should be the same in the Washout and in the Baseline. In other words, in order to subserve the function of *motor performance*, the neuronal population of M1 must transmit analogous commands before and after the adaptation experience. On the other hand, this and other studies provide evidence for neural plasticity in M1 associated with motor learning. In the present study, we show that plastic changes in memory cells outlast the exposure to the force field, reflecting the development of an internal model. These findings suggest that M1 is also involved in *motor learning*. But how can these two functions, of motor performance and motor learning, be achieved by the same neuronal population? Two findings reported here are relevant to this issue. First, two classes of memory cells were found. With regard to the change of preferred direction, these two classes balanced each other in the Washout. Second, when the entire neuronal population was considered, the changes of preferred direction matched the changes observed for muscles. Taken together, these findings suggest that while single neurons change their activity when a new internal model is developed (motor learning), the entire neuronal population reorganizes itself to transmit a signal appropriate for the behavioral goal (motor performance).

The curl force fields used in this experiment imposed a constraint on the effects of adaptation on muscular activity. In accord with the predictions illustrated in Figure 1D,

[2] See the appendix to the thesis for a mathematical formulation of this argument.

the preferred direction (Pd) of muscles rotated in the direction of the external force in the Force epoch and rotated back in the Washout epoch. Incidentally, this confirms previous results from a study on humans performing an identical learning task (Thoroughman and Shadmehr, 1999). For neurons, we found several classes of cells, including memory cells that have different Pd in the Washout compared to the Baseline. Thus, *single cells* did not simply reflect the changes of muscle activity. The *neuronal population*, however, matched the changes observed for muscles. As a population, the Pd of neurons shifted in the direction of the applied force in the Force epoch and shifted back in the opposite direction in the Washout epoch. The magnitude of the Pd shift of the neuronal population (16.2 deg Force-Baseline; -14.3 deg Washout-Force) was smaller, though comparable, to that observed for muscles (18.8 deg Force-Baseline; -21.7 deg Washout-Force).

The match between the neuronal population and the muscle activity could be accounted for by the presence of both Class I and Class II memory cells. On the one hand, Class I memory cells (*x-y-y*) typically shifted their Pd in the direction of the force field in the Force epoch and retained this shift in the Washout epoch. On the other hand, Class II memory cells (*x-x-y*) did not change their Pd in the Force epoch. Their Pd, however, shifted in the Washout epoch in the direction *opposite* to the previous force field. In the Washout epoch, the shifts of Pd of the Class I and Class II memory cells balanced each other. As a result, for the neuronal population, the changes of Pd between the Washout and the Baseline essentially averaged to zero. Notably, the percentages of the Class I and Class II memory cells were similar (19% versus 22%).

In our interpretation, Class I and Class II memory cells are complementary correlates of motor performance and motor learning. After re-adaptation in the non-perturbed condition (Washout), the neuronal population returns to a state statistically indistinguishable from the initial state (Baseline). Correspondingly, the motor performance, as dictated by the activity of the neuronal population, assumes similar values in terms of both the kinematics and the dynamics of movements. At the single cell level, however, the activity of neurons after re-adaptation still reflects the previous adaptation to the force field. Such plasticity parallels the development of an internal model of the dynamic environment.

Neuronal plasticity and short- versus long-term motor learning

In the present study, we used the correlation coefficient (CC) as an indicator of behavioral performance. From a psychophysical standpoint, the observation of the CC revealed several stages of motor learning. First, within each session the CC increased across trials in the Force epoch, as illustrated in Figure 2A. We refer to this stage as motor adaptation, or short-term learning. Second, we computed the mean CC in the Force epoch for each session (i.e. for each day) and studied its trend across sessions. The mean CC increased, and reached a plateau within 15-25 sessions in the same force field (data not shown). Third, for both monkeys, the mean CC reached a plateau within fewer sessions for the second force field than for the first force field (6-8 days for the second field versus 15-25 days for the first field) (Padoa-Schioppa et al., 1998). We refer to these last two stages as long-term learning. Interestingly, these stages closely parallel those obtained in previous reports on the learning of motor sequences (Hikosaka et al., 2000).

The present study investigated the neural correlates of motor adaptation. Independently of its significance for long-term learning, the neuronal plasticity observed

here occurred within a single session. In this respect, it should be more precisely referred to as short-term plasticity. Previous studies have demonstrated that individual neurons can reflect the acquisition of a conditioned response within several minutes of sensorimotor associations (Mitz et al., 1991; Aosaki et al., 1994; Chen and Wise, 1995; Wise et al., 1998). A recent experiment revealed neuronal activity underlying rapid motor adaptation in the superior colliculus, concordant with progressively shorter reaction times (Dorris et al., 2000). Overall, a growing body of evidence supports the idea that neuronal plasticity can occur over a very short period of time. Mechanisms previously proposed in a number of studies, such as the unmasking of pre-existing horizontal synaptic connections, could account for the plasticity observed here together with its time scale (Donoghue, 1995; Hess et al., 1996; Dinse et al., 1997; Huntley, 1997; Laubach et al., 2000).

The data reported here were collected starting from the first day the monkeys were exposed to the force fields, up to sessions well within the long-term learning plateau. Different classes of cells, including memory cells, were recorded in all phases of the long-term learning curve, and sometimes in the same session. Although we cannot conclude from the present data that the neuronal plasticity observed here is directly related to long-term motor learning, the fact that the neurons exhibiting plasticity were found in the behavioral plateau remains intriguing. Indeed, some indication suggests that the monkeys' behavior was not completely stationary even when the mean CC had reached the plateau. After completion of the present study, one of the monkeys was used for a follow-up experiment where the two force fields were presented within the same session (DiLorenzo, 1999). In that experiment, the results of which will be presented elsewhere, the monkey underwent the following sequence of epochs: Baseline, Force A, Washout, Force B, Washout, Force A, Washout. Force fields A and B were the same clockwise and counterclockwise force fields used here, with the order of presentation counterbalanced across sessions. Although the monkey was already familiar with both force fields, we observed that the performance in the second force field was generally worse than the performance in the first force field. In other words, the mean CC in the second force field was lower, independent of which force field was presented first (clockwise or counterclockwise). This interference would not be expected had the monkey learned both force fields so well that their corresponding internal models could be switched on and off at "no cost." Instead, this observation suggests that even in the plateau region of the long-term learning the monkeys were still completing the development of the internal models for the force fields.

In the interpretation proposed, the neuronal plasticity reflects the development of an internal model of the movement dynamics. A distinct and complementary interpretation can also be considered. The changes of the tuning curves outlasting the dynamic adaptation might reflect the temporal "non-stationarity" of the cortex. In an always-changing environment, the nervous system constantly reorganizes itself to meet its needs. In the motor areas of the cerebral cortex, the reorganization occurs to accomplish the desired motor acts. While subsequent changes overwrite each other, any time the nervous system encounters a new environment a sub-population of neurons modify the activity to accommodate the new conditions. In this view, our observations are the fingerprints of a continuous reorganization of the nervous system, suggesting that neuronal plasticity is the rule rather than an exception.

Kinematic versus "load" modulation of M1 neurons

Consistent with previous experiments, the present results provide evidence that the movement-related neuronal activity in primary motor cortex can be modulated by loads. Earlier work demonstrated that the discharge of many motor cortical cells varies with muscle activity (Evarts, 1968; Humphrey et al., 1970; Thach, 1978; Cheney and Fetz, 1980; Fromm, 1983). Neuronal activity increased when the monkey moved against an opposing load, and decreased when the load facilitated the movements. More recently, the responses of motor cortical neurons were systematically examined in monkeys performing center-out planar movements, compensating for a load that pulled the arm in eight different directions (Kalaska et al., 1989). The clockwise and counterclockwise curl forces used in our experiment imposed a load whose direction was always orthogonal to the direction of movement. The modulations of neuronal activity we obtained were therefore not readily comparable to those obtained by Kalaska and colleagues. A close examination of Figure 6 of that study, however, reveals that the preferred direction of that M1 neuron rotates in the direction of the force, similar to what we observed in the present work.

Though of a smaller proportion, we also found neurons that appeared to encode the direction of movement independently of changes in muscle activity. The percentage of kinematic cells obtained in the current study (9-34%, depending on the parameter) is smaller than the 41% obtained in a study in which the direction of movement and muscle activity was dissociated using opposing and assisting torque load (Crutcher and Alexander, 1990), though comparable to that documented in other studies (Kalaska et al., 1989; Scott and Kalaska, 1997). More recently, in a behavioral task dissociating muscle activity, direction of joint movement and direction of movement in space, it was demonstrated that muscle-like neuronal activity and activity that reflected the direction of joint movement in space coexisted in M1 (Kakei et al., 1999). The authors suggested that both "muscles" (28/88 neurons) and "movements" (44/88 neurons) are represented in the primary motor cortex. These results, together with those obtained in other studies (Georgopoulos et al., 1992; Shen and Alexander, 1997; Zhang et al., 1997), suggested that M1 harbors dynamic processes that translate stimulus representation into motor outputs.

In our statistical analysis, the kinematic category was always the null hypothesis. In other words, we classified cells based on *changes* of their parameters, and we included them in the class of kinematic cells if no changes were observed. Thus, no strong claims can be made regarding the functional role of kinematic cells. Furthermore, when multiple parameters were considered at the same time, the large majority of neurons showed some change across epochs. On the other hand, our task provided a strong constraint on the activity of muscles, namely a shift of the preferred direction. Indeed, the argument based on the vectorial summation of the force exerted by muscles and the force exerted by the manipulandum (illustrated in Figure 1D) would predict that the shift of preferred direction occurs for *any* muscle directionally tuned in the task. It is thus surprising that a relatively large population of cells does not show any shift of preferred direction across epochs (kinematic cells, 34%). In this regard, it is also noteworthy that in the present study the monkeys were not only switching between different dynamic environments, but were also learning a new force field. The kinematic cells were thus not only non-

correlated with the dynamics of the movements, but also "resistant" to a motor learning experience.

Changes of Average firing frequency

Changes of neuronal activity across behavioral epochs occurred in the preferred direction (Pd), the average firing frequency (Avf) and the tuning width (Tw). At the population level, we noted a general increase of the Avf as the monkey performed across the three behavioral epochs. The fact that the Avf continued to increase in the Washout suggests that factors other than the load imposed by the external force should be considered. One possibility is that this increase is related to the adaptation process, similar to the shift of Pd. An alternative explanation, however, is that the monkeys became fatigued as they continued the task, such that more cortical output was required to generate muscle contractions adequate for movement. In a study in which the activity of motor cortex neurons was recorded in monkeys trained to perform self-paced isometric contractions, 50% (13/26) of the neurons increased and 31% (8/26) decreased in discharge frequency during muscle fatigue (Belhaj-Saif et al., 1996). Therefore, we cannot rule out the possibility that the change of Avf observed in the current study reflects, at least in part, fatigue of the cortico-motor circuitry.

Movement speed

It has been proposed that the activity of M1 reflects movement speed (Moran and Schwartz, 1999). In the following, we explicitly address the issue of whether speed fluctuations can explain our observations and we conclude that they cannot.

Because the trajectories were essentially straight in all three epochs, we referred to a modified version of the model of Moran and Schwartz: $m(\vartheta) = v(\vartheta)\cos(\vartheta - \phi)$, where $m(\vartheta)$ was the firing rate of the cell and $v(\vartheta)$ was the speed. Thus, the tuning curve of cells was the product of a spatial, cosine-shaped, tuning curve and a speed tuning curve $v(\vartheta)$. For each day, we computed the speed tuning curve in the three epochs. The speed profile was integrated from the movement onset to the end of movement, and the tuning curves were computed as was done for neurons.

To test for uniformity of distribution across directions, we first combined all the days, separately for the two force fields. We obtained six speed tuning curves (3 epochs x 2 force fields), none of which was significantly non-uniform (all $pR>0.40$, Rayleigh test). Thus, the hypothesis that changes of neuronal Pd correlate with changes of speed can be rejected. Furthermore, it can be shown that, independently of the shape of $v(\vartheta)$, the homogeneous distribution of neuronal preferred directions in all three epochs is sufficient to exclude this hypothesis. We also performed a correlation analysis on a cell-by-cell basis. For each cell, we computed the corresponding speed tuning curve $v(\vartheta)$ and its Pd. Then we studied the correlation between changes of neuronal Pd and changes of the corresponding speed Pd, separately for each pair of epochs (Force-Baseline, Washout-Force and Washout-Baseline). For a cell to participate in this analysis, we imposed the conditions of directional non-uniformity on both the neuronal and the speed tuning curves (condition $pR<0.05$, Rayleigh test). When defined, the changes of speed Pd were essentially at random. Consistently, none of the three correlation was significant (all $r^2<2\%$). We conclude that changes of neuronal Pd do not correlate with fluctuations of speed.

To test for changes of average speed across epochs, we first combined the data of both monkeys and both force fields (91 days total). We found no changes in the Force compared to the Baseline (mean=2%, p=0.13), and a modest increase in the Washout compared to the Force (mean=5%, p=0.03). We then investigated on a cell-by-cell basis whether the change in neuronal Avf correlated with speed fluctuations. For each pair of epochs, we computed the correlation between the changes of neuronal Avf and the changes of average speed. None of these were significant (all r^2<14%). We conclude that the changes of neuronal Avf do not correlate with fluctuations of speed.

As no instance satisfied both the conditions of directional non-uniformity and unimodality for both the neuronal and the speed tuning curve, the correlation could not be studied for the Tw.

Taken together, these results confirm that the kinematics were essentially constant throughout the task and that changes of neuronal activity across epochs reflect the change of movement dynamics and the adaptation to the force field.

Conclusions

In conclusion, we presented a paradigm that dissociates movement kinematics from movement dynamics and motor performance from the effects of motor adaptation. By choosing a specific, rotation invariant, dynamic perturbation we were able to make stringent predictions on the effects of the perturbation on muscle activity. We then used the muscles as a framework to interpret the neuronal activity recorded from M1. We presented evidence of neuronal plasticity associated with dynamic adaptation and development of a new internal model. In response to the changing dynamics of the environment, neurons changed their firing rate and spatial tuning properties. Plastic changes outlasted the exposure to the perturbation. Remarkably, changes of neuronal activity across behavioral conditions combined in a way adequate to support both functions of motor performance and motor learning.

Methods

Behavioral task

Two adult male macaque monkeys (*Macaca nemestrina*) were used in the experiment. Both monkeys performed with their right arm. The monkeys held a two-link low-friction manipulandum and performed the reaching task in an electrically isolated enclosure (Figure 1A). Two torque motors at the base of the manipulandum could apply perturbing force field upon the hand of the monkey. The monkeys forearm was positioned approximately parallel to the ground and the monkeys could move their arm freely during the task. Movements were confined to the horizontal plane. A computer monitor, situated 75 cm in front of the monkey and slightly below eye level, displayed the targets of the movement and a cursor representing the position of the manipulandum handle. The center square and peripheral targets were represented by squares of 14 by 14 mm (corresponding to ca 1 degree of visual angle) and the cursor by a square of 3 by 3 mm (ca 0.2 degree of visual angle).

The behavioral paradigm was a delayed, visually guided, reaching task (Figure 1B). A center square appeared in the center of the monitor before the beginning of each trial. The monkeys moved the cursor into the center square to initiate the trial. After

1,000 msec, a peripheral target appeared randomly at one of eight locations evenly spaced in a circle corresponding to 10 cm of actual distance in the center-out movement. The monkeys held the cursor within the center square for a variable period of 800 to 1,200 msec after the appearance of the peripheral target. The center square was then extinguished (the "GO" signal). The monkeys had to move and acquire the peripheral target within 1,200 msec after the "GO" signal appeared and remain within the peripheral target for another 1,000 msec to complete the task and receive a juice reward. During the movement, the trajectory had to be confined to an area subtended by an angle of 60 deg on both sides of the line connecting the center square and the peripheral target. Such a large spatial window was used to accommodate the possible perturbations of movements. The same time constraints and spatial windows were used for the three behavioral epochs. The trial was terminated if the monkeys made a mistake at any time during the task, and a new trial was initiated after a randomly selected inter-trial interval of 1 to 2 seconds.

In each session, the monkeys performed in three behavioral epochs (Baseline – no force; Force epoch – force field; Washout – no force), each with approximately 160 successful trials. The force fields used in the current experiments were vector fields **F=BV**, where **B** is a constant viscosity matrix and **V** is the instantaneous hand velocity vector in Cartesian coordinates (Shadmehr and Mussa-Ivaldi, 1994). For **B,** we chose an anti-diagonal rotation matrix [0 b; -b 0] that defined a viscous, curl force field. The force field was viscous in that the magnitude of the applied forces was proportional to the instantaneous hand speed ($\|\mathbf{V}\|$) and curl in that the force direction was orthogonal to the instantaneous hand velocity (**V**). We chose $b = \pm 0.07$ N sec/m. Depending on the sign, **F** was clockwise (CK, $b>0$) or counterclockwise (CCK, $b<0$).

The monkeys performed at an 80% success rate (in the Baseline epoch), after 4 to 6 months of training on the behavioral task. At no time during training were the monkeys exposed to the force fields used for recordings. Recording sessions using the two force fields were run in blocks, with each block occurring over a period of 1 to 5 months. The CK force field was studied first for both monkeys. The quality of the performance was quantified with a correlation coefficient (CC, see below). In each session, the CC showed an adaptation curve (Figure 2A). Over sessions, the adaptation became faster (shorter ramp) and better (higher asymptote). Monkey B underwent 40 sessions (CK) and 10 sessions (CCK) with the two force fields respectively. The mean CC approximately reached plateau after 25 and 6 sessions respectively. Monkey M underwent 25 sessions (CK) and 16 sessions (CCK) with the two force fields respectively. The mean CC reached plateau after 15 and 8 sessions respectively. During the sessions of the plateau region, the CC reached asymptote and the trajectories became straight within 30 trials in each epoch (Padoa-Schioppa et al, 1998).

Surgery, recording, electrical microstimulation and animal care

After training and under aseptic stereotaxic surgery, we implanted a restraint device on the skull and a recording well (18 mm, inner diameter) over the left primary motor cortex (M1). The location of M1 was verified by magnetic resonance imaging prior to surgery. The monkeys were given antibiotics and pain medications, and were allowed full rest for at least one week following the surgery. The NIH guidelines on the care and use of animals were strictly adhered to throughout the experiment.

Vinyl-coated tungsten electrodes (1-3 MΩ impedance) were used for recordings. Electrodes were advanced initially in the experiment through a hydraulic microdrive with a depth resolution of 1 μm and later by manually rotating a threaded rod carrying the electrode in a set-screw system at an approximate depth resolution of 30 μm (300 μm /turn). Up to three electrodes were used in each session. Electrical signals were passed through a head stage (AI 401, Axon Instruments) and an amplifier (Cyberamp 380, Axon Instruments) and filtered at a high and low cutoff of 10K Hz and 300 Hz, respectively. Action potentials were detected by threshold crossing and waveforms (1.75 msec duration, 25 kHz) were recorded (Experimenter's WorkBench 5.1, DataWave Technology) and digitized for subsequent clustering.

Electrical microstimulation were performed in separate sessions to verify the recording locations. A train of 20 biphasic charge balanced pulse pairs (pulse width=0.1msec, train duration = 60 msec) was delivered at 330 Hz. At most sites, muscle twitches in the shoulder and forearm were elicited with a current magnitude of 20 μ Amp.

We manually implanted teflon-insulated wires into the Pectoralis, Deltoid, Biceps, Triceps and Brachioradialis muscles in separate sessions. The electromyographic (EMG) activity was recorded, rectified, and integrated over the movement-related time window. The response magnitudes were normalized and submitted to the same analyses used for cells. 16 instances of muscles were considered in the final sample (3 Pectoralis, 5 Deltoid, 4 Biceps, 2 Triceps and 2 Brachioradialis).

Both monkeys were euthanized at the end of the experiment. They were given an overdose of pentobarbital sodium and then perfused transcardially with heparinized saline, followed by buffered Formalin. The brain was removed from the skull following standard procedures. Examination of the penetration marks on the surface of the brain revealed that they were primarily concentrated on the anterior bank of the central sulcus, at a location corresponding to the arm area of the primary motor cortex (Figure 8).

Data analysis

The correlation coefficient (CC) was defined as in human studies. Briefly, from each trajectory $(x(t), y(t))$ we extracted the speed profile $\mathbf{v} = (\dot{x}^2(t) + \dot{y}^2(t))^{1/2}$. We then derived an ideal speed profile **u** through an iterative process through all trials in the Baseline. The vectors **v** and **u** were aligned at their maximum and the CC was defined as the normalized covariance of **v** and **u** (see Shadmehr and Mussa-Ivaldi, 1994 for details):

$$CC(\mathbf{v},\mathbf{u}) = \frac{\mathrm{cov}(\mathbf{v},\mathbf{u})}{\sigma(\mathbf{v})\sigma(\mathbf{u})}$$

In essence, the CC quantifies the similarity between the actual and the ideal speed profiles.

Individual neurons recorded from the same electrode were first separated through manual clustering. Only cells whose waveform was convincingly consistent throughout the recordings (as valued by visual inspection) were considered for further analysis.

All the results on the neuronal and muscular activity refer to the same movement-related time period (from 200 msec before the movement onset to the end of the movement). The onset and termination of the movement were defined with a speed threshold criterion (4 cm/sec) during the acceleration and deceleration phase of the movement. In each session, we arbitrarily considered that the monkeys had reached the

steady state region after they had performed four successful trials in each direction of movement. Only the remaining trials were considered for further analysis.

The activity of each neuron was separately analyzed in the Baseline, Force field and Washout epochs. For each epoch and for each direction we considered the mean activity across trials. We obtained three tuning curves and we defined the preferred direction (Pd), average firing rate (Avf) and tuning width (Tw). Pd was as the direction of the vector average of the tuning curve. Avf was the average of the tuning curve. Tw was the angle over which the firing frequency was higher than half the maximum of the tuning curve. The Tw was not defined for multimodal cells, for which the directions with firing frequency higher than half the maximum were non-continuous.

Our analysis focused on cells with Avf>1Hz. Of the 162 neurons considered, 137 neurons satisfied this criterion in all three behavioral epochs. 64 neurons had a significantly non-uniform activity across the eight directions in all three epochs (Rayleigh test. pR<0.05). 25 neurons were unimodal in all three epochs.

The neuronal recordings were carried out over several months. No effort was made to locate the cortical layer of the recording sites. Thus, we cannot ascertain whether the different classes of neurons were segregated in different cortical layers. However, different classes of neurons were recorded in the same locations on the surface and sometimes even from the same electrode (i.e. at the same time).

Because our results rest upon the changes observed in tuning curves, several concerns were considered. In general, since the change of Pd of neurons was consistently in the direction of the perturbing force, random sources of noise can hardly account for the alterations of neuronal activity. In addition, we analyzed only neurons with excellent recording stability, addressing the concern of poor isolation. Finally, monkeys adopted a stable body position and a stereotypical arm configuration while performing the task, suggesting that the changes of neuronal activity did not reflect postural changes (Scott and Kalaska, 1995, 1997; Sergio and Kalaska, 1997).

Statistical analysis of tuning curves

We statistically compare the three parameters (Pd, Avf and Tw) across epochs using the following method. In each epoch, we repeatedly measure the firing rate t_i of the cell for movements in the direction i, and $i=1,...8$. We indicate with $t_i(j)$ the j^{th} measure of t_i, and we have $j = 1...n_i$ and $n_i \approx 20$. t_i is a random variable with expectation value μ_i and finite variance $Var(t_i)$. If μ_i is the expected firing rate of the cell for movements in direction i, a parameter is a function:

$$p=P(\mu_i) \qquad (1)$$

and we want to compare values of p obtained in different epochs. The best estimate we have for μ_i is:

$$m_i = \frac{1}{n_i}\sum_{j=1}^{n_i} t_i(j) \qquad (2)$$

namely the average of many measures of the firing rate t_i. The variance $Var(t_i)$ can be estimated through:

$$Var(t_i) \approx s_i^2 = \frac{1}{n_i - 1}\sum_{j=1}^{n_i}(t_i(j) - m_i)^2 \qquad (3)$$

For high values of n_i ($n_i \approx 20$ in our case), m_i can be safely treated as a Gaussian variable $m_i : N(\mu, \sigma_i^2)$. Furthermore, because a liner combination $f=ax+by+c$ of Gaussian variables $x : N(\mu, \sigma^2)$ and $y : N(\mu, \sigma^2)$ is itself a Gaussian variable with $f : N((a+b)\mu + c, (a^2+b^2)\sigma^2)$ (Devore, 1990, p.212), we have: $\sigma_i^2 = Var(t_i)/n_i$. Thus, we can consider m_i as a measure of μ_i affected by a square error σ_i^2. Note that while the expectation value of s_i^2 is $Var(t_i)$, independent of the number of measures n_i, the expectation value of σ_i^2 is $Var(t_i)/n_i$, a decreasing function of n_i.

The idea of the method is to propagate to the parameter p the error of measure σ_i^2 of μ_i. We develop the parameter $p=P(\mu_i)$ close to μ_i at the first order in $(m_i - \mu_i)$:

$$P(m_i) \approx P(\mu_i) + \sum_i \left.\frac{\partial P}{\partial m_i}\right|_{\mu} (m_i - \mu_i) \qquad (4)$$

This approximation is best for smooth functions $P(m_i)$, and for small values of $|m_i - \mu_i|$. The expectation value of $|m_i - \mu_i|$ is σ_i^2, which is smaller for higher n_i. Following Eq.(4), p is Gaussian, with:

$$p : N\left(P(\mu_i), \sum_i \left(\left.\frac{\partial P}{\partial m_i}\right|_{\mu}\right)^2 \sigma_i^2\right) \equiv N\left(P(\mu_i), \sigma_p^2\right) \qquad (5)$$

We are left with the problem of comparing two Gaussian variables, for which we have the measures of the mean values and the estimates of the variances. This can be done with a conventional z-test.

The cells presented in this paper were classified by running three z-tests. We obtained three p-values for the three pairs of epochs (p_{fb} for Force-Baseline, p_{wf} for Washout-Force, p_{wb} for Washout-Baseline). Cells were classified as kinematic, dynamic, or memory for a given parameter by setting a threshold $\alpha = 0.05$, below which we rejected the null hypothesis. For instance, we classified as dynamic a cell with $p_{fb} < \alpha$, $p_{wf} < \alpha$, $p_{wb} > \alpha$. Analogously, we did for the other categories of cells. We also had some dubious cases, for instance when $p_{fb} < \alpha$, $p_{wf} > \alpha$, $p_{wb} > \alpha$. The first p-value indicates an activity in the Force epoch different to the one in the Baseline, but neither of the differences between Washout-Force and Washout-Baseline is significant. We proceeded in this case according to the lowest p-value, so that we classified the cell as dynamic if $p_{wf} < p_{wb}$, and as memory if $p_{wf} > p_{wb}$.

Acknowledgments

We thank Brian Benda for participating at an early stage of the present work and Dan DiLorenzo for helping us with the EMG recordings. We are also thankful to Matt Tresch,

Andrea d'Avella, Philippe Saltiel and Emanuel Todorov for helpful discussions and to Lori Markson for editing the manuscript. This study was supported by the NIH grant number MN481185.

References

1. Aosaki, T., Tsubokawa, H., Ishida, A., Watanabe, K., Graybiel, A.M., and Kimura, M. (1994) Responses of tonically active neurons in the primate's striatum undergo systematic changes during behavioral sensorimotor conditioning. J. Neurosci. 14, 3969-3984.
2. Balhaj-Saif, A., Fourment, A., and Maton, B. (1996) Adaptation of the precentral cortical command to elbow muscle fatigue. Exp. Brain Res. 111, 405-416.
3. Borsook, D., Becerra, L., Fishman, S., Edwards, A., Jennings, C.L., Stojanovic, M., Rapinicolas, L., Ramachandran, V.S., Gonzalez, R.G., and Breiter, H. (1998) Acute plasticity in the human somatosensory cortex following amputation. Neuroreport 9, 1013-1017.
4. Chen, L.L., and Wise, S.P. (1995) Neuronal activity in the supplementary eye field during acquisition of conditional oculomotor associations. J. Neurophysiol. 73, 1101-1121.
5. Cheney, P.D., and Fetz, E.E. (1980) Functional classes of primate corticomotoneuronal cells and their relation to active force. J. Neurophysiol. 44, 773-791.
6. Classen, J., Liepert, J., Wise, S.P., Hallett, M., and Cohen, L.G. (1998) Rapid plasticity of human cortical movement representation induced by practice. J. Neurophysiol. 79, 1117-1123.
7. Crutcher, M.D., and Alexander, G.E. (1990) Movement-related neuronal activity selectively coding either direction or muscle pattern in three motor areas of the monkey. J. Neurophysiol. 64, 151-163.
8. Devore, J.L. (1990) Probability and statistics for engineering and sciences (Brooks/Cole, Pacific Grove CA).
9. DiLorenzo, D.J. (1999). Correlates of motor performance in the primary motor cortex. MIT Ph.D. Thesis.
10. Dinse, H.R., Godde, B., Hilger, T., Haupt, S.S., Spengler, F., and Zepka, R. (1997) Short-term functional plasticity of cortical and thalamic sensory representations and its implication for information processing. Adv. Neurol. 73, 159-178.
11. Donoghue, J.P. (1995) Plasticity of adult sensorimotor representations. Curr. Opinion Neurobiol. 5, 749-754.
12. Dorris, M.C., Pare, M., and Munoz, D.P. (2000) Immediate neural plasticity shapes motor performance. J. Neurosci. 0:RC52, 1-5.
13. Elbert, T., Pantev, C., Wienbruch, C., Rockstroh, B., and Taub, E. (1995) Increased cortical representation of the fingers of the left hand in string players. Science 270, 305-307.
14. Evarts, E.V. (1968) Relation of pyramidal tract activity to force exerted during voluntary movement. J. Neurophysiol. 31, 14-27.
15. Faggin, B.M. Nguyen, K.T., and Nicolelis, M.A. (1997) Immediate and simultaneous sensory reorganization at cortical and subcortical levels of the somatosensory system. Proc. Natl. Acad. Sci. (USA) 94, 9428-9433.
16. Fisher, N.I. (1993). Statistical Analysis of Circular Data (Cambridge University Press).

17. Florence, S.L., and Kaas, J.H. (1995) Large-scale reorganization at multiple levels of the somatosensory pathway follows therapeutic amputation of the hand in monkeys. J. Neurosci. 15, 8083-8095.
18. Fromm, C. (1983) Changes of steady state activity in motor cortex consistent with the length-tension relation of muscle. Pfluegers Arch. 398, 318-323.
19. Gandolfo, F., Li, C.-S.R., Benda, B. Padoa-Schioppa, C., and Bizzi, E. (2000) Cortical correlates of motor learning in monkeys adapting to a new dynamic environment. Proc. Natl. Acad. Sci. (USA) 97, 2259-2263.
20. Georgopoulos, A.P., Ashe, J., Smyrnis, N., and Taira, M. (1992) The motor cortex and the coding of force. Science 256, 1692-1695.
21. Hess, G., Aizenman, C.D., and Donoghue, J.P. (1996) Conditions for the induction of long-term potentiation in layer II/III horizontal connections of the rat motor cortex. J. Neurophysiol. 75, 1765-1778.
22. Hikosaka, O., Sakai, K., Nakahara, H., Lu, X., Miyachi, S., Nakamura, K., and Rand, M.K. (2000). Neural mechanisms for learning of sequential procedures. In the New Cognitive Neurosciences, M.S Gazzaniga, ed. (MIT press, Cambridge MA), pp 553-572.
23. Humphrey, D.R., Schmidt, E.M., and Thompson, W.D. (1970) Predicting measures of motor performance from multiple cortical spike trains. Science 179, 758-762.
24. Huntley, G.W. (1997) Correlation between patterns of horizontal connectivity and the extend of short-term representational plasticity in rat motor cortex. Cereb. Cortex 7, 143-56.
25. Kakei, S., Hoffman, D.S., and Strick, P.L. (1999) Muscle and movement representations in the primary motor cortex. Science 285, 2136-2139.
26. Kalaska, J.F., Cohen, D.A.D., Hyde, M.L., and Prud'homme, M. (1989) A comparison of movement direction-related versus load direction-related activity in primate motor cortex, using a two-dimensional reaching task. J. Neurosci. 9, 2080-2102.
27. Karni, A., Meyer, G., Jezzard, P., Adams, M.M., Turner, R., and Ungerleider, L.G. (1995) Functional MRI evidence for adult motor cortex plasticity during motor skill learning. Nature 377, 155-158.
28. Laubach, M., Wessberg, J., and Nicolelis, M.A. (2000) Cortical ensemble activity increasingly predicts behaviour outcomes during learning of a motor task. Nature 40: 567-571.
29. Manger, P.R., Woods, T.M., and Jones, E.G. (1996) Plasticity of the somatosensory cortical map in macaque monkeys after chronic partial amputation of a digit. Proc. Royal Soc. London (B) 263, 933-939.
30. Mitz, A.R., Godschalk, M., and Wise, S.P. (1991) Learning-dependent neuronal activity in the premotor cortex: activity during the acquisition of conditional motor associations. J. Neurosci. 11, 1855-1872.
31. Moran, D.W., and Schwartz, A.B. (1999) Motor cortical representation of speed and direction during reaching. J. Neurophysiol. 82:2676-2692.
32. Nakamura, K., Sakai, K., and Hikosaka, O. (1998) Neuronal activity in medial frontal cortex during learning of sequential procedures. J. Neurophysiol. 80, 2671-2687.

33. Nudo, R.J., Milliken, G.W., Jenkins, W.M., and Merzenich, M.M. (1996) Use-dependent alterations of movement representations in primary motor cortex of adult squirrel monkeys. J. Neurosci. 16:785-807.
34. Padoa-Schioppa, C., Sadr, J., Li, C.-S. R., Benda, B., DiLorenzo, D., Gandolfo, F., and Bizzi, E. (1998) Psychophysical correlates of long-term force-field adaptation and motor memory consolidation in monkey. Soc. Neurosci. Abstr. 24: 406.
35. Pascual-Leone, A., Grafman, J., and Hallett, M. (1994) Modulation of cortical motor output maps during development of implicit and explicit knowledge. Science 263, 1287-1289.
36. Recanzone, G.H., Schreiner, C.E., and Merzenich, M.M. (1993) Plasticity in the frequency representation of primary auditory cortex following discrimination training in adult owl monkeys. J. Neurosci. 13, 87-103.
37. Sakai, K., and Miyashita, Y. (1991) Neural organization for the long-term memory of paired associates. Nature 354, 152-155.
38. Scott, S.H., and Kalaska, J.F. (1995) Changes in motor cortex activity during reaching movements with similar hand paths but different arm postures. J. Neurophysiol. 73, 2563-2567.
39. Scott, S.H., and Kalaska, J.F. (1997) Reaching movements with similar hand paths but different arm orientations. I. Activity of individual cells in motor cortex. J. Neurophysiol. 77, 826-852.
40. Sergio, L.E., and Kalaska, J.F. (1997) Systematic changes in directional tuning of motor cortex cell activity with hand location in the workspace during generation of static isometric forces in constant spatial directions. J. Neurophysiol. 78, 1170-1174.
41. Shadmehr, R., and Mussa-Ivaldi, F.A. (1994) Adaptive representation of dynamics during learning of a motor task. J. Neurosci. 14, 3208-3224.
42. Shen, L., and Alexander, G.E. (1997) Neural correlates of a spatial sensory-to-motor transformation in primary motor cortex. J. Neurophysiol. 77, 1171-1194.
43. Thach, W.T. (1978) Correlation of neural discharge with pattern and force of muscular activity, joint position, and direction of intended next movement in motor cortex and cerebellum. J. Neurophysiol. 41, 654-676.
44. Thoroughman, K.A., and Shadmehr, R. (1999) Electromyographic correlates of learning an internal model of reaching movements. J. Neurosci. 19, 8573-8588.
45. Wise, S.P., Moody, S.L., Blomstrom, K.J., and Mitz, A.R. (1998) Changes in motor cortical activity during visuomotor adaptation. Exp Brain Res. 121: 285-299.
46. Xerri, C., Merzenich, M.M., Peterson, B.E., and Jenkins, W. (1998) Plasticity of primary somatosensory cortex paralleling sensorimotor skill recovery from stroke in adult monkeys. J. Neurophysiol. 79, 2119-2148.
47. Zhang, J., Riehle, A., Requin, J., and Kornblum, S. (1997) Dynamics of single neuron activity in monkey primary motor cortex related to sensorimotor transformation. J. Neurosci. 17, 2227-2246.

Figure legends

Figure 1. *The experimental setup and the behavioral paradigm.* **A**. The monkey held a two-link low-friction manipulandum. Two torque motors mounted at the base of the manipulandum and connected independently to each joint enabled specific forces to be applied. **B**. The trial structure of the delayed, visually instructed, reaching task (see text). **C**. The clockwise curl force field used in the experiment is plotted in velocity space. The direction of the perturbing force is orthogonal to the hand velocity and the magnitude proportional to the hand speed. **D**. Predictions of change in the preferred direction (Pd) of muscles' EMG during exposure to a curl field. In the absence of external forces (Left), only muscles (green) exert a force upon the hand of the monkey. When a clockwise force field is introduced (Right), two forces are present: the force exerted by the muscles (green) and the force exerted by the manipulandum (red). The vector sum of these two forces gives a resultant force (blue) pointing in a direction shifted clockwise. The Pd of each muscle, represented in real space, shifts in the Force epoch compared to the Baseline. For all muscles this shift occurs in the same direction, namely the direction of the external force. When the force is turned off, the Pd of each muscle returns to its original value.

Figure 2. *Correlation coefficient and movement trajectories in the three behavioral epochs.* **A.** The correlation coefficient (CC) was close to 1 in the Baseline (performance close to ideal). In the Force epoch, the CC dropped abruptly and gradually recovered, reaching a steady state. In the Washout the CC briefly decreased again (aftereffect), and then quickly returned to the original levels. **B.** Trajectories recorded in the same day. Note that the deviations observed in the aftereffect mirror the early effects of the force field.

Figure 3. *Examples of cells.* The tuning curves are plotted in polar coordinates. For each cell, the three plots represent the movement-related activity in the Baseline (left), in the Force epoch (center), and in the Washout (right). In each plot, the circle in dashed line represents the average activity during the center hold time window, when the monkey holds the manipulandum inside the center square and waits for instructions. **A**, **B**, **C** and **D** are examples of kinematic (*x-x-x*), dynamic (*x-y-x*), memory I (*x-y-y*), and memory II (*x-x-y*) cells, in terms of the modulation of the Pd. A neuron could display modulation in more than one parameter. For instance, the neuron shown in **B** has dynamic property both in terms of the Pd and the Tw, and **E** shows a neuron that has memory property both in terms of the Avf and the Pd. **F** shows a neuron collected in a control experiment, in which no force field was used. The Pd remained unchanged across the three arbitrarily divided behavioral epochs, each consisting of 200 successful trials. All cells **A-E** were recorded with a clockwise force field. Cells **A-C** are from monkey B, cells **D-F** are from monkey M. All plots are normalized to the maximal activity across the three epochs. The labels on the left refer to the changes of Pd.

Figure 4. *Distribution of preferred directions.* Each line represents the Pd of a single neuron. Circular statistics showed that the distribution is homogeneous across directions in all three epochs (see text).

Figure 5. *Histograms.* Changes in the preferred direction (**A**), average firing frequency (**B**), and tuning width (**C**) for the activity of M1 neurons as a population during the movement-related time period in the force adaptation task. The arrows in (**A**) indicate the direction of the force field. The preferred directions are "flipped" for cells recorded with the CK force field. The plots in the first column represent the difference between the Force and Baseline epochs, the second column the difference between the Washout and Force epochs, and the third column the difference between the Washout and Baseline epochs. The vertical axis represents the number of cells. In each plot, M is the median of the histogram, m is the mean of the histogram, and p is the *p*-value obtained from a *t*-test (circular *t*-test for Pd and Tw).

Figure 6. *Scatter plots.*
Diagonal plots. Cells were separately classified according to the changes of Pd (**Aa**, top left), the changes of Avf (**Bb**, center), and the changes of Tw (**Cc**, bottom right). In each plot, the x-axis represents the change in the measure in the Force epoch compared to the Baseline, and the y-axis represents the change in the Washout compared to the Force epoch. The kinematic cells (black) do not show any significant change either for the x or the y measure, and are close to the origin. The dynamic cells (blue) show a change in the Force epoch compared to the Baseline, and the opposite effect in the Washout compared to the Force epoch. These cells lie on the diagonal over the second and fourth quadrant. The "*x-y-y*" cells (or memory I cells) are represented in green. These cells show a significant change between the Force epoch and the Baseline, but not between the Washout and the Force epoch. Thus, they lie on the x-axis. The "*x-x-y*" cells (or memory II cells) are represented in red and lie on the y-axis. The "*x-y-z*" cells are represented in gray. The arrows in **Aa** indicate the direction of the force field. The two monkeys (B and M) and the two force fields, clockwise (CK) and counterclockwise (CCK), are represented by the symbols: circles (B, CK), squares (B, CCK), triangles (M, CK), and diamonds (M, CCK).
Off-diagonal plots. The off-diagonal plots compare the classification of cells based upon different parameters. For each neuron, the position on the axes represents the changes of one parameter (axes), while the color represents the category based upon a different parameter (color). The conventions for colors are the same as for the diagonal plots. **Ab** (top center): the axes refer to the changes of Pd (axes: Pd), while the colors refer to the changes of Avf (color: Avf). The neurons shown in plot Ab are the same neurons shown in plot Aa. However, in plot Ab there is no systematic relationship between the position and the colors. In other words, there is no consistent correspondence between the classification based upon the two parameters Pd and Avf. **Ba** (center left) further testifies the independence between the changes of Avf (axes: Avf) and the changes of Pd (color: Pd). Note that of the 137 neurons shown in plot Bb, only 64 are present in plot Ba; these 64 are the neurons that were significantly tuned in all three epochs and that could be classified according to the Pd. **Ac** (axes: Pd; color: Tw) and **Ca** (axes: Tw, color: Pd) illustrate the relations between the changes of Pd and the changes of Tw. **Bc** (axes: Avf; color: Tw) and **Cb** (axes: Tw, color: Avf) illustrate the relations between the changes of Avf and the changes of Tw. Only the 25 neurons that could be classified according to the Tw are shown in plots Ac, Ca, Bc, Cb.

Figure 7. *Muscles EMG.* EMG activity recorded with a clockwise (CK) force field. The EMG activity was rectified and integrated over the same movement-related time window used for cells. For each muscle, the Pd shifts in the CK direction in the Force epoch, and in the CCK direction in the Washout.

Figure 8. *Gross histology.* Reconstruction of the recording sites on the surface of the brain for the two monkeys. The circles illustrate the number of cells recorded from the corresponding coordinates. CS central sulcus, AS arcuate sulcus, PS principal sulcus.

Tables

Table 1: Classification of cells recorded in the force field adaptation task.

	Preferred Direction	Average Firing Rate	Tuning Width
Kinematic (*x-x-x*)	22 (34%)	13 (9%)	7 (28%)
Dynamic (*x-y-x*)	14 (22%)	18 (13%)	3 (12%)
Memory I (*x-y-y*)	12 (19%)	29 (21%)	5 (20%)
Memory II (*x-x-y*)	14 (22%)	22 (16%)	5 (20%)
Other (*x-y-z*)	2 (3%)	55 (40%)	5 (20%)
Total	64 (100%)	137 (100%)	25 (100%)

Table 2. Muscles.

	Preferred Direction	Average Firing Rate	Tuning Width
Kinematic (*x-x-x*)	2 (17%)	4 (25%)	3 (30%)
Dynamic (*x-y-x*)	6 (50%)	2 (13%)	4 (40%)
Memory I (*x-y-y*)	1 (8%)	5 (31%)	2 (20%)
Memory II (*x-x-y*)	0	2 (13%)	0
Other (*x-y-z*)	3 (25%)	3 (19%)	1 (10%)
Total	12 (100%)	16 (100%)	10 (100%)

Figures

Figure 1

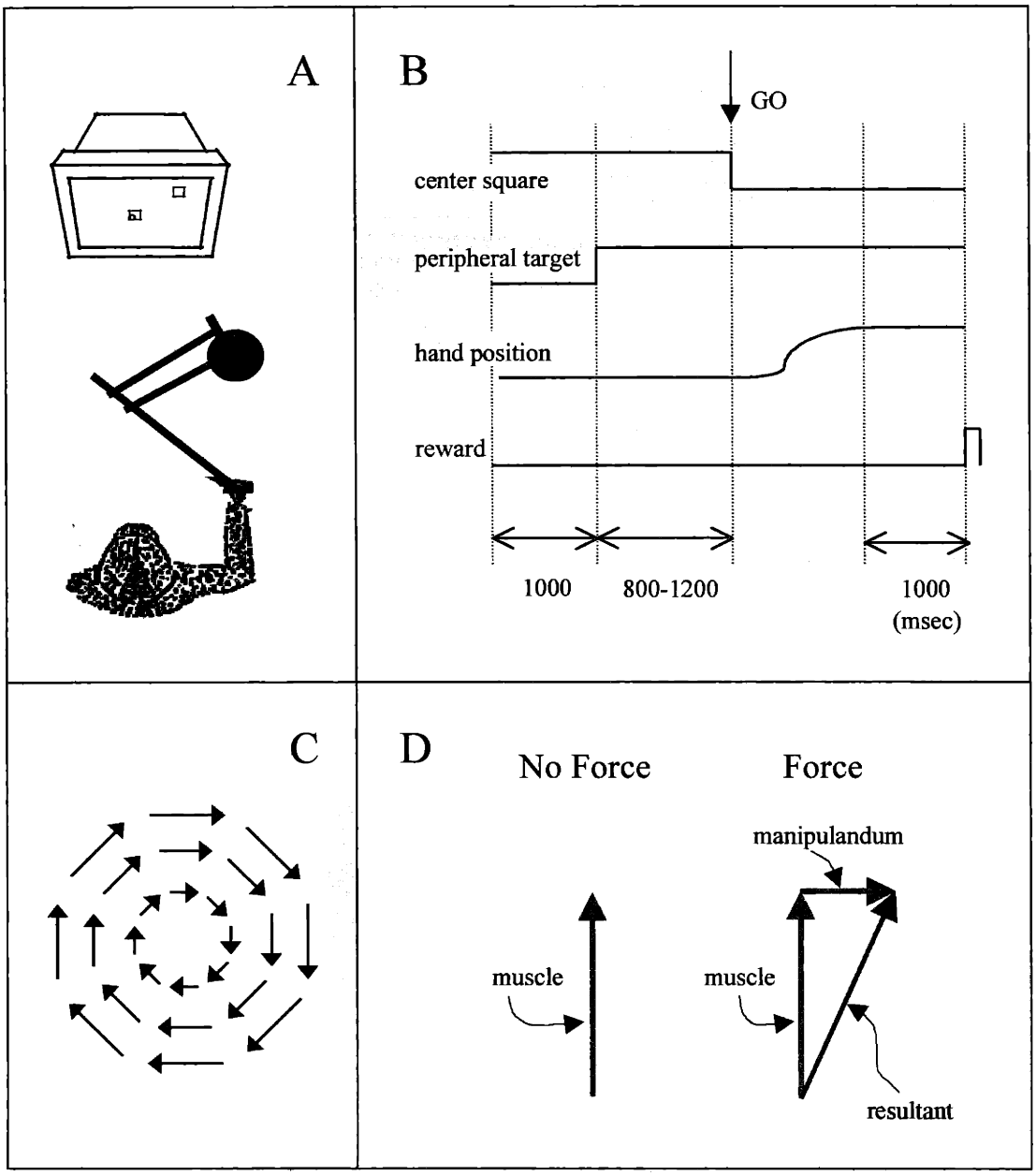

Figure 2

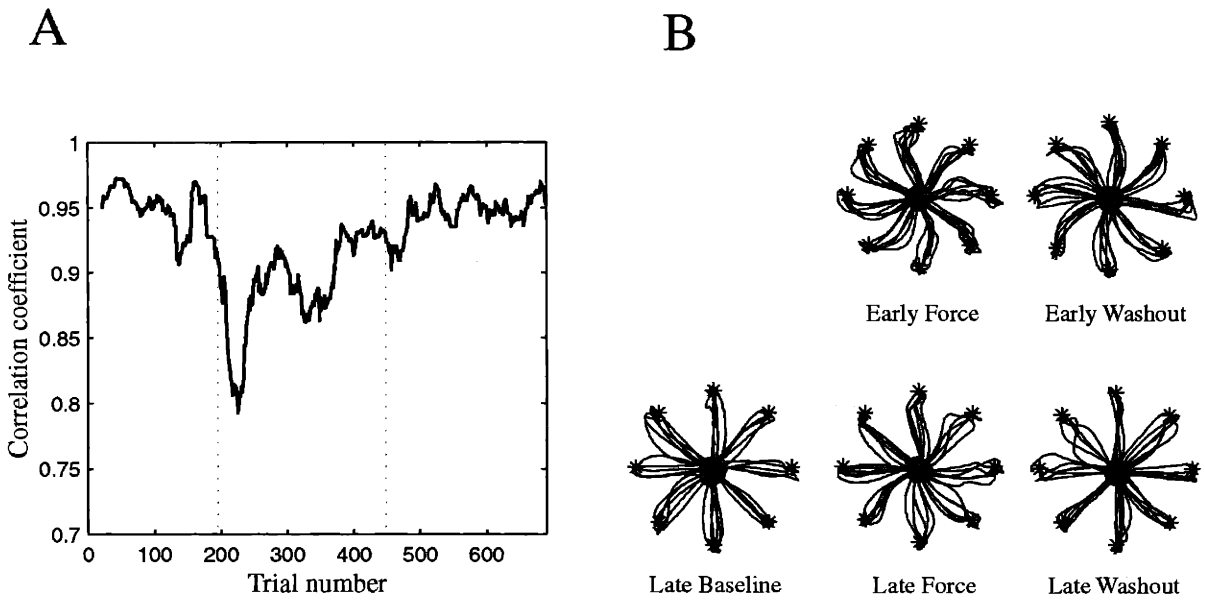
A
B
Correlation coefficient
1
0.95
0.9
0.85
0.8
0.75
0.7
0
100
200
300
400
500
600
Trial number
Early Force
Early Washout
Late Baseline
Late Force
Late Washout

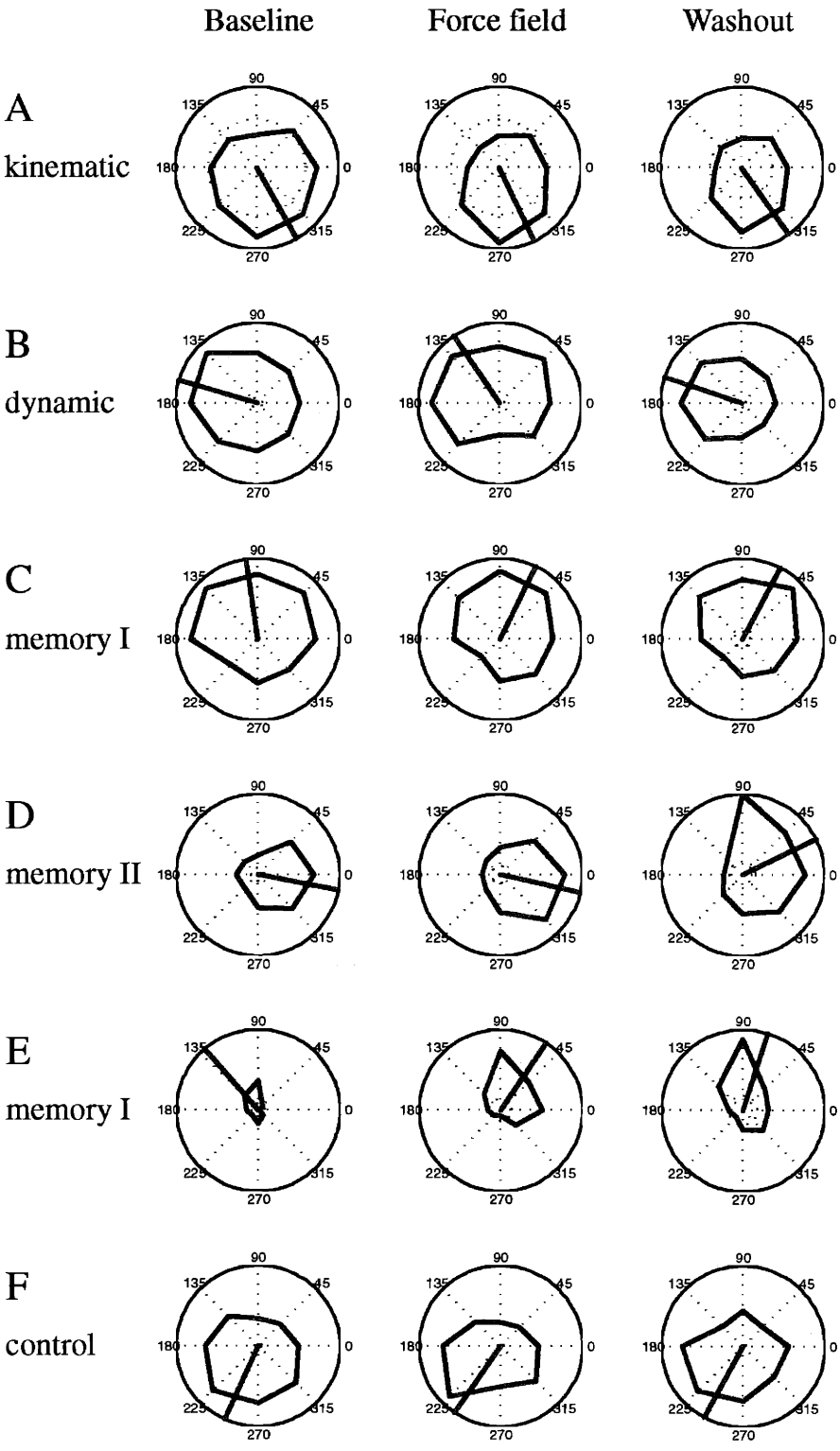
Baseline
Force field
Washout
A
kinematic
B
dynamic
C
memory I
D
memory II
E
memory I
F
control
90
135
45
180
0
225
315
270

Figure 4

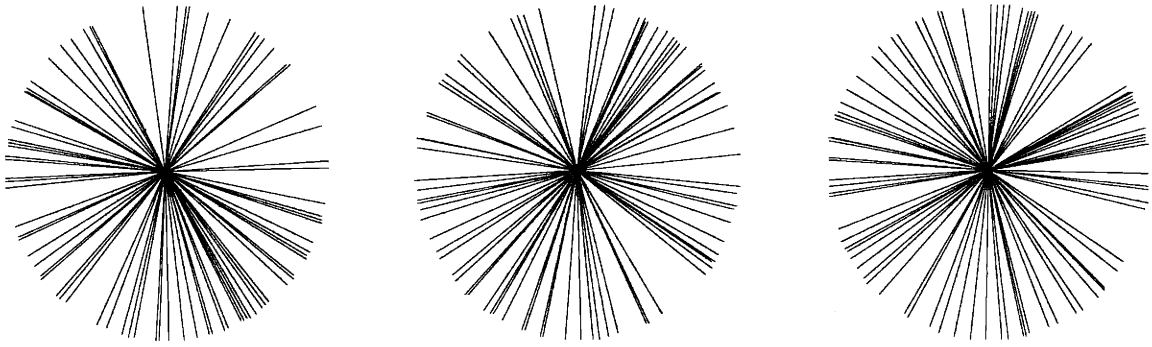

Baseline Force field Washout

Figure 5

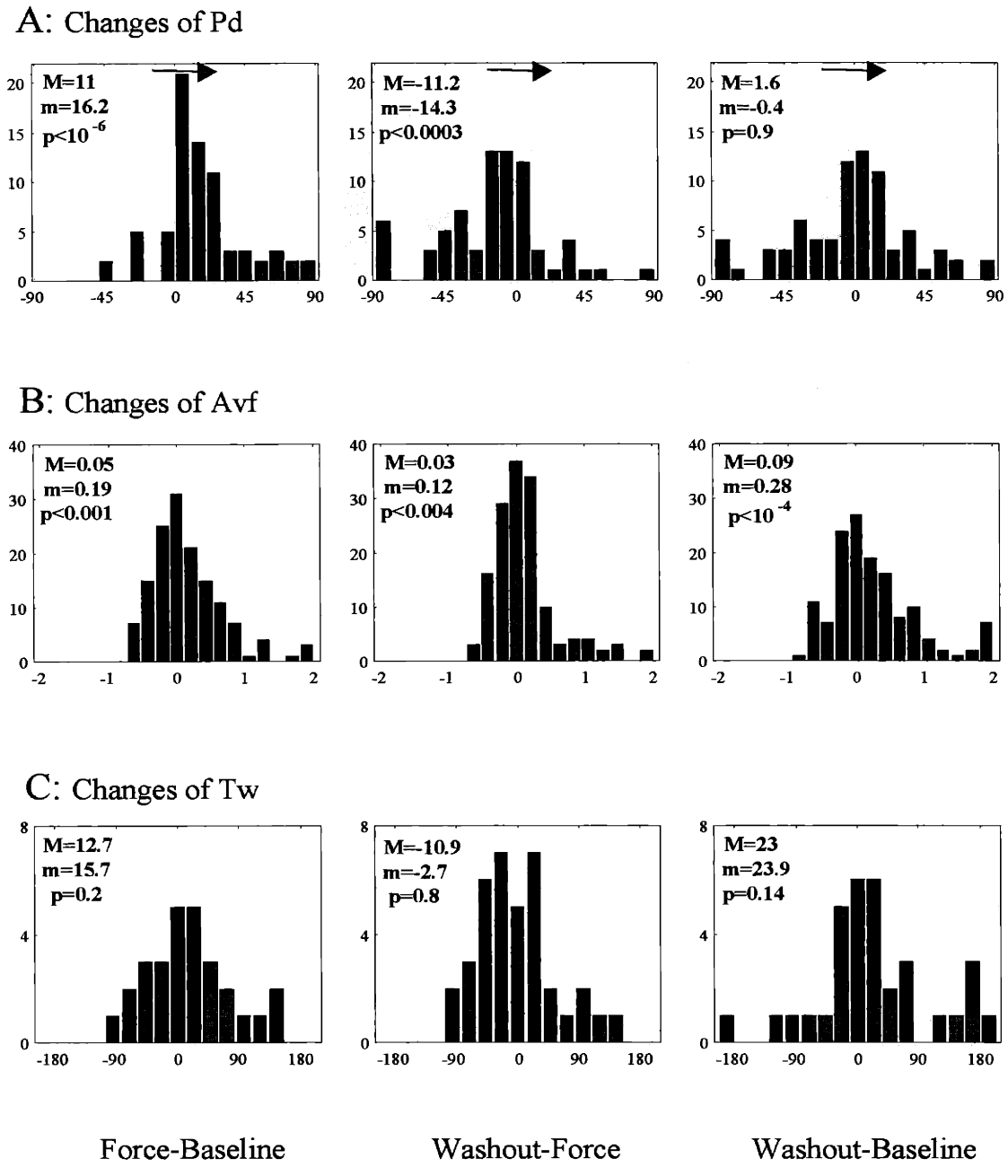
A: Changes of Pd
M=11
m=16.2
p<10 -6
M=-11.2
m=-14.3
p<0.0003
M=1.6
m=-0.4
p=0.9
B: Changes of Avf
M=0.05
m=0.19
p<0.001
M=0.03
m=0.12
p<0.004
M=0.09
m=0.28
p<10 -4
C: Changes of Tw
M=12.7
m=15.7
p=0.2
M=-10.9
m=-2.7
p=0.8
M=23
m=23.9
p=0.14
Force-Baseline
Washout-Force
Washout-Baseline

Figure 6

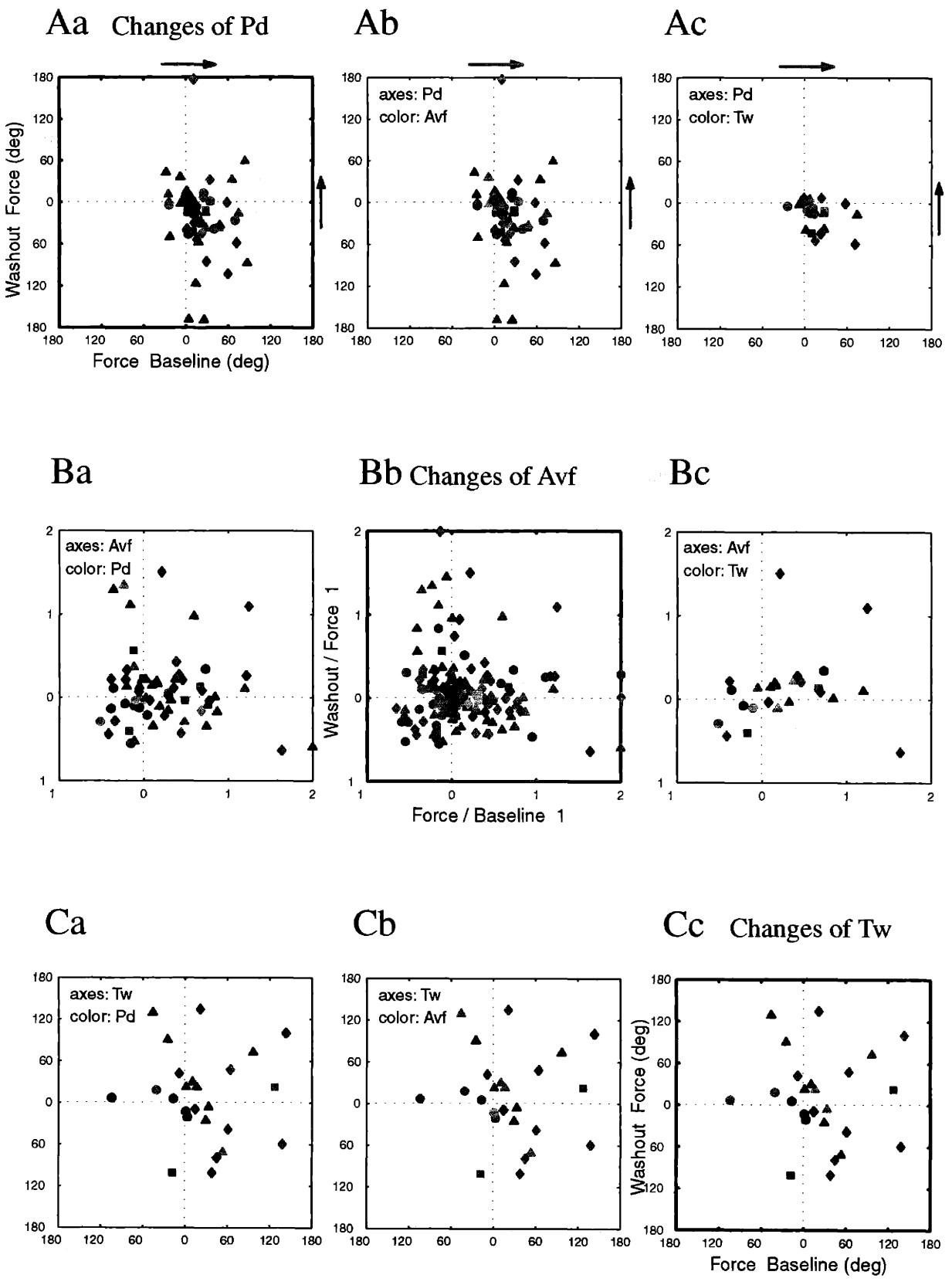
Aa Changes of Pd
Ab
Ac
axes: Pd
color: Avf
axes: Pd
color: Tw
Washout Force (deg)
Force Baseline (deg)
Ba
Bb Changes of Avf
Bc
axes: Avf
color: Pd
axes: Avf
color: Tw
Washout / Force 1
Force / Baseline 1
Ca
Cb
Cc Changes of Tw
axes: Tw
color: Pd
axes: Tw
color: Avf
Washout Force (deg)
Force Baseline (deg)

Figure 7

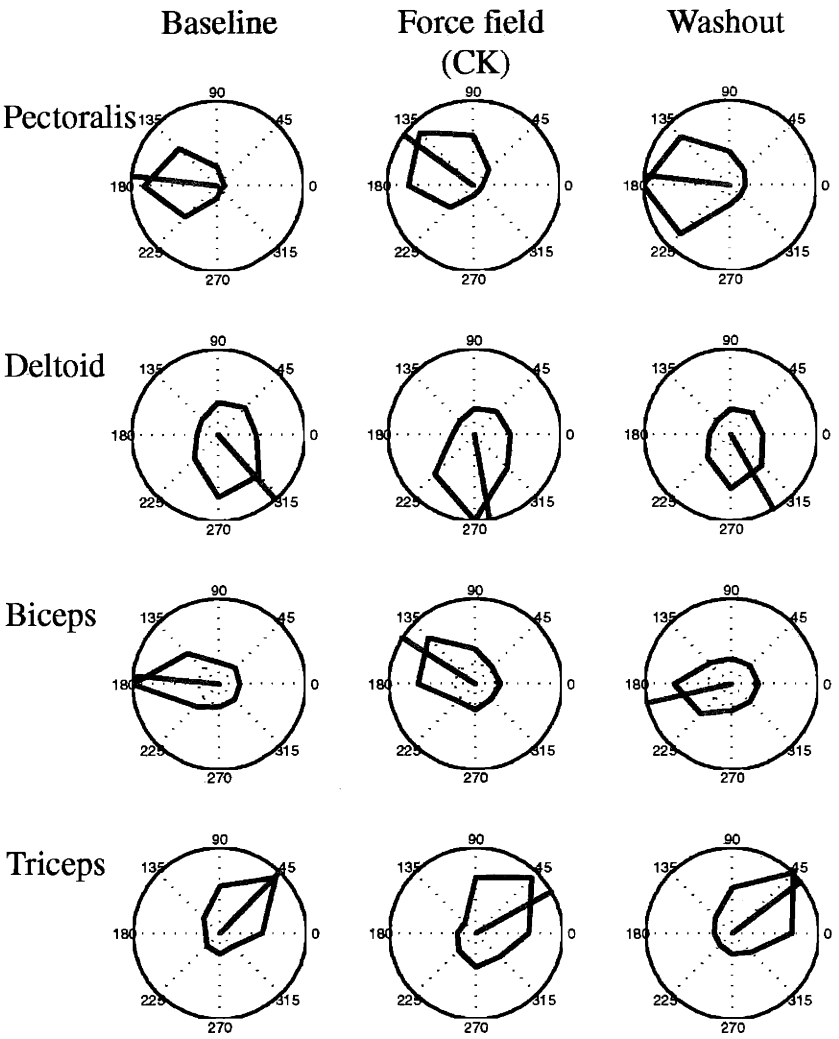
Baseline
Force field (CK)
Washout
Pectoralis
Deltoid
Biceps
Triceps
90
45
0
315
270
225
180
135

Figure 8

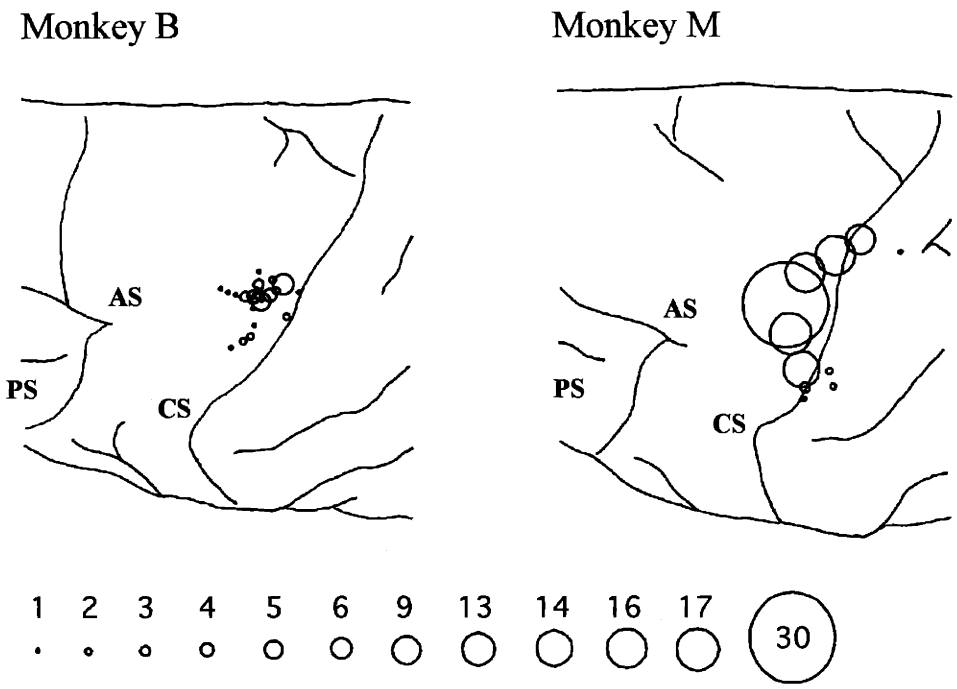

Chapter 4. Neuronal plasticity in the supplementary motor area[1]

We recorded the activity of 252 neurons in the supplementary motor area (SMA) of two monkeys executing visually instructed delayed reaching movements. The neuronal activity was recorded before, during and after exposure to an external perturbing force field, which the monkeys learned to adapt to. Neurons in the SMA process the dynamics of movements both during motor planning and during motor execution. Here we show that neurons in SMA exhibit a variety of plastic changes when monkeys acquire a new internal model. Some neurons –initially not tuned –become directionally tunes as a result of adaptation (tune-in cells), as other neurons leave the pool (tune-out cells). In other cases, neurons that remain directionally tuned throughout the recordings change their activity pattern as a result of adaptation (memory cells). Plastic changes outlast the exposure to the perturbation, and remain after the monkeys re-adapt to the non-perturbed conditions. These results extend for the SMA findings previously described for the primary motor cortex (M1). They indicate that when a new internal model for the dynamics is acquired, plastic changes are widespread across cortical areas.

[1] Elsewhere in the thesis, Chapter 4 is referred to as (Padoa-Schioppa, Li and Bizzi, in preparation).

Introduction

The mechanics of movements is described at two different levels: the dynamics and the kinematics. For a reaching movement, the actual dynamics describes the forces –exerted by contracting muscles –that cause the movement ($f(t)$). The actual kinematics describes the position of the hand and the joint angles in time ($x(t)$), together with the time derivatives ($\dot{x}(t)$, $\ddot{x}(t)$). After Newton, the dynamics and the kinematics are related in the equation $f(t) = m \cdot \ddot{x}(t)$, which fully describes actual movements. From the point of view of the central nervous system (CNS), it is widely assumed that executing visually guided reaching movements requires a sequence of mental operations. For our purposes, these operations can be grouped in (i) processing of the visual stimuli (including all stages "upstream" of the kinematics, such as making the decision to reach); (ii) designing the desired kinematics; and (iii) computing the corresponding desired dynamics (Bernstein, 1967; Saltzman, 1979; Alexander and Crutcher, 1990a; Kalaska and Crammond, 1992; Mussa-Ivaldi and Bizzi, 2000). Assuming that in normal conditions the desired and the actual movements (kinematics and dynamics) coincide, two fundamental issues are open. First, what kinematic and dynamic variables are exactly coded? For instance, the end-point, or the total time, or the curvature of the trajectories are all valid kinematic variables. Likewise, the total force or the joint torques are valid dynamic variables. Second, how are these variables processed in the CNS? The present work investigated aspects of this second issue. Specifically, we investigated how neurons in the motor areas of the frontal lobe process the dynamics of movements.

Considering the psychophysics, the CNS as a whole can be thought to control movements by the use of internal models (Shadmehr and Mussa-Ivaldi, 1994; Wolpert, Ghahramani and Jordan, 1995; Krakauer, Ghilardi and Ghez, 1999; Flanagan et al., 1999; Merfeld, Zupan and Peterka, 1999; for reviews see Wolpert and Ghahramani, 2000; Desmurget and Grafton, 2000; Kawato, 1999). With respect to the movement dynamics, internal models describe the dynamics of the limb and the environment. Work in humans and monkeys showed that new internal models can be acquired when subjects adapt to a new dynamics environment (i.e., to a perturbing force) (Shadmehr and Mussa-Ivaldi, 1994; Gandolfo et al., 2000). In addition, new internal models for the dynamics allow some generalization (Shadmehr and Mussa-Ivaldi, 1994; Gandolfo, Mussa-Ivaldi and Bizzi, 1996; Thoroughman and Shadmehr, 2000) and undergo consolidation (Brashers-Krug, Shadmehr and Bizzi, 1996). Finally, internal models for the dynamics are learned independently of other internal models, e.g. internal models for the kinematics (Krakauer, Ghilardi and Ghez, 1999; Flanagan et al., 1999).

Considering the physiology, although a number of cortical areas in the frontal lobe are known to project directly to the spinal cord (He, Dum and Strick, 1993, 1995), their functions are still largely unknown. In a series of experiments, we investigated how the movement dynamics is processed in four of these areas, namely the primary motor cortex (M1), the supplementary motor area (SMA), the dorsal premotor area (PMd), and ventral premotor area (PMv). Our research focused on two complementary aspects. First, how do neurons in these areas process the internal models for the dynamics? Second, how is their activity modified when a new internal model is acquired? The present report focuses on the SMA.

One important discovery in the past decade has been that the traditionally defined "*SMA*" (Penfield and Welch, 1951; Woolsey et al., 1952) includes two distinct areas: the rostral pre-SMA (or F6), and the caudal SMA-proper (or SMA, or F3; here referred to as SMA). The preSMA and the SMA differ in many respects. Most importantly, the SMA sends direct projections to the spinal cord, whereas the preSMA does not (Luppino et al 1994; He, Dum and Strick, 1995; Rouiller et al., 1996; Dum and Strick, 1991). Consistently, simple movements are elicited by electrical stimulation of the SMA with relatively low currents, while stimulation of pre-SMA triggers more complex movements, and with a higher threshold (Luppino et al., 1991). In addition, the preSMA and the SMA have different cortico-cortical connections. The SMA is interlinked with M1 and with other premotor areas that project to the cord, whereas the preSMA receives direct inputs from the prefrontal cortex and is interlinked with the anterior cingulate area (Luppino et al., 1993; Luppino, Matelli and Rizzolatti, 1990, Bates and Goldman-Rakic, 1993). Finally, the two areas differ for their cytoarchitectonical organization, as giant pyramidal cells are found in the SMA but not in the preSMA (Matelli et al., 1991; for review see Geyer et al., 2000).

While the anatomy of SMA is now rather well identified, much less is known about its functions, essentially because of two combined reasons. First, most of the available studies predate the distinction between preSMA and SMA. Second, most of the studies on the undivided "*SMA*" searched the neuronal correlates of early and complex motor functions (Tanji, Taniguchi and Saga, 1980; Tanji and Kurata 1985ab; Okano and Tanji, 1987; Mushiake, Inase and Tanji, 1991; Thaler et al., 1995; Chen et al., 1995; for a review of human studies see Picard and Strick, 1996, 2001). In contrast, the studies that considered preSMA and SMA separately –either by direct contrast or by meta-analyses – have generally concluded that high and complex functions are better associated with the preSMA rather than with the SMA (Matsuzaka, Aizawa and Tanji, 1992; Matsuzaka and Tanji, 1996; Picard and Strick, 1996, 2001; Alexander and Crutcher, 1990b; Nakamura, Sakai and Hikosaka, 1998; see also Hikosaka et al 2000). As a consequence, the literature on the undivided "*SMA*" is most likely inherited by the preSMA, leaving the SMA essentially unexplored. This notwithstanding, two complementary characteristics of the neuronal activity on the SMA emerge from the literature. On the one hand, the SMA seems more involved in motor planning than the M1 (Alexander and Crutcher, 1990; Tanji and Mushiake, 1996). On the other hand, the SMA also seems directly involved in motor execution (Matsuzaka, Aizawa and Tanji, 1992; Crutcher and Alexander, 1990; Alexander and Crutcher, 1990b; Hikosaka et al 2000). In the present study, we show that neurons in the SMA process the dynamics of the movement (i.e., a late computational stage) during *motor planning* and during *motor execution*. In addition, we show that neurons in the SMA undergo a variety of plastic changes when a new internal model for the dynamics is acquired. Parts of this work were presented elsewhere (Padoa-Schioppa, Li and Bizzi, 2000, submitted).

Methods

The experimental setup and behavioral paradigm were essentially the same used for a previous study of M1 (Li, Padoa-Schioppa and Bizzi, 2001). The NIH guidelines on the care and use of animals were adhered throughout the experiment.

Behavioral task

Two young male rhesus monkeys (*Macaca mulatta*), C and F, took part in the experiment. Both monkeys weighted 6.5-7.5 Kg, and both performed with their right arm. In the experiment, the monkeys sat on a chair in an electrically isolated enclosure. They grab the handle of a two degrees of freedom robotic arm (the manipulandum), which allowed free movements confined to a horizontal plane. A computer monitor placed vertically 75 cm in front of the monkeys displayed the position of the handle (cursor: 3x3-mm square, ca to 0.2° of visual angle) and the targets of the reaching movements (16x16 mm squares, ca 1° of visual angle). All the movements were from a central location (center square) to one of eight peripheral targets (peripheral squares), equally spaced along a circle (45° apart). Actual reaching movements were 8 cm in length.

The monkeys performed an instructed delayed reaching task. At the beginning of each trial, the center square appeared on the monitor, and the monkey moved the cursor into the center square to initiate the trial. After 1s, a peripheral square (*cue*) appeared randomly at one of the eight peripheral locations. The monkey held the cursor within the center square for a randomly variable delay (0.5-1.5 s) before the center square was extinguished (*go* signal). The monkey had then to move and acquire the peripheral square within 3 s, and to remain within the peripheral square for 1 s to receive a juice reward (*rew*). During the task, the trajectories were confined within 60° on both sides of the line passing through the center square and peripheral square. The trial was immediately aborted if the monkey made an error, and another trial started after an inter-trial interval (*iti*) of 0.8-1.2 s. The peripheral targets were pseudo-randomly chosen.

Two motors attached at the base of the robotic arm allowed turning on and off perturbing forces (force fields). We used one of the two force fields described by $\mathbf{F}=\mathbf{BV}$, where $\mathbf{B}$ is the rotation matrix $\mathbf{B}=[0, -b; b, 0]$, with $b=\pm 0.06$ Ns/m, and $\mathbf{V}$ is the instantaneous velocity vector. Thus, the force field $\mathbf{F}$ was viscous (proportional in strength to the velocity $\mathbf{V}$) and curl (orthogonal in direction to the velocity $\mathbf{V}$). Depending on the sign of "b" the force field was clockwise (CK) or counterclockwise (CCK). In each session, the monkeys performed in three subsequent behavioral epochs: Baseline (no force), Force epoch, and Washout. Each epoch lasted for approximately 20 successful trials for each direction (ca 160 trials total). Only one of the two force fields (CK or CCK) was used in each session.

During the training (4-6 months), monkeys were only exposed to the non-perturbed reaching task, and the force fields were only introduced for the recordings. For monkey C, recording sessions with the two force fields were run in blocks (27 sessions with the CK force field, followed by 28 sessions with the CCK force field). Monkey F was tested on the CCK force field only (40 sessions). Sometimes, recording sessions began after the monkey had performed in non-perturbed conditions for up to 300 trials, leaving us the time to wait for the brain to stabilize and accurately set the threshold for the spikes. Each recording session lasted approximately 1-2 hours, after which we let the monkeys work as long as they continued. We ran no more than one session per day.

On separate control sessions we followed the usual procedure for recording sessions without ever introducing the perturbing force field. Thus, in control sessions the monkey performed in three arbitrarily divided epochs of approximately 160 successful trials each. Control sessions were intermixed with experimental sessions (16 control sessions in total).

Surgery and identification of the recording area

After training was completed, aseptic stereotaxic surgery was performed to put a restraint device on the skull and a recording well (inner diameter: 28 mm and 19 mm for monkeys C and F, respectively). Chambers were centered on the midline, and in anterior coordinates A=22 and A=18 for monkeys C and F, respectively. The monkeys were given antibiotics and pain medications, and were allowed to fully rest for at least one week after the surgery.

The SMA was identified through electrical microstimulation (monkey C) and histology (monkey F). For microstimulation, we used a train of 20 biphasic pulse pairs (width=0.1msec, duration=60 msec), at 330 Hz and 10-40 μ Amp. Before the recordings, we extensively stimulated the left medial wall and we obtained a map closely matching that of Luppino and colleagues (Luppino et al., 1991). Monkey F was euthanized at the end of the experiment. We marked the recording sites with electrolytic lesions (cathodal current, 20 μ A, 2 min). We then administered an overdose of pentobarbital sodium, and perfused the monkey transcardially with heparinized saline, followed by buffered Formalin. The brain was marked with electrodes dipped in black ink, removed from the skull, photographed, sectioned (coronal plane, 28 μ m sections), and Nissl-stained. Recordings were located in the medial wall, caudal to the alignment with the genu of the arcuate sulcus. Microscopic inspection revealed that the recording region was poorly laminated, and lied within 6 mm rostral to tissue displaying a single line of giant pyramidal cells, thus identifying the SMA (Matelli, Luppino and Rizzolatti, 1991).

Recordings

Two computers were used in the experiments. One computer recorded the position and velocity of the manipulandum (at the frequency of 100 Hz) and controlled the motors. A second computer (synchronized with the first computer) recorded the behavioral events and the neuronal activity.

For neuronal recordings, we used vinyl-coated tungsten electrodes (1-3 MΩ impedance). We advanced electrodes by manually rotating a threaded rod carrying the electrode in a set-screw system, at an approximate depth resolution of 30 μm (300 μm /turn). Up to eight electrodes were used in each session. Electrical signals acquired by the electrodes passed through a head stage (AI 401, Axon Instruments) and an amplifier (Cyberamp 380, Axon Instruments), and were filtered at a high and low cutoff of 10 kHz and 300 Hz, respectively. Data from each electrode were recorded and displayed using commercially available software (Experimenter's WorkBench 5.3, DataWave Technology). Electrical signals from each electrode were continuously sampled at a frequency of 20 kHz. Action potentials were detected by threshold crossing. Waveforms (1.75 msec duration) were recorded on line and saved for subsequent analysis.

Data analysis: psychophysics

We defined the correlation coefficient (CC) as the normalized co-variance between the actual speed profile and an ideal speed profile (Shadmehr and Mussa-Ivaldi, 1994; Li, Padoa-Schioppa and Bizzi, 2001). For each actual trajectory $(x(t), y(t))$ we extracted the speed profile $\mathbf{v} = (\dot{x}^2(t) + \dot{y}^2(t))^{1/2}$. Thus, **v** was a vector of instantaneous speeds, sampled at 100 Hz. We derived the ideal speed profile **u** with an iterative process, separately for each movement direction and for each session. We then aligned **u** and **v** at their maximum and computed the $CC(\mathbf{v},\mathbf{u})=Cov(\mathbf{v},\mathbf{u}) / (\sigma(\mathbf{v})\,\sigma(\mathbf{u}))$. Thus, the values of the CC ranged between –1 and 1, and were close to 1 for actual trajectories close to ideal.

To compare movements with similar kinematics, we disregarded for each epoch the first four successful trials in each direction. Loose time constraints were imposed on the RT during the experiments. In the analysis, we excluded anticipatory movements (RT<200 msec) and outliers (RT>400 msec). The remaining trials (>88%)were considered for further analysis. For each trial we defined the movement onset (*mo*) and movement end (*me*), with threshold-crossing criteria on the speed (4 cm/sec).

Data analysis: neurons

The neuronal recordings were first subjected to a clustering analysis, to separate one ore more individual neurons recorded form the same electrode from each other and from other sources of noise. Clustering was performed using a commercially available software (Autocut 3, Datawave Technology), with a semi-manual procedure. We visually inspected the waveforms after the clustering, and often repeated the procedure one or more times. Only cells with convincingly consistent waveform throughout the session were considered for further analysis.

We analyzed the activity of single neurons in 4 separate time windows. The center hold time (CH, *cue*-500 msec to *cue*), serving as a control time window; the delay time (DT, *go*-500 msec to *go*); the movement time (MT, *mo*-200 msec to *me*); the target hold time (TH, *rew*-500 msec to *rew*). For each neuron and for each time window, we analyzed the spiking activity separately in the Baseline, Force epoch and Washout. We averaged the activity across trials, and obtained a tuning curve for each epoch. To characterize the tuning curves, we defined three parameters: the preferred direction (Pd), the average firing frequency (Avf), and the tuning width (Tw). The Pd of the neuron was defined as the direction of the vector average of the eight vectors representing the activity recorded for the eight movement directions. The Avf was defined as the average of the neuronal activity across the eight directions. The Tw was defined as the angle over which the firing frequency was higher than half of the maximal activity across the eight directions (maximum of the tuning curve). These parameters were defined for any given tuning curve, subject to the following pre-conditions. First, we only considered tuning curves with an Avf > 1 Hz. Second, the Pd and Tw were only defined for tuning curves displaying a significantly unimodal distribution across directions, as stated by the Rayleigh test ($p<0.01$, see Fisher p70). Third, the Tw was only defined for strictly unimodal cells, for which the directions with firing frequency higher than half the maximum were continuous.

To analyze the changes of Pd over the entire population, we "flipped" the data recorded with the CK force field to obtain positive values when the Pd shifted in the direction of the external force.

Classification of cells

Significant changes across epochs for the three parameters Pd, Avf and Tw were stated according to the method previously described in detail (Li, Padoa-Schioppa and Bizzi, 2001). Briefly, given the 8-dimensional firing rate $\vec{m}$, the 8-dimensional standard error $\vec{\sigma}$ (due to trial-by-trial variability in the activity of the cell) can be thought of as an error of measure for $\vec{m}$. For each parameter $p=P(\vec{m})$, we derived an error σ_p using an error-propagation method. We then compared the values of the parameter across epochs with a *z*test ($p<0.05$), using the squared derived errors as estimates of the variances.

Individual cells were classified separately for each parameter (Pd, Avf and Tw) and for each time window (CH, DT, MT, and TH). We refer to the Pd to illustrate the criteria of classification. Cells that did not change their Pd across epochs (*x*-*x*-*x*) were named "kinematic cells," because the desired kinematics remained essentially unchanged throughout the session. Cells that changed their Pd in the Force epoch compared to Baseline and returned to the original Pd in the Washout (*x*-*y*-*x*) were named "dynamic cells," because the dynamics of the movement were the same in the Baseline and the Washout but different in the Force epoch (where the monkeys compensate for the external force). Cells changed their Pd in the Force epoch compared to the Baseline, and maintained in the Washout their newly acquired Pd (*x*-*y*-*y*) were named "memory cells," because they appeared to keep trace of the adaptation experience even after the monkey had returned to the non-perturbed conditions. More precisely, *x*-*y*-*y* cells were named "memory I cells," as distinguished from "memory II cells," whose Pd did not in the Force epoch compared to Baseline, but changed in the Washout compared to the Force epoch (*x*-*x*-*y*). Thus, memory II cells were complementary to memory I cells. Finally, cells that changed their Pd in the Force epoch and again in the Washout (*x*-*y*-*z*) were named "other cells". The same criteria were applied for the Avf and the Tw.

For the statistical analysis of the population, we used conventional methods of linear and circular statistics (Fisher, p75-76).

Comparing the results of different classifications

SMA cells were classified for their changes across behavioral epochs separately for the four time windows and three parameters. One of the goals of the present study was to compare the results of such classification across time windows (CH, DT, MT, and TH), and across parameters (Pd, Avf, and Tw). In addition, we wanted to compare the results recorded here for the SMA with that recorded for the M1 (Gandolfo et al., 2000; Li, Padoa-Schioppa and Bizzi, 2001) and for the PMd and PMv (Xiao, Padoa-Schioppa and Bizzi, in preparation). We performed these comparisons using a Pearson's χ^2 analysis (Freeman, 1987), which we chose (over the likelihood ratio) because our contingency tables came sometimes with empty locations. For this same reason, we performed the comparison separately across time windows, across parameters, and across areas.

When comparing the classifications across time windows, we considered one parameter (e.g., the Avf) and two time windows (e.g., the DT and MT). We then addressed specific questions such as the following. Given that each given cell can be classified differently in the two time windows (e.g., "kinematic" in the DT, and "dynamic" in the MT), are *coincident* classifications more frequent than would be expected if they occurred by chance? Having five possible classes (kinematic, dynamic,

memory I, memory II, and other), we studied the 5x5 contingency table (5 DT-classes x 5 MT-classes) where the element n_{ij} is equal to the number of cells classified as "*i*" and "*j*" in the two time windows, respectively. We then compute the matrix:

$$\chi_{ij}^2 = \frac{(n_{ij} - m_{ij})^2}{m_{ij}}$$

where:

$$m_{ij} = \frac{\sum_i n_{ij} \sum_j n_{ij}}{\sum_{i,j} n_{ij}}$$

and Pearson's χ^2 is given by:

$$\chi^2 = \sum_{i,j} \chi_{ij}^2$$

In essence, the matrix element χ_{ij}^2 quantifies how unlikely is the value n_{ij} given all the other values n_{lk}, and χ^2 quantifies how unlikely is the matrix *n* if the distribution across raw is independent of the distribution across columns (or vice versa). In our case, χ^2 indicated whether the classification in the DT and MT were at all inter-dependent, against the null hypothesis of homogeneity. To assess more specifically whether the two classifications coincided more frequently than expected by chance, we computed the trace:

$$Tr = \sum_{i=j} \chi_{ij}^2$$

Because it is the sum of the diagonal elements of χ_{ij}^2, *Tr* precisely quantifies how unlikely are coincident classifications.

When comparing the classifications across parameters, we considered one time window (e.g., the MT) and two parameters (e.g., the Pd and the Avf). We then addressed specific questions such as the following. Given that each given cell can be classified differently for the two parameters (e.g., "dynamic" for the Pd and "memory I" for the Avf), are *coincident* classifications more frequent than would be expected if they occurred by chance? Again, we studied the 5x5 contingency table, which we analyzed like before. In particular, we computed both $\chi^2 = \sum_{i,j} \chi_{ij}^2$ and $Tr = \sum_{i=j} \chi_{ij}^2$.

When comparing across areas we addressed the general question whether the division of cells into classes were the same in the different areas. Considering for instance how cells are classified for their changes of Pd in the MT time window, we studied the 3x5 contingency matrix given by the three areas (PMd, SMA, and M1) and the five classes (kinematic, dynamic, memory I, memory II, and other). The value of Pearson's $\chi^2 = \sum_{i,j} \chi_{ij}^2$ indicated whether there were any generic difference across areas, against the null hypothesis of homogeneity. In addition, the decomposed values χ_{ij}^2 indicated specific deviance from chance. We could therefore address specific questions such as the following. Are there comparatively more memory I cells in the M1 than expected by chance? Using this same approach we compared the results obtained for the SMA experimental cells with that obtained for the SMA control cells.

In all these analyses we imposed a significance threshold of $p<0.05$.

Electromyographic activity

In separate sessions, we recorded the electromyographic (EMG) activity of the muscles Pectoralis, Deltoid, Biceps, Triceps and Brachioradialis while the monkey performed in the task. We manually implanted Teflon-insulated wires in the shoulder and arm muscles. The EMG were recorded continuously, at the frequency of 1 kHz. In the analysis, we rectified and integrated the EMG over the same time windows used for the neurons. We obtained EMG's tuning curves, which we normalized and submitted to the same analysis used for neurons.

Results

Psychophysics

The psychophysics of the task has been previously described for humans (Shadmehr and Mussa-Ivaldi, 1994) and monkeys (Gandolfo et al., 2000; Li, Padoa-Schioppa and Bizzi, 2001). The present study confirmed those results, as illustrated in Figure 1. In the absence of external perturbation (Figure 1a, Baseline), hand trajectories were essentially straight, and the speed profile were close to ideal, as quantified by the correlation coefficient (CC, Figure 1b). When we introduced a CK force field (Force epoch), the hand trajectories were initially deviated (Figure 1a, Early Force), and the values of the CC dropped. But as the monkey adapted to the perturbing force, the trajectories returned straight (Figure 1a, Late Force), very much like that recorded in the Baseline. The adaptation process is well illustrated by the increase of the CC, which gradually returned to high values. When we removed the force field, we observed an "aftereffect" (Figure 1a, Early Washout), as the trajectories were initially deviated in a way that mirrored the deviation observed in the Early Force. After a short re-adaptation, however, the trajectories returned straight (Figure 1a, Late Washout) and the CC regained the original values.

Over days, the adaptation process improved. This long term-learning was observed by computing the average CC in the Force epoch for each session, and by plotting it against the session number, separately in the three epochs (Figure 1C).

EMG activity

The choice of viscous, curl force fields **F=BV** offered two advantages. First, no perturbing force was ever present when the monkey held their hand still (**V=0**). In particular, no external force was ever present –even in the Force epoch –during the instructed delay (DT). Second, because the force field was curl, it imposed predictable and consistent changes onto the EMG activity of muscles during the movement time (MT). Specifically, by comparing the preferred direction (Pd) recorded in the Force epoch with that recorded in the Baseline, we observed a shift of Pd in the direction of the external force field.

Figure 2 illustrates the EMG activity of one representative muscle (triceps longhead). The three columns represent the three epochs (Baseline, Force epoch, Washout), and the four raw represent the four time windows (CH, DT, MT, TH). In each panel, the muscle's tuning curve is plotted in blue in polar coordinates, and the preferred direction (Pd) is plotted in red. The Pd is only defined for directionally tuned EMG

activity. It can be noticed that there is no directional activity in either the CH, or DT. With respect to the MT, the Pd of the muscle is oriented towards 21° in the Baseline. In the Force epoch –after adaptation to the CCK field –the Pd of the muscle shifts by 28° in the direction of the external force (the CCK direction). In the Washout, the Pd of the muscle shifts back, essentially to that originally recorded in the Baseline.

Similar shifts of Pd in the direction of the external force in the Force epoch, and back in the opposite direction in the Washout were observed for all the muscles we recorded from. We defined the shift of Pd to be positive when it occurred in the direction of the external force, and we averaged across muscles. Considering the population of muscles, we found a significant shift of Pd in the Force epoch compared to the Baseline (mean shift 19.2°, $p<0.003$, *t*test), a significant shift back in the Washout compared to the Force epoch (mean shift -15.4°, $p<0.03$, *t*test), and no significant shift when the Washout was compared to the Baseline (mean shift 4.4°, $p=0.06$, *t*test).

The shift of Pd observed for muscles is simply predicted considering the mechanics of the forces acting upon the hand of the monkey in the Force epoch, and has been described for both humans (Thoroughman and Shadmehr, 1999; Shadmehr and Moussavi, 2000) and monkeys (Li, Padoa-Schioppa and Bizzi, 2001). For the current purposes, the crucial point is that the Pd of all the muscles shifts in the *same* direction (the direction of the external force field), independently of the initial Pd. Thus, the shift of Pd observed for muscles provides a framework to interpret the neuronal data.

Neuronal database

We recorded the activity of 252 SMA cells in the adaptation task. In addition, we recorded the activity of 46 SMA cells in control sessions.

Figures 4-10 illustrate the activity of 6 representative cells recorded in the SMA in the adaptation task (Figures 4-9) and one control cell (Figure 10). For each cell, we show the activity recorded in the three behavioral epochs (columns Baseline, Force epoch, Washout), and in the four time windows (raw CH, DT, MT, and TH), plotted in polar coordinates. For clarity of exposure, we describe different aspects observed in the activity of single neurons in separate sections here below.

Directional tuning

The percentages of directionally tuned cells for the three behavioral epochs and in the four time windows are shown in Table 1. As expected, negligible percentages of cells passed the statistical test in the CH. In contrast 44%-49% of cells (depending on the behavioral epoch) were directional tuned in the DT. These percentages increased in the MT, to 59%-66%. In the TH, 53%-58% of cells were tuned.

We also analyzed the distribution of Pd around the clock for the entire population (Figure 3). The null hypothesis of homogeneity held for all three epochs, and all three time windows (minimal $p>0.04$, Rayleigh test), with the only exception of the Force epoch and MT time window ($p<0.002$, Rayleigh test).

Dynamically-tuned cells, tune-in cells, and tune-out cells

As the monkey adapted to the perturbing force, the activity of neurons in the SMA changed. Some cells that were not tuned in the Baseline became tuned in the Force epoch following the adaptation, and lost their tuning again in the Washout. Other cells that were

originally tuned in the Baseline lost their tuning in the Force epoch, to regain it in the Washout. These two types of cells were grouped in the class of "dynamically-tuned" cells, because the changes observed in their directional tuning appeared dynamic in nature. Figure 4 illustrates one example of dynamically-tuned cell (MT activity). In total, dynamically-tuned cells counted for 10% of the SMA population (MT time window).

We also found another group of cells –named "tune-in" cells –that were initially not tuned in the Baseline and acquired a directional tuning in the Force epoch (Gandolfo et al., 2000). Unlike dynamically-tuned cells, however, tune-in cells maintained their newly acquired tuning in the Washout, after the monkey had re-adapted to the non-perturbed conditions. Thus, tune-in cells appeared to maintain a trace of the adaptation experience after re-adaptation in the Washout. One example of tune-in cell is illustrated in Figure 5.

We also found a group of cells –named "tune-out" cells –that were initially tuned in the Baseline, lost their tuning in the Force epoch, and failed to regain their tuning in the Washout. Thus, the changes observed for tune-in cells and tune-out cells appeared memory in nature. In total, tune-in cells and tune-out cells counted for 14% and for 8% of the population, respectively (analysis done on the MT).

We compared the incidence of dynamically-tuned, tune-in and tune-out cells recorded in the SMA with that recorded in the M1, PMd and PMv by analyzing the 4x4 contingency table (4 areas x 4 groups: dynamically-tuned, tune-in, tune-out, tuned-throughout). In general, we found significant differences between areas ($\chi^2 = 50.85$; d.o.f.=9; $p<10^{-7}$). In particular, more dynamically-tuned cells were found in the PMd than in the other areas (decomposed $\chi^2 = 6.53$; d.o.f.=1; $p<0.02$). With respect to the SMA, we found a lower incidence of tune-out cells than in the other areas (decomposed $\chi^2 = 8.27$; d.o.f.=1; $p<0.01$).

Changes of Preferred direction: DT

Cells that remained directionally tuned throughout the three epochs were analyzed and classified for their changes in preferred direction (Pd), separately for the DT, MT and TH time windows.

Figure 6 illustrates the activity of a kinematic cell, classified according to the changes of Pd. Considering the DT time window (second raw), the Pd of the cell remains essentially constant throughout the session (*x-x-x*). Because the desired kinematics remained unchanged throughout the three epochs, this cell was classified as kinematic cell.

Figure 7 illustrates the activity of a dynamic cell recorded with a CK force field, and classified according to the changes of Pd. The DT activity is shown in the second raw. In the Force epoch, the Pd of the cell shifts in the direction of the external force (i.e., in the CCK direction) compared to the Baseline. In the Washout, the Pd shifts in the opposite direction, back to that recorded in the Baseline (*x-y-x*). Because the dynamics of the movement were the same in the Baseline and in the Washout, but different in the Force epoch, this cell was classified as dynamic cell.

Figure 8 illustrates the activity of a memory I cell recorded in the SMA with a CK force field, and classified according to the changes of Pd. Again, the DT activity is illustrated in the second raw. In the Force epoch, the Pd of the cell shifts in the direction of the external force (i.e., the CK direction) compared to the Baseline. However, after re-

adaptation in the Washout, the Pd remained oriented in the newly acquired direction (*x-y-y*). Thus, the cell appeared to maintain a trace of the previously adaptation experience. We therefore classified this cell as memory I cell.

Considering the entire SMA population, a total of 68 cells could be classified according to their changes of Pd in the DT time window. The majority of these cells was classified as kinematic (37 cells, 55%). However, we also found dynamic cells (7 cells, 10%), memory I cells (15 cells, 22%) and memory II cells (8 cells, 12%). These percentages are summarized in Table 2.

We also analyzed the shifts of Pd at the population level. We computed the shift of Pd for each cell, and defined positive the shifts that occurred in the direction of the external force. We then averaged the shift of Pd across the SMA population, for the three between-epochs comparisons (Force-Baseline; Washout-Force; Washout-Baseline). Comparing the Force epoch with the Baseline, we found that neurons in the SMA shifted their Pd significantly in the direction of the external force (mean shift = 11.1°, $p<0.02$, *t*test). Conversely, SMA neurons quasi-significantly shifted their Pd back in the opposite direction in the Washout compared to the Force epoch (mean shift = -7.2°, $p=0.054$, *t*test). No significant shift of Pd was observed for the population when comparing the Washout with the Baseline (mean shift = 5.6°, $p=0.3$, *t*test). These changes of Pd observed for the neuronal population are summarized in Figure 11 and in Table 3.

Qualitatively, the shifts of Pd observed for SMA neurons during the delay (DT) match the shifts of Pd observed for muscles during the upcoming movements (MT). Three points should however be stressed. First, no EMG activity was present during the DT (see Figure 2). Second, no force was actually present ($\mathbf{F}=\mathbf{BV}=0$), because the monkey was not moving ($\mathbf{V}=0$). Third, because the extent of the delay was randomly chosen, the monkey could not pre-initiate the movement. Thus, the DT activity genuinely reflects the planning of the movement. The changes of Pd indicate that neurons in the SMA process the dynamics of the upcoming movement during motor planning. In a previous report, we showed that –in the Force epoch –the shift of Pd occurs progressively over the course of the delay, indicating that neurons in the SMA process a kinematics-to-dynamics transformation (Padoa-Schioppa, Li and Bizzi, submitted). We also showed how the shift of Pd at the end of the delay correlates with the goodness of adaptation (quantified by the initial direction of the upcoming movement), and anti-correlates with the following reaction time, necessary to initiate the movement.

Changes of Preferred direction: MT

The cells illustrated in Figures 6-8 to exemplify the classes of kinematic, dynamic and memory I cells –as defined for the DT time window –also make the case for the MT time window. Considering the MT activity of the cell in Figure 6 (third raw), the Pd is essentially constant throughout the three epochs (*x-x-x*). Therefore, the cell was classified as kinematic for it's changes of Pd in the MT.

The cell in Figure 7 was recorded with a CK force field. Considering the MT activity (third raw), the Pd of the cell shifts in the direction of the external force in the Force epoch compared to the Baseline. In the Washout, the Pd shifts back in the opposite direction, essentially to its original orientation (*x-y-x*). Therefore, the cell was classified as dynamic for it's changes of Pd in the MT.

The cell in Figure 8 was recorded with a CCK force field. Again, considering the MT activity (third raw), the Pd of the cell shifts in the direction of the external force in

the Force epoch compared to the Baseline. In the Washout, the cell maintains its newly acquired Pd (*x-y-y*). Thus, this cell was classified as memory I cell for its changes of Pd in the MT.

Figure 9 illustrates the activity of a memory II cell recorded in the SMA with a CCK force field. In the DT (second raw), the cell is not directionally tuned. Considering the MT time window (third raw), the Pd is essentially unchanged in the Force epoch compared to the Baseline. In the Washout, however, the Pd of the cell shifts in the direction *opposite* to the previously experienced force field, namely the CK direction (*x-x-y*). Thus, this cell was classified as memory II cell for it's changes of Pd in the MT. Note that the shift of Pd of memory II cells seems to balance in the Washout the shift of Pd of memory I cells (Li, Padoa-Schioppa and Bizzi, 2001).

In total, we could classify 117 SMA cells according to their changes of Pd in the MT. Of these, 33 cells (28%) were kinematic, 35 cells (30%) were dynamic, 23 cells (20%) were memory I, 16 cells (14%) were memory II, and 10 cells (9%) were "other" cells. These percentages are summarized in Table 2.

Considering the entire population of SMA in the MT, we observe shifts of Pd similar to that observed for the EMG activity of muscles, and for neurons in the M1. As a population, neurons in the SMA show a significant shift of Pd in the Force epoch compared to the Baseline (mean shift =16.6°, $p<10^{-6}$, *t*test). Comparing the Washout with the Force epoch, we see a significant shift back in the opposite direction (mean shift =-9.7°, p<0.001, *t*test). In contrast, no significant shift is observed when comparing the Washout and the Baseline (mean shift =3.9°, p=0.2, *t*test). The changes of Pd observed for the neuronal population are summarized in Figure 11 and in Table 3.

Changes of Preferred direction: TH

We found that some cells also changed their Pd in the TH, and one case of memory I cell is shown in Figure 8. The percentages of cells in the various classes are summarized in Table 2. Considering the entire SMA population in the TH, however, we found no significant shifts of Pd in either the Force epoch compared to the Baseline (mean shift =3.4°, p=0.3, *t*test) or in the Washout compared to the Force epoch (mean shift =-0.1°, p=1, *t*test). These averages are summarized in Figure 11 and in Table 3.

Control cells

Figure 10 illustrates the activity of one control cell, recorded in a session were no force field was ever introduced. It can be seen that the Pd of the cell is quite stable throughout the session, in all time windows. We analyzed all control cells with the same procedure used for experimental cells. Considering the entire population of control cells, no significant shifts of Pd were observed either in the Force epoch or in the Washout, in any time window (DT, MT or TH; 9 comparisons total, maximal mean shift =6.2°, minimal p=0.2). Consider single control cells we occasionally found significant changes of Pd. In particular with respect to the MT time window, we recorded 55% of kinematic, 3% of dynamic, 18% of memory I, 21% of memory II, and 3% of "other" cells (33 cells total). We contrasted these percentages with the corresponding values recorded for experimental cells (see Table 2) with a χ^2 analysis, and found that the distribution of classes were significantly different for the two populations ($\chi^2 = 15.06$, d.o.f.=4, p<0.005). More

specifically, we found a significant "excess" of kinematic cells in the control group (decomposed $\chi^2 = 4.10$, d.o.f.=1, $p<0.05$).

Changes of Average firing frequency

We analyzed the changes of average firing frequency (Avf) across behavioral epochs, and we classified all single SMA neurons separately in the CH, DT, MT and TH time windows. For example, the cell illustrated in Figure 8 was classified as memory I cell for its changes of Avf in both the MT and TH time windows. The percentages of cells in the various classes are reported in Table 2.

Considering the entire population, we found a general increase in Avf in the Force epoch compared to the Baseline, and a further –though more limited –increase in the Washout compared to the Force epoch. The increase in Avf was present in all time windows, as summarized in Figure 11 and Table 3. Significant increases of Avf were however also found for control cells. Moreover, by direct contrast we failed to find significant differences between the changes of Avf recorded in the Force epoch for the experimental cells and that recorded in the analogous behavior epoch for control cells. With respect to cells that were recorded in the adaptation task, the increases in Avf observed for the population of SMA are similar to that recorded for the populations of M1, PMd and PMv.

Changes of Tuning width

We analyzed the changes of tuning width (Tw) of single cells across behavioral epochs, and we classified single SMA neurons separately in the DT, MT and TH time windows. The percentages of cells in the various classes are reported in Table 2.

Considering the entire population, we found a general increase in Tw in all time windows, both in the Force epoch and in the Washout. This increase, however, did not reach significance level, except for the MT time window, when the Washout was compared to the Baseline. The changes of Tw for the entire population are summarized in Figure 11 and Table 3.

Consistency of classification across time windows (DT and MT)

The cells shown in Figures 6-8 appear to have a rather consistent changes of Pd across time windows. For instance, cell in Figure 7 is classified as dynamic for its changes of Pd recorded in either the DT or the MT. Were cells always as consistent? To address this question, we combined the classification in the DT with that in the MT in a 5x5 contingency table, which we analyzed with a χ^2 statistics. With respect to the changes of Pd, we found no evidence to reject the null hypothesis of homogeneity (Pearson's $\chi^2 = 16.85$, d.o.f.=16, p=0.4). Further computing the trace $Tr = \sum_{i=j} \chi_{ij}^2$ we quantified whether the classification across time windows coincided more often than expected by chance. We found no statistical evidence of such consistency ($Tr = 2.84$, d.o.f.=4, p=0.6).

With respect to the changes of Avf, in contrast, we found that the classification in the DT and MT time windows were highly predictive of each other. Considering the entire contingency matrix, we rejected the null hypothesis of homogeneity (Pearson's $\chi^2 = 63.98$, d.o.f.=16, $p<10^{-6}$). Furthermore, the deviance from homogeneity were largely

explained by the trace of the matrix $Tr = 44.55$, which indicated that the two classifications coincided more frequently than expected by chance (d.o.f.=4, $p<10^{-8}$). The rest of the matrix, considered with out the trace, did not indicate any further deviance from homogeneity.

We did not perform this analysis for the Tw, because only 7 cells could be considered.

Consistency of classification across parameters

We also investigated whether the classification of cells was consistent across parameters. We found that although the classifications performed according to different parameters did not always coincide (e.g., see Figure 6), coincident classifications occurred more frequently than expected by chance. Considering the MT time window, we first combined the classification for the Pd with that for the Avf in a 5x5 contingency table. We then computed the matrix χ^2_{ij} imaged in Figure 12. Considering the entire matrix, the null hypothesis of homogeneity should not be rejected (Pearson's $\chi^2 = 17.57$, d.o.f.=16, p=0.35). However, considering the trace Tr by itself, we find a significant coincidence between the two classifications ($Tr = 9.82$, d.o.f.=4, $p<0.05$). In other words, the classification for the changes of Pd and that for the changes of Avf coincide more often than would be expected by chance.

Combining the classification of the Pd with that of the Tw, we found no significant departure from homogeneity at the level of the entire matrix (Pearson's $\chi^2 = 18.18$, d.o.f.=16, p=0.3), nor a significant coincidence considering the trace only ($Tr = 2.83$, d.o.f.=4, p=0.6). Likewise, combining the classification of the Avf with that of the Tw, we found no significant departure from homogeneity at the level of the entire matrix (Pearson's $\chi^2 = 13.65$, d.o.f.=16, p=0.6), nor a significant coincidence considering the trace only ($Tr = 1.88$, d.o.f.=4, p=0.8).

Discussion

Neuronal plasticity in the SMA

In the present study, we investigated the neuronal plasticity associated with the development of a new internal model for the dynamics. We described a variety of plastic changes in the activity of neurons recorded from the SMA. As a consequence of the acquisition of the new internal model, new neurons in the SMA become committed to the task (tune-in cells), as other neurons leave the pool (tune-out cells). In addition, cells that are task-related before, during, and after the learning process exhibit changes in their activity patterns that outlast exposure to the perturbation (memory cells). These changes in the activity of single neurons combine in such a way that the output of the neuronal population of SMA after re-adaptation is statistically not distinguishable from that before adaptation. This characteristic phenomenon –which we previously described for the primary motor cortex (Li, Padoa-Schioppa and Bizzi, 2001) –is consistent with the understanding that neurons in the motor cortices subserve both functions of motor performance and motor learning.

The present results extend to the SMA and complements findings previously described for the M1 (Gandolfo et al., 2000; Li, Padoa-Schioppa and Bizzi, 2001). First,

we showed that the movement dynamics is processed across multiple cortical areas of the frontal lobe (see also Xiao, Padoa-Schioppa and Bizzi, in preparation). Second, we showed that when a new internal model is acquired, plastic changes occur in multiple cortical areas, not just in the M1. Third, thanks to a larger data set, we addressed for the SMA questions remained open for the M1. In particular, we could compare the results of different classification of cells, and we found significant *coincidences* of classification across parameters and across time windows.

However, the present study falls short of addressing the issue of whether the short-term plasticity observed in our experiments has any direct relevance for long-term learning. Monkey in the present experiment "learned" throughout the recordings, and we did not observe clear differences between the early and the late sessions. A more careful analysis and additional data might help shed light on this issue.

The following two papers present a direct contrast between cortical areas (Xiao, Padoa-Schioppa and Bizzi, in preparation; Padoa-Schioppa and Bizzi, in preparation). The present data indicate, however, that the SMA is at one time "upstream" and very similar to the M1. On the one hand, neurons in the SMA process the kinematics-to-dynamics transformation during motor planning, well before the engagement of M1 (Padoa-Schioppa, Li and Bizzi, submitted). On the other hand, a late computational stage –the movement dynamics –is processed in both the SMA and the M1. With particular respect to the learning-related neuronal plasticity, we report similar results for the two areas, though M1 appears slightly more "plastic". In the M1, 41% of cells are classified as memory I or II for their changes of Pd in the MT time window, against 34% of cells in the SMA (and 25% in the PMd).

Interpretative limits

We classified cells depending on how their activity changed in the presence and after the exposure to a dynamic perturbation. Cells that did not show any changes were classified as kinematic. Cells whose activity changed across epochs were classified as dynamic, memory, or other, respectively. Invariant cells were defined "kinematic" because the kinematics of the movement remained essentially invariant across epochs. The interpretation of invariant cells as kinematic cells is however subject to two limitations. First, a failure to detect significant changes is a poor statement of invariance. In other words, the activity of cells that appeared invariant to us may really have changed, but to a lesser extent than we were able to detect. Note, however, that this limitation does not apply to the case were we see a *progressive* change (Padoa-Schioppa, Li and Bizzi, submitted). Second, the kinematics of the movement was not the only quantity to remain unchanged across epochs. In particular, the visual instructions also remained unchanged across epochs. Thus, neurons that remained invariant could in principle be processing any computational stage "upstream" of the dynamics, including the visual stimuli and the kinematics. We chose the label "kinematic" for parsimony, assuming that the kinematics is the last stage processed *before* the dynamics.

Acknowledgments

We are thankful to Matt Tresch and Philippe Saltiel for valuable discussion, and to Margo Cantor and Sylvester Szczepanowski for technical assistance. This research was supported by the National Institute of Health (NIH grant MN481185).

References

1. Alexander, G.E. & Crutcher, M.D. Preparation for movement: neural representations of intended direction in three motor areas of the monkey. *J. Neurophysiol.* **64,** 133-150 (1990a).
2. Alexander, G.E. & Crutcher, M.D. Neural representation of the target (goal) of visually guided arm movements in three motor areas of the monkey. *J. Neurophysiol.* **64,** 164-178 (1990b).
3. Bates, J.F. & Goldman-Rakic, P.S. Prefrontal connections of medial motor areas in the rhesus monkey. *J. Comp. Neurol.* **336,** 211-228 (1993).
4. Bernstein, N. *The coordination and regulation of movements.* (Pergamon Press, Oxford, 1967).
5. Brashers-Krug, T., Shadmehr, R., & Bizzi, E. Consolidation in human motor memory. *Nature* **382,** 252-255 (1996).
6. Chen, Y.C., Thaler, D., Nixon, P.D., Stern, C.E. & Passingham, R.E. The functions of the medial premotor cortex. II. The timing and selection of learned movements. *Exp. Brain Res.* **102,** 461-473 (1995).
7. Crutcher, M.D. & Alexander, G.E. Movement-related neuronal activity selectively coding either direction or muscle pattern in three motor areas of the monkey. *J. Neurophysiol.* **64,** 151-163 (1990).
8. Desmurget, M. & Grafton, S. Forward modeling allows feedback control for fast reaching movements. *Trends Cogn. Sci.* **4**, 423-431 (2000).
9. Dum, R.P. & Strick, P.L. The origin of corticospinal projections from the premotor areas in the frontal lobe. *J. Neurosci.* **11,** 667-689 (1991).
10. Fisher, N.I. *Statistical analysis of circular data.* (Cambridge University Press, Cambridge, 1993).
11. Flanagan J.R., Nakano, E., Imamizu, H., Osu, R., Yoshioka, T. & Kawato, M. Composition and decomposition of internal models in motor learning under altered kinematic and dynamic environments. *J. Neurosci.* **19,** (RC34) 1-5 (1999).
12. Freeman, D.H. *Applied categorical data analysis.* (Marcel Dekker, Inc., New York, 1987).
13. Gandolfo, F., Li, C.-S., Benda, B.J., Padoa-Schioppa, C. & Bizzi, E. Cortical correlates of learning in monkeys adapting to a new dynamical environment. *Proc. Natl. Acad. Sci. USA* **97**, 2259-2263 (2000).
14. Gandolfo, F., Mussa-Ivaldi, F.A. & Bizzi, E. Motor learning by field approximation. *Proc. Natl. Acad. Sci. USA* **93**, 3843-3846 (1996).
15. Geyer, S., Matelli, M., Luppino, G. & Zilles, K. Functional neuroanatomy of the primate isocortical motor system. *Anat. Embryol. (Berl.).* **202**, 443-474 (2000).
16. He, S.Q., Dum, R.P. & Strick, P.L. Topographic organization of corticospinal projections from the frontal lobe: motor areas on the lateral surface of the hemisphere. *J. Neurosci.* **13,** 952-980 (1993).
17. He, S.Q., Dum, R.P. & Strick, P.L. Topographic organization of corticospinal projections from the frontal lobe: motor areas on the medial surface of the hemisphere. *J. Neurosci.* **15,** 3284-3306 (1995).
18. Hikosaka, O. *et al.* In: *The New Cognitive Neuroscience* (Ed Gazzaniga, M.S.) 553-572 (MIT Press, Cambridge MA, 2000).

19. Kalaska, J.F. & Crammond, D.J. Cerebral cortical mechanisms of reaching movements. *Science* **255,** 1517-1523 (1992).
20. Kawato, M. Internal models for motor control and trajectory planning. *Curr. Opin. Neurobiol.* **9**, 718-727 (1999).
21. Krakauer, J.W, Ghilardi, M.F. & Ghez, C. Independent learning of internal models for kinematic and dynamic control of reaching. *Nat. Neurosci.* **2**, 1026-1031 (1999).
22. Mussa-Ivaldi, F.A. & Bizzi, E. Motor learning through the combination of primitives. *Phil. Trans. R. Soc. Lond.* B **355,** 1755-1769 (2000).
23. Li, C-S.R., Padoa-Schioppa, C. & Bizzi, E. Neural correlates of motor performance and motor learning in the primary motor cortex of monkeys adapting to an external force field. *Neuron* **30,** 593-607 (2001).
24. Luppino, G., Matelli, M., Camarda, R. & Rizzolatti, G. Corticocortical connections of area F3 (SMA-proper) and area F6 (pre-SMA) in the macaque monkey. *J. Comp. Neurol.* **338,** 114-140 (1993).
25. Luppino, G., Matelli, M., Camarda, R. & Rizzolatti, G. Corticospinal projections from mesial frontal and cingulate areas in the monkey. *Neuroreport* **5,** 2545-2548 (1994).
26. Luppino, G., Matelli, M. & Rizzolatti, G. Cortico-cortical connections of two electrophysiologically identified arm representations in the mesial agranular frontal cortex. *Exp. Brain Res.* **82,** 214-218 (1990).
27. Luppino, G., Matelli, M., Camarda, R.M., Gallese, V. & Rizzolatti, G. Multiple representations of body movements in mesial area 6 and the adjacent cingulate cortex: an intracortical microstimulation study in the macaque monkey. *J. Comp. Neurol.* **311,** 463-482 (1991).
28. Matelli, M., Luppino, G. & Rizzolatti, G. Architecture of superior and mesial area 6 and the adjacent cingulate cortex in the macaque monkey. *J. Comp. Neurol.* **311,** 445-462 (1991).
29. Matsuzaka, Y., Aizawa, H. & Tanji, J. A motor area rostral to the supplementary motor area (presupplementary motor area) in the monkey: neuronal activity during a learned motor task. *J. Neurophysiol.* **68,** 653-662 (1992).
30. Matsuzaka, Y. & Tanji, J. Changing directions of forthcoming arm movements: neuronal activity in the presupplementary and supplementary motor area of monkey cerebral cortex. *J. Neurophysiol.* **76**, 2327-2342 (1996).
31. Merfeld D.M., Zupan L. & Peterka R.J. Humans use internal models to estimate gravity and linear acceleration. *Nature* **398**, 615-618 (1999).
32. Mushiake, H., Inase, M. & Tanji, J. Neuronal activity in the primate premotor, supplementary, and precentral motor cortex during visually guided and internally determined sequential movements. *J. Neurophysiol.* **66,** 705-718 (1991).
33. Mussa-Ivaldi, F.A. & Bizzi, E. Motor learning through the combination of primitives. *Phil. Trans. R. Soc. Lond.* B **355,** 1755-1769 (2000).
34. Nakamura, K., Sakai, K., & Hikosaka, O. Neuronal activity in medial frontal cortex during learning of sequential procedures. *J. Neurophysiol.* **80,** 2671-2687 (1998).
35. Okano, K. & Tanji, J. Neuronal activities in the primate motor fields of the agranular frontal cortex preceding visually triggered and self-paced movement. *Exp. Brain Res.* **66,** 155-166 (1987).

36. Padoa-Schioppa, C. & Bizzi, E. Neuronal activity in five motor areas of the frontal lobe during visually instructed reaching movements. (In preparation).
37. Padoa-Schioppa, C., Li, C.-S.R. & Bizzi, E. Planning movements: kinematics-to-dynamics transformation in the supplementary motor area. (Submitted).
38. Penfield, W. & Welch, K. The supplementary motor area of the cerebral cortex. *Arch. Neurol. Psychiatry* **66,** 289-317 (1951).
39. Picard, N. & Strick, P.L. Motor areas of the medial wall: a review of their location and functional activation. *Cereb. Cortex* **6,** 342-353 (1996).
40. Picard, N. & Strick, P.L. Imaging the premotor areas. *Curr. Opin. Neurobiol.* **11**, 663-672 (2001).
41. Rouiller, E.M., Moret, V., Tanne, J. & Boussaoud, D. Evidence for direct connections between the hand region of the supplementary motor area and cervical motoneurons in the macaque monkey. *Eur. J. Neurosci.* **8,** 1055-1059 (1996).
42. Saltzman, E. Levels of sensorimotor representation. *J. Math. Psychol.* **20,** 91-163 (1979).
43. Shadmehr, R. & Moussavi, Z.M. Spatial generalization from learning dynamics of reaching movements. *J. Neurosci.* **20**, 7807-7815 (2000).
44. Shadmehr, R. & Mussa-Ivaldi, F.A. Adaptive representation of dynamics during learning of a motor task. *J. Neurosci.* **14,** 3208-3224 (1994).
45. Tanji, J. & Kurata, K. Contrasting neuronal activity in supplementary and precentral motor cortex of monkeys. I. Responses to instructions determining motor responses to forthcoming signals of different modalities. *J. Neurophysiol.* **53,** 129-141 (1985a).
46. Tanji, J. & Kurata, K. Contrasting neuronal activity in supplementary and precentral motor cortex of monkeys. II. Responses to movement triggering vs. nontriggering sensory signals *J. Neurophysiol.* **53,** 142-152 (1985b).
47. Tanji, J. & Mushiake, H. Comparison of neuronal activity in the supplementary motor area and primary motor cortex. *Cog. Brain Res.* **3,** 143-150 (1996).
48. Tanji, J., Taniguchi, K. & Saga, T. Supplementary motor area: neuronal response to motor instructions. *J. Neurophysiol.* **43,** 60-68 (1980)..
49. Thaler, D., Chen, Y.C., Nixon, P.D., Stern, C.E. & Passingham, R.E. The functions of the medial premotor cortex. I. Simple learned movements. *Exp. Brain Res.* **102,** 445-460 (1995).
50. Thoroughman, K.A & Shadmehr, R. Electromyographic correlates of learning an internal model of reaching movements. *J. Neurosci.* **19**, 8573-8588 (1999).
51. Thoroughman, K.A & Shadmehr, R. Learning of action through adaptive combination of motor primitives. *Nature* **12**, 742-747 (2000).
52. Wolpert, D.M & Ghahramani Z. Computational principles of movement neuroscience. *Nat. Neurosci.* **3**, 1212-1217 (2000).
53. Wolpert, D.M, Ghahramani Z. & Jordan, M.I. An internal model for sensorimotor integration. *Science* **269,** 1880-1882 (1995).
54. Woolsey, C.N., Settlage, P.H., Meyer, D.R., Sencer, W., Pinto Hamuly, T. & Travis, A.M. Patterns of localization in precentral and "supplementary" motor areas and their relation to the concept of premotor area. *Res. Publ. Assoc. Nerv. Ment. Dis.* **30,** 231-250 (1952).
55. Xiao, J., Padoa-Schioppa, C. & Bizzi, E. Neuronal activity in the dorsal and ventral premotor areas of monkeys adapting to a new dynamic perturbation. (In preparation).

Figure legends

Figure 1. Psychophysics of short- and long-term motor learning. **A.** Hand trajectories. In the Baseline (Late Baseline), the hand trajectories are straight, from the central location to the eight peripheral targets. When a CK force field is introduced, the trajectories are initially deviated (Early Force). As the monkey continues in the task, however, the trajectories gradually return straight (Late Force), and similar to that observed in the Baseline. Thus, the monkeys learn to transform the same desired kinematics into a new, adapted, dynamics (short-term learning). In the Early Washout, the trajectories deviate in a way that mirrors that observed in the Early Force (aftereffect). The monkey, however, rapidly re-adapts to the non perturbed conditions, and the trajectories return straight (Late Washout). **B.** Correlation coefficient, one session. For each trial, we computed the correlation coefficient (CC) between the actual speed profile and an ideal speed profile. The CC (y-axis) is plotted here against the trial number (x-axis). The CC ranges in values between –1 and 1, and is close to 1 when the speed profile is close to ideal. In the Baseline, the CC has high values (CC~0.98). When we introduce the CK force, the CC drops sharply (CC<0.80). As the monkey adapts, the CC gradually recovers. When the force is then removed, we observe a brief aftereffect (CC~0.93), before the monkey fully re-adapts. The values of the CC are smoothed in 10-trials bins. **C.** Correlation coefficient, all sessions. For each session, we averaged the CC over trials, separately in the three behavioral epochs (Baseline, Force epoch, Washout). Here we plot the mean CC (y-axis) against the session number (x-axis), separately for the Baseline (black, face-up triangles), the Force epoch (blue circles), and the Washout (green, face-down triangles). All the 28 sessions where monkey C was presented with the CCK force field are shown. For the Baseline and the Washout, the mean CC remained high throughout the recordings. For the Force epoch, the mean CC increased over sessions (long-term learning). Note that the monkey was still "learning" throughout the recording period.

Figure 2. Electromyographic activity. EMG activity of the triceps-longhead muscle, recorded with the CCK force field. The tuning curve (blue) and the Pd (red) are plotted in polar coordinates, separately for the four time windows (CH, DT, MT, TH) and for the three epochs (Baseline, Force epoch, Washout). The activity is normalized to the maximum across the 12 panels, and the Pd is defined only for directionally tuned activity. No directional EMG are present in either the CH (first raw) or the DT (second raw). Considering the MT (third raw) in the Force epoch, the EMG activity modifies compared to the Baseline, and the Pd shifts in the CCK direction (i.e., the direction of the external force). The shift of Pd in direction of the external force was consistent for all muscles, and due to the vector sum between the force of the muscle and the external force. In the Washout, the activity of the muscle returned to that observed in the Baseline, and the Pd shifted back. Considering the TH (fourth raw), we observe a more modest shift, which was not consistent for all the muscles. This suggests that the EMG activity in the TH was positional, because viscous force fields (**F=BV**) equal zero when the hand is still (**V**=0).

Figure 3. Distribution of Pd. All SMA neurons are shown. Circular statistics indicated that the distribution of Pd around the clock was always homogeneous (minimal $p>0.04$, Rayleigh test), except for the Force epoch-MT time window ($p<0.002$, Rayleigh test).

Figure 4. A dynamically-tuned cell. The tuning curve of the cell is plotted in blue in polar coordinates, separately for the three epochs and for the four time windows. The Pd –defined only for directionally tuned activity –is plotted in red. The radial scale (*9Hz*) is the same for all 12 panels, and is indicated in *italic* for the top left panel (CH, Baseline). The activity of this cell was very scarce in the CH and DT, throughout the three epochs. Considering the MT (third raw), low activity and no directional tuning is present in the Baseline. In the Force epoch, the activity increases and the cell becomes directionally tuned. In the Washout, however, the activity of the cell returns to that observed in the Baseline and the cell loses its directional tuning. These changes are dynamic in nature, as the dynamics of the movement were the same in the Baseline and in the Washout, but different in the Force epoch.

Figure 5. A "tune-in" cell. The CH, DT and TH activity of this cell remained scarce throughout the session. Considering the MT (third raw), scarce activity is present in the Baseline. However, after adaptation in the Force epoch, the cell becomes sharply tuned. In the Washout, after the monkey re-adapts of the non-perturbed conditions, the cell maintains the new directional tuning. Thus, this cell maintains a memory of the newly acquired internal model for the dynamics. All conventions are as in Figure 4.

Figure 6. A kinematic cell (*x-x-x*). Considering either the DT (second raw) or the MT (third raw), the Pd of the cell remains essentially constant throughout the three epochs. We classified this cell as kinematic for its changes of Pd, because the desired kinematics of the movement remained the same throughout. Note that –unlike the Pd –the Avf of the cell changed across epochs. Considering for instance the changes of Avf in the CH, the cell has memory I properties. All conventions are as in Figure 4.

Figure 7. A dynamic cell (*x-y-x*). This cell was recorded with a CK force field. The cell is directionally tuned both in the DT and in the MT, in all three epochs. Considering the DT activity (second raw), the Pd of the cell shifts in the Force epoch compared to the Baseline in the direction of the external force (CK direction). In the Washout, the Pd of the cell shifts back to that observed in the Baseline. Therefore, we classified the cell as dynamic for its changes of Pd in the DT. Considering the MT activity (third raw), the cell exhibits similar changes. The Pd of the cell shifts in the CK direction in the Force epoch, and shifts back in the Washout essentially to that observed in the Baseline. Thus, the cell was classified as dynamic also for its changes of Pd in the MT. Note that the shift of Pd is quantitatively more pronounced in the MT than in the DT, though qualitatively analogous in the two time windows. All conventions are as in Figure 4.

Figure 8. A memory I cell (*x-y-y*). The activity of this cell –recorded with a CCK force field –is directionally tuned in the DT, MT and TH time windows. The cell is classified as memory I cell for its changes of Pd in all three time windows. Considering –for instance –the DT activity (second raw), the activity of the cell modifies in the Force epoch compared to the Baseline and the Pd shifts in the CCK direction (the direction of the external force). In the Washout, the activity of the cell and the Pd remain that observed in the Force epoch. Because the cell appeared to maintain a trace of the

adaptation experience, we classified it as memory I cell. Considering the MT time window, we observe similar changes. Here again, the shift of Pd (and the overall changes) are quantitatively more pronounced in the MT than in the DT, but qualitatively analogous. This cell was classified as memory I cell also for its changes of average firing rate (Avf), in both the MT and TH time windows. In contrast, the CH activity of the cell remained stable throughout the session. All conventions are as in Figure 4.

Figure 9. A memory II cell (*x-x-y*). The activity of this cell –recorded with a CCK force field –is directionally tuned in the MT throughout the three epochs. In the Force epoch, the activity of the cell remained essentially unchanged compared to the Baseline. In the Washout, however, the activity modified, and the Pd shifted in the CK direction, that is the direction *opposite* to the previously experienced external force. Thus, the cell was classified as memory II cell. All conventions are as in Figure 4.

Figure 10. A control cell. This cell was recorded in a session where no perturbing force was ever introduced, and the monkey performed in Baseline-like conditions throughout the session. The Pd of the cell remained essentially unchanged throughout the three – arbitrarily defined –behavioral epochs, in the DT, MT, and TH time windows. Note, however, that the Avf of the cell increased over the course of the session. All conventions are as in Figure 4.

Figure 11. Population changes. Summary of the changes observed at the population level for the three parameters preferred direction (Pd), average firing rate (Avf), and tuning width (Tw) (values in Table 3). **Changes of Pd** (left column). Consider first the DT (top displayed panel). The black line connects three data-points, corresponding –on the x-axis –to the Baseline (Bl), the Force epoch (Ff), and the Washout (Wo). The y-axis represents the shifts of Pd, where "zero" is the Pd in the Baseline and positive values are shifts in the direction of the external force. Vertical lines indicate the error bars. In the DT, SMA neurons shifted their Pd in the Force epoch compared to the Baseline. The red asterisk indicates that this shift was significant. In the Washout, SMA neurons shifted their Pd back in the opposite direction. The two blue "vertical" asterisks indicate that the Pd in the Washout was statistically different from that in the Force epoch, but the same as that in the Baseline. Similar shifts of Pd are observed in the MT. In contrast, no significant shifts of Pd are observed in the TH. **Changes of Avf** (center column). Consider the CH (top panel). Again, the x-axis corresponds to the three epochs (Bl, Ff, and Wo). The y-axis represents percentage changes of Avf compared to the Baseline. The single red asterisk indicates a significant increase of Avf in the Force compared to the Baseline. The two "horizontal" red asterisks indicate that in the Washout the Avf was significantly higher than that in both the Force epoch and the Baseline. Similar increases are observed in the DT, MT, and TH. In the MT, the increase of Avf in the Washout does reach significance if compared to the Baseline, but not if compared to the Force epoch. **Changes of Tw** (right column). Here the y-axis represents increases in the Tw compared to the Baseline. In general, we observe an increase of Tw in all three time windows. However, this increase reaches significance level only in the MT, when comparing the Washout with the Baseline (red asterisk).

Figure 12. Consistency of classification across parameters (Pd and Avf). The matrix χ^2_{ij} is here imaged in color scale (hot colors red and yellow for high values, cold color blue for low values). Raw represent the classification of cells for their changes of Pd, columns represent the classification of cells for their changes of Avf. If we name n_{ij} the number of cells classified as "*i*" and "*j*" for the two parameters respectively, the matrix element χ^2_{ij} quantifies how unlikely is the value n_{ij}, given all the other values n_{kl}. The point here is that hot colors (i.e., high χ^2_{ij}) are found on the main diagonal, indicating that coincident classifications are more frequent than would be expected by chance.

Figure 13. Results of microstimulation of the left medial wall (monkey C). Recordings were concentrated in the arm area.

Tables

Table 1. SMA, percentage of cells directionally tuned.

	Baseline	Force epoch	Washout
CH	13	13	7
DT	44	49	46
MT	59	65	66
TH	54	53	58

Table 2. SMA, classes of cell (percentages).

	Preferred direction			Average firing freq.			Tuning width		
	DT	MT	TH	DT	MT	TH	DT	MT	TH
Kinematic	55	28	47	13	10	7	47	31	38
Dynamic	10	30	10	9	10	8	6	22	14
Memory I	22	20	19	24	22	24	18	28	28
Memory II	12	14	16	31	18	19	24	13	17
Other (*x*-*y*-*z*)	1	9	9	32	40	42	6	6	3
N cells (tot)	68	117	94	205	228	210	17	32	29

Table 3. SMA, Population changes of activity (means).

		Force – Baseline	Washout – Force	Washout – Baseline
Change of Pd	DT	m=11.1° p<0.02 *	m=-7.2° p=0.054	m=5.6° p=0.3
	MT	m=16.6° $p<10^{-6}$ *	m=-9.7° p<0.001 *	m=3.9° p=0.2
	TH	m= 3.4° p=0.3	m=-0.1° p=1	m=4.3° p=0.3
Change of Avf	CH	m=0.26 $p<10^{-7}$ *	m=0.12 $p<10^{-3}$ *	m=0.42 $p<10^{-5}$ *
	DT	m=0.29 $p<10^{-5}$ *	m=0.14 $p<10^{-4}$ *	m=0.48 $p<10^{-4}$ *
	MT	m=0.26 $p<10^{-6}$ *	m=0.01 p=0.7	m=0.21 $p<10^{-4}$ *
	TH	m=0.30 $p<10^{-5}$ *	m=0.09 p<0.03 *	m=0.36 $p<10^{-6}$ *
Change of Tw	DT	m= 8° p=0.5	m= 10° p=0.4	m= 23° p=0.2
	MT	m= 11° p=0.3	m= -6° p=0.5	m= 24° p<0.04 *
	TH	m= 20° p=0.052	m= -7° p=0.5	m= 11° p=0.4

Figure 1

Figures

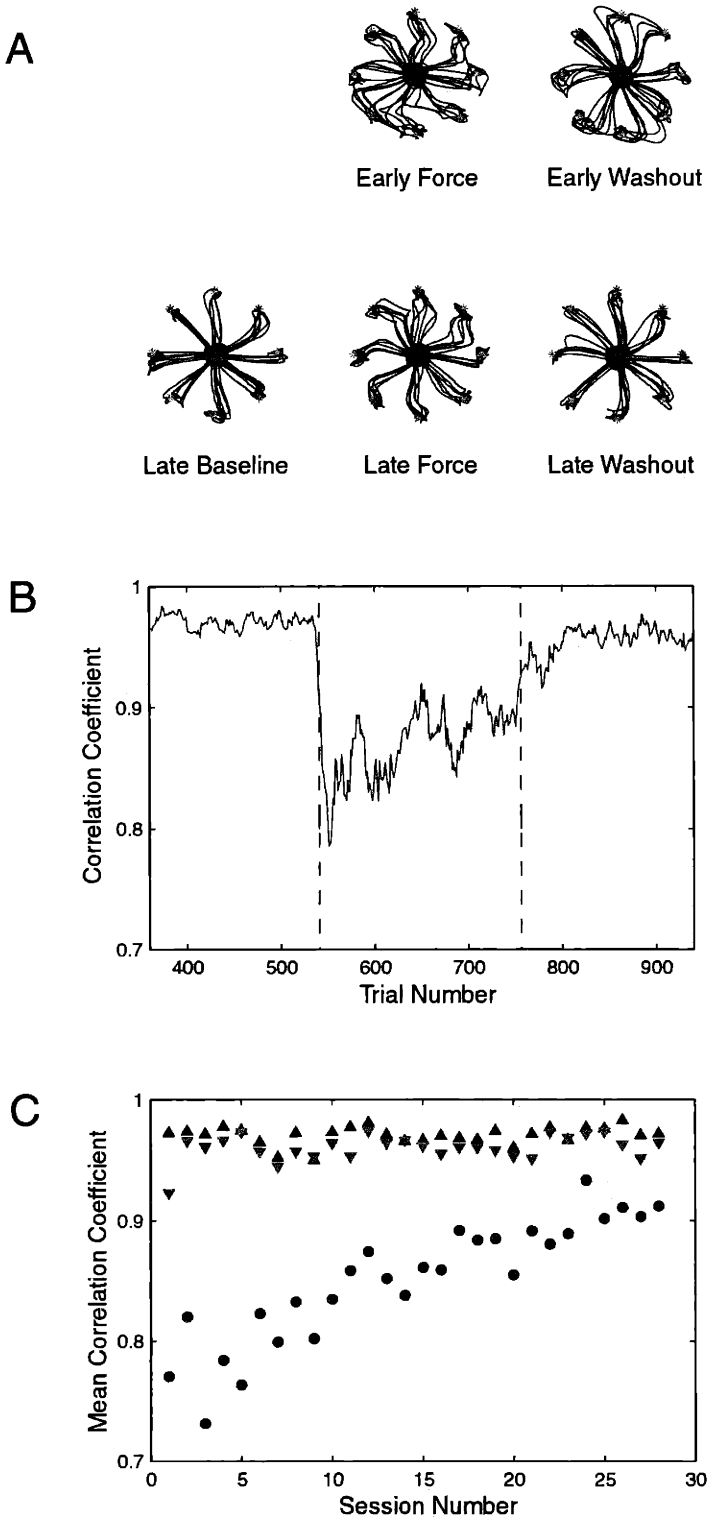

Figure 2

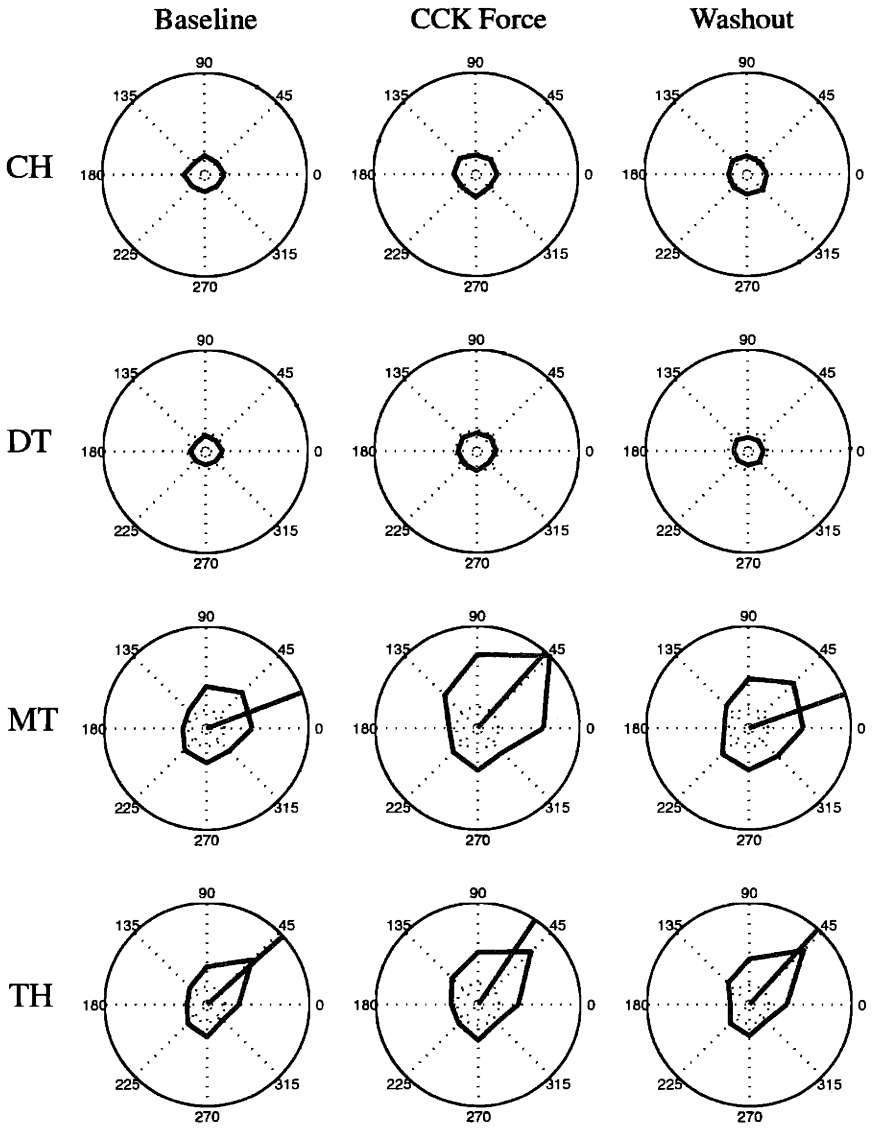
Baseline
CCK Force
Washout
CH
DT
MT
TH
90
135
45
180
0
225
315
270

Figure 3

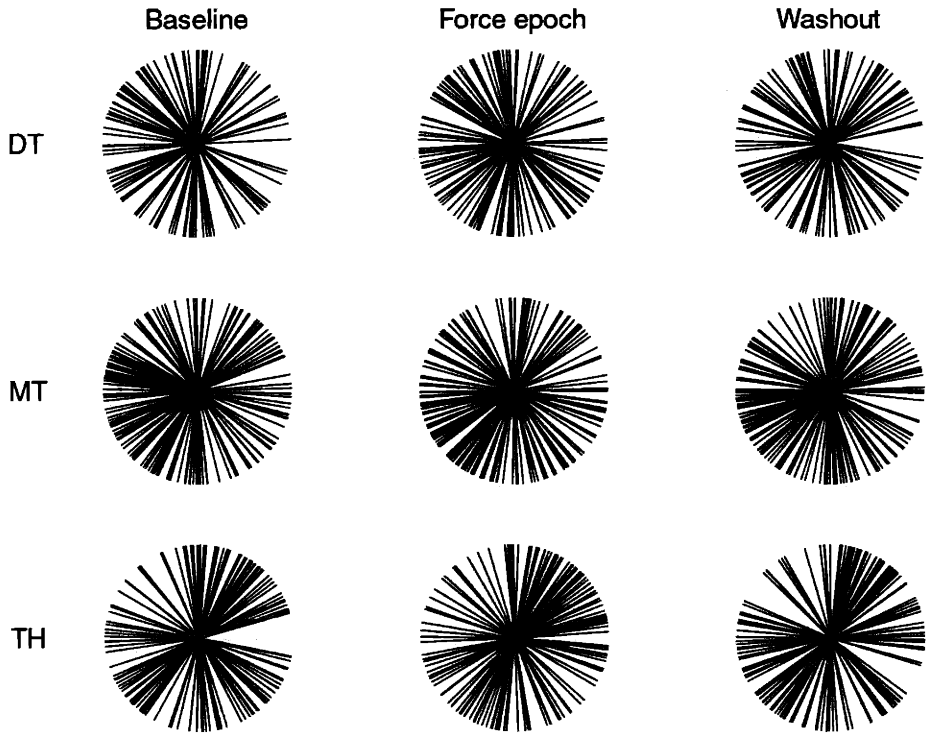

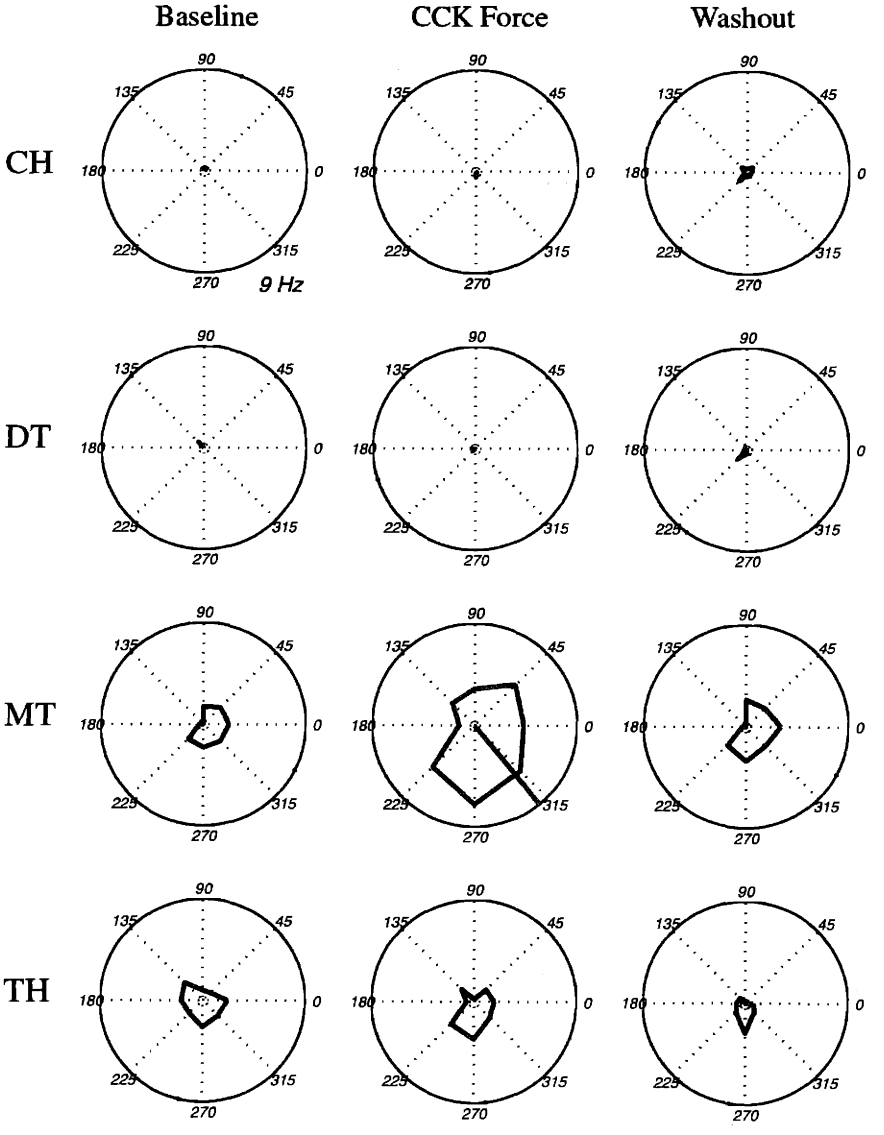
Baseline
CCK Force
Washout
CH
DT
MT
TH
90
45
0
315
270
225
180
135
9 Hz

Figure 5

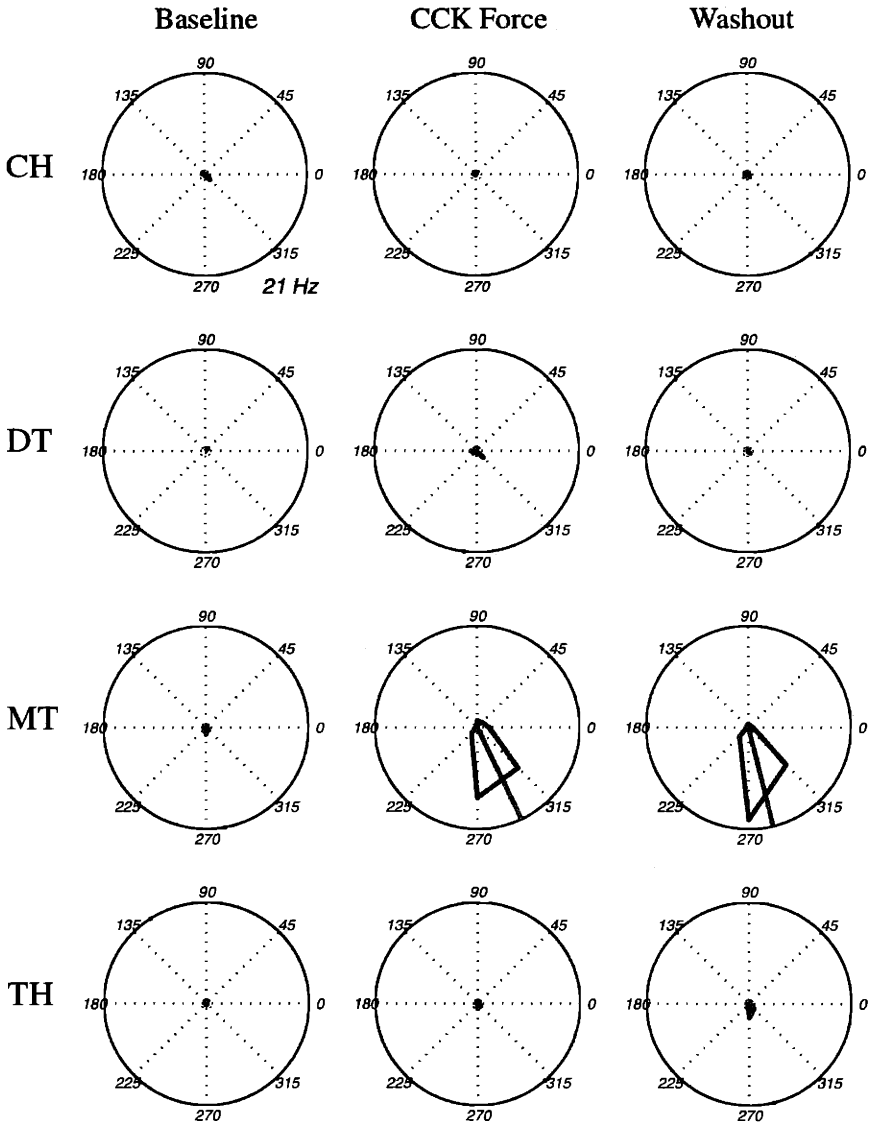
Baseline
CCK Force
Washout
CH
DT
MT
TH
90
135
45
180
0
225
315
270
21 Hz

Figure 6

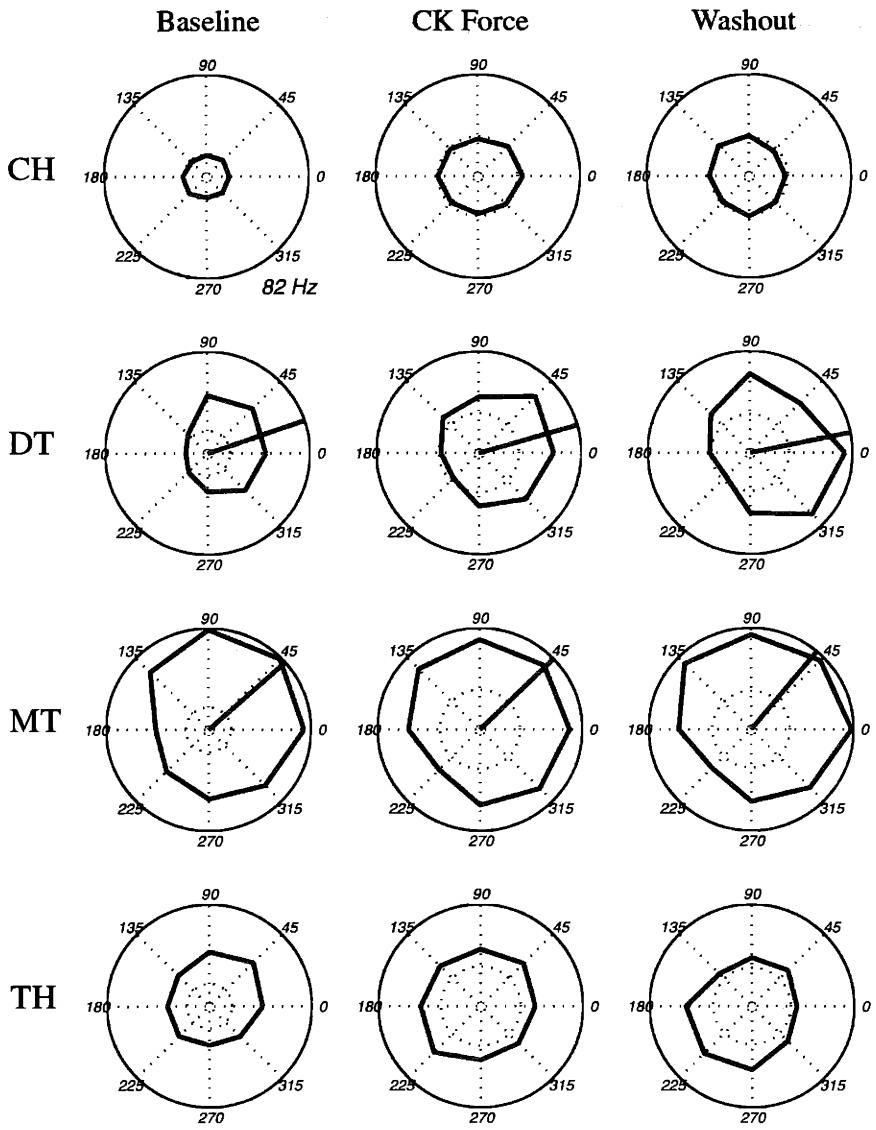
Baseline
CK Force
Washout
CH
DT
MT
TH
82 Hz
90
45
0
315
270
225
180
135

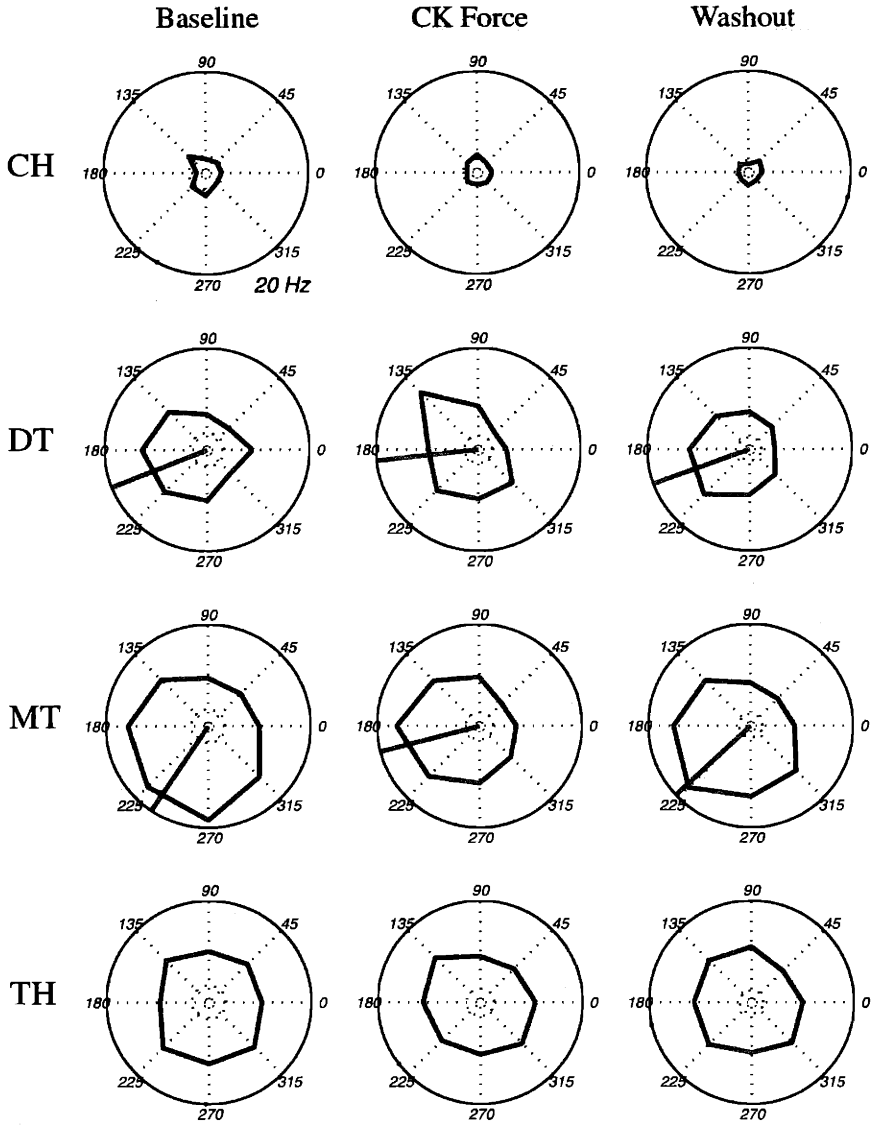
Baseline
CK Force
Washout
CH
DT
MT
TH
90
45
0
315
270
225
180
135
20 Hz

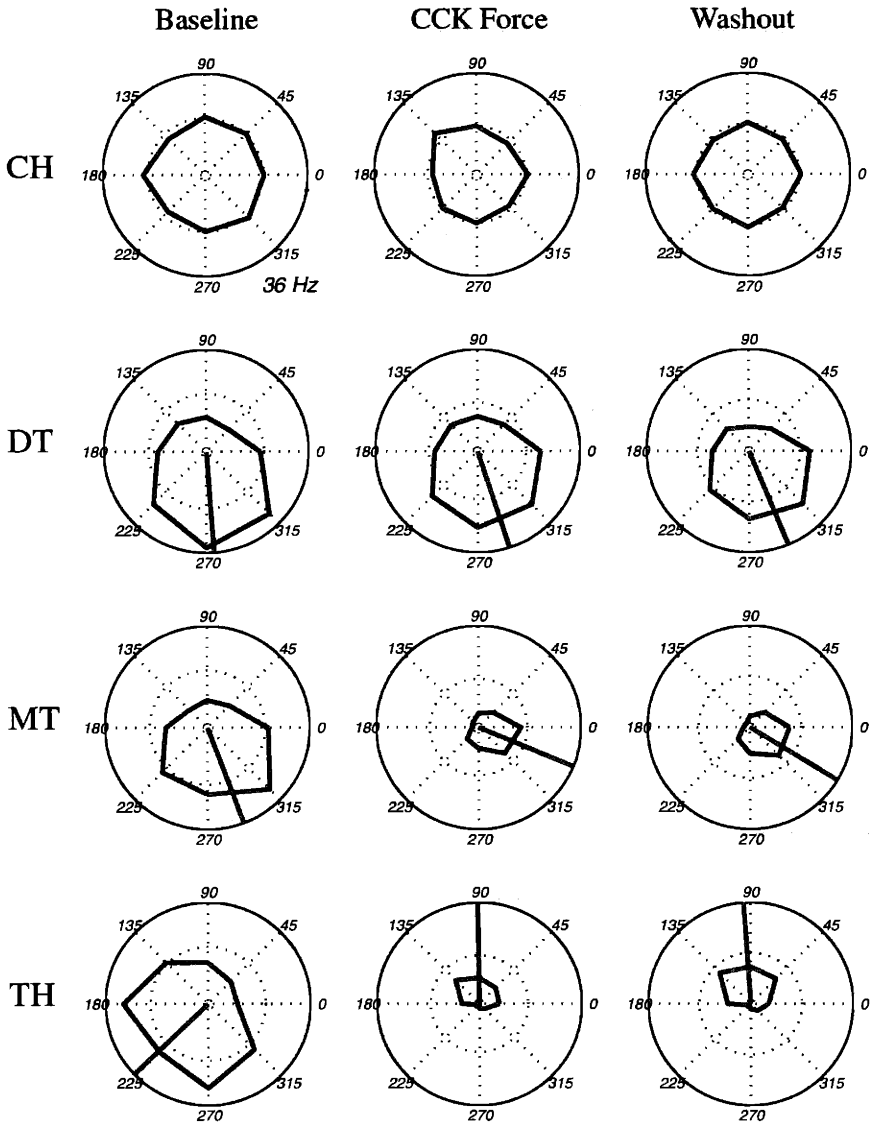
Baseline
CCK Force
Washout
CH
DT
MT
TH
90
45
0
315
270
225
180
135
36 Hz

Figure 9

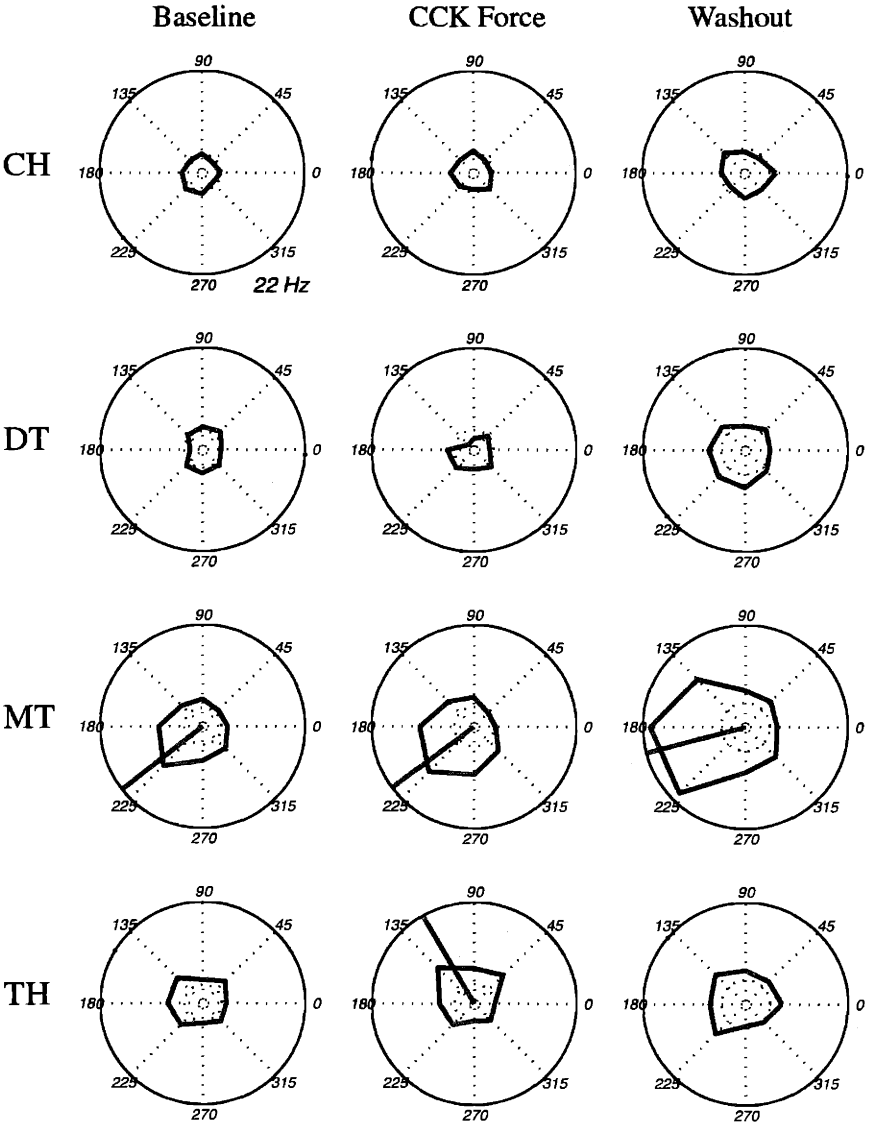
Baseline
CCK Force
Washout
CH
DT
MT
TH
90
45
0
315
270
225
180
135
22 Hz

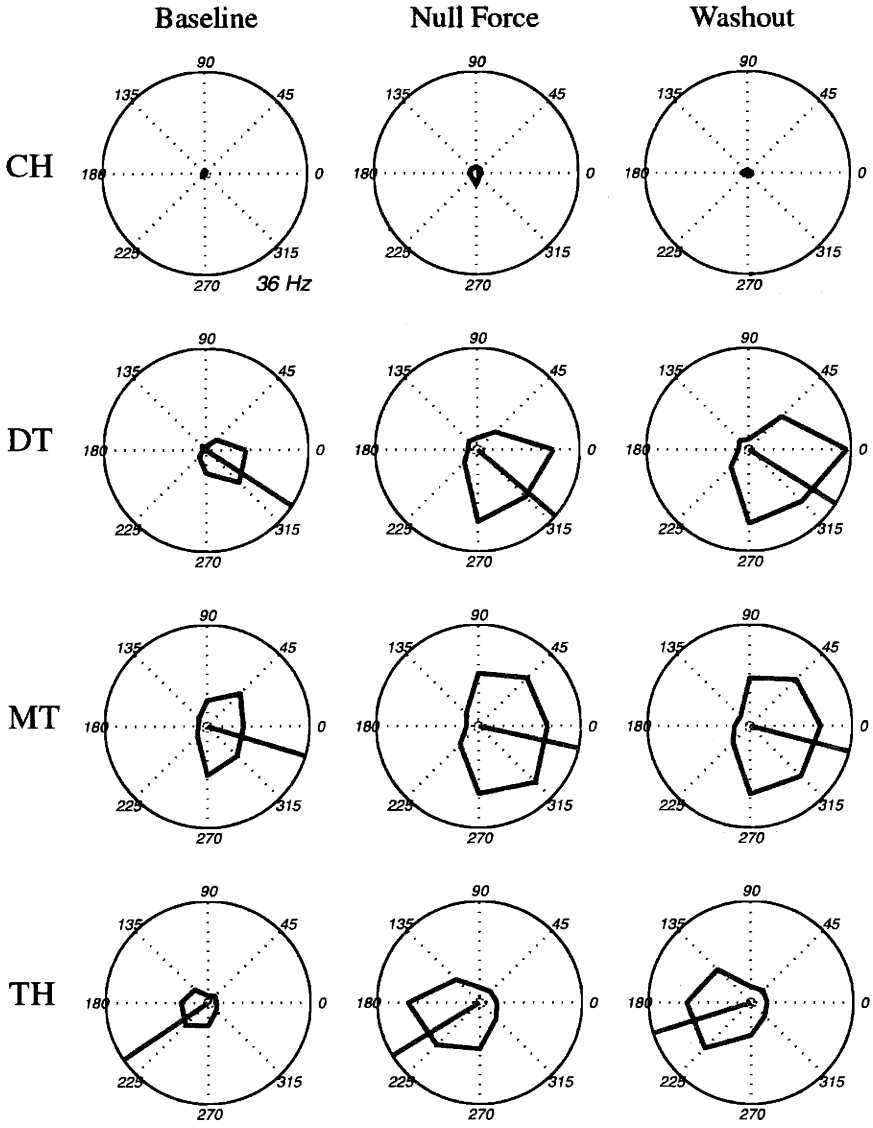
Baseline
Null Force
Washout
CH
DT
MT
TH
90
45
0
315
270
225
180
135
36 Hz

Figure 11

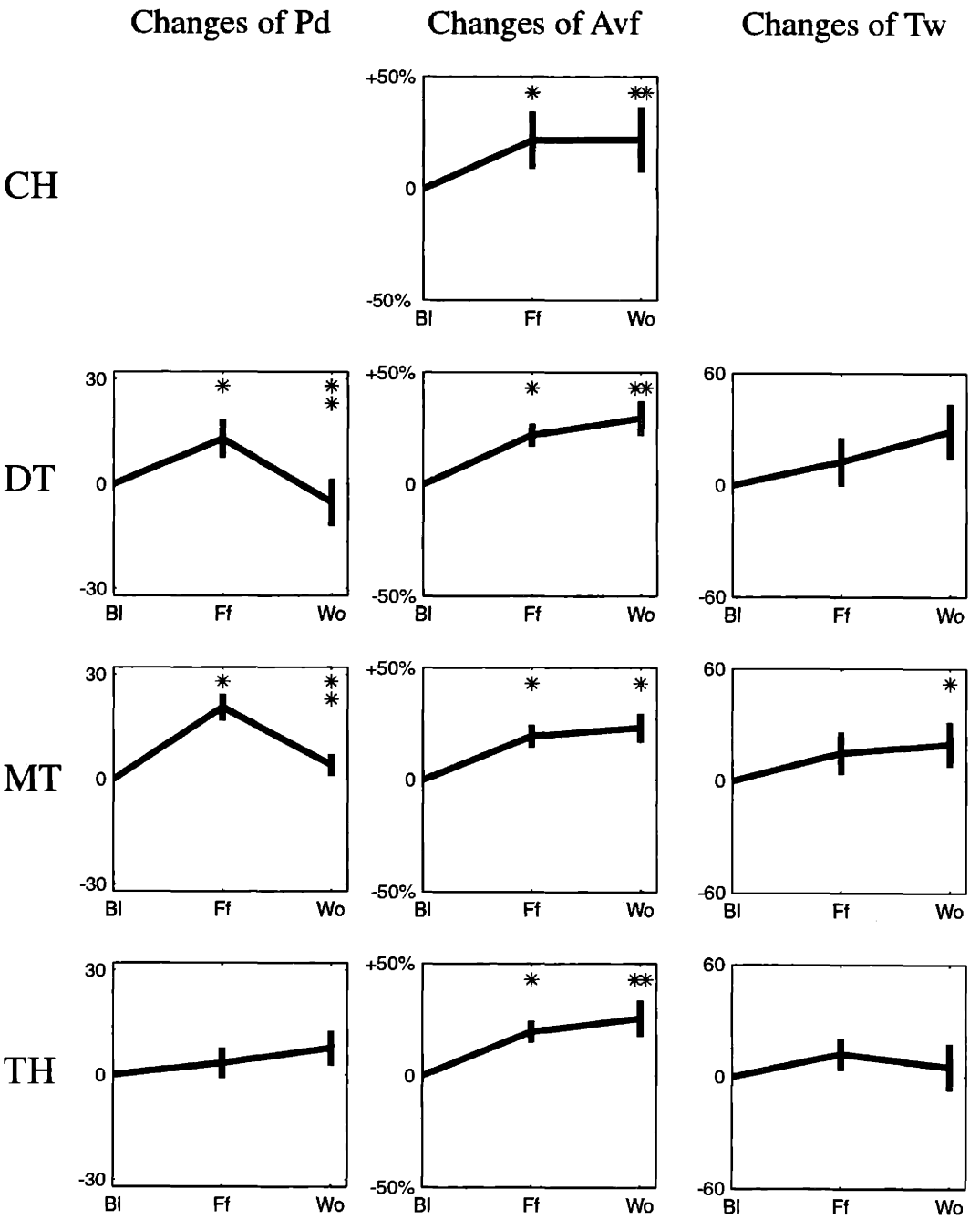
Changes of Pd
Changes of Avf
Changes of Tw
CH
DT
MT
TH
+50%
0
-50%
30
-30
60
-60
Bl
Ff
Wo

Figure 12

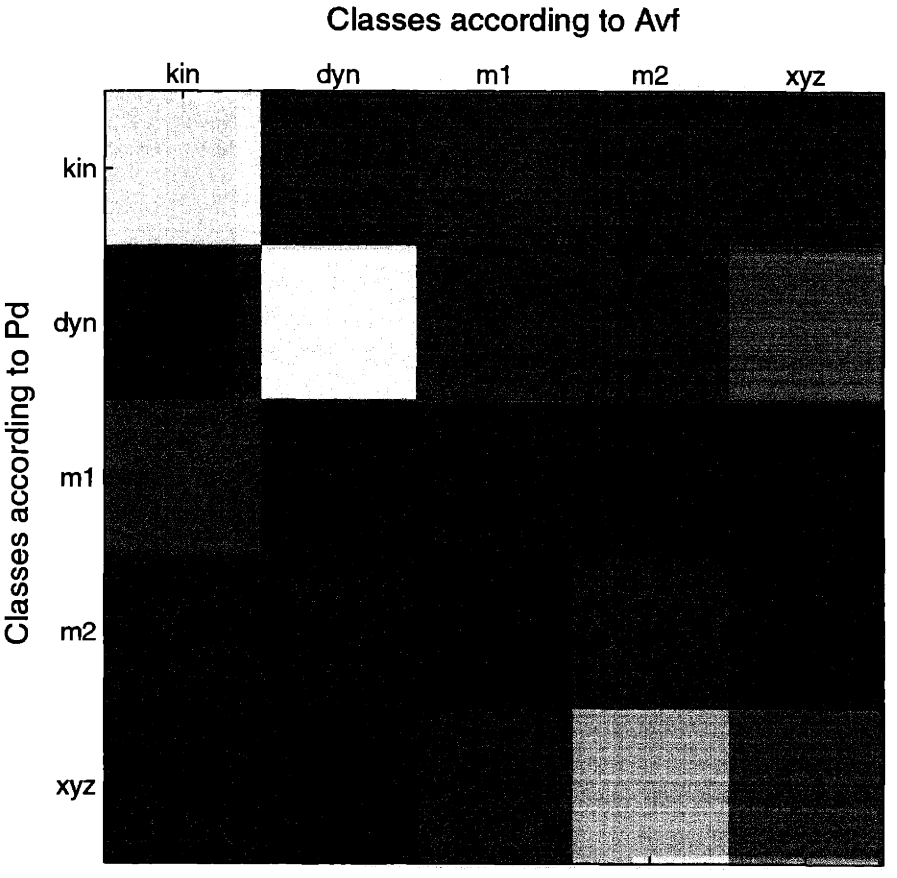
Classes according to Avf
kin
dyn
m1
m2
xyz
Classes according to Pd
kin
dyn
m1
m2
xyz

Figure 13

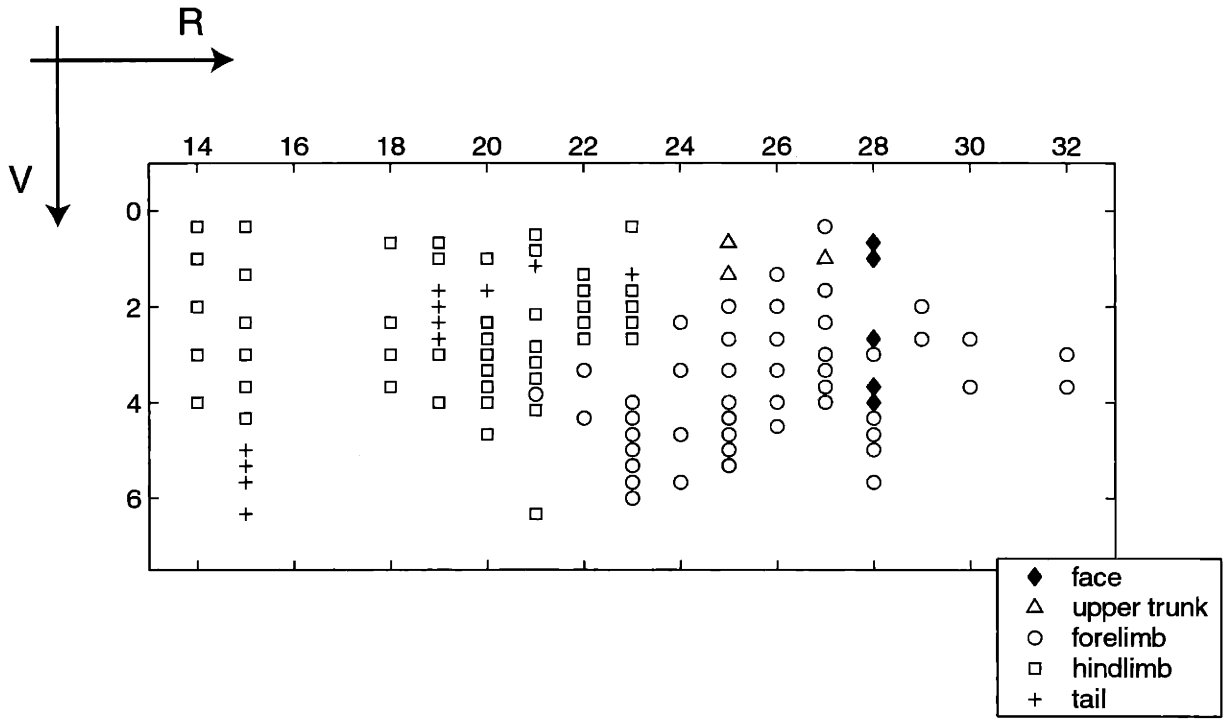
R
V
14
16
18
20
22
24
26
28
30
32
0
2
4
6
face
upper trunk
forelimb
hindlimb
tail

Chapter 5. Neuronal plasticity in the dorsal and ventral premotor areas[1]

We investigated the activity of neurons in the dorsal premotor cortex (PMd) and ventral premotor cortex (PMv) of two monkeys adapting to a novel dynamic environment (a force field). Monkeys performed visually instructed, delayed reaching movements, while holding the handle of a robotic arm. We found that during the instructed delay that followed the cue and preceded the go signal, the dynamics of the upcoming movement was reflected in the activity of neurons in PMd but not in PMv. In contrast both PMd and PMv reflected the dynamics of the movement during movement execution. Evidence of neuronal plasticity associated with the development of a new internal model for the dynamics was found in both areas, although more prominently in PMv than in PMd. These results indicate that the movement dynamics is widely represented across cortical areas.

[1] Elsewhere in the thesis, Chapter 5 is referred to as (Xiao, Padoa-Schioppa and Bizzi, in preparation).

Introduction

According to the traditional "serial" view, the "premotor" areas harbor early sensorimotor processes and funnel their output into the primary motor cortex (M1), which directly controls the execution of movements through its sub-cortical and spinal projections. With respect to M1, a long-lasting debate has been whether *during motor execution* neurons in M1 process aspects of the movement kinematics, of the movement dynamics, or both (Evarts, 1968; Thach, 1978; Georgopoulos et al., 1982; 1983; Fromm, 1983; Kettner, Schwartz and Georgopoulos, 1988; Flament and Hore, 1988; Kalaska et al., 1989; Crutcher and Alexander, 1990; Georgopoulos et al., 1992; Scott and Kalaska, 1995, 1997; Moran and Schwartz, 1999; Kakei, Hoffman and Strick, 1999; Johnson and Ebner, 2000; Todorov, 2000; Li, Padoa-Schioppa and Bizzi, 2001; Scott et al., 2001). The terms of this debate, together with the serial view of cortical motor control may explain why relatively fewer studies investigated the dynamics-related activity of neurons in areas other than M1. The past few years have however witnessed enlightening progresses.

With respect to the anatomy, two findings are mostly relevant. First, the original "premotor" Broadmann area 6 has been subdivided over the years into a number of distinct motor areas (Luppino et al., 1991; Matelli, Luppino and Rizzolatti, 1991; Luppino et al., 1993; He, Dum and Strick, 1993; 1995). Second, it was found that several of these motor areas –not only M1 –send direct projections to the spinal cord. Specifically, direct projections to the cord originate from the dorsal premotor area (PMd), the ventral premotor area (PMv), the supplementary motor area (SMA), the dorsal and ventral cingulate motor areas, and from the M1 (Dum and Strick, 1991; He, Dum and Strick, 1993; 1995). With respect to the physiology, the traditional serial view has been questioned by numerous studies that recorded the activity of neurons in multiple motor areas at the same time and consistently found extensive functional overlaps across areas (Thach, 1978; Alexander and Crutcher, 1990ab; Crutcher and Alexander, 1990; Scott and Kalaska, 1997; Scott, Sergio and Kalaska, 1997; Kakei, Hoffman and Strick, 2001; Fetz, 1992). These results lead some investigators to propose that different cortical areas contribute "in parallel" to the control of movements (Crutcher and Alexander, 1990; Dum and Strick, 1991; Prut and Fetz, 1999). Finally, with respect to the debate on M1, recent advances cast doubt on the arguments supporting the kinematic view (Todorov, 2000; Scott et al., 2001; Scott and Kalaska 1997), whereas converging data indicate that the dynamics of movement is reflected in M1 (Evarts, 1968; Thach, 1978; Fromm, 1983; Kalaska et al., 1989; Crutcher and Alexander, 1990; Georgopoulos et al., 1992; Li, Padoa-Schioppa and Bizzi, 2001).

Taken together, these results suggest that the "premotor" areas might process significantly later computations than previously thought. More specifically, we hypothesized that the movement dynamics may be processed in all cortical areas that send direct projections to the cord. Some previous work on isometric activity supports this hypothesis for the PMd (Werner, Bauswein and Fromm, 1991) and the for PMv (Hepp-Reymond et al., 1994, 1999). In addition, dynamics-related (or load-dependent) activity was described in the SMA (Crutcher and Alexander, 1990), the putamen (Crutcher and Alexander, 1990), and the dentate and interpositus nuclei of the cerebellum (Thach, 1978). In contrast, no dynamics-related activity was found in area 5 (Kalaska et

al., 1990), which lacks direct projections to the cord. In the present study, we extend the investigation of the dynamics-related activity in the PMd and PMv in three respects. First, we recorded the neuronal activity before and during full reaching movements. Second, we recorded the plastic changes associated with the acquisition of a new internal model for the dynamics. Third, we recorded from both the PMd and the PMv, and from the SMA and the M1 in parallel experiments. Here we show that neurons in the PMd process the dynamics of the upcoming movement during motor planning. In this respect, the PMd shares properties characteristic of the SMA. In contrast, during motor planning the PMv and the M1 are essentially silent. In addition, we show that during motor execution both the PMd and the PMv reflect the dynamics of the movement. Finally, with respect to the development of a new internal model, we show that plastic occur in both the PMd and the PMv, though in different proportions (more in the PMv than in the PMd). In conclusion, our results argue against a strictly serial view, because processing of the movement dynamics is widely present across several cortical areas. However, they also argue against a strictly parallel view, because clear areas clearly differ for the timing of their activation.

Methods

The experimental setup, recording techniques and data analysis were essentially the same previously described (Li, Padoa-Schioppa and Bizzi, 2001), with minor differences.

Behavioral paradigm

Two young female rhesus monkeys (R and N), weighting 5-5.5 Kg, participated in the experiment. The monkeys sat on a chair in an electrically isolated enclosure. With their right arm, they grab the handle of a two degrees of freedom robotic arm (the manipulandum). The manipulandum allowed free movements limited to a horizontal plane. A computer monitor, placed vertically 75 cm in front of the monkeys, indicated the position of the handle (3x3-mm square, ca 0.2° of visual angle) and the targets of the movements (12x12-mm squares, ca 1° of visual angle). All reaching movements were from a central location to one of eight peripheral targets, equally spaced along a circle and 45° apart from each other. Actual reaching movements were 6 cm in length.

The monkeys performed an instructed delayed reaching task. In each trial, the center square appeared on the screen. The monkeys acquired the center square (beginning of the trial), and waited for further instruction for 1 sec. One peripheral square then appeared on the screen (the *cue*), indicating the target of the reaching movement. Monkeys had to maintain the cursor still in the center target for a delay period of randomly variable duration (1.1-1.9 sec). At the end of the delay, the center square was extinguished (*go* signal), prompting the monkeys to move. Monkeys had to acquire the peripheral target within 1.8 sec, and to maintain the cursor within the peripheral square for an additional 1 sec to receive a juice reward (*rew*). After an inter-trial interval (*iti*) of 1 sec, the sequence started over again. During the movement, the monkeys had to maintain the trajectory within an angle of 60° on both sides of the straight line passing through the center and the peripheral square. The trial was immediately aborted if the monkey made an error, and another trial started, after the *iti*. Peripheral targets were pseudo-randomly chosen.

Two motors attached at the base of the robotic arm allowed to turn force fields on and off. In the experiment, we used one of two force fields, described by **F=BV**, where **B** is an anti-diagonal 2x2 rotation matrix **B**=[0, -b; b, 0] and **V** is the instantaneous velocity vector. Thus, the forces were in strength proportional to the velocity (viscous) and in direction orthogonal to the velocity (curl). Depending on the sign of "b", this defines one of two force fields, clockwise (CK) or counterclockwise (CCK). For the intensity of the forces, we used b=0.07. In each experimental session, the monkeys performed in three subsequent behavioral epochs: Baseline (no force, ca 160 trials), Force epoch (ca 160 trials), Washout (no force, ca 160 trials). In the Force epoch, one of the two force fields (CK or CCK) was introduced. The same timing and spatial constraints were maintained throughout the session.

During the training (4-6 months), the monkeys were only exposed to the non-perturbed conditions. The force fields were introduced only during the recordings. In total, monkey R performed in 28 and 27 sessions with the CK and CCK force fields, respectively. Monkey N performed 4 and 5 sessions with the CK and CCK force fields, respectively. For both monkeys, sessions with the two force fields were interspersed.

Surgery, microstimulation and gross anatomy

Before the training, and under aseptic stereotaxic surgery, we implanted a head-restraining device on the skull of the monkeys. At the end of training, we performed a second aseptic stereotaxic surgery and implanted a recording chamber (18 mm, inner diameter) over the left hemisphere. For both monkeys, we centered the chambers on (A=16, L=-15). During the surgery, we could clearly observe the genu of the arcuate sulcus. After surgery, the monkeys were given antibiotics and pain medications.

Before the first recording session and at the end of several recording sessions, we performed electrical microstimulation. We used a train of 20 biphasic charge balanced pulse pairs (pulse width=0.1msec, train duration=60 msec), delivered at 330 Hz and variable amplitude (20-120 μ Amp). Recording were concentrated in areas were arm movements could be elicited.

Both monkeys were euthanized at the end of the experiment. They were given an overdose of pentobarbital sodium and then perfused transcardially with heparinized saline, followed by buffered Formalin. The recording locations were marked with electrodes dipped in black ink. The brain was then removed from the skull, and photographed. The NIH guidelines for the use and care of animals in laboratory were followed throughout the experiments.

Recordings

The recording procedures were that previously described (Padoa-Schioppa, Li and Bizzi, in preparation). The trajectories (position and velocity) were recorded at the frequency of 100 Hz. For the neuronal recordings, vinyl-coated tungsten electrodes (1-3 MΩ impedance) were manually advanced with a set-screw system (approximate depth resolution of 30 μm). Electrical signals were acquired, passed through a head stage (AI 401, Axon Instruments) and an amplifier (Cyberamp 380, Axon Instruments), filtered (high and low cutoffs of 10 kHz and 300 Hz, respectively), and displayed on a computer monitor (sampling frequency of 20 kHz) using a commercial software (Experimenter's WorkBench 5.3, DataWave Technology). Action potentials –detected by threshold

crossing –were saved to disk (waveforms of 1.75 msec duration) for subsequent analysis. Eight electrodes were used in each recording session. No effort was made to locate the cortical layer of the recordings.

Data analysis: psychophysics

For each movement, we defined the movement onset (*mo*) and the movement end (*me*) with a threshold-crossing criterion (4 cm/sec) on the speed. The psychophysics was analyzed using a correlation coefficient (CC), as previously described (Shadmehr and Mussa-Ivaldi, 1994; Li, Padoa-Schioppa and Bizzi, 2001). The CC is a measure of similarity between the speed profile of an actual trajectory and an ideal speed profile. Its values range between –1 and +1, and are close to +1 when the actual speed profile is close to ideal.

In order to compare the neuronal activity across trials with similar kinematics, we disregarded the first four successful trials in each movement direction. Only the remaining trials were considered for further analysis. One of the aims of the experiment was to investigate the neuronal activity related to the movement dynamics during the instructed delay (see below). No time constraints on the reaction time (RT) were imposed during the experiment. In the analysis of the delay activity we excluded anticipated movements (RT<200 msec) as well as outliers (RT>500 msec). Only the remaining trials (>89%) were considered for subsequent analysis.

Data analysis: neurons

The clustering was performed using either a custom-written software (described in Li, Padoa-Schioppa and Bizzi, 2001), or a commercially available software (Autocut 3, Datawave Technology). In both cases, waveforms were visually inspected for stability and only cells with convincingly consistent waveform throughout the session were considered for further analysis.

We considered the neuronal activity of single neurons in 4 separate time windows: the center hold time (CH, *cue*-500 msec to *cue*); the delay time (DT, *go*-500 msec to *go*); the movement time (MT, *mo*-200 msec to *me*); the target hold time (TH, *rew*-500 msec to *rew*). For each neuron and for each time window, the activity was separately analyzed in the Baseline, Force epoch and Washout. For each epoch, we averaged the activity across trials, and obtained a tuning curve. We defined three parameters to characterize the tuning curves. The preferred direction (Pd) was defined as the direction of the vector average of the eight activity vectors. The average firing frequency (Avf) was defined as the scalar average of the neuronal activity across the eight directions. The tuning width (Tw) was defined as the angle over which the firing frequency was higher than half of the maximal neuronal activity among the eight directions (maximum of the tuning curve). The parameters were defined subject to the following pre-conditions. First, only tuning curves with an Avf>1Hz were considered. Second, the Pd and Tw were only defined for tuning curves displaying a significantly unimodal distribution across directions, as stated by the Rayleigh test ($p<0.01$, see Fisher, 1993, p70). Third, the Tw was only defined for strictly unimodal cells, for which the directions with firing frequency higher than half the maximum were continuous.

Classification of cells

For each parameter, significant changes across epochs were stated using an error-propagation procedure previously described in detail (Li, Padoa-Schioppa and Bizzi, 2001). We used a significance threshold of $p<0.05$. Cells were divided in classes depending on the changes across behavioral epochs and separately for the three parameters. With respect to the changes of Pd, we named "kinematic" cells that maintained their Pd unchanged across epochs (*x-x-x*). Cells whose Pd changed in the Force epoch compared to Baseline and returned to the original orientation in the Washout (*x-y-x*) were named "dynamic" cells, because the dynamics of the movement were the same in the Baseline and the Washout, but different in the Force epoch. Cells whose Pd changed in the Force epoch and remained in the Washout in their newly acquired orientation (*x-y-y*) were named "memory I," because they appeared to keep trace of the adaptation experience after the monkey had re-adapted to the non-perturbed conditions. A complementary group of cells, whose Pd did not change in the Force epoch but changed in the Washout (*x-y-y*) were named "memory II" cells. Finally, cells whose Pd changed in the Force epoch and again in the Washout (*x-y-z*) were named "other" cells. The same classification criteria were applied for the changes of Avf and Tw.

Neurons were separately classified for the changes observed in different time windows. Thus, single cell could be classified as "kinematic" in the DT and as "dynamic" in the MT. To compare the results of different classifications, we analyzed the 5x5 contingency table where the element n_{ij} equals the number of cells classified as "*i*" and "*j*" in the two time windows, respectively. In particular, we studied the matrix χ^2_{ij} such that Pearson's χ^2 is given by $\chi^2 = \sum_{i,j} \chi^2_{ij}$ (Freeman, 1987). To investigate whether classifications according to different parameters coincided more frequently than expected by chance, we studied the trace $Tr = \sum_{i=j} \chi^2_{ij}$ (for details, see Padoa-Schioppa, Li and Bizzi, in preparation). Using a similar approach, we compared the classifications obtained for different areas.

Results

Psychophysics

The present study confirms the psychophysical results previously described for monkeys (Gandolfo et al., 2000; Li, Padoa-Schioppa and Bizzi, 2001) and humans (Shadmehr and Mussa-Ivaldi, 1994). In absence of external perturbation, the hand trajectories are essentially straight, with bell-shaped speed profiles. When the force field is introduced, trajectories are initially deviated, and gradually return straight as the monkeys adapt to the external force field. This convergence suggests that the desired kinematics remains unchanged and that the monkey develop a new internal model for the dynamics to implement that desired kinematics (Shadmehr and Mussa-Ivaldi, 1994). When the force is removed, the monkeys show a transient aftereffect, and rapidly re-adapt to the non-perturbed conditions. The process of adaptation (or short-term learning) can be quantified with the correlation coefficient (CC). Typically, the CC is high in the Baseline, drops early in the Force epoch, and gradually recovers in the Force epoch, temporarily drops

early in the Washout, and readily returns to the initially high values. Over sessions, the adaptation becomes faster (fewer trials to plateau) and better (higher plateau), indicating a process of long-term learning (Li, Padoa-Schioppa and Bizzi, 2001). In the present study sessions with the two force fields were intermixed. As shown in Figure 1, we found evidence of long-term learning.

We did not record the electromyographic (EMG) activity of the two monkeys used for the present study. However, we recorded the EMG of other monkeys performing in the same task (Li, Padoa-Schioppa and Bizzi, 2001; Padoa-Schioppa, Li and Bizzi, submitted), and other recordings were also done in humans (Thoroughman and Shadmehr, 1999; Shadmehr and Moussavi, 2000). Curl force fields impose a shift onto the preferred direction (Pd) of single muscles in the Force epoch compared to the Baseline. Importantly, the Pd of all the muscles shifts in the direction of the external force, independently of their initial Pd. In the Washout, the Pd of muscles shifts back to that observed in the Baseline. The shift of Pd is essentially due to the vector sum of the internal (muscular) force with the force exerted by the manipulandum (for an heuristic argument, see Li, Padoa-Schioppa and Bizzi, 2001; for a more realistic model, see Thoroughman and Shadmehr, 1999). In monkeys, we found that the Pd of muscles shifts on average by 18-20° in the Force epoch compared to Baseline. Other researchers predicted and observed an analogous shift of Pd in humans performing the same task. Reflected in the activity of neurons, the shift of Pd can be regarded as a fingerprint of the new dynamics (see also discussion in Li, Padoa-Schioppa and Bizzi, 2001).

Neuronal database

In total, we recorded the activity of 142 PMd cells and 143 PMv cells (Figure 2). Each cell was separately analyzed in the four time windows CH, DT, MT and TH and in the three epochs Baseline, Force epoch and Washout.

Directional tuning

The percentages of directionally tuned cells for the PMd are shown in Table 1. As expected, a negligible percentage of cells passed the tuning test in the CH. Considering the Baseline, in the DT 41% of cells in PMd are directionally tuned. The number of directionally tuned cells increases only slightly in the MT, to 47% of cells. In contrast, fewer cells are tuned in the TH (22%). Table 2 shows the corresponding percentages for the PMv. It can be observed that for both areas the highest percentage of directionally tuned cells is observed in the MT. The most important difference between the two areas is that in the DT there are many more directionally tuned cells in PMd than in PMv. In other words, considering the entire population, the PMd engages in the task at an earlier time than PMv. Considering the percentages of directionally tuned cells in the Force epoch and in the Washout strengthens these observations.

We also analyzed the circular distributions of preferred direction (Pd), separately for the three time windows (DT, MT and TH) and for the three epochs (Baseline, Force epoch and Washout). For the PMd, the distributions of Pd are shown in Figure 3a. Circular statistics indicated that the distribution was homogeneous in all three time windows and all three behavioral epochs (minimal $p>0.015$, Rayleigh test). We repeated the same analysis for the PMv (Figure 3b). Again, we found that the distribution of Pd

were homogeneous in all three time windows and all three epochs (minimal $p>0.035$, Rayleigh test).

Dynamically-tuned cells, tune-in cells, and tune-out cells

As the monkeys adapted to the force field, the activity of the cells modified. In particular, we observed a group of cells that were initially not tuned in the Baseline, became tuned in the Force epoch, and lost their tuning again in the Washout. We also observed other cells that were originally tuned in the Baseline, lost their tuning in the Force epoch, but regained their tuning in the Washout. These two groups of cells, which appeared *dynamic* in nature, were named "dynamically-tuned" cells. Figure 4a-b illustrates two examples of dynamically-tuned cells recorded in the PMd (the activity refers to the MT). In total, we found that the group of dynamically-tuned cells accounted for 14% of cells in the PMd, and for 10% of cells in the PMv (MT activity).

We also found a group of cells whose changes outlasted the exposure to the perturbation. "Tune-in" cells were initially not tuned in the Baseline, and acquired a directional tuning in the Force epoch following adaptation to the perturbing force. In the Washout, however, tune-in cells maintained their newly acquired directional tuning. Tune-in cells, which appeared *memory* in nature, were found in PMd and PMv, in different proportions. One example of tune-in cell recorded in the PMv with a CCK force field is shown in Figure 5a. In total, the group of tune-in cells accounted for 16% of PMd cells, and for 15% of PMv cells.

We also observed a group of "tune-out" cells. Tune-out cells were originally tuned in the Baseline, but lost their tuning in the Force epoch, and remained non-tuned in the Washout. One example of tune-out cell recorded in the PMv with a CK force field is shown in Figure 5b. In total, the group of tune-out cells accounted for 14% of PMd cells, and for 25% of PMv cells.

We compared the incidence of dynamically-tuned, tune-in and tune-out cells recorded in the PMd and PMv with that recorded in the SMA and M1 by analyzing the 4x4 contingency table (4 areas x 4 groups; groups: dynamically-tun; tune-in; tune-out; tuned-throughout). In general, different areas were not homogeneous ($\chi^2=50.85$; d.o.f.=9; $p<10^{-7}$). In particular, we found significantly more dynamically-tuned cells in the PMd than in the other areas (decomposed $\chi^2=6.53$; d.o.f.=1; $p<0.02$). We also found significantly fewer tune-out cells in the PMv than in the other areas (decomposed $\chi^2=13.34$; d.o.f.=1; $p<10^{-3}$).

PMd, Changes of Preferred direction: DT

We classified cells into the classes kinematic, dynamic, memory I, memory II, and "other," separately for each of the three time windows (DT, MT, TH), and for each of the three parameters (Preferred direction, Average firing frequency, and Tuning width). With respect to the Preferred direction (Pd), we classified only cells that showed a consistent directional tuning throughout the three behavioral epochs (Baseline, Force epoch, and Washout).

Considering the PMd with respect to the delay activity (DT), the vast majority of cells was either kinematic or dynamic (38% and 41%, respectively). Figure 6a shows an example of kinematic cell recorded in the PMd with a CK force field. The Pd of the cells remains essentially unchanged across epochs. The cell shown in Figure 6b was recorded

with a CK force field and was classified as dynamic according to its changes of Pd. In the Force epoch, the Pd shifts in the CK direction (i.e., the direction of the external force). In the Washout the Pd shifts back to its original direction.

In total, 34 PMd cells could be classified in the DT. Of these, 38% were kinematic, 41% were dynamic, 12% were memory I, and 9% were memory II. This PMd population is shown in a scatter plot in Figure 7a. The x-axis indicates the shift of Pd in the Force epoch compared to Baseline, and the y-axis indicates the shift of Pd in the Washout compared to the Force epoch. Positive values correspond to shifts in the direction of the external force. Each symbol represents one cell, and cells are color-coded according to their class. Kinematic cells (black), whose Pd does not change across epochs, lie close to the origin of the axes. Dynamic cells (blue), while Pd shifts in one direction in the Force epoch (positive x-axis for shifts in direction of the external force), and in the opposite direction in the Washout, lie one the diagonal through the second and fourth quadrant. Memory I cells (green), whose Pd changes on the Force epoch but not in the Washout, lie on the x-axis. In contrast, memory II cells lie on the y-axis: their Pd does not change in the Force and changes in the Washout.

We quantified the shift of Pd for the entire PMd population. For each cell exhibiting a directional tuning in both the Baseline and the Force epoch we computed the shift of Pd. We then averaged the shifts across the entire population. On average, the PMd population showed a shift of Pd of 11.0° in the direction of the external force in the Force epoch compared to Baseline. This shift reached significance level in the DT ($p<0.05$, *t*test), indicating that during motor planning neurons in the PMd process the dynamics of the upcoming movement. Comparing the Pd in the Washout with that in the Force epoch, we observed the opposite trend, as the Pd of cells in PMd significantly shifted in the direction opposite to the previously experienced force field (mean shift = -8.5°, $p<0.05$, *t*test). No significant shift was observed comparing the Pd in the Washout with that in the Baseline (mean shift = -2.7°, $p=0.5$, *t*test).

PMv, Changes of Preferred direction: DT

Of the 150 neurons recorded in the PMv, only 9 neurons were directionally tuned in the DT consistently in all three epochs (Baseline, Force epoch, and Washout) and could therefore be classified according to their changes of Pd. Of these 9 neurons, 6 (67%) neurons were classified as kinematic, 1 (11%) neuron was classified as dynamics, and 1 (11%) neuron was classified as memory I. All the percentages relative to the classification of PMv neurons are reported in Table 5. Considering the entire PMv population, we observed no significant shift of Pd in the delay in the Force epoch compared to Baseline (mean shift = -3.1°, $p=0.8$, *t*test). Likewise, no shift of Pd was observed in the Washout compared either to the Force epoch (mean shift = 0°, $p=1$, *t*test) or to the Baseline (mean shift = -6.6°, $p=0.6$, *t*test).

PMd, Changes of Preferred direction: MT

Figure 8a-d shows the movement-related (MT) activity of a kinematic, a dynamic, a memory I, and a memory II cells recorded in the PMd. For the kinematic cell (Figure 8a), the Pd is essentially constant across epochs. For the dynamic cell (Figure 8b), recorded with a CCK force field, the Pd shifted in the direction of the external force in the Force epoch compared to the Baseline. In the Washout, the Pd shifted back to the original

direction. The cell shown in Figure 8c is an example of memory I cell, recorded with a CCK force field. The Pd of the cell shifts in the direction of the external force in the Force epoch compared to Baseline, and remains shifted in its new direction in the Washout. The memory II cell shown in Figure 8d shows a complementary pattern. In the Force epoch, where a CK force field was introduced, the Pd of the cell remained unchanged. In the Washout, however, the Pd shifted in the direction opposite to the previously experienced force field (i.e., the Pd sifts CCK).

A total of 37 PMd cells could be classified according to their changes of Pd in the MT time window. In particular, we found 8 (22%) kinematic cells, 16 (43%) dynamic cells, 4 (11%) memory I cells, 5 (14%) memory II cells, and 4 (11%) "other" cells. The changes of Pd for this population are shown in the scatter plot in Figure 7b.

We then considered the shift of Pd for the entire population is the MT time window. Most importantly, we found a significant shift of Pd in the direction of the force field in the Force epoch compared to Baseline (mean shift = 11.0°, $p<0.04$, *t*test). In other words, as the monkeys adapted to the perturbation, the neurons in their PMd consistently shifted their Pd in the direction of the external force. Comparing the Washout with the Force epoch, we found a significant shift of Pd in the opposite direction (mean shift = -14.0°, $p<0.02$, *t*test). These two shifts were of comparable magnitude, and no significant shift was observed comparing the Washout with the Baseline (mean shift = -6.0°, $p=0.09$, *t*test).

PMv, Changes of Preferred direction: MT

A total of 26 PMv could be classified according to their changes of Pd in the MT time window. As summarized in Table 5, we found that 35% of PMv cells were kinematic, 19% were dynamic, 8% were memory I, 23% were memory II and 15% were "other". Considering the entire population, we found a significant shift of Pd in the Force epoch compared to the Baseline. As was observed for the PMd, for the M1 and for the muscles' EMG, the shift of Pd occurred in the direction of the external force. On average over the PMv population, we found a shift of 11.5° ($p<0.03$, *t*test). In the Washout, the Pd of the PMv population shifted back in the direction opposite to the previously experienced force field, by –19.0° ($p<0.01$, *t*test) on average. We found no significant shift of Pd when comparing the Washout with the Baseline (mean shift 11.7°, $p=0.2$, *t*test). The changes of Pd for the PMv population are summarized in Table 6.

PMd, Changes of Preferred direction: TH

Only a limited population of PMd cells (16 cells) could be classified in respect of the changes of Pd in the target hold time (TH). Of these, the vast majority was kinematic (56%), as exemplified by the cell shown in Figure 9. The scatter plot in Figure 7c shows the entire population. The percentages of cells in the various classes are also summarized in Table 3, for the three time windows DT, MT, and TH.

Considering the entire population in the TH, we found no significant shifts of Pd across epochs (minimal $p=0.1$, *t*test). The shifts of Pd for the relevant PMd populations relative to the DT, MT and TH time windows are also shown in the histograms displayed in Figure 10 and summarized in Table 4.

PMv, Changes of Preferred direction: TH

A total of 8 PMv neurons could be classified according to their changes of Pd in the TH. Of these, 6 (63%) neurons were classified as kinematic. The shifts of Pd for the relevant PMv populations relative to the DT, MT and TH time windows are also shown in the histograms displayed in Figure 11 and summarized in Table 5.

Changes of Average firing rate in PMd and PMv

We analyzed the changes of average firing rate (Avf) both at the single cell level and for the neuronal populations of PMd and PMv. In general, a consistent result was that the Avf increased in the Force epoch compared to the Baseline, and did not change in the Washout compared to the Force epoch. This could be observed both at the single cell and at the population level, in both PMd and PMv.

Single cells were classified into the kinematic, dynamic, memory I and II, and "other" classes. We found that the different classes of cells were present in all time windows in both epochs and both areas. In general, we observed high percentages of "other" cells, compared to what found by classifying cells according to the Pd and Tw. The percentages for PMd and PMd, for all time windows (DT, MT and TH) are summarized in Table 3 and Table 5, respectively.

Considering the entire population, we observed a higher activity in the Washout than in the Baseline. This result was consistent for all time windows (CH, DT, MT, and TH) and in both PMd and PMv. The PMd and PMv population changes of Avf across epochs are summarized in Table 4 and Table 6, respectively.

Changes of Tuning width in PMd and PMv

Only small numbers of single cells could be classified according to the changes of Tw, because of the relatively strict criteria imposed as pre-condition. Nonetheless, we could observe all classes of cells in the MT time window, in PMd. For example, Figure 8b shows the MT activity of a PMd cell, recorded with a CCK force field. According to the changes of Tw, the cell is dynamic. The Tw increases in the Force field compared to the Baseline, and return to approximately the original value in the Washout. This cell is also dynamic in respect to the changes of Pd.

In Tables 3 and 5, we report the percentages of PMd cells and PMv cells found in the different classes for the DT, MT and TH time window. Considering the neuronal population, we observed in the PMd a significant increase of Tw in the Force epoch compared to Baseline (mean increase = 22°, $p<0.03$) in the MT time window. The Tw increased further in the Washout. As summarized in Table 4 for the PMd, we did not observe other consistent changes of Tw in the other time windows. Likewise, no consistent changes of Tw were observed in the population of PMv, as summarized in Table 6.

Consistency of classification across time windows

We studied the consistency of classification across time windows. With respect to the changes of Pd, however, we had too few cells classified both in the DT and the MT (17 cells and 4 cells in the PMd and PMv, respectively) to do this analysis.

With respect to the changes of Avf, we found that the classification across time windows often coincided, though such consistency did not reach significance level. This

result was found in both the PMd and the PMv. More precisely, considering for the PMd the 5x5 contingency matrix given by the classification of cells in the DT and MT time windows, we obtained for the Pearson's $\chi^2 = 23.18$ (d.o.f.=16, p=0.11) and for the trace $Tr = 8.22$ (d.o.f.=4; p=0.08). However, considering the contingency matrix given by the CH and MT time window, we obtained a significant effect for both the Pearson's $\chi^2 = 30.54$ (d.o.f.=16, p<0.02) and for the trace $Tr = 14.95$ (d.o.f.=4; p<0.005). Similar significant coincidence effects were observed when we combined the DT with the CH, the MT with the TH, and the DT with the TH.

Considering for the PMv the changes of Avf in the DT and MT time windows, we obtained a significant effect both for the Pearson's $\chi^2 = 43.71$ (d.o.f.=16, p<0.001) and for the trace $Tr = 22.66$ (d.o.f.=4; p<0.001). Similar significant coincidence effects were observed when we combined all the other possible pairs of time windows (CH and DT, CH and MT, DT and TH, MT and TH, CH and TH)

We did not perform this analysis for the changes of Tw, because too few cells could be considered in both the DT and MT time windows (8 cells and 0 cells in the PMd and PMv, respectively).

Topographical distribution of cell classes

We investigated whether the different classes of cells appeared topographically distributed on the surface of the brain. In particular, we analyzed the classification operated according to the shift of Pd. We did not find any obvious topographical organization, as cells of different classes were often recorded from the same location.

Discussion

The curl force fields used in the experiments impose on the preferred direction (Pd) of muscles a consistent shift toward the direction of the external force. In previous studies, we observed that the Pd-shift of muscles is matched by analogous Pd-shifts of neurons in the primary motor cortex (M1) and supplementary motor area (SMA), indicating that neurons in these areas process the dynamics of movements. Likewise in the present study, we used the shift of Pd to detect the dynamics-related activity of neurons in the PMd and PMv. We investigated two complementary issues. First, how the dorsal and ventral premotor areas (PMd and PMv) process the dynamics of the movement. Second, how neurons in the PMd and PMv modify their activity patterns when subjects learn a new internal model for the dynamics.

One important result of the study is that neurons in the PMd shift their Pd *during motor planning* (prior to the *go* signal). Significant shifts in the DT are observed both at the level of single cells (53% of neurons) and at the level of the population (mean shift 10.4°, p<0.05). In other words, during motor planning neurons in the PMd process the dynamics of the upcoming movement. In this respect, the PMd share properties characteristic of the SMA (Padoa-Schioppa, Li and Bizzi, submitted). In contrast, little neuronal activity is recorded in M1 and PMv during the DT, and no significant shifts of Pd are observed.

With respect to the neuronal activity *during motor execution*, we found that the dynamics of movements is reflected in both PMd and PMv. Significant shifts of Pd are

observed both for single cells (65% and 43% of cells in PMd and PMv, respectively) and for the neuronal populations. The finding that the movement-related activity of both the PMd and PMv reflects the movement dynamics is consistent with previous reports (Werner, Bauswein and Fromm, 1991; Hepp-Reymond et al., 1994). Quantitatively, the shifts of Pd recorded for the population of PMd (mean shift 11.0°, $p<0.04$ in the Force-Baseline; -14.0°, $p<0.02$ in the Washout-Force) and PMv (mean shift 11.5°, $p<0.03$ in the Force-Baseline; -19.0°, $p<0.01$ in the Washout-Force) are close to that recorded in the M1 (mean shifts 16.2°, $p<10^{-6}$ in the Force-Baseline; -14.3°, $p<0.001$ in the Washout-Force) and SMA (mean shifts 16.6°, $p<10^{-6}$ in the Force-Baseline; -9.7°, $p<0.001$ in the Washout-Force).

One major aim of the present study was to investigate the neuronal correlates in the PMd and PMv of the development of a new internal model for the dynamics. The experimental design allowed dissociating the activity related to motor *performance* from the changes of neuronal activity underlying motor *learning*. With respect to the PMd we report a partially negative result. In general, the neuronal plasticity observed in the PMd is much less diffused than that recorded in the M1 and SMA. Considering in particular the shifts of Pd in the MT time window, only 25% of PMd cells was classified as memory I or II. The corresponding percentages for the M1 and SMA are 41% and 34%, respectively. A χ^2 analysis indicated significant differences in the classifications obtained for the PMd, the SMA and the M1 for the changes of Pd in MT time window (Pearson's $\chi^2 = 15.81$, d.o.f.=8, $p<0.05$). With respect to the PMv, the results fall in between that for the PMd and that of M1. Considering again the shifts of Pd in the MT, 31% of PMv cells was classified as memory I or II.

Taken together, the results of the PMd, SMA, M1, and PMv indicate that the movement dynamics is indeed processed in a rather distributed fashion across multiple areas, thus arguing against a strictly serial view. However, our data also argue against a strictly parallel hypothesis, because we found dynamics-related activity during the delay in the PMd but not in the PMv (or in the M1). In this respect, our findings are consistent with the conclusions of numerous previous studies (Wise, Weinrich and Mauritz, 1983; Wise and Mauritz, 1985; Mauritz and Wise, 1986; Kurata and Wise, 1988; Vaadia, Kurata and Wise, 1988; Riehle and Requin, 1989; Crammond and Kalaska, 1994,1996; Johnson et al., 1996, Shen and Alexander, 1997ab; Johnson et al., 1999; Hoshi and Tanji, 2000).

Considering the timing of activation, the results suggest that the PMd and the SMA are "close" to each other, and "upstream" of the M1. In other words, the emerging picture is consistent with the view that the contributions of the PMd, SMA, and M1 are orderly organized (in the order PMd, SMA, M1) and yet largely overlapping (see Padoa-Schioppa and Bizzi, in preparation). Considering the *plasticity* underlying the development of a new internal model for the dynamics, the results appear somewhat paradoxical. While we observe a similar order, the direction seem counter-intuitive: the PMd is less "memory" and more purely "dynamic" than the SMA, which is less "memory" and more purely "dynamic" than the M1. Additional theoretical and experimental work is needed to further investigate this issue.

Acknowledgments

We thank Margo Cantor and Sylvester Szczepanowski for technical assistance. This research was supported by the National Institute of Health (NIH grant MN481185).

References

1. Alexander, G.E. & Crutcher, M.D. Preparation for movement: neural representations of intended direction in three motor areas of the monkey. *J. Neurophysiol.* **64,** 133-150 (1990a).
2. Alexander, G.E. & Crutcher, M.D. Neural representation of the target (goal) of visually guided arm movements in three motor areas of the monkey. *J. Neurophysiol.* **64,** 164-178 (1990b).
3. Crammond, D.J. & Kalaska, J.F. Modulation of preparatory neuronal activity in dorsal premotor cortex due to stimulus-response compatibility. *J. Neurophysiol.* **71,** 1281-1284 (1994).
4. Crammond, D.J. & Kalaska, J.F. Differential relation of discharge in primary motor cortex and premotor cortex to movements versus actively maintained postures during a reaching task. *Exp. Brain Res.* **108**, 45-61 (1996).
5. Crutcher, M.D., and Alexander, G.E. (1990) Movement-related neuronal activity selectively coding either direction or muscle pattern in three motor areas of the monkey. J. Neurophysiol. 64, 151-163.
6. Dum, R.P. & Strick, P.L. The origin of corticospinal projections from the premotor areas in the frontal lobe. *J. Neurosci.* **11,** 667-689 (1991).
7. Evarts, E.V. Relation of pyramidal tract activity to force exerted during voluntary movement. *J. Neurophysiol.* **31,** 14-27 (1968).
8. Fetz, E.E. Are movement parameters recognizably coded in the activity of single neurons? *Behav. Brain Sci.* **15,** 679-690 (1992).
9. Fisher, N.I. *Statistical analysis of circular data.* (Cambridge University Press, Cambridge, 1993).
10. Flament, D. & Hore, J. Relations of motor cortex neural discharge to kinematics of passive and active elbow movements in the monkey. *J. Neurophysiol.* **60**, 1268-1284 (1988).
11. Freeman, D.H. *Applied categorical data analysis.* (Marcel Dekker, Inc., New York, 1987).
12. Fromm, C. Changes of steady state activity in motor cortex consistent with the length-tension relation of muscle. *Pfluegers Arch.* **398,** 318-323 (1983).
13. Gandolfo, F., Li, C.-S., Benda, B.J., Padoa-Schioppa, C. & Bizzi, E. Cortical correlates of learning in monkeys adapting to a new dynamical environment. *Proc. Natl. Acad. Sci. USA* **97**, 2259-2263 (2000).
14. Georgopoulos, A.P., Ashe, J., Smyrnis, N. & Taira, M. The motor cortex and the coding of force. *Science* **256**, 1692-1695 (1992).
15. Georgopoulos, A., Caminiti, R., Kalaska, J. & Massey, J. Spatial coding of movement: a hypothesis concerning the coding of movement direction by motor cortical populations. *Exp. Brain Res. (Supp.)* **7,** 327-336 (1983).
16. Georgopoulos, A., Kalaska, J., Caminiti, R. & Massey, J. On the relations between the direction of two-dimensional arm movements and cell discharge in primate motor cortex. *J. Neurosci.* **2,** 1527-1537 (1982).
17. He, S.Q., Dum, R.P. & Strick, P.L. Topographic organization of corticospinal projections from the frontal lobe: motor areas on the lateral surface of the hemisphere. *J. Neurosci.* **13,** 952-980 (1993).

18. He, S.Q., Dum, R.P. & Strick, P.L. Topographic organization of corticospinal projections from the frontal lobe: motor areas on the medial surface of the hemisphere. *J. Neurosci.* **15,** 3284-3306 (1995).
19. Hepp-Reymond, M.C., Husler, E.J., Maier, M.A. & Qi, H.X. Force-related neuronal activity in two regions of the primate ventral premotor cortex. *Can. J. Physiol. Pharmacol.* **72,** 571-579 (1994).
20. Hepp-Reymond, M.C., Kirkpatrick-Tanner, M., Gabernet, L., Qi, H.X. & Weber, B. Context-dependent force coding in motor and premotor cortical areas. *Exp. Brain Res.* **128,** 123-133 (1999).
21. Hoshi, E. & Tanji, J. Integration of target and body-part information in the premotor cortex when planning action. *Nature* **408**, 466-470 (2000).
22. Johnson, M.T. & Ebner, T.J. Processing of multiple kinematic signals in the cerebellum and motor cortices. *Brain Res. Brain Res. Rev.* **33**, 155-168 (2000).
23. Johnson, P.B., Ferraina, S., Bianchi, L. & Caminiti, R. Cortical networks for visual reaching: physiological and anatomical organization of frontal and parietal lobe arm regions. *Cereb. Cortex* **6,** 102-119 (1996).
24. Johnson, M.T.V., Coltz, J.D., Hagen, M.C. & Ebner, T.J. Visuomotor processing as reflected in the directional discharge of premotor and primary motor cortex neurons. *J. Neurophysiol.* **81,** 875-894 (1999).
25. Kakei, S., Hoffman, D.S. & Strick, P.L. Muscle and movement representations in the primary motor cortex. *Science* **285,** 2136-2139 (1999).
26. Kakei S, Hoffman DS, Strick PL. Direction of action is represented in the ventral premotor cortex. *Nat. Neurosci.* **4**, 1020-1025 (2001).
27. Kalaska, J.F., Cohen, D.A.D., Hyde, M.L. & Prud'homme, M. A comparison of movement direction-related versus load direction-related activity in the primate motor cortex, using a two-dimensional reaching task. *J. Neurosci.* **9,** 2080-2102 (1989).
28. Kalaska, J.F., Cohen, D.A., Prud'homme, M. & Hyde, M.L. Parietal area 5 neuronal activity encodes movement kinematics, not movement dynamics. *Exp. Brain Res.* **80**, 351-364 (1990).
29. Kettner, R.E., Schwartz, A.B. & Georgopoulos, A.P. Primate motor cortex and free arm movements to visual targets in three-dimensional space. III. Positional gradients and population coding of movement direction from various movement origins. *J. Neurosci.* **8**, 2938-2947 (1988).
30. Kurata, K. & Wise, S.P. Premotor cortex of rhesus monkeys: set-related activity during two conditional motor tasks. *Exp. Brain Res.* **69**, 327-343 (1988).
31. Li, C-S.R., Padoa-Schioppa, C. & Bizzi, E. Neural correlates of motor performance and motor learning in the primary motor cortex of monkeys adapting to an external force field. *Neuron* **30,** 593-607 (2001).
32. Luppino, G., Matelli, M., Camarda, R.M., Gallese, V. & Rizzolatti, G. Multiple representations of body movements in mesial area 6 and the adjacent cingulate cortex: an intracortical microstimulation study in the macaque monkey. *J. Comp. Neurol.* **311,** 463-482 (1991).
33. Luppino, G., Matelli, M., Camarda, R. & Rizzolatti, G. Corticocortical connections of area F3 (SMA-proper) and area F6 (pre-SMA) in the macaque monkey. *J. Comp. Neurol.* **338,** 114-140 (1993).

34. Matelli, M., Luppino, G. & Rizzolatti, G. Architecture of superior and mesial area 6 and the adjacent cingulate cortex in the macaque monkey. *J. Comp. Neurol.* **311,** 445-462 (1991).
35. Mauritz, K.H. & Wise, S.P. Premotor cortex of the rhesus monkey: neuronal activity in anticipation of predictable environmental events. *Exp. Brain Res.* **61**, 229-244 (1986)
36. Moran, D.W. & Schwartz, A.B. Motor cortical representation of speed and direction during reaching. *J. Neurophysiol.* **82,** 2676-2692 (1999).
37. Padoa-Schioppa, C. & Bizzi, E. Neuronal activity in five motor areas of the frontal lobe during visually instructed reaching movements. (In preparation).
38. Padoa-Schioppa, C., Li, C.-S.R. & Bizzi, E. Planning movements: kinematics-to-dynamics transformation in the supplementary motor area. (Submitted).
39. Padoa-Schioppa, C., Li, C.-S.R. & Bizzi, E. Neuronal activity in the supplementary motor area of monkeys adapting to a new dynamic perturbation. (In preparation).
40. Prut, Y. & Fetz, E.E. Primate spinal interneurons show pre-movement instructed delay activity. *Nature* **401,** 590-594 (1999).
41. Riehle, A. & Requin, J. Monkey primary motor and premotor cortex: single-cell activity related to prior information about direction and extent of an intended movement. *J. Neurophysiol.* **61,** 534-549 (1989).
42. Scott, S.H. & Kalaska, J.F. Changes in motor cortex activity during reaching movements with similar hand paths but different arm postures. *J. Neurophysiol.* **73,** 2563-2567 (1995).
43. Scott, S.H. & Kalaska, J.F. Reaching movements with similar hand paths but different arm orientations. I. Activity of individual cells in motor cortex. *J. Neurophysiol.* **77,** 826-852 (1997).
44. Scott, S.H., Gribble, P.L., Graham, K.M. & Cabel, D.W. Dissociation between hand motion and population vectors from neural activity in motor cortex. *Nature* **413,** 161-165 (2001).
45. Scott, S.H., Sergio, L.E. & Kalaska, J.F. Reaching movements with similar hand paths but different arm orientations. II. Activity of individual cells in dorsal premotor cortex and parietal area 5. *J. Neurophysiol.* **78**, 2413-2426 (1997).
46. Shadmehr, R. & Moussavi, Z.M. Spatial generalization from learning dynamics of reaching movements. *J. Neurosci.* **20**, 7807-7815 (2000).
47. Shadmehr, R. & Mussa-Ivaldi, F.A. Adaptive representation of dynamics during learning of a motor task. *J. Neurosci.* **14,** 3208-3224 (1994).
48. Shen, L. & Alexander, G.E. Neural correlates of a spatial sensory-to-motor transformation in primary motor cortex. *J. Neurophysiol.* **77,** 1171-1194 (1997a).
49. Shen, L. & Alexander, G.E. Preferential representation of instructed target location versus limb trajectory in dorsal premotor area. *J. Neurophysiol.* **77,** 1195-1212 (1997b).
50. Thach, W.T. Correlation of neural discharge with pattern and force of muscular activity, joint position, and direction of intended next movement in motor cortex and cerebellum. *J. Neurophysiol.* **41**, 654-676 (1978).
51. Thoroughman, K.A & Shadmehr, R. Electromyographic correlates of learning an internal model of reaching movements. *J. Neurosci.* **19**, 8573-8588 (1999).

52. Todorov, E. Direct cortical control of muscle activation in voluntary arm movements: a model. *Nat. Neurosci.* **3,** 391-398 (2000).
53. Vaadia, E., Kurata, K. & Wise, S.P. Neuronal activity preceding directional and nondirectional cues in the premotor cortex of rhesus monkeys. *Somatosens. Mot. Res.* **6**, 207-230 (1988).
54. Werner, W., Bauswein, E. & Fromm, C. Static firing rates of premotor and primary motor cortical neurons associated with torque and joint position. *Exp. Brain Res.* **86,** 293-302 (1991).
55. Wise, S.P. & Mauritz, K.H. Set-related neuronal activity in the premotor cortex of rhesus monkeys: effects of changes in motor set. *Proc. R. Soc. Lond. B Biol. Sci.* **223**, 331-354 (1985).
56. Wise, S.P., Moody, S.L., Blomstrom, K.J. & Mitz, A.R. Changes in motor cortical activity during visuomotor adaptation. *Exp. Brain Res.* **121,** 285-299 (1998).
57. Wise, S.P., Weinrich, M. & Mauritz, K.H. Motor aspects of cue-related neuronal activity in premotor cortex of the rhesus monkey. *Brain Res.* **260**, 301-305 (1983).

Figure legends

Figure 1. Psychophysics of the task. **A.** The plot illustrates the values of the correlation coefficient (CC, y-axis) as a function of trial number (x-axis) in one representative session. Values of the CC range between –1 and 1, and are close to 1 for movements close to ideal. The CC has high values in the Baseline. It drops at the beginning of the Force epoch and gradually recovers as the monkeys adapt to the perturbing force. In the Washout, after a short re-adaptation phase, the CC returns to the high values observed in the Baseline. **B.** Over sessions, the adaptation became faster (shorter ramp) and better (higher plateau). This process of long-term learning is illustrated by plotting the mean CC (y-axis) against the session number (x-axis), separately for the three epochs. Sessions with the CK force field (red color) and the CCK force field (blue color) were intermixed. For both force fields, the mean CC recorded in the Force epoch increased over sessions (long-term learning).

Figure 2. Reconstruction of the recording sites for monkeys R (left) and N (right). CS central sulcus; AS arcuate sulcus; PS principal sulcus.

Figure 3. Distribution of preferred directions. We show the distribution of Pd for the three epochs (Baseline, Force epoch and Washout) and for the three time windows (DT, MT and TH). We show the distributions both for the PMd (top) and for the PMv (bottom). In all cases, circular statistics indicates a homogeneous distribution of Pd around the clock

Figure 4. Dynamically-tuned cells. Two examples of dynamically tuned cells recorded from the PMd. In both cases, the figure shows the movement-related activity (time window MT). **A.** This cell has a very low and not directionally-tuned activity in the Baseline. In the Force epoch, the cell becomes directionally tuned. In the activity of the cell returns similar to that observed in the Baseline. **B.** A complementary pattern is shown in B. This cell is very active and directionally tuned in the Baseline, and loses its tuning when the monkey adapts to the perturbing force field. In the Washout, the cell recovers the tuning observed in the Baseline. These changes are dynamic in nature, because the dynamics of the movement is identical in the Baseline and in the Washout, but different in the Force epoch where the monkey compensates for the external force field.

Figure 5. Tune-in and Tune-out cells. The Figure illustrates the movement-related activity (MT time window) of two cells recorded from the PMv. **A.** Example of tune-in cell. The activity of the cell is low and not directionally tuned in the Baseline. In the Force epoch –and following adaptation to the external force field –the activity increases and the cell becomes directionally tuned. In the Washout, the cell maintains the newly acquired directional tuning. Thus, in the Washout the cell maintains a trace of the previous adaptation experience. **B.** Example of Tune-out cell. This cell is initially tuned, and looses its tuning following adaptation to the force filed. In the Washout, the cell remains not-tuned.

Figure 6. Delay activity of two PMd cells. Both cells were recorded with a CK force field. **A.** This cell is directionally tuned in all three epochs, and its Pd remains essentially unchanged throughout the session. Thus, this cell was classified as kinematic with respect to its changes of Pd in the DT. **B.** The Pd of this cell shifted in the Force epoch in the direction of the external force field, namely the CK direction. In the Washout, the Pd shifted back to that observed in the Baseline. Thus, this cell was classified as dynamic with respect to its changes of Pd in the DT. This example indicates that *during motor planning* neurons in the PMd process the dynamics of the upcoming movement.

Figure 7. Scatter plots. The three plots refer to the changes of Pd across epochs observed in the PMd in the three time windows (DT, top; MT, center; TH, bottom). In each plot, the x-axis indicates the shift of Pd in the Force epoch compared to the Baseline, and the y-axis indicates the shift of Pd in the Washout compared to the Force epoch. Positive values indicate shifts of Pd in the direction of the external force. The entire PMd population is plotted, and cells are color-coded according to their class. Kinematic cells (black color) –whose Pd do not change in either the Force epoch or the Washout –lie close to the origin of the axes. Dynamic cells (blue color) –whose Pd shift in opposite directions in the Force epoch compared to the Baseline and in the Washout compared to the Force epoch –lie along the diagonal cutting the second and fourth quadrant. Typically, the Pd of dynamic cells shifts in the direction of the external force in the Force epoch, and in the opposite direction in the Washout. Therefore, most dynamic cells lie in the fourth quadrant. Memory I cells (green color) –whose Pd shifts in the Force epoch compared to the Baseline, but does not shift in the Washout compared to the Force –lie along the x-axis. Memory II cells (red color) –whose Pd does not shift in the Force epoch compared to the Baseline, but does shift in the Washout compared to the Force –lie along the y-axis. The percentages for the various classes in the three epochs are shown on the right. It can be noticed that a consistent amount of cells reflect the dynamics of the upcoming movement during the delay (DT).

Figure 8. Classes of cells. All four cells were recorded with a CCK force field. The cells in **A.** and **B.** were recorded from the PMd, The cells in **C.** and **D.** were recorded from the PMv.

Figure 9. Target-hold time activity. This cell was recorded in PMd with a CK force field, and the figure illustrates the activity recorded during the target-hold time (TH time window). The Pd of the cell remains essentially constant through out the three epochs.

Figure 10. PMd, population histograms. The histograms illustrate the Shift of Pd observed for the entire PMd population in the three time windows. Significant shifts of Pd are observed in the DT and MT time windows (red asterisks).

Figure 11. PMv, population histograms. The histograms illustrate the Shift of Pd observed for the entire PMv population in the three time windows. Significant shifts of Pd are observed in the MT time windows (red asterisks).

Tables

Table 1. PMd, percentage of cells directionally tuned.

	Baseline	Force epoch	Washout
CH	3	1	1
DT	41	44	34
MT	47	52	49
TH	22	25	10

Table 2. PMv, percentage of cells directionally tuned.

	Baseline	Force epoch	Washout
CH	4	8	1
DT	25	21	19
MT	49	43	39
TH	15	20	19

Table 3. PMd, classes of cells (percentages).

	Preferred direction			Average firing freq.			Tuning width		
	DT	MT	TH	DT	MT	TH	DT	MT	TH
Kinematic	38	22	56	9	7	6	26	35	40
Dynamic	41	43	25	18	20	16	21	12	20
Memory I	12	11	0	14	16	23	21	18	20
Memory II	9	14	13	29	16	20	21	18	0
Other (*x*-*y*-*z*)	0	11	6	30	40	36	11	18	20
N cells (tot)	34	37	16	114	122	101	19	17	5

Table 4. PMd, Population changes of activity (means).

		Force – Baseline	Washout – Force	Washout – Baseline
Change of Pd	DT	m=10.4° p<0.05 *	m= -8.5° p<0.05 *	m= -2.7° p=0.5
	MT	m=11.0° p<0.04 *	m=-14.0° p<0.02 *	m= -6.0° p=0.09
	TH	m=10.0° p=0.1	m= 2.8° p=0.7	m= 0.8° p=0.9
Change of Avf	CH	m=0.33 $p<10^{-3}$ *	m=0.03 p=0.5	m=0.26 p<0.002 *
	DT	m=0.27 $p<10^{-4}$ *	m=0.09 p=0.2	m=0.25 $p<10^{-3}$ *
	MT	m=0.17 p<0.002 *	m=0.06 p=0.2	m=0.18 p<0.004 *
	TH	m=0.23 p<0.002 *	m=0.05 p=0.2	m=0.24 $p<10^{-3}$ *
Change of Tw	DT	m= 8° p=0.6	m= 6° p=0.6	m=14° p=0.3
	MT	m=22° p<0.03 *	m= 22° p=0.2	m=31° p<0.005 *
	TH	m=34° p=0.1	m=-10° p=0.7	m= 1° p=1

Table 5. PMv, classes of cells (percentages).

	Preferred direction			Average firing freq.			Tuning width		
	DT	MT	TH	DT	MT	TH	DT	MT	TH
Kinematic	67	35	63	14	7	14	67	75	0
Dynamic	11	19	13	10	14	9	0	13	0
Memory I	11	8	13	27	23	23	0	0	100
Memory II	0	23	13	19	17	20	0	0	0
Other (*x-y-z*)	11	15	0	30	39	35	33	13	0
N cells (tot)	9	26	8	124	137	123	3	8	1

Table 6. PMv, Population changes of activity (means).

		Force – Baseline	Washout – Force	Washout – Baseline
Change of Pd	DT	m= 3.1° p=0.8	m= 0.0° p=1	m= -6.6° p=0.6
	MT	m=11.5° p<0.03 *	m=-19.0° p<0.01 *	m=-11.7° p=0.2
	TH	m=15.1° p=0.2	m=-27.6° p<0.02 *	m= -9.2° p=0.6
Change of Avf	CH	m=0.14 p<0.01 *	m=0.07 p=0.2	m=0.19 p<0.01 *
	DT	m=0.11 p<0.03 *	m=0.06 p=0.2	m=0.10 p=0.1
	MT	m=0.14 p<0.01 *	m=0.01 p=0.9	m=0.11 p=0.09
	TH	m=0.13 p<0.01 *	m=0.12 p=0.06	m=0.24 p<0.01 *
Change of Tw	DT	m=-71° p=0.3	m= 30° p=0.4	m=-58° p=0.2
	MT	m= 3° p=0.9	m=-16° p=0.5	m= 23° p=0.05
	TH	m= 42° p=1	m= 4° p=0.2	m= 47° p=1

Figure 1

Figures

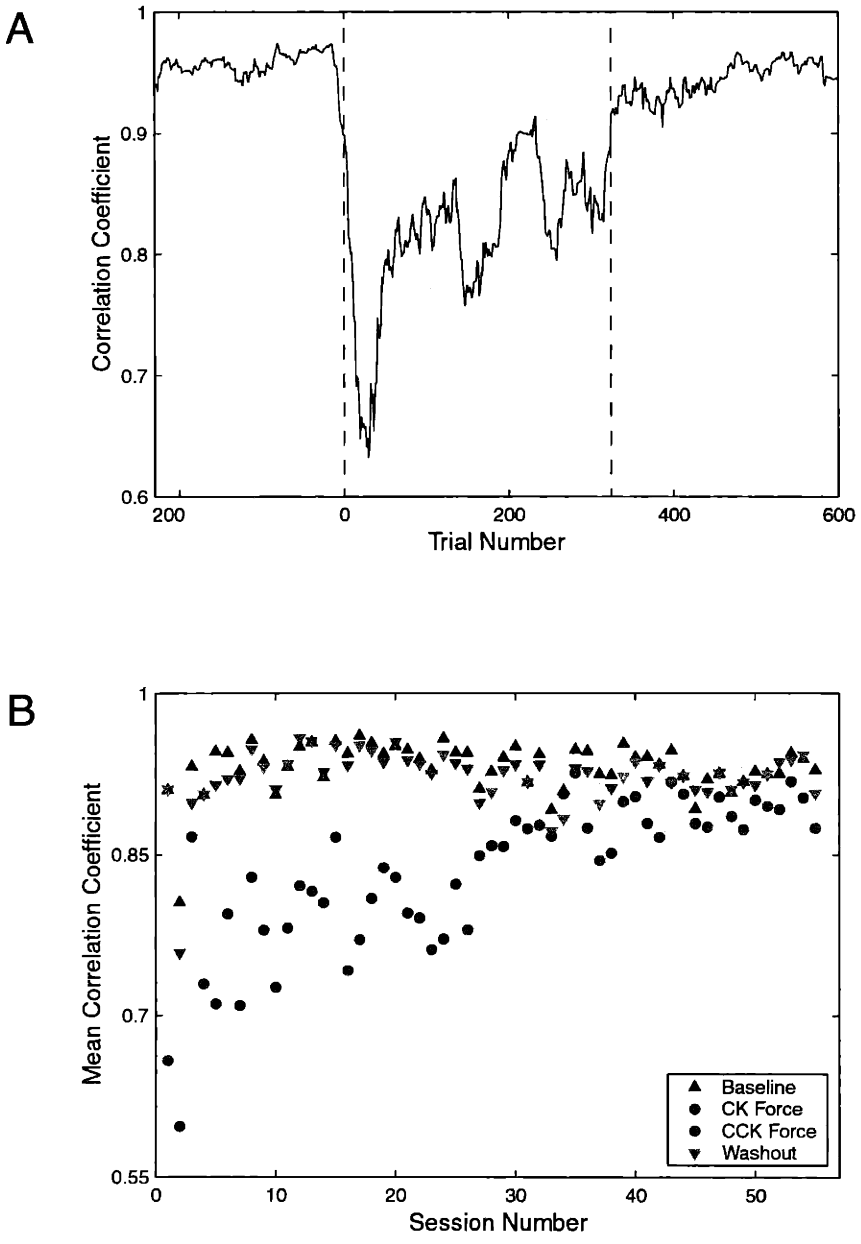

Figure 2

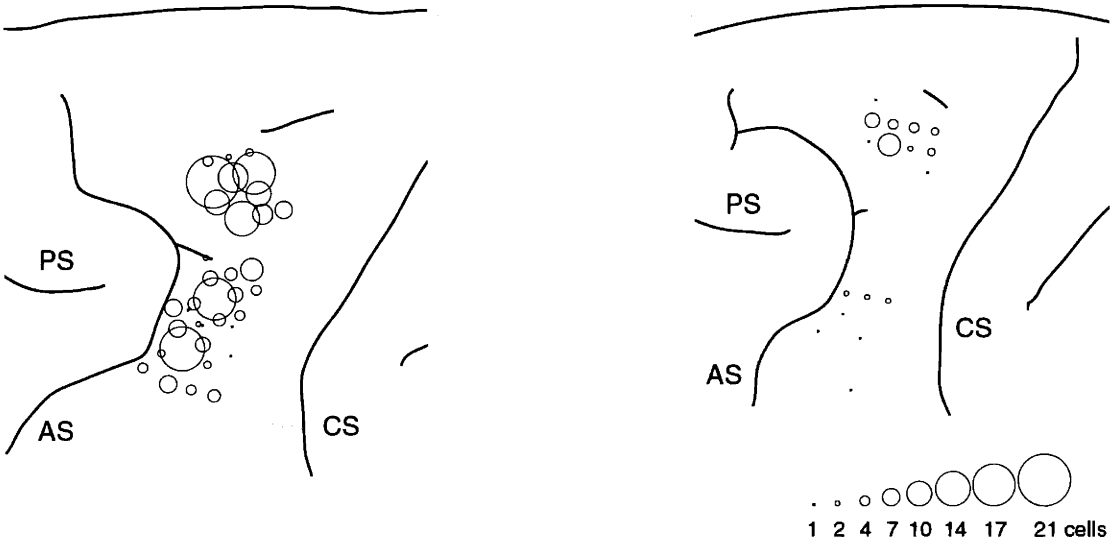

A. PMd

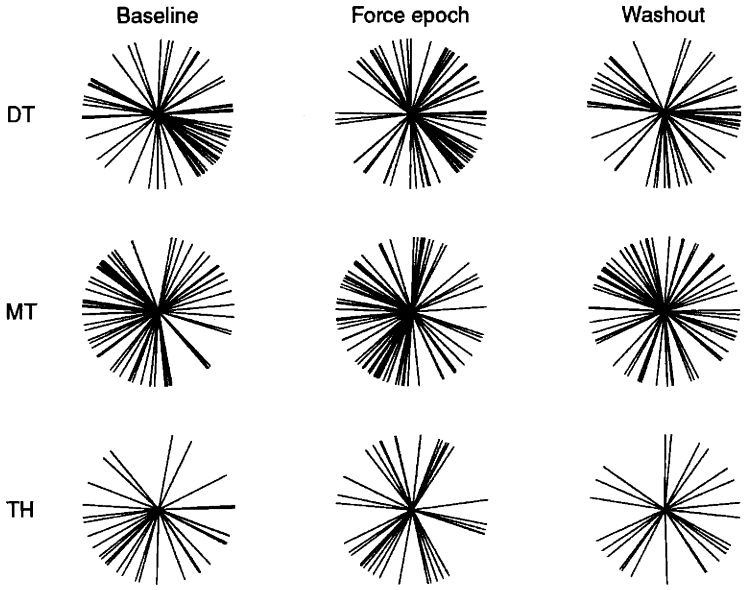
Baseline
Force epoch
Washout
DT
MT
TH

B. PMv

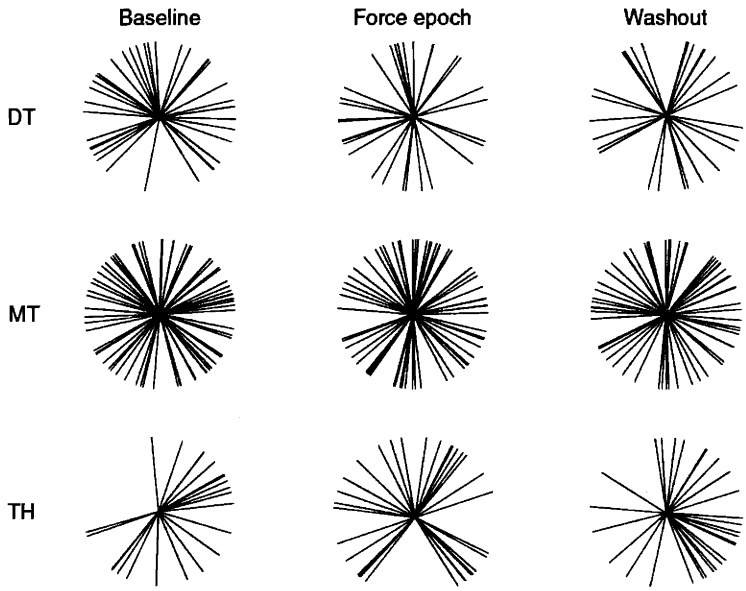
Baseline
Force epoch
Washout
DT
MT
TH

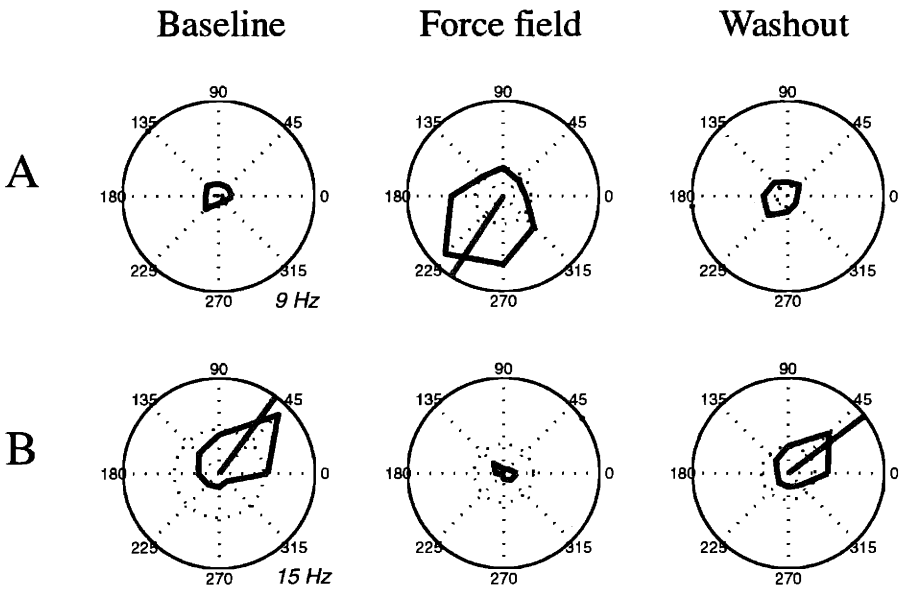
Baseline
Force field
Washout
A
B
90
135
45
180
0
225
315
270
9 Hz
15 Hz

Figure 5

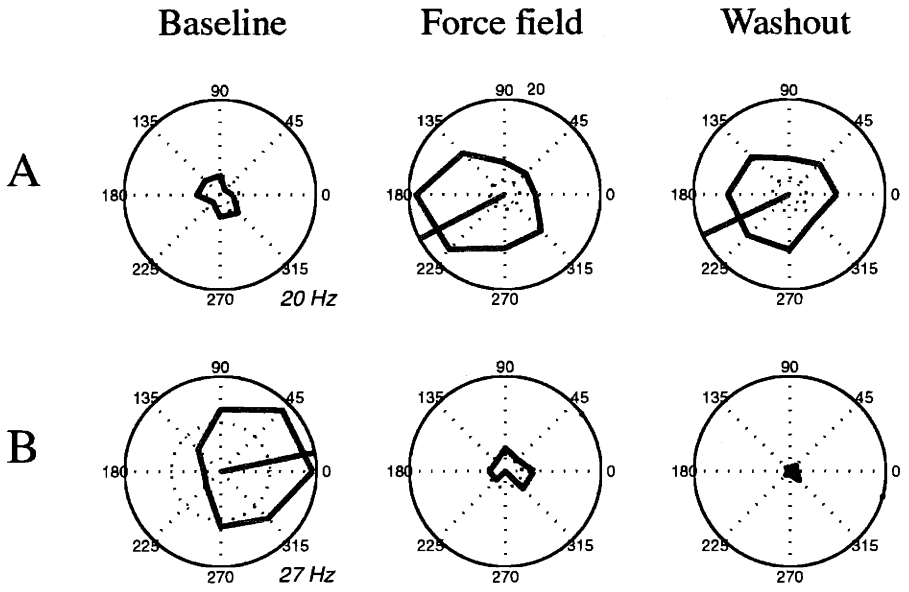
Baseline
Force field
Washout
A
B
90
135
45
180
0
225
315
270
20
20 Hz
27 Hz

Figure 6

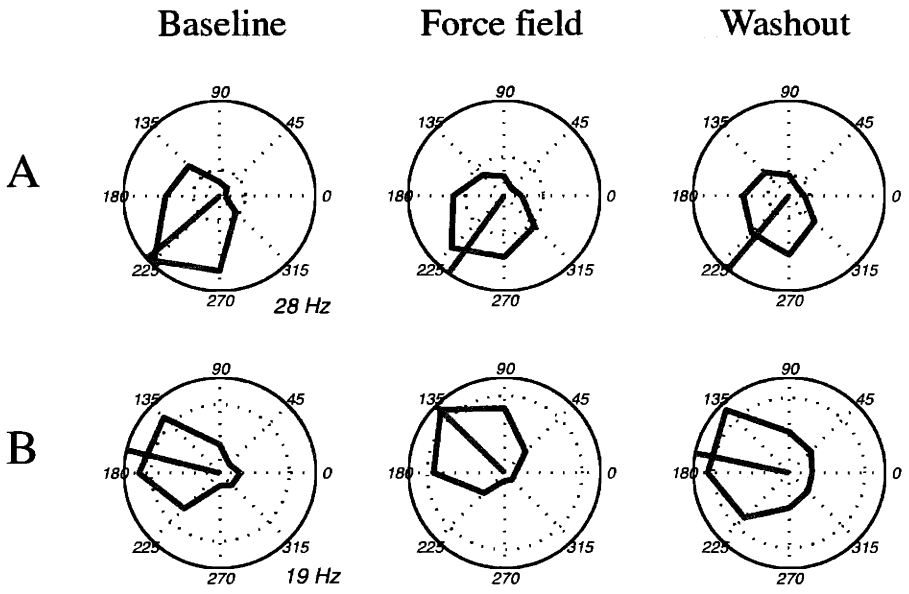
Baseline
Force field
Washout
A
B
90
135
45
180
0
225
315
270
28 Hz
19 Hz

Figure 7

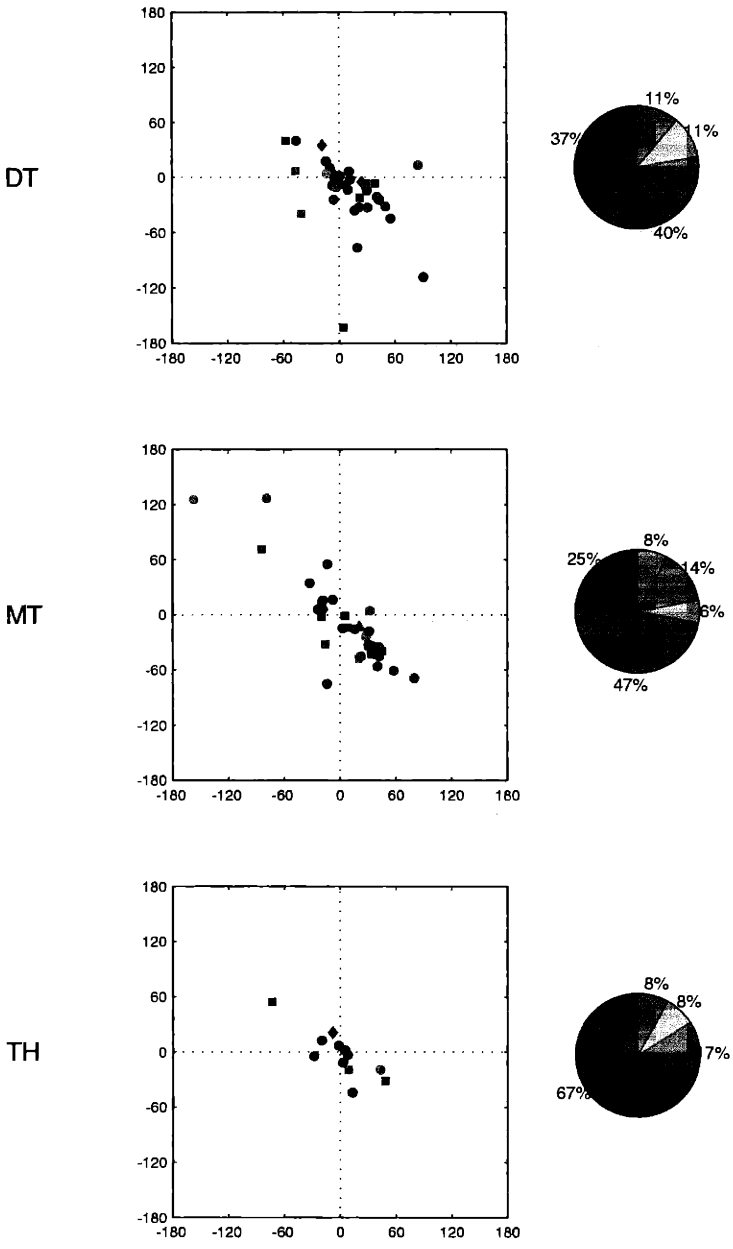
DT
MT
TH
180
120
60
0
-60
-120
-180
-180 -120 -60 0 60 120 180
11%
11%
37%
40%
8%
25%
14%
6%
47%
8%
8%
7%
67%

Figure 8

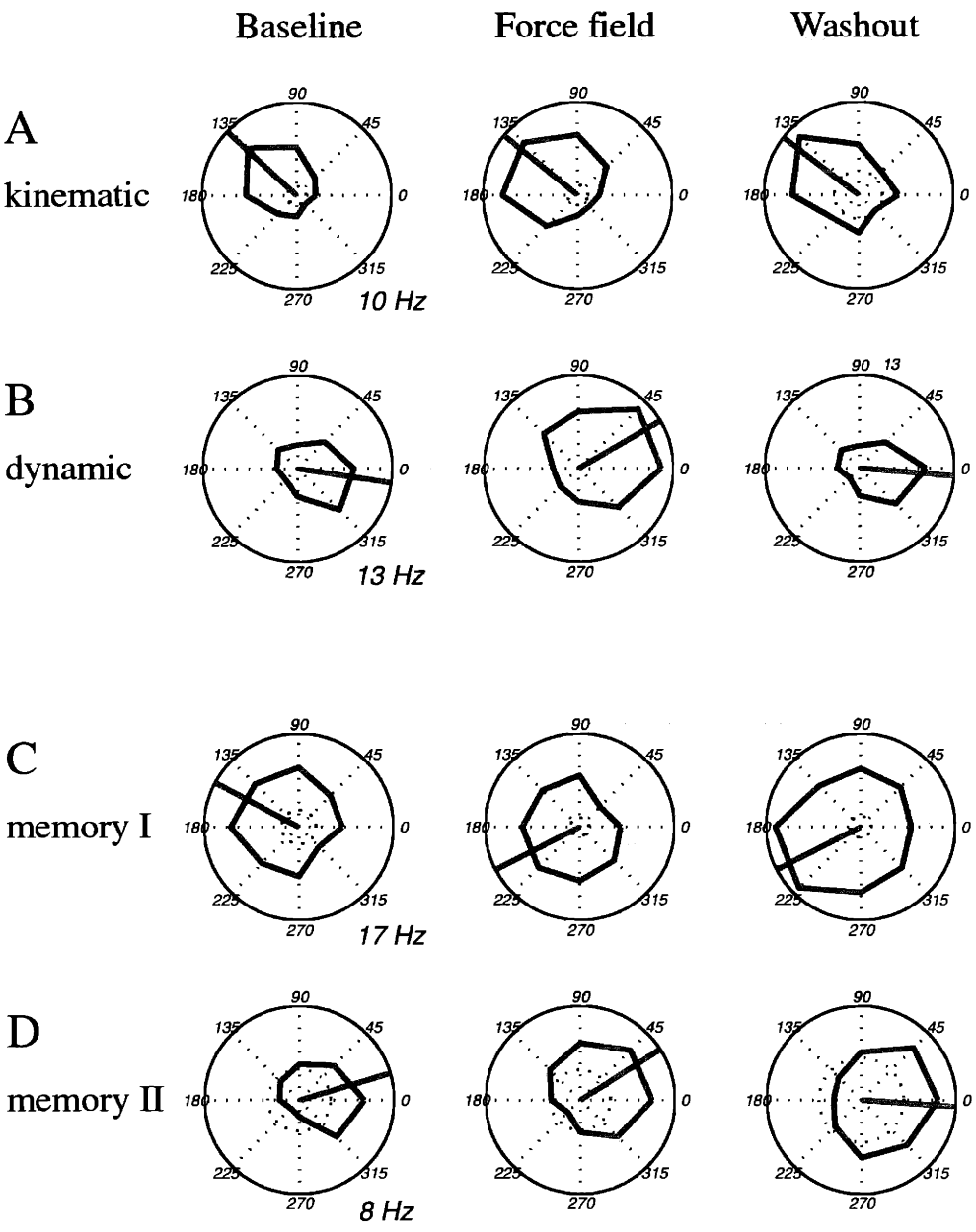
Baseline
Force field
Washout
A
kinematic
B
dynamic
C
memory I
D
memory II
90
45
0
315
270
225
180
135
10 Hz
13 Hz
17 Hz
8 Hz

Figure 9

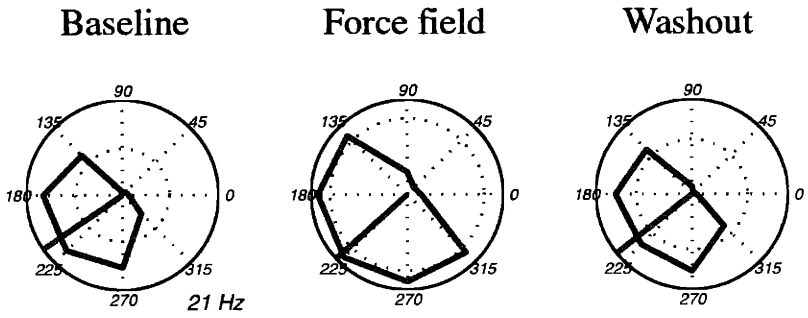

Figure 10

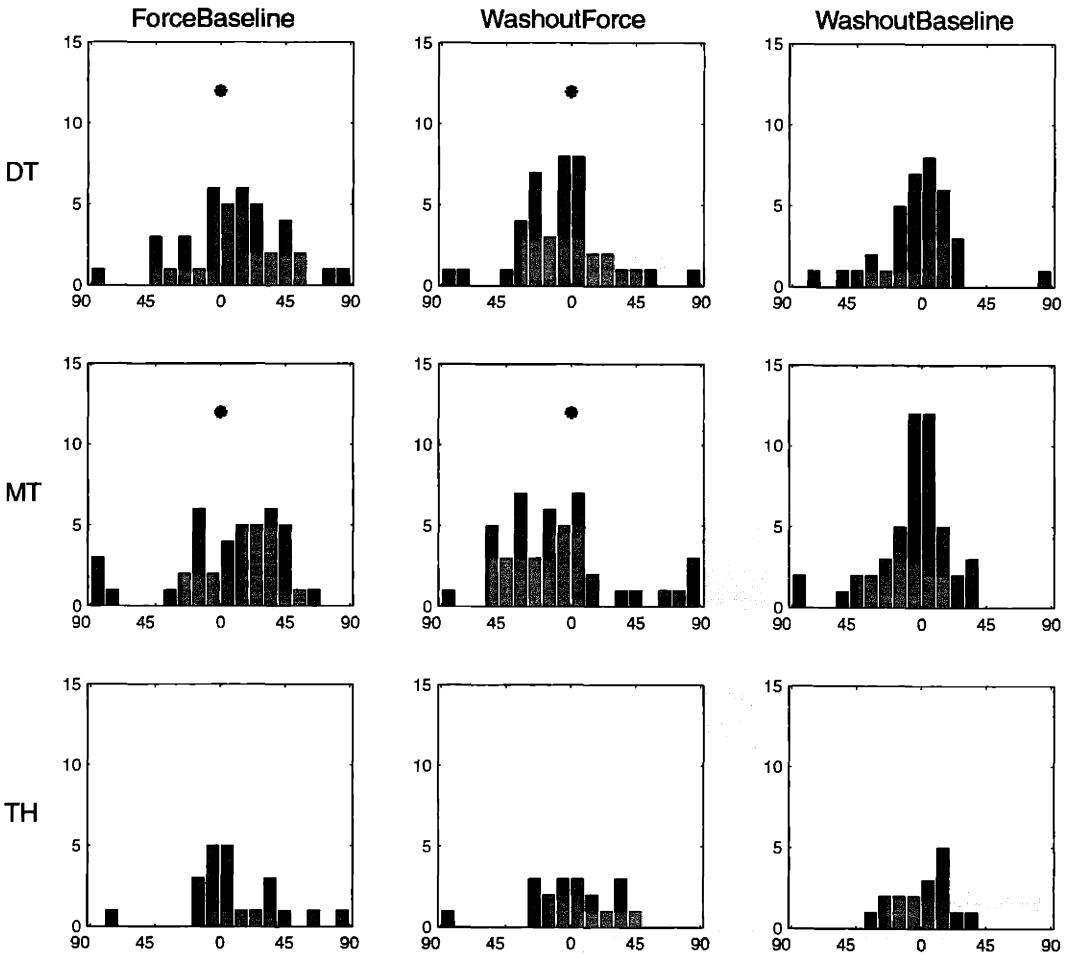
ForceBaseline
WashoutForce
WashoutBaseline
DT
MT
TH
15
10
5
0
90
45
0
45
90

Figure 11

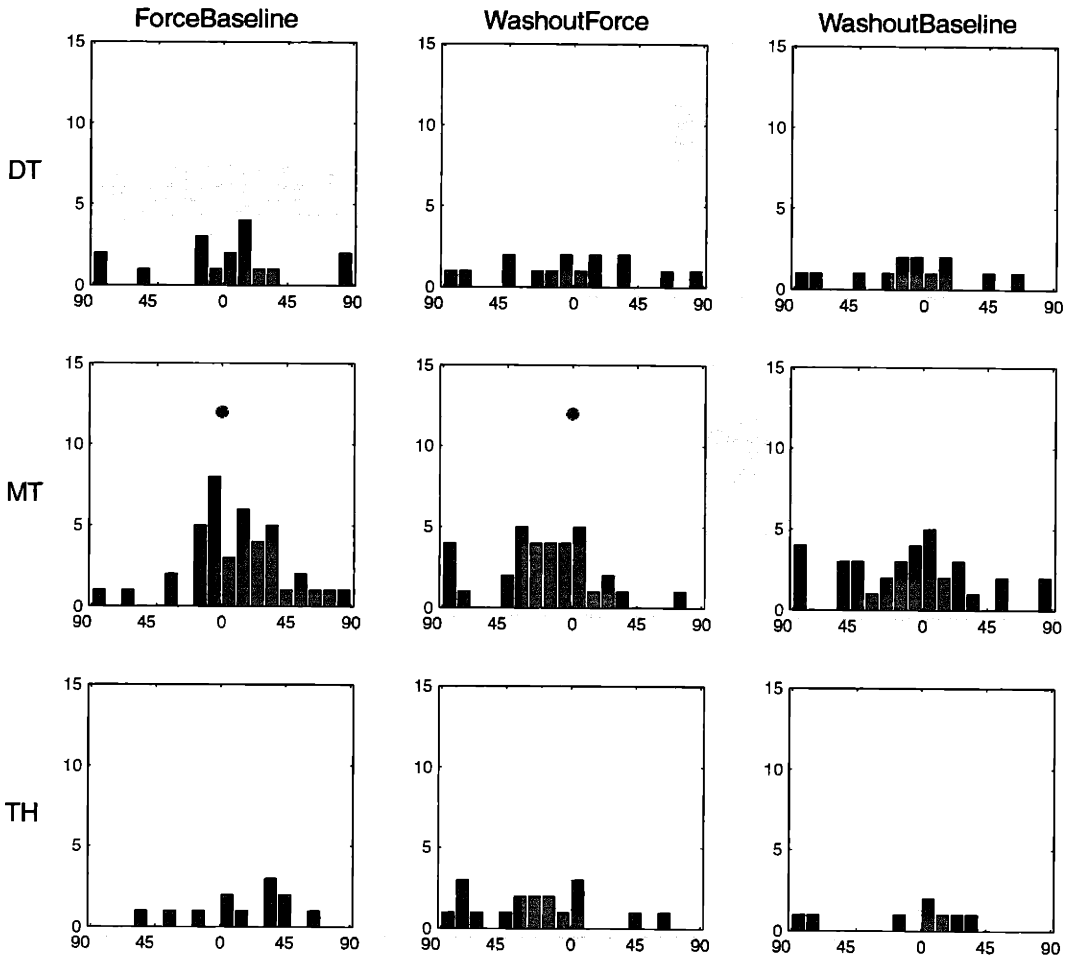
ForceBaseline
WashoutForce
WashoutBaseline
DT
MT
TH
15
10
5
0
90
45
0
45
90

Chapter 6. Neuronal activity in five motor areas during reaching movements[1]

We compare the activity profiles of over 900 neurons recorded in the primary motor cortex (M1), supplementary motor area (SMA), pre-supplementary motor area (preSMA), dorsal premotor cortex (PMd), and ventral premotor cortex (PMv). We analyze the modulation and directional selectivity of cells in different time windows prior to and during visually instructed delayed reaching movements. All cortical areas (with the partial exception of the PMv) appear largely task-related. However, different areas appear to fall in the "logical" sequence: preSMA, PMd, SMA, and M1, as indicated by several independent measures. Thus, the emerging picture contains both elements of serial and parallel organization. These results also help characterize the SMA, indicating that it lies closest and just "upstream" of M1 among the areas under consideration.

[1] Elsewhere in the thesis, Chapter 6 is referred to as (Padoa-Schioppa and Bizzi, in preparation).

Introduction

Over the past century an increasing number of motor areas have been identified in the frontal lobe of the cerebral cortex. Within the two Broadmann areas 4 and 6, most recent studies count six or seven motor fields: the primary motor cortex (M1, or F1), the dorso-caudal premotor area (PMdc, or F2, hereafter PMd), the dorso-rostral premotor area (PMdr, or F7), the ventro-caudal premotor area (PMvc, or F4, hereafter PMv), the ventro-rostral premotor area (PMvr, or F5), the supplementary motor area (SMA, or SMA-proper, or F3), and the presupplementary motor area (preSMA, or F6). In addition, three or four motor areas have been described in the cingulate sulcus and cingulate girus (cingulate motor areas CMAr, CMAd, and CMAv). So far, these anatomical subdivisions have not been followed by clear functional distinctions. The case of reaching movements is perhaps paradigmatic. At least seven of the nine or ten cortical motor areas listed above contain a representation of the forelimb (M1, PMd, PMv, preSMA, SMA, CMAd, and CMAv) and thus presumably participate in different forms to the control of reaching movements. The traditional view was that multiple "premotor" areas process "high" aspects of movement and feed with their output the area M1, which controls the execution of movements through its corticospinal projections. A strict interpretation of this serial view is however challenged by anatomical and physiological evidence. First, recent studies[1, 2] found direct projections to the cord originating from multiple areas, including the M1, SMA, PMd, PMv, CMAd and CMAv. Second, studies that recorded from multiple areas and made one particular dissociation (e.g., between the instructing stimulus and the instructed movement) generally found very extensive functional overlaps between areas (but also significant differences)[3-24]. Based on these considerations, several authors proposed that numerous cortical areas control movements in parallel[7, 25,26].

In a series of experiments[27-29] we studied the activity of five motor areas of the frontal lobe of monkeys performing visually instructed reaching movements. Specifically, we recorded neurons in the M1, SMA, preSMA, PMd and PMv. In particular, our studies investigated the neuronal correlates of the inverse dynamics (a "late" processing stage), which we isolated from other processing levels by introducing an external dynamic perturbation (a force field). Computationally, the CNS can be thought to process the inverse dynamics by the use of internal models, and previous work showed that new internal models for the dynamics can be acquired through experience[30-34] In our experiments, we investigated how neurons in these different areas process the internal model for the dynamics, and how their activity modifies when a new internal model is acquired (neuronal plasticity). Like other before, our experiments failed to trace clear-cut functional boundaries between areas, although we did record some distinctive features. For instance, we found (only) in the SMA and PMd neurons that process the dynamics of the upcoming movement *during motor planning*. In contrast, neurons that process dynamics *during motor execution* were present in all areas (M1, SMA, PMd, and PMv). With respect to the development of a new internal model, we found neuronal plasticity in all areas, but in different proportions. In particular, plastic changes were more frequent in the M1 than in the SMA, and more frequent in the SMA than in the PMd.

The present study is a first attempt to compare the activity of different areas directly with each other. Our analysis is focused here of the *timing* of activation. For each trial, we define multiple time windows from prior to the presentation of the instruction to the end of movement, and we analyze the activity and directional selectivity of the cells in all areas. We report two main results. First, all areas are largely task-related (with the partial exception of the PMv). All areas are increasingly active over the course of the trial, and maximally active during the execution of the movement. Second, areas are differentially active at different times, and naturally fall in the "logical" sequence: preSMA, PMd, SMA , M1 (and PMv). Different measures of modulation and timing consistently indicate this same sequence. For instance, early activity (prior to and shortly after the *cue*) is most frequent in the preSMA and orderly less frequent in the PMd, SMA, and M1, whereas movement-related activity is most frequent in the M1 and orderly less frequent in the SMA, PMd, and preSMA. Thus, the emerging picture resembles that of subsequent overlapping waves.

The present analysis is rather extensive, and the results are largely consistent with previous reports that contrasted the activity of two or three different areas[3-23]. We consider particularly interesting the results obtained here for the SMA. It is nowadays recognized that the traditionally defined "*SMA*" includes two distinct areas, the preSMA and the SMA-proper (or SMA) (see ref. [35] for review). It is also relatively clear that the preSMA is more remote from the actual implementation of movements than the SMA, and that the "early" and "complex" motor functions once attributed to the undivided "*SMA*" area better associated with the preSMA[35-41, 8]. For this reason, however, little is currently known of the SMA-proper. Our results show that the SMA is indeed closely related to the late stages of motor planning and to motor execution. In the picture of overlapping waves, SMA appears to be the closest area and just upstream to M1.

The present results can constitute a framework to compare the neuronal plasticity associated with the development of a new internal model observed in the PMd, SMA and M1.

Methods

Here we pooled and analyzed data collected from 6 monkeys across three different studies (database summarized in Table 1). The three studies were carried in the same experimental setup, and the paradigm and procedures used were essentially the same. The details on experimental procedures used in each study are described in the corresponding reference paper[26-28]. The monkeys were two male *Macaca nemestrina* (B and M, see ref. [26]), two male *Macaca mulatta* (F and C, see ref. [27]), and two female *Macaca mulatta* (R and N, see ref. [28]). Here we only review the experimental methods briefly, describe the current analysis, and outline some of the differences across studies.

Experimental setup, behavioral task and data collection

The monkeys sat in an electrically insulated enclosure and executed reaching movements instructed by squares that appeared on a computer monitor. During the experiments, the monkeys held the handle of a two-degrees of freedom robotic arm. The position of the handle was indicated by a cursor on the screen, and movements were confined to a horizontal plane. In each trial, a center square appeared in the center of the monitor, and

the monkey had to acquire the center square to initiate the trial. After 1 s, a peripheral square appeared in one of eight locations (*cue*). The eight peripheral locations were equally spaced on a circle around the center square. After a variable-duration delay, the center square was extinguished. This was the *go* signal that prompted the monkey to move. The monkeys had then to acquire the peripheral square and wait within the peripheral square for 1 s before receiving a drop of juice for reward.

Attached to the robotic arm were two motors that could exert upon the hand of the monkey perturbing forces, described by force fields. Force fields were vector fields $\mathbf{F}=B\mathbf{V}$, where $\mathbf{F}$ is the force, $\mathbf{V}$ is the hand velocity and B is a 2x2 rotation matrix (0 b; -b 0). Thus, the force was always in strength proportional to the velocity (viscous), and in direction orthogonal to the velocity (curl). Depending on the sign of b, the force was clockwise or counterclockwise.

Each session consisted of three behavioral epochs. A Baseline, where no force was applied; a Force epoch, where a force field was introduced; and a Washout, where the force field was removed. Each epoch lasted about 15-20 trials per movement direction (120-160 trials total). Force fields were never introduced during the training, prior to the recordings. In the Force epoch, monkeys showed typical patterns of dynamics adaptation (short-term learning). Their hand trajectory –initially deviated –returned straight over trials. In the Washout, hand trajectories initially deviated in a way that mirrored that seen in the early Force epoch (aftereffect), and then returned straight. Over sessions, the adaptation became faster and better (long-term learning). In some sessions (control sessions) no force field was ever introduced, and the monkey performed in three arbitrarily defined epochs of 120-160 trials.

During the experiments, we recorded the hand trajectories and velocity at a sampling rate of 100 Hz. Neuronal recordings were carried over using 1-8 electrodes and commercially available software. During the experiments, spikes were identified with a threshold crossing criteria and waveforms were saved to disk for subsequent analysis.

Recording areas were identified through microstimulation (monkeys C, B, M, R, N) and gross histology (monkeys F, B, M, R, N).

Data analysis

Neuronal data were clustered off line using either a custom-written or a commercially available software. Waveforms were always inspected for stability across epochs, and only stable cells were included in subsequent analysis.

In the analysis, we aligned trials in correspondence of the following events: the presentation of the cue (cue), the go signal (go), the movement onset (mo), the movement end (me), and the delivery of the reward (rew). For each trial, the mo and the me were identified with a threshold-crossing criterion on the speed (4 cm/s).

We studied the activity profile of each cell aligning trials with the cue, with the go, and with the mo. For each cell, we identified the preferred direction (Pd, see below), and we defined the preferred hemifield (PH) as the 180° centered in the Pd. The opposite hemifield was named anti-preferred hemifield (APH). We then computed the PH activity profile by pooling together all the trials corresponding to movements towards the four directions within the PH. Analogously, we computed the APH activity profile by pooling together all the trials corresponding to movements towards the four directions within the

APH. We also computed the ALL activity profile, by pooling together all the trials in all directions.

The quantitative analysis of the activity profiles was aimed at comparing the activity of different areas at different times. We defined multiple profile variables, with the following intents. First, we tried to capture aspects that appeared most salient when the profiles were inspected visually. Second, we tried to be exhaustive and avoid biases between areas. Third, we tried to be non-redundant and define variables *a priori* mutually independent.

We analyzed the activity profiles in the following time windows. We considered the reference "*rest*" activity as the activity in a 400 msec-long time window (*cue*-700 : *cue*-300). We then defined five other 400 msec-long time windows: the *aftercue* (*cue*+100 : *cue*+500); the *delay* (*go*-400 : *go*); the *RT* (*go*-200 : *go*+200); the *early mov* (*mo*-200 : *mo*+200); and the *late mov* (*mo* : *mo*+400). The activity of each of the *aftercue*, *delay*, *RT*, *early mov*, and *late mov* was separately compared with the *rest* activity with an ANOVA ($p<0.01$). For this comparison, we considered the activity profile obtained with all the trials in all directions (ALL activity profile). This analysis assessed whether the activity in a given time window (e.g., the *delay*) differed from *rest* more than would be expected from the intrinsic variability in the *rest* activity itself (analysis of variance). This approach is meaningful if the activity within the time window under study remains relatively stable. We therefore chose 400 msec-long time windows (and not longer), to avoid rejecting cells whose profile had a narrow peak. In addition, the ANOVA analysis is only justified if the two sets include measures statistically independent from each other. Because our profiles sampled the cell activity with 80 msec-wide sliding time bins, 20 msec apart from one another, the same spike was effectively counted in 4 subsequent time bins. To avoid under-estimating the variability within the *rest* time window and within the time window under study, we included in this analysis every fourth time bin of the activity profile. For this analysis, we considered both significant increases and significant decreases of activity.

We used the same time windows to analyze the directional selectivity. We defined the variables *delay dir selec*, *RT dir selec*, *early mov dir selec*, and *late mov dir selec*. The goal of these analyses was to state whether the PH activity profile (preferred hemifield) was significantly different from the APH activity profile (anti-preferred hemifield). The significance of this difference was stated with a bootstrap analysis, as follows. First, we computed the actual preferred direction and (Pd), the PH and APH profiles, and the difference D_{actual} between the two profiles (integrated in the corresponding time window):

$$D_{actual} = \int_{time\_window} PH_{actual} - APH_{actual}$$

Then, we reassigned each trial to a randomly chosen movement direction. We computed the new bootstrap Pd_{boot}, the PH_{boot} and APH_{boot} profiles, and the difference D_{boot} between the two profiles:

$$D_{boot(i)} = \int_{time\_window} PH_{boot(i)} - APH_{boot(i)}$$

We repeated this procedure for N=500 times, and obtained a set of $D_{boot(i)}$ with i=1...500. Finally we considered the actual difference D_{actual} to be significantly greater than zero if four or less of the $D_{boot(i)}$ exceeded D_{actual} ($p<0.01$). Note that in the analysis of the profiles we did not impose any pre-condition before computing the Pd. Thus, the Pd was

initially defined for all cells. The bootstrap analysis performed here is thus analogous to the tests on the directional tuning of the cells used elsewhere [42, 43, 13, 27], with the difference that the test used here imposes to the cell the minimal request to "distinguish" between hemifield.

We also defined the two additional variables *precue* and *early dir selec*. For the variable *precue*, we analyzed whether the ALL activity profile had a consistent trend (increase or decrease) in the time window (*cue*-640 : *cue*). A trend was considered significant based upon a linear regression analysis ($p<0.01$). For the variable *early dir selec*, we analyzed the PH and APH profiles. We considered that there was a significant *early dir selec* if the PH profile consistently exceeded the APH profile for at least 15 consecutive time bins (300 msec) starting within 350 msec after the *cue*.

Note that the variables defined above are quasi-independent from each other. This is because there is no *a priori* correlation between pairs of "modulation" variables (*aftercue*, *delay*, *RT*, *early mov*, and *late mov*), except for contiguous overlapping variables (e.g., *early mov* and *late mov*). Likewise, there is no *a priori* correlation between pairs of "dir selec" variables (*early dir selec*, *delay dir selec*, *RT dir selec*, *early dir selec*, and *late dir selec*), except for the contiguous overlapping variables (e.g., *early mov dir selec* and *late mov dir selec*). Moreover, there is no *a priori* correlation between "modulation" and "dir selec" pairs of variables.

This description was completed considering that the cell was significantly *task-related* if at least one of the previously defined variables was significant. Table 2 summarizes all the profile variables defined.

Preferred direction

The preferred direction of each cell was identified as the direction of the vector average of the eight directional activation (corresponding to the eight movement directions) recorded in the time window (*mo*-200 : *me*). The choice of this window may appear somewhat arbitrary in the present context. However, although the Pd does not remain strictly constant throughout the trial[44-46], there still is a relatively good correspondence between measures of the Pd at different times.

Differences across monkeys

The differences across monkeys/studies include the size of the monkeys (6.5-7.5 Kg for F and C; 5-5.5 Kg for R and N; 11-13.5 Kg for B and M), the size of the squares and the center-out distance of the movement (scaled to the size of the monkeys); the duration the variable delay (0.5-1.5 s for F and C; 1.1-1.9 for R and N; 0.8-1.2 s for B and M); the experimenters performing the recordings and off-line clustering. In particular, no constraints were imposed on the reaction time (RT, time from the *go* to the *mo*) during all the experiments, and different monkeys performed with different RT. Monkeys C and F had the most consistent behavior, as >88% of their RT fell in the time window (200-400 msec). For monkeys R and N, >89% of RT fell in the time window (200-500 msec). Monkeys B and M had a less consistent behavior, and often (>25% of trials) anticipated the movement (RT<200 msec). (Presumably, this was because the delay was less variable in their experiment.) To accommodate differences across monkeys, we included in the analysis only trials with RT within the time window (150-500 msec), and we did not

consider cells recorded from monkeys B and M in the analysis of the *delay* and *RT* variables.

Results

Database

We analyzed a total of 903 cells, recorded from five cortical areas (preSMA, PMd, SMA, M1, and PMv) and from six monkeys. The database, divided for monkeys and areas, is illustrated in Table 1. Unless otherwise specified, the following analysis refers to the Baseline epoch, which was in each session the block of trials prior to the introduction of the perturbing force field.

Table 2 summarizes all the profile variables defined here, with the relative time windows and statistical tests. The gray areas indicate the "modulation" variables. Note that the profile variables naturally form a chronological sequence (top to bottom in Table 2).

Activity profiles: preSMA

Figure 1a-e shows the activity profile of five cells recorded from the preSMA. In each plot, the black and gray lines indicate the PH and APH activity, respectively. A significant *precue* activity was most frequently found in the preSMA, as exemplified by the cell shown in Figure 1a. In the 450-550 msec prior to the *cue*, the cell activity ranges the 3-5 Hz. Before the *cue*, the cell's activity raises gradually, and at the *cue* the activity ranges the 11-13 Hz. Of course, the *precue* activity is not directionally selective, because no stimulus is present at that time. However, in the *precue* period the monkey expects an upcoming instruction. Shortly after the *cue* (*cue*+200 msec), the PH and APH profiles of the cell separate, and the cell becomes directionally selective (*early dir selec*). In the *delay*, the activity of the cell remains sustained, and directionally selective (*delay dir selec*). However, shortly after the *go* –and before the *mo* –both the PH and APH activity profiles decay, and the cell looses its directional selectivity. The peak activity of the cell (red dot) is observed in the *cue* alignment, and occurs 280 msec after the *cue*.

Figure 1b illustrates the activity profile of another preSMA cell. In this case, the cell is clearly task-related (i.e., modulated during the trial), but not directionally selective. The activity of the cell –initially very low –raises sharply after the *go* signal, and sharply falls back within 400 msec. Note that the activity peak is also visible in the *mo* alignment (right panel). However, the peak observed in the *go* alignment is higher.

A rather striking case of *precue* activity is shown in Figure 1c. The activity of this cell –initially very low –raises in the 500 msec prior to the *cue* and drops shortly after the *cue*. Later in the trial, the cell has a second –directionally selective –response peak. The peak activity is recorded when trials are aligned with the *go* signal, 480 msec after the *go*.

Figure 1d shows another example of directionally non-selective cell. During the *precue*, the activity of the cell increases from 12-15 Hz to 22-26 Hz. The activity continues to increase during the delay, and after the *go* signal, and reaches its peak 100 msec before the *mo*. After the *mo*, the activity drops, and returns to that observed at rest. Over the entire trial, however, no directional selectivity is observed. From a strictly motor point of view, modulation in the task implies directional selectivity. Thus, the activity of this cell does not appear purely "motor".

Figure 1e shows an example of inhibited activity. Prior to the *cue*, the activity of the cell drops from over 80 Hz down to 12-14 Hz. The activity of the cells remains very low in the *delay*, but raises again after the *go* signal. During the movement, the activity profile of the cell is directionally selective. The PH and APH profiles drop at the end of the movement, and then gradually return high. In this case again, although the cell certainly appears task-related, its activity profile is not readily interpreted as purely "motor".

In conclusion, the following characteristics were observed in preSMA cells. First, significant *precue* activity was relatively frequent. Second, early responses to the *cue* and the *go* signal were also relatively frequent. Third, we found several cells with non-directionally selective modulations. Compared to the other areas, the activity profiles of preSMA cells were more often difficult to interpret as purely "motor". These characteristics are quantified in Table3.

Activity profiles: PMd

Like cells in preSMA, cells in PMd often showed a *precue* activity. Furthermore, PMd cells often became directionally selective shortly after the *cue* (*early dir selec*). For instance, the activity profile of the cell in Figure 2a gradually increased over the 500 msec prior to the *cue*. Within 220 msec after the *cue* the cell also became directionally selective, and the PH profile reached its peak in the *cue* alignment, 560 msec after the *cue*. At the *go* signal the cell was still directionally selective, but the PH activity dropped shortly thereafter, before the *mo*. Figure 2b shows another example of cell with an early response, that extinguishes by the *mo*. In this case, however, there is no *precue* activity.

Both early response and late "motor" response were common in the PMd, and often coexisted in the same cell. The cell in Figure 2c becomes directionally selective 260 msec after the *cue*, and maintains its selectivity until after the end of the movement. During the delay, the cell is mostly modulated by the fact that the APH profile (gray) is inhibited. In contrast, the PH profile shows a substantial response after the *go* signal, reaching its peak 60 msec after the *go*. Note that the activity of the cell remains directionally selective after the end of the movement, a characteristic often observed also in SMA and M1.

Figure 2d shows another cell were early and late components coexisted. In this case, the cell has a *precue* response, and becomes directionally selective shortly (200 msec) after the *cue* (*early dir selec*). The cell, however, also exhibits a sharp movement-related activity starting shortly before the *mo* and peaking 160 msec after the *mo* (*mo* alignment).

Yet another case of coexistence of early and late components is shown in Figure 2e. In this case, we observe a transient and directionally selective response, time-locked with the presentation of the *cue* (peak circa 160 msec after the *cue*). The activity profile of the cell shows some directional selectivity in the *delay*, followed by a sharp raise after the *go* signal. The peak activity of this cell was observed 500 msec after the *mo*.

In conclusion, we observed the following characteristics for the activity profiles of PMd cells. First, significant *precue* and *early dir selec* were relatively frequent, though less frequent than in the preSMA. Second, PMd cells were frequently directionally selective at the end of the delay (*delay dir selec*) and shortly after the *go* signal (*RT dir selec*). Third, many PMd cells also showed a classic movement-related component. Early

components and late components often coexisted in the activity of single cells. These characteristics are quantified in Table3.

Activity profiles: SMA

Figure 3a-e illustrates the activity profiles of five representative cells recorded from the SMA. A vivid example of "delay" cell is shown in Figure 3a. At *rest*, the activity of the cell ranges the 25-33 Hz. After the *cue*, the activity profile increases, and becomes directionally selective 240 msec after the *cue*. The PH profile continues to increase, then remains essentially stable until after the *go* signal. After the *go* –and prior to the *mo* –the activity of the cells drops. The cell looses its directional selectivity shortly after the *mo*, when the activity returns close to that observed at *rest*.

The cell in Figure 3b has a similar response early after the cue. However, this cell maintains its directional selectivity throughout the trial. The *delay dir selec* is mostly due to the inhibition of the APH profile (gray). In contrast, the PH profile increases slightly within the delay, but shows a sharp response time-locked with the *go* signal. The PH profile reaches its peak 160 msec after the *go*.

Another representative SMA cell is shown in Figure 3c. Here, the activity is very low (0-2 Hz) at *rest*, and slightly increases over the course of the delay. However, the activity increases further –and more dramatically –following the *go* signal. The peak activity –visible in both the center and the right panel –is sharper and higher in the *go* alignment, suggesting that the *go* signal is a more salient event for this cell. During the movement, the activity profile gradually drops, and looses its directional selectivity.

The *delay dir selec*-tivity of the cell in Figure 3d seems at first incongruent with the directional selectivity observed during the movement, because the PH profile lies below the APH profile before and just after the *go* signal. In fact, the APH profile is essentially stable, whereas the PH profile is partially inhibited prior to the *go* signal, and has a substantial "motor" response during the RT and the movement.

The cell in Figure 3e has a somewhat depressed (but directionally selective) activity during the delay, followed by a classical "motor" response. After the *go* signal, the PH activity profile sharply increases and reaches its peak 120 msec into the movement, while the APH activity remains depressed.

In conclusion, these examples illustrate three characteristics of SMA cells. First, SMA cells had only seldom a *precue* and *early dir selec* components. Second, they often became directionally selective during the delay (*delay dir selec*), and particularly during the RT (*RT dir selec*). Third, the activity peak of SMA cells was often time-locked with the *go* signal. These characteristics are quantified in Table3.

Activity profiles: M1

Most frequently, cells in M1 were significantly modulated only during the movement. Their modulation and directional selectivity often began after the *go* signal, reaching a peak at or close to the *mo*, as observed in the *mo* alignment.

One such example is shown in Figure 4a. During the delay, the activity of this cell was mildly depressed in a directionally non-selective fashion. Shortly after the *go* signal, the PH activity raised sharply, and reached a peak 60 msec before the *mo*. The APH activity showed a complementary depression, reaching a minimum peak shortly after the

mo. Notably, the cell remained directionally selective at the end of movement, possibly indicating a positional signal.

The activity profile of cell in Figure 4b remained low and not-modulated during the delay. After the *go* signal, the PH activity raised sharply, reaching a peak at the *mo* (*mo* alignment). Note also that the APH profile of this cell (gray) has a late movement-related peak.

The cell illustrated in Figure 4c was not modulated during the delay. The cell became, however, directionally selective after the *go* signal, when the PH profile sharply increased to values several folds higher than *rest*. The peak activity was highest in the *mo* alignment, and occurred 100 msec after the *mo*. The cell in Figure 4d did show a directional selectivity in the delay. After the *go* signal, however, the PH activity increased by many folds, reaching its peak 120 msec after the *mo*. Finally, we sometimes observed late peaks in the activity profiles. Figure 4e shows one such example, where the PH profile of the cell reached a peak 480 msec after the *mo*.

In conclusion, we observed the following characteristics for M1 cells. First, any modulated activity or directional selectivity prior to the *go* was rather infrequent. Second, most activity peaks were aligned with the *mo*. Third, the peak activity was often several times higher than *rest*. These characteristics are quantified in Table3.

Activity profiles: PMv

The activity profile of PMv cells was relatively less frequently task-related. Considering task-related cells, the activity profiles were sometimes similar to that observed in M1. Three such examples are shown in Figure 5a-c. In all three cases, the cells are not modulated prior to the *go* signal, and have a strong directionally selective response after the *go*. For cells in Figure 5a and 5b, the response occurs in the RT, prior to the *mo*. For the cell in Figure 5c, the response begins at the *mo*, and the PH profile reaches its peak 220 msec into the movement.

In several cases, the PH and APH profiles of PMv cells were qualitatively similar, though quantitatively different. For instance, the cell in Figure 5d showed a broad movement-related activity profile, which reached its PH peak 320 msec after the *mo*. However, the PH and APH profiles have very similar patterns.

Other cells, such as that illustrated in Figure 6e, were clearly modulated by the task, but in a directionally non-selective fashion. For the cell in Figure 5e, the modulation begins after the *go* signal and occurs as a depression of the activity.

In conclusion, we observed the following peculiarities for PMv cells. First, many cells were not task-related. Second, the activity profiles of task-related cells were in some cases similar to that observed in M1, with little delay activity, movement-related modulation, and activity peak aligned with the *mo*. In general, however, the activity profiles of PMv cells appeared less readily interpretable than that of the PMd, SMA and M1. These characteristics are quantified in Table3.

Quantitative comparison across areas

We analyzed the activity profile of each neuron by computing all the variables defined in Table2. For each area and for each variable, we computed the percentage of neurons that passed the significance test. The percentages obtained are presented in Table3. For instance, we learn from the first row of Table3 that a significant *precue* activity was

present in 32% of preSMA cells, in 20% of PMd cells, in 13% of SMA cells, in 12% of M1 cells, and in 13% of PMv cells.

Inspection of the percentages shown in Table3 reveals several important points. First, the activity of neurons in all areas was for the vast majority modulated during the task (last row in Table3). For preSMA, PMd, SMA, and M1 92-97% of cells passed at least one significance test. As partial exception, "only" 81% of PMv cells displayed some modulation (see Discussion). Second, in all areas the neuronal activity was chiefly movement-related. Comparison of the (similarly defined) variables *aftercue*, *delay*, *early movement*, and *late movement* shows that for all areas the percentage of modulated neurons increased over the trial. Considering for example SMA, we find a significant *aftercue* activity for 3% of cells. The percentage of modulated cells increases in the *delay* to 44% of cells, in the *early movement* to 57% of cells, and in the *late movement* to 67% of cells. Similar trends can be observed in other areas, also considering the variables quantifying the directional selectivity.

The most interesting result emerges from Table3 when we compare the *order* of different areas, for different variables. Considering the first row of Table3 (*precue*), we observe a clear gradient across areas: more *precue* activity is present in preSMA (32%) than in PMd (20%), whereas a reduced *precue* activity is present in SMA (13%), M1 (12%), and PMv (13%). In other words, during the *precue*, preSMA is the "leading" area. The same trend is found when we observe the variables *aftercue* (second row) and the *early dir selec* (third row of Table3). For instance, the percentage of cells with a significant *early dir selec* is highest in the preSMA (28%), and orderly decreasing in the PMd (24%), the SMA (20%), the M1 (11%), and the PMv (9%). Again, early after the *cue*, the preSMA appears to be the "leading" area. Note that the *precue*, *aftercue*, and *early dir selec* are *a priori* independent variables

The order of different areas changes over the time course of the trial. Considering the variable *delay*, it can be observed that the PMd and the SMA are progressively more present (the percentages are comparable with that of the preSMA), while the M1 and PMv "lag behind". Considering the variable *delay dir selec*, PMd becomes the leading area (25%), followed by the preSMA (22%), and the SMA (18%). In M1 and PMv, only few cells still pass the test (7% and 3%, respectively). If we now consider the variable *RT dir selec*, the leading area becomes SMA (45%), while M1 "catches-up". Finally, during the early movement (*early mov*, *early mov dir selec*) M1 becomes the leading area, with SMA, PMd and preSMA orderly less modulated.

Thus, the areas preSMA, PMd, SMA and M1 appear to fall in a "logical" sequence, maintained across time windows. The emerging picture can be illustrated by a cartoon (Figure 6), where the x-axis represents time, the y-axis represent the "task-relatedness," and different areas appear as subsequent, overlapping waves of increasing magnitude. For each area, the task-relatedness increases over the trial, and reach its maximum during the movement. Yet, areas appear in a clear order. On the one hand, preSMA "enters" the scene first, orderly followed by the PMd, SMA and M1. On the other hand, the most task-related area during the movement is M1, orderly followed by the SMA, PMd and preSMA.

Few additional remarks should be made on Table 3. First, the "modulation" variables (*aftercue*, *delay*, *RT*, *early mov*, *late mov*) are analogous to each other and somewhat complementary to the "dir selec" variables (*early dir selec*, *delay dir selec*, *RT*

dir selec, *early mov dir selec*). It is not necessarily meaningful to directly compare variables of the two groups (e.g., *aftercue* with *early dir selec*, or *delay* with *delay dir selec*). In fact, the "dir selec" variables seem to run "ahead of time" compared to the "modulation" variables (for instance, compare the order between areas indicated by *RT* with that indicated by *RT dir selec*). Second, excluding the PMv, the summary depicted in Figure 6 captures all the *order* relations between areas, except for one value (the *late mov dir selec* for the PMd, in parenthesis in Table 3).

In all respects, the PMv (rightmost column in Table 3) is the less task-related area. For every variable, the percentage of PMv cells passing the relative test is the lowest among areas (note that PMv cells were recorded and analyzed together with PMd cells). Moreover, the PMv does not seem to have a natural position in Table 3. Thus, the rightmost column should not be interpreted as indicative of a specific position in the "logical" sequence of areas. Data from the PMv were included here for completeness, but additional work is necessary to further investigate its properties.

Population activity profiles and profile peaks

For each area, we computed the population activity profile by averaging the activity profiles of all cells. The population PH and APH profiles for the five areas are shown in Figure 7a-e. The population profiles reflect the characteristics found in the cell-by-cell analysis described above. For instance, the preSMA is the first area to show a PH/APH separation shortly after the *cue*, followed by the PMd. The delay activity is clearly modulated and directionally selective in the preSMA, PMd and SMA, but not in the M1 and PMv. In correspondence of the movement execution, all five areas show a peak of activity, but with different *relative* modulations. The population activity peak is comparatively highest in M1 (~2.2 times the rest activity), and orderly lower in the SMA (~1.9 times the rest activity), the PMd (~1.9 times the rest activity), the preSMA (~1.4 times the rest activity), and in the PMv (~1.5 times the rest activity).

We also analyzed the peaks of the activity profiles. For each cell we considered the maximal activity peak across the three alignment (*cue*, *go*, and *mo*). The histograms shown in Figure 7a-e illustrate the distribution of activity peaks for the five areas under consideration. For each area, we computed the percentage of cells whose PH profile reached its peak (1) during the delay (between the *cue* and the *go*); (2) aligned with the *go* (after the *go*); and (3) aligned with the *mo*. The values for the five areas are shown in Table 4. Essentially, the analysis of the peaks provides results consistent with the previous conclusions. For instance, cells that reached their activity peak within the delay were most commonly found in the preSMA (14%), and orderly less in the PMd (13%), the SMA (6%), and the M1 (4%). One interesting result of this analysis is that for a large percentage of SMA cells (41%) the peak activity was observed when trials were aligned at the *go* signal, rather than at the *mo*. In contrast, the activity peak of most M1 cells (71%) was observed when trials were aligned at the *mo*.

Discussion

The present study analyzed the activity of a large database of neurons recorded from five motor areas of the frontal lobe during visually instructed, delayed reaching movements. We compared the modulation and directional selectivity of neurons in separate time windows, spanning from prior to the presentation of the instruction to late into the movement. We presented here two main results. First, all areas appeared largely task-related, and all areas were increasingly modulated within the trial. Second, different areas fell in a "logical" sequence. Multiple distinct and independent measures of timing and modulation consistently indicate the same order: preSMA, PMd, SMA, and M1 (the position of the PMv is dubious at this time). The emerging picture –resembling that of subsequent but overlapping waves –contains both elements of serial and parallel organization. Serial, in that distinct areas fall in a precise order. Parallel, in that distinct areas largely overlap.

The present results area largely consistent with previous studies comparing two or three different areas. In particular, numerous studies contrasted the activity of the PMd and M1. In general, these studies concluded or indicate that the PMd lies "upstream" of M1 (refs. [5, 10, 12-14, 16-19, 45]). Likewise, several studies contrasted the activity of the preSMA and SMA. These studies generally concluded or indicate that the preSMA is rather remote from, whereas the SMA is more intimately related to the implementation of the actual movement[6-8, 11, 21, 37-41]. In contrast, few studies compared the activity of the newly defined SMA with either the M1 or the PMd (old works that did not distinguish the SMA from the preSMA are not valid). Thus, our third major result is to "put on the map" the SMA. In general, our data indicate that of the areas under consideration the PMd, SMA and M1 are –in this order –the most purely "motor". More specifically, the SMA appears to be the closest and just "upstream" of M1 among the areas considered here.

Acknowledgments

This research was supported by the National Institute of Health (NIH grant MN481185).

References

1. He, S.Q., Dum, R.P. & Strick, P.L. Topographic organization of corticospinal projections from the frontal lobe: motor areas on the lateral surface of the hemisphere. *J. Neurosci.* **13,** 952-980 (1993).
2. He, S.Q., Dum, R.P. & Strick, P.L. Topographic organization of corticospinal projections from the frontal lobe: motor areas on the medial surface of the hemisphere. *J. Neurosci.* **15,** 3284-3306 (1995).
3. Thach, W.T. Correlation of neural discharge with pattern and force of muscular activity, joint position, and direction of intended next movement in motor cortex and cerebellum. *J. Neurophysiol.* **41,** 654-676 (1978).
4. Kurata, K. & Wise, S.P. Premotor and supplementary motor cortex in rhesus monkeys: neuronal activity during externally- and internally-instructed motor tasks. *Exp. Brain Res.* **72,** 237-248 (1988).
5. Riehle, A. & Requin, J. Monkey primary motor and premotor cortex: single-cell activity related to prior information about direction and extent of an intended movement. *J. Neurophysiol.* **61,** 534-549 (1989).
6. Alexander, G.E. & Crutcher, M.D. Preparation for movement: neural representations of intended direction in three motor areas of the monkey. *J. Neurophysiol.* **64,** 133-150 (1990a).
7. Crutcher, M.D. & Alexander, G.E. Movement-related neuronal activity selectively coding either direction or muscle pattern in three motor areas of the monkey. *J. Neurophysiol.* **64,** 151-163 (1990).
8. Alexander, G.E. & Crutcher, M.D. Neural representation of the target (goal) of visually guided arm movements in three motor areas of the monkey. *J. Neurophysiol.* **64,** 164-178 (1990b).
9. Werner, W., Bauswein, E. & Fromm, C. Static firing rates of premotor and primary motor cortical neurons associated with torque and joint position. *Exp. Brain Res.* **86,** 293-302 (1991).
10. Riehle, A. & Requin, J. The predictive value for performance speed of preparatory changes in neuronal activity of the monkey motor and premotor cortex. *Behav. Brain Res.* **53,** 35-49 (1993).
11. Halsband, U., Matsuzaka, Y. & Tanji, J. Neuronal activity in the primate supplementary, pre-supplementary and premotor cortex during externally and internally instructed sequential movements. *Neurosci. Res.* **20,** 149-155 (1994).
12. Fu, Q.G., Flament, D., Coltz, J.D. & Ebner, T.J. Temporal encoding of movement kinematics in the discharge of primate primary motor and premotor neurons. *J. Neurophysiol.* **73,** 836-854 (1995).
13. Johnson, P.B., Ferraina, S., Bianchi, L. & Caminiti, R. Cortical networks for visual reaching: physiological and anatomical organization of frontal and parietal lobe arm regions. *Cereb. Cortex* **6**, 102-119 (1996).
14. Crammond, D.J. & Kalaska, J.F. Differential relation of discharge in primary motor cortex and premotor cortex to movements versus actively maintained postures during a reaching task. *Exp. Brain Res.* **108**, 45-61 (1996).

15. Cadoret, G. & Smith, A.M. Comparison of the neuronal activity in the SMA and the ventral cingulate cortex during prehension in the monkey. *J. Neurophysiol.* **77,** 153-166 (1997).
16. Scott, S.H. & Kalaska, J.F. Reaching movements with similar hand paths but different arm orientations. I. Activity of individual cells in motor cortex. *J. Neurophysiol.* **77,** 826-852 (1997a).
17. Scott, S.H. & Kalaska, J.F. Reaching movements with similar hand paths but different arm orientations. I. Activity of individual cells in dorsal premotor cortex and parietal area 5. *J. Neurophysiol.* **78,** 2413-2426 (1997b).
18. Shen, L. & Alexander, G.E. Neural correlates of a spatial sensory-to-motor transformation in primary motor cortex. *J. Neurophysiol.* **77,** 1171-1194 (1997a).
19. Shen, L. & Alexander, G.E. Preferential representation of instructed target location versus limb trajectory in dorsal premotor area. *J. Neurophysiol.* **77,** 1195-1212 (1997b).
20. Donchin, O., Gribova, A., Steinberg, O., Bergman, H. & Vaadia, E. Primary motor cortex is involved in bimanual coordination. *Nature* **395,** 274-278 (1998).
21. Shima, K. & Tanji, J. Neuronal activity in the supplementary and presupplementary motor areas for temporal organization of multiple movements. *J. Neurophysiol.* **84,** 2148-2160 (2000).
22. Wessberg, J., *et al.* Real-time prediction of hand trajectory by ensembles of cortical neurons in primates. *Nature* **408,** 361-365 (2000).
23. Donchin, O., Gribova, A., Steinberg, O., Bergman, H., Cardoso de Oliveira, S. & Vaadia, E. Local field potentials related to bimanual movements in the primary and supplementary motor cortices. *Exp. Brain Res.* **140,** 46-55 (2001).
24. Kakei S, Hoffman DS, Strick PL. Direction of action is represented in the ventral premotor cortex. *Nat. Neurosci.* **4,** 1020-1025 (2001).
25. Dum, R.P. & Strick, P.L. The origin of corticospinal projections from the premotor areas in the frontal lobe. *J. Neurosci.* **11,** 667-689 (1991).
26. Prut, Y. & Fetz, E.E. Primate spinal interneurons show pre-movement instructed delay activity. *Nature* **401,** 590-594 (1999).
27. Li, C-S.R., Padoa-Schioppa, C. & Bizzi, E. Neural correlates of motor performance and motor learning in the primary motor cortex of monkeys adapting to an external force field. *Neuron* **30,** 593-607 (2001).
28. Padoa-Schioppa, C., Li, C-S.R. & Bizzi, E. Neuronal activity in the supplementary motor area of monkeys adapting to a new dynamic perturbation. (In preparation).
29. Xiao, J., Padoa-Schioppa, C. & Bizzi, E. Neuronal activity in the dorsal and ventral premotor areas of monkeys adapting to a new dynamic perturbation. (In preparation).
30. Shadmehr, R. & Mussa-Ivaldi, F.A. Adaptive representation of dynamics during learning of a motor task. *J. Neurosci.* **14,** 3208-3224 (1994).
31. Brashers-Krug, T., Shadmehr, R., & Bizzi, E. Consolidation in human motor memory. *Nature* **382,** 252-255 (1996).
32. Flanagan J.R., Nakano, E., Imamizu, H., Osu, R., Yoshioka, T. & Kawato, M. Composition and decomposition of internal models in motor learning under altered kinematic and dynamic environments. *J. Neurosci.* **19,** (RC34) 1-5 (1999).
33. Krakauer, J.W, Ghilardi, M.F. & Ghez, C. Independent learning of internal models for kinematic and dynamic control of reaching. *Nat. Neurosci.* **2**, 1026-1031 (1999).

34. Gandolfo, F., Li, C.-S., Benda, B.J., Padoa-Schioppa, C. & Bizzi, E. Cortical correlates of learning in monkeys adapting to a new dynamical environment. *Proc. Natl. Acad. Sci. USA* **97**, 2259-2263 (2000).
35. Geyer, S., Matelli, M., Luppino, G. & Zilles, K. Functional neuroanatomy of the primate isocortical motor system. *Anat. Embryol. (Berl.).* **202**, 443-474 (2000).
36. Luppino, G., Matelli, M., Camarda, R.M., Gallese, V. & Rizzolatti, G. Multiple representations of body movements in mesial area 6 and the adjacent cingulate cortex: an intracortical microstimulation study in the macaque monkey. *J. Comp. Neurol.* **311,** 463-482 (1991).
37. Matsuzaka, Y., Aizawa, H. & Tanji, J. A motor area rostral to the supplementary motor area (presupplementary motor area) in the monkey: neuronal activity during a learned motor task. *J. Neurophysiol.* **68,** 653-662 (1992).
38. Matsuzaka Y, Tanji J. Changing directions of forthcoming arm movements: neuronal activity in the presupplementary and supplementary motor area of monkey cerebral cortex. *J. Neurophysiol.* **76**, 2327-2342 (1996).
39. Hikosaka, O. *et al.* In: *The New Cognitive Neuroscience* (ed Gazzaniga, M.S.) 553-572 (MIT Press, Cambridge MA, 2000).
40. Picard, N. & Strick, P.L. Motor areas of the medial wall: a review of their location and functional activation. *Cereb. Cortex* **6,** 342-353 (1996).
41. Picard, N. & Strick, P.L. Imaging the premotor areas. *Curr. Opin. Neurobiol.* **11**, 663-672 (2001).
42. Georgopoulos, A., Kalaska, J., Caminiti, R. & Massey, J. On the relations between the direction of two-dimensional arm movements and cell discharge in primate motor cortex. *J. Neurosci.* **2,** 1527-1537 (1982).
43. Battaglia-Mayer, A. *et al.* Early coding of reaching in the parietoccipital cortex. *J. Neurophysiol.* **83,** 2374-2391 (2000).
44. Sergio, L.E. & Kalaska, J.F. Systematic changes in directional tuning of motor cortex cell activity with hand location in the workspace during generation of static isometric forces in constant spatial directions. *J. Neurophysiol.* **78,** 1170-1174 (1997).
45. Johnson, M.T.V., Coltz, J.D., Hagen, M.C. & Ebner, T.J. Visuomotor processing as reflected in the directional discharge of premotor and primary motor cortex neurons. *J. Neurophysiol.* **81,** 875-894 (1999).
46. Padoa-Schioppa, C., Li, C.-S.R. & Bizzi, E. Planning movements: kinematics-to-dynamics transformation in the supplementary motor area. (Submitted).

Figure legends

Figure 1. Activity profiles of five preSMA cells. **A.** The three panels show the activity profile of one cell obtained aligning the trials with the presentation of the *cue* (left panel), with the *go* signal (center panel), and with the movement onset (*mo*, right panel). The plots illustrate the activity profiles of the preferred hemifield (PH, black) and anti-preferred hemifield (APH, gray). In all three panels, the x-axis indicates the time in msec, and "zero" is the corresponding alignment (*cue*, *go*, *mo*). The y-axis indicates the firing frequency of the cell. The scale –the same for all three panels –is indicated only on left panel (in Hz). The activity profiles are computed in 80-msec time bins, shifted by 20 msec. The red dot on x-axis of the left panel indicates the time (*cue*+350 msec) at which the PH profile reaches its peak (only the highest of the three peaks obtained for the three alignments is indicated). This cell has a significant *precue* activity, as the activity profiles gradually increase prior to the presentation of the *cue*. The cell has also a significant *early dir selec*-tivity, because the PH and APH profiles separate 200 msec after the *cue*. The cell maintains its modulation and directional selectivity throughout the delay and reaction time (RT), and looses its selectivity shortly before the *mo*. **B.** This cell has a sharp activity peak, time-locked with the *go* signal, but not directionally selective. **C.** This cell has a striking *precue* activity, which drops shortly after the *cue*. It also has a later – directionally selective –activity peak. **D.** This cell is modulated (*precue*, *aftercue*, *delay*, *RT*, *early mov*, and *late mov*), but not directionally selective in any time window. Thus, its activity appears not purely "motor". **E.** The activity of this cell is mostly inhibited during the trial (see scale on the left). However, the cell has a directionally selective modulation during the movement.

Figure 2. Activity profiles of five PMd cells. All conventions as in Figure 1A. **A.** This cell has a significant *precue* activity, and an *early dir selec*-tivity. The PH activity profile reaches its peak 560 msec after the *cue*, after which the profile of the cell gradually decreases. The cell still remains directionally selective throughout the RT. Its activity eventually drops at or shortly after the *mo*. **B.** This cell has an *early dir selec*-tive response. The PH profile continues to increase over the course of the delay and after the *go* signal. During the RT, however, the activity drops and the cell looses its directional selectivity shortly after the *mo*. **C.** This cell becomes directionally selective 260 msec after the *cue*, and maintains its directional selectivity throughout the trial. During the delay, the APH profile drops, while the PH profile remains relatively stable. After the *go*, however, the PH profile increases for a typical "motor" response, reaching its peak 60 msec after the *mo*. **D.** The activity profile of this cells shows both early and late components. The cell remains directionally selective from early after the *cue* throughout the movement. The PH profile reaches its peak 160 msec after the *mo*. **E.** Another case of cell with both early and late components.

Figure 3. Activity profiles of five SMA cells. All conventions as in Figure 1A. **A.** This cell is somewhat similar to cells observed in the preSMA (Figure 1A) and PMd (Figure 2A). **B.** This cell becomes directionally selective 240 msec after the *cue*, and maintains its selectivity throughout the trial. The APH profile of the cell is mostly inhibited, whereas the PH profile has a peak of activity 160 msec after the *go* signal. **C.** The activity

of this typical SMA cell is low and not modulated before the *cue*, and gradually becomes modulated and directionally selective over the course of the delay. After the *go*, the activity of the cell sharply increases, and then gradually decays during the movement. The peak of the cell is highest when trials are aligned with the *go* signal, and occurs 220 msec after the *go*. **D.** In this case the cell is directionally selective in the delay, but in a way (apparently) incongruent with that in the movement. In fact, the APH profile remains essentially stable throughout the delay, whereas the PH profile is inhibited. After the *go* signal, the PH profile has a sharp raise, similar to the responses often observed in M1. **E.** During the delay, the activity of this cell is gradually depressed. After the *go* signal, however, the PH profile raises and remains high throughout the movement, reaching its peak 120 msec after the *mo*. Thus, this cell has a mild delay activity, followed by a "classic" motor response.

Figure 4. Activity profiles of five M1 cells. All conventions as in Figure 1A.**A.** The activity profile of this M1 cell remains directionally non-selective (though mildly depressed) throughout the delay. After the *go*, the PH profile increases and reaches its peak 60 msec before the *mo*, in the *mo* alignment. In contrast, the APH profile activity decreases, and reaches a minimum shortly after the *mo*. The cell remains directionally tuned throughout and after the movement, possibly indicating a position-dependent signal. **B.** The profile of this cells is not modulated prior to the *go* signal, and sharply raises during the RT. The PH profile reaches its peak at the *mo*, before decaying. **C.** This cell has a similar profile than that in B., except that the PH profile reaches its peak 100 msec after the *mo*, and that the cell maintains a directional selectivity after the end of the movement. **D.** In this case, the cell has some directional selectivity during the delay, and increases its activity more substantially during the RT. The PH profile reaches its peak 120 msec after the *mo*. **E.** This cell has a late peak, occurring 480 msec after the *mo*.

Figure 5. Activity profiles of five PMv cells. All conventions as in Figure 1A. **A. B. and C.** The activity profiles of these cells are not modulated prior to the *go*. After the *go*, the cells have substantial PH responses, similar to that observed in the activity profiles of many M1 cells (Figure 4). The PH profiles reach their peak before or after the *mo*. **D.** In this case the PH and APH profiles are qualitatively very similar, though quantitatively different. **E.** This cell is task-related (modulated during the trial), but not directionally selective.

Figure 6. Emerging picture. Areas are represented by subsequent and overlapping waves of increasing magnitude, in their "logical" order (preSMA, PMd, SMA, and M1).

Figure 7. Activity profiles for the five areas preSMA, PMd, SMA, M1, PMv. The black and gray line represent the population PH and APH activity profiles, respectively. The histograms refer to the maximal activity peaks. The time scale (x-axis) is the same as for the activity profiles. The y-axis represent the number of cells. The scale –common to all three alignments –is shown on the right of the right panel. **A.** PreSMA. **B.** PMd. **C.** SMA. **D.** M1 (the activity profile includes only data from monkeys R and N; see methods for details). **E.** PMv.

Tables

Table 1: Neuronal database.

	PreSMA	PMd	SMA	M1	PMv	Total
F			59			59
C	105 (26)		239 (46)			344 (72)
R		108		54	133	295
N		34			10	44
B				47		47
M				114 (7)		114 (7)
Total	105 (26)	142	298 (46)	215 (7)	143	903 (79)

Legend. Neuronal database. We recorded from six monkeys (rows F, C, R, N, B, and M) and from five cortical areas (columns PreSMA, PMd, SMA, M1, and PMv). Values in the Table indicate the number of cells recorded from each monkey/area. We included in the analysis both experimental and control cells (903 cells total). The number of control cells for each group is indicated in parenthesis.

Table 2: Profile variables.

	Time window	Statistical test	p-value
"rest"	*cue*-700 : *cue*-300		
1. Precue	*cue*-640 : *cue*	Linear regression	p<0.01
2. Aftercue	*cue*+100 : *cue*+500	ANOVA against "rest"	p<0.01
3. Early dir selec	*cue* : *cue*+350	1st of 15 consecutive signs	
4. Delay	*go*-400 : *go*	ANOVA against "rest"	p<0.01
5. Delay dir selec	*go*-400 : *go*	Bootstrap (new dir assign)	p<0.01
6. RT	*go*-200 : *go*+200	ANOVA against "rest"	p<0.01
7. RT dir selec	*go*-200 : *go*+200	Bootstrap (new dir assign)	p<0.01
8. Early mov	*mo*-200 : *mo*+200	ANOVA against "rest"	p<0.01
9. Early mov dir selec	*mo*-200 : *mo*+200	Bootstrap (new dir assign)	p<0.01
10. Late mov	*mo* : *mo*+400	ANOVA against "rest"	p<0.01
11. Late mov dir selec	*mo* : *mo*+400	Bootstrap (new dir assign)	p<0.01
12. Task-related	(*any*)	At least one of the previous	

Legend. Profile variables. We defined 11 quasi-independent variables and one cumulative variable (*task-related*). In the Table, the colors distinguish between "modulation" variables (light gray) and the corresponding "dir selec" variables (white). The dark gray is reserved for the remaining variables *precue*, *early dir selec*, and *task-related*. See Methods for detail on the statistical tests.

Table 3 Percentages.

	PreSMA	PMd	SMA	M1	PMv
1. Precue	32	20	13	12	13
2. Aftercue	10	6	3	3	1
3. Early dir selec	28	24	20	11	8
4. Delay	49	46	44	43	38
5. Delay dir selec	27	28	22	14	8
6. RT	42	48	44	30	35
7. RT dir selec	39	43	46	39	22
8. Early mov	48	51	57	70	43
9. Early mov dir selec	45	51	52	53	32
10. Late mov	57	58	67	81	53
11. Late mov dir selec	51	(46)	54	60	45
12. Task-related	94	91	92	96	85

Legend. For each area (columns) and for each variable (rows), the Table indicates the percentage of cell that passed the relative statistical test (for details, see Table 2 and Methods). Comparing the percentages obtained for different areas at different times, we observe that areas fall in a "logical" sequence. Early in the trial (rows 1., 2., and 3.) preSMA is the "leading" area, with PMd, SMA, and M1 orderly less represented. During the delay (row 4.) PMd and SMA catch up. PMd becomes the leading area (row 5.), followed by the preSMA, SMA and M1. In the RT, the SMA outnumbers the preSMA (row 6.), and the PMd, thus becoming the leading area (row 7.). Finally, the M1 takes over during the movement (rows 8.-11.), orderly followed by the SMA, PMd, and preSMA. Note that the "dir selec" variables tend to run ahead of the "modulation" variables. The emerging picture is represented by a cartoon in Figure 6. The cartoon qualitatively captures all the data in the Table relative to the preSMA, PMd, SMA, and M1, except for one (preSMA, *late mov dir selec*, in parenthesis in the Table).

Table 4. Peak alignments.

	PreSMA	PMd	SMA	M1	PMv
Cue : Go	14	13	6	4	7
Go	32	17	41	7	22
Mo	28	42	30	72	40
Other	26	29	23	17	31

Legend. The values indicate the percentages of cells for which the maximal activity peak was observed (1) during the delay (between the *cue* and the *go*), (2) aligned with the *go* (and after the *go*), and (3) aligned with the *mo* (within 1 sec after the *mo*). Cells whose maximal activity peak fell outside these time windows, or that were not modulated in the task (as indicated by the variable *task-related*) were counted as "other". Thus, all the cells are counted in the Table, and each cell is counted only once.

Figures

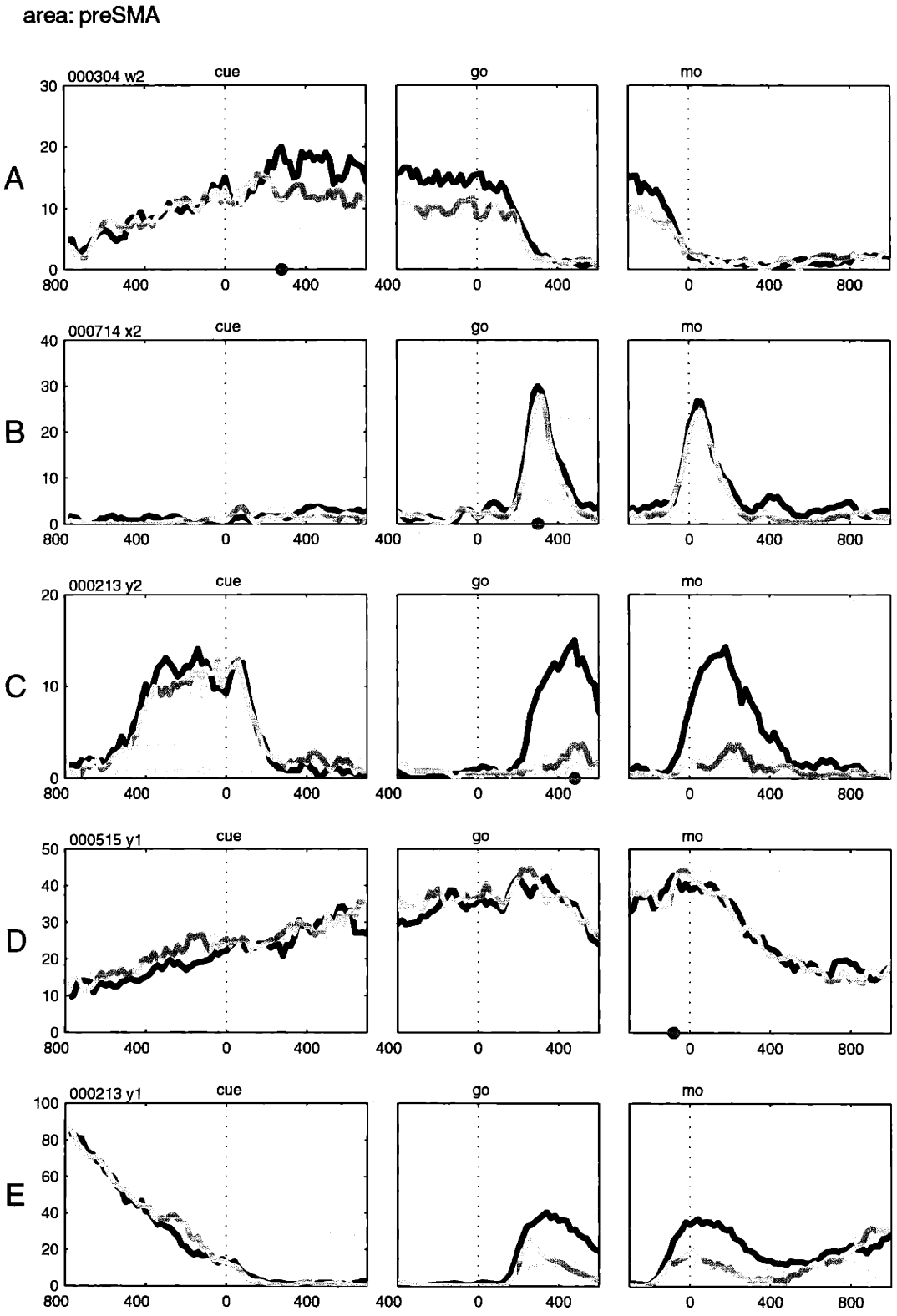
area: preSMA
A
000304 w2
cue
go
mo
B
000714 x2
C
000213 y2
D
000515 y1
E
000213 y1

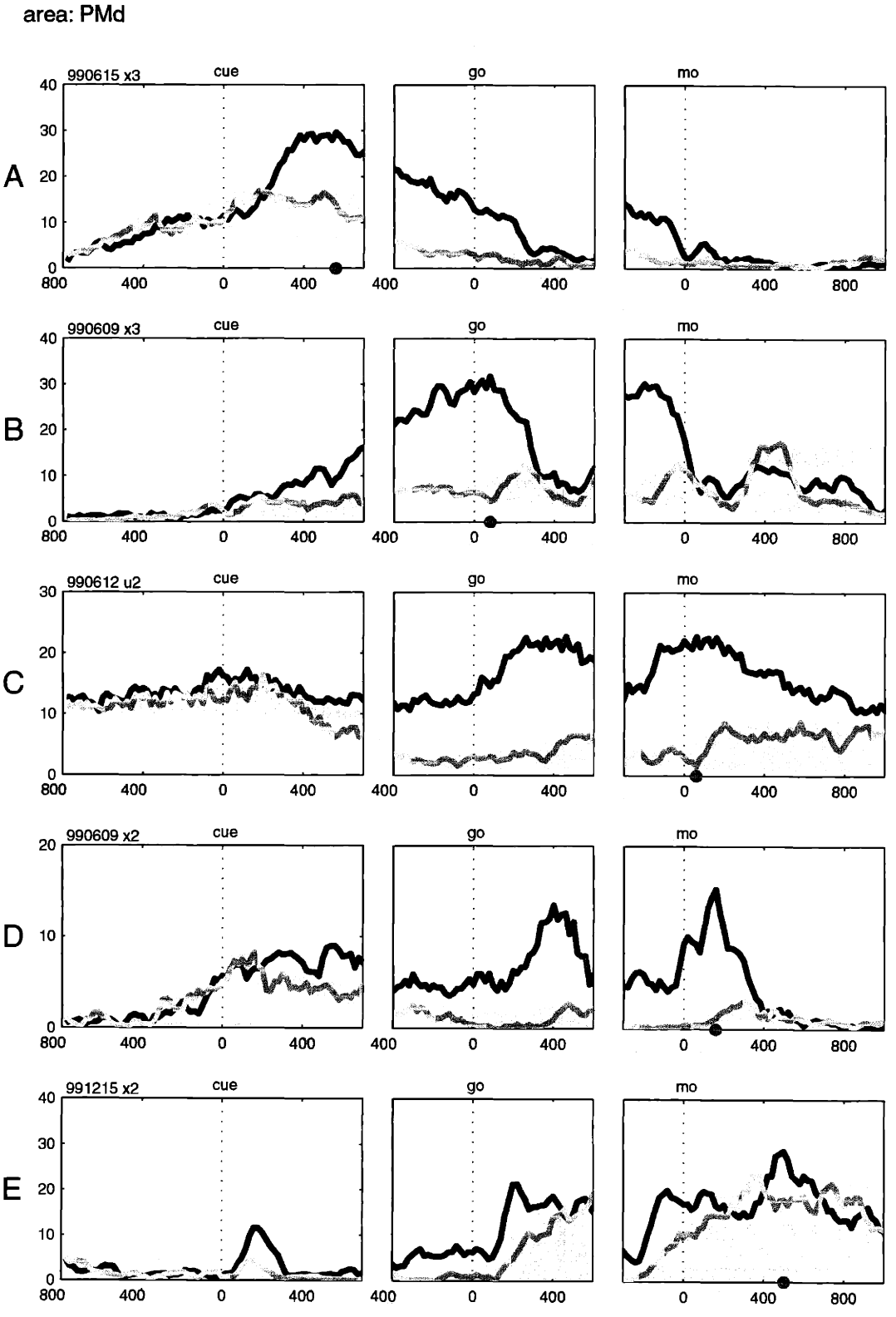
area: PMd
A
990615 x3
cue
go
mo
B
990609 x3
cue
go
mo
C
990612 u2
cue
go
mo
D
990609 x2
cue
go
mo
E
991215 x2
cue
go
mo

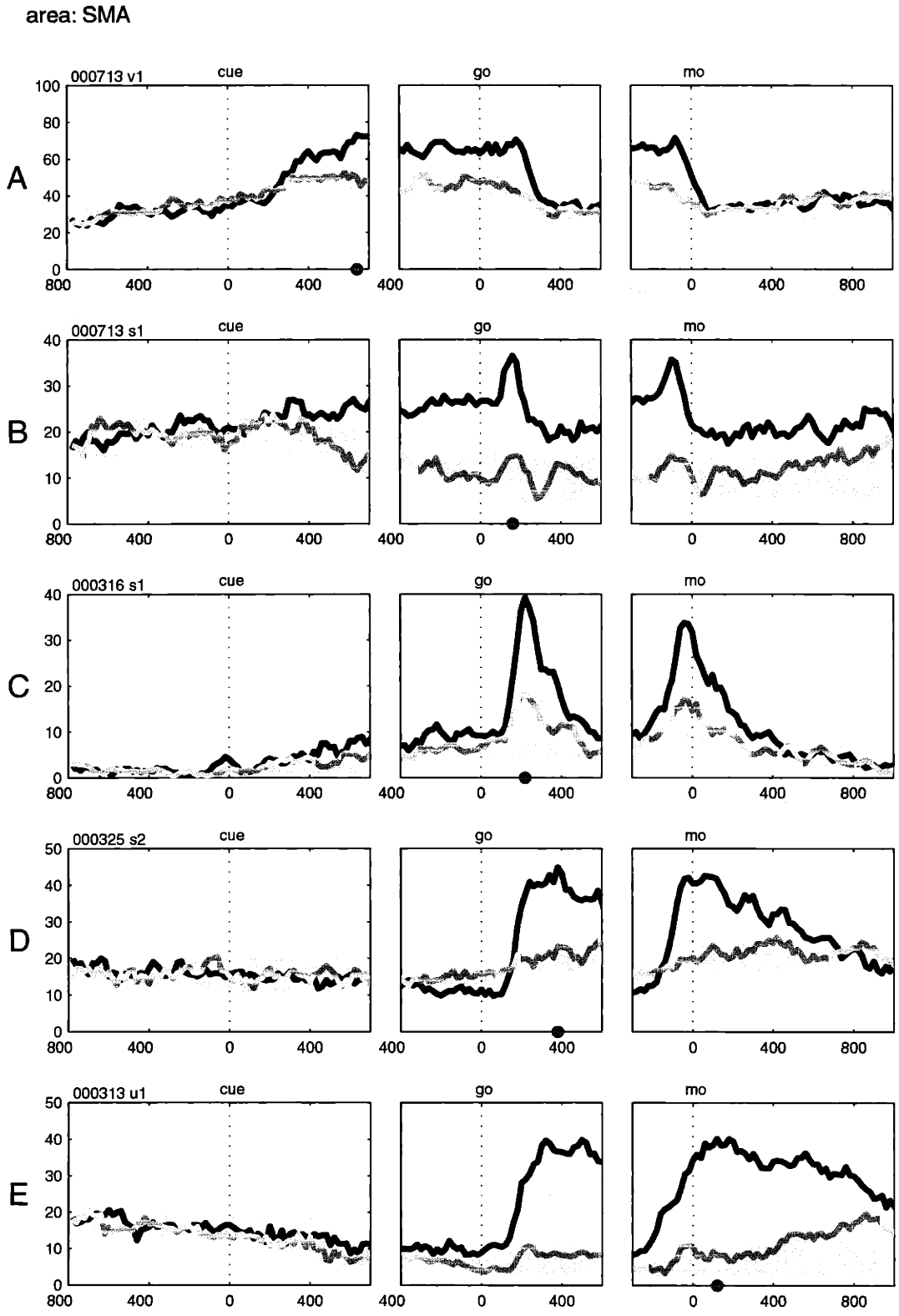
area: SMA
A
000713 v1
cue
go
mo
B
000713 s1
C
000316 s1
D
000325 s2
E
000313 u1

Figure 4

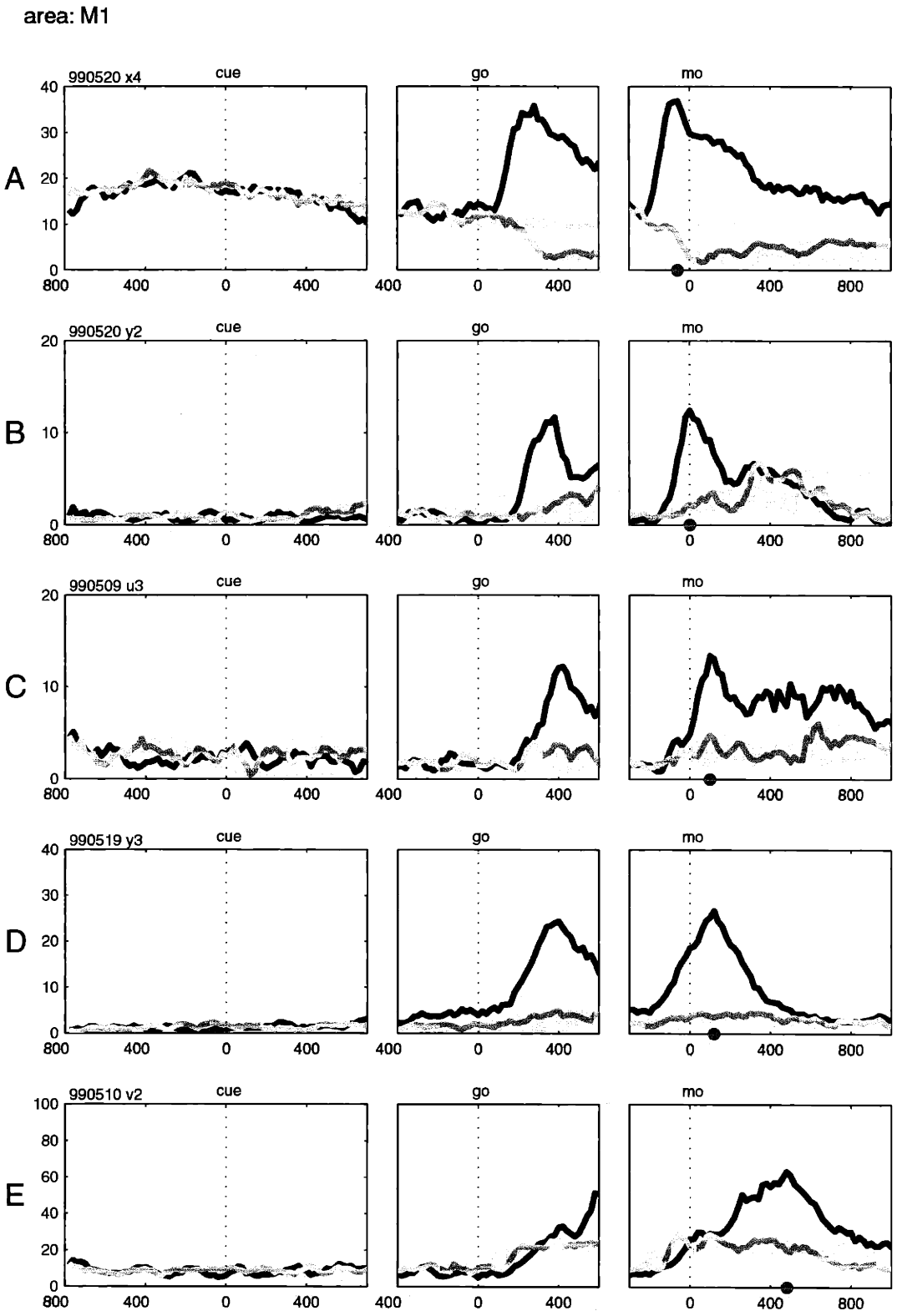
area: M1
A
990520 x4
cue
go
mo
B
990520 y2
C
990509 u3
D
990519 y3
E
990510 v2

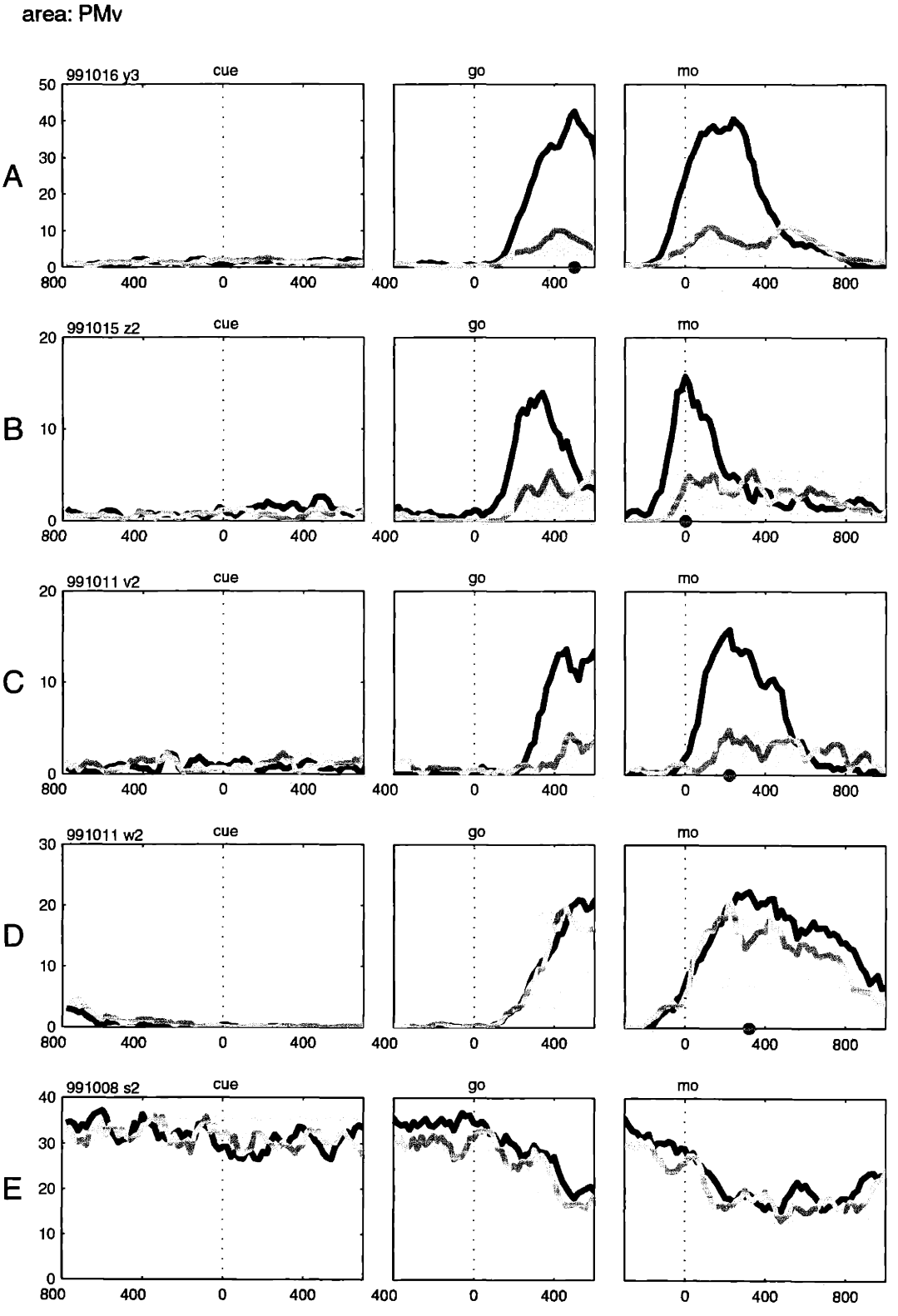
area: PMv
A
991016 y3
cue
go
mo
B
991015 z2
C
991011 v2
D
991011 w2
E
991008 s2

Figure 6

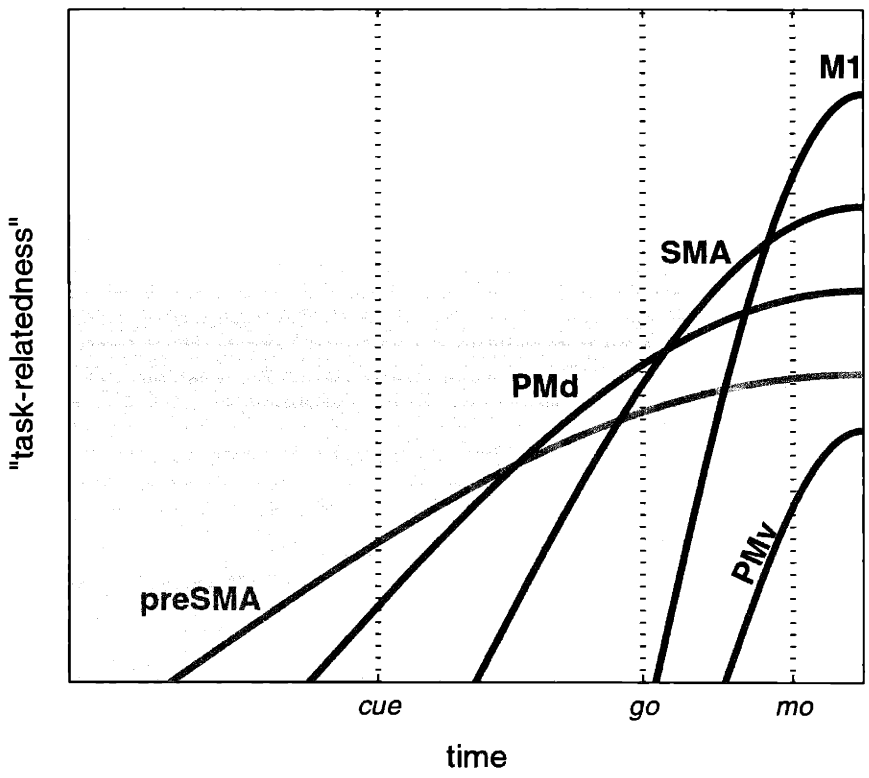

Figure 7

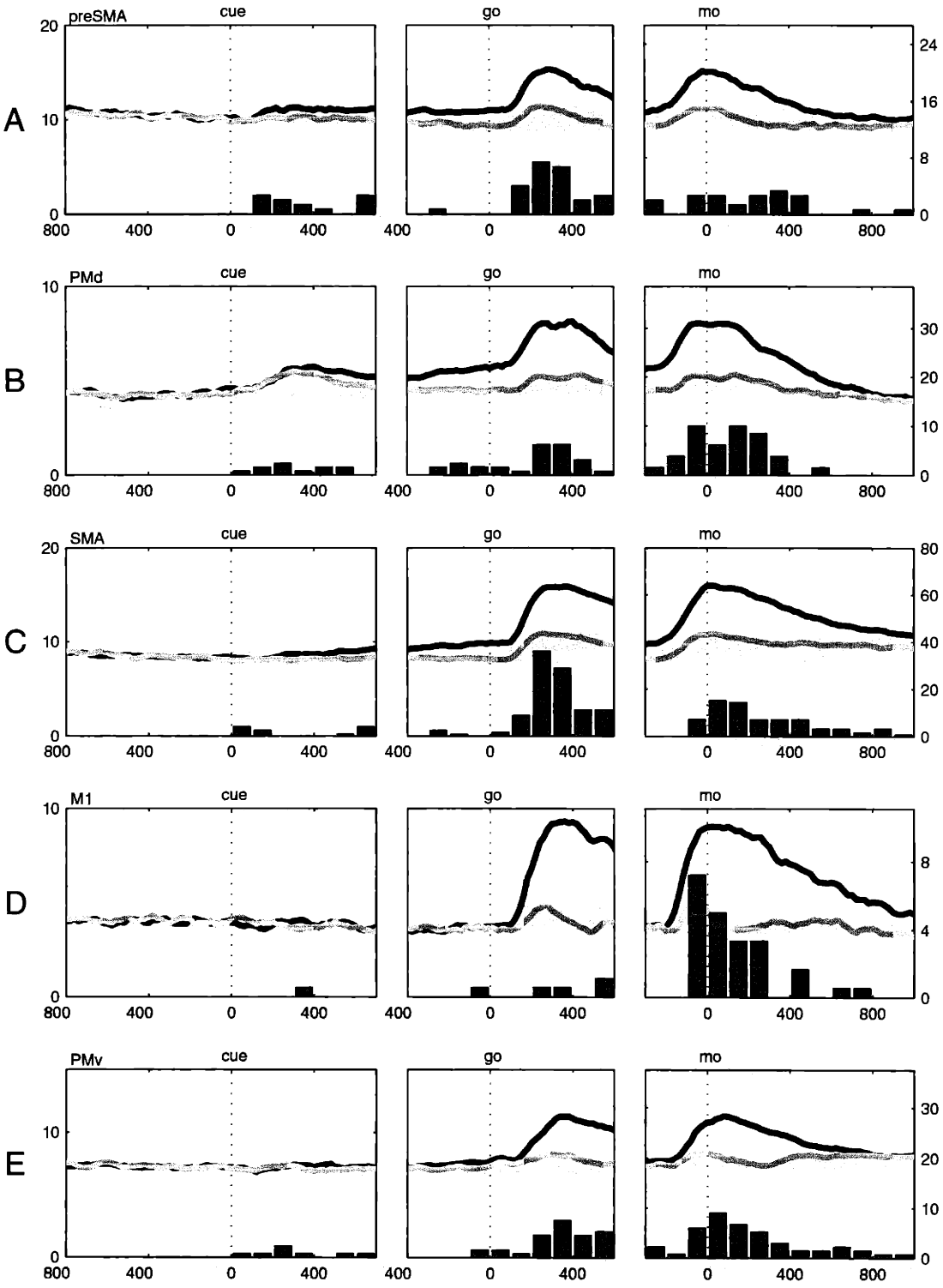

Chapter 7. Conclusions

The studies collected in this thesis describe how five motor areas of the frontal lobe process the dynamics of movements. In particular, we investigated three themes. First, how does the CNS process the kinematics-to-dynamics transformation necessary for movements? Second, how does the activity of neurons modify when we learn to process a new dynamics? Third, how does the activity of different areas combine to control movements? Our main results can be summarized and re-ordered as follows.

First, the neuronal activity of different motor areas largely overlap, but also fall in a clear "logical" sequence, where the preSMA, PMd, SMA, and M1 appear orderly. In particular, the SMA is of the areas under consideration the "closest" to the M1. In contrast, the PMv is more difficult to interpret.

Second, neurons in both the PMd and the SMA process the dynamics of the upcoming movement *during motor planning*, at a time when the M1 is essentially silent. In particular, the activity of neurons in the SMA reflects a kinematics-to-dynamics transformation. The correlates of this transformation can be observed both at the level of the population and at the level of single neurons[3].

Third, processing of the movement dynamics *during motor execution* is widespread across areas that project to the spinal cord, as we observed in the PMd, SMA, M1 and PMv[4].

Fourth, when monkeys acquire a new internal model for the dynamics extensive plastic changes occur in all motor areas, though in different proportions. In particular, more plasticity is observed in the M1, not-as-much in the SMA, and less in the PMd.

Fifth, in particular in the M1, plastic changes recorded after learning and after re-adaptation combine in a statistically meaningful way. Considered globally, the neuronal population after learning is not distinguishable from before learning. Yet, memory of that learning experience is maintained at the level of single neurons. This combination is consistent with the understanding that the M1 subserves both functions of motor performance and motor learning.

---

[3] We did not present the analogous results for the PMd because this analysis requires a rather large data set, which we do not have available for the PMd. However, the fact that PMd neurons process the dynamics during planning suggests that the neuronal correlates of the KD transformation might not be found uniquely in the SMA.

[4] We did not present any result for the preSMA, which does not project to the cord, because our preSMA data are limited.

Though exciting, these results are in many respects not conclusive. Future work, both experimental and analytical, may address questions opened on all three themes. With respect to the kinematics-to-dynamics transformation (KD transformation), addressable questions include the following. Can the neuronal correlates of the KD transformation be traced down to the activity of a single neuron *in a single trial*? Can the KD transformation be observed also in other areas (i.e., the PMd and the cingulate motor areas)? How general is the finding that a *transformation* is processed by single neurons (e.g., is this true for other sensorimotor transformations "upstream" of the KD)? What really is "K" in "KD" (the desired kinematics is only one candidate, see discussion in Chapter 2)?

With respect to the neuronal plasticity associated with motor learning, the following major question remains pending. Is the plasticity we described (a short-term plasticity) of any relevance for long-term learning? Addressable in principle, this issue is difficult to track. Given that with current techniques single neurons cannot be recorded from for longer than a few hours, the way left is that of a careful statistical analysis of a large data set. Our data on the SMA (252 neurons) may or may not be sufficient for that, as future analysis will tell.

With respect to how the activity of different areas (that project to the cord) combines to control movement, one question is: What about the dorsal and ventral cingulate motor areas? Very little is known about either of them, and recordings thereby shall provide interesting and novel insights.

Although numerous questions remain unanswered, we find it encouraging that some of them can possibly be addressed.

Appendix. Changes of EMG activity in the presence of external forces

In a series of experiments, we recorded the activity of neurons in the motor areas of monkeys executing reaching movements. To investigate how neurons process the dynamics of movements we compared the activity recorded in the absence or in the presence of external force fields. We interpreted changes of neuronal activity across conditions using as a framework the changes observed in the electromyographic (EMG) activity of muscles. To this end, the crucial observation was that curl force fields impose onto the EMG of muscles a consistent shift of preferred direction (Pd) in the direction of the external force. The shift –we argued –occurs for all muscle in the same direction, independently of their initial Pd. We supported this point with experimental data from six muscles of the arm and with an heuristic model of how the external perturbing forces vector-sum with the internal muscle forces (see Figure 1d in Li, Padoa-Schioppa and Bizzi, 2001). The goal of the present Appendix is to make that heuristic argument mathematically rigorous. We will design a rather general model of how external and internal forces combine, and derive explicit predictions for two specific cases of external forces: curl forces (of interest here) and radial fields (i.e., assistive/resistive loads, largely used in previous studies). The advantages of the present model are its simplicity and its generality. The main limit is that the model is only valid *ad equilibrium*.

During non-perturbed movements, the activity of contracting muscles produces a force that ultimately moves the hand. If we indicate with $\vec{\mu}$ the activity of muscles and with $\vec{F}$ the resulting force, we can write:

$$\vec{F} = \Phi(\vec{\mu}) \qquad (1.1)$$

$$\vec{\mu} = \Gamma(\vec{F}) \qquad (1.2)$$

where Φ in Eq.(1.1) is a function containing the biomechanics of the arm, and Γ in Eq.(1.2) is the function inverse of Φ (so that $\Gamma = \Phi^{-1}$). Note that in Eqs.(1.1) and (1.2), $\vec{F}$ is a 2-dimensional vector (for planar movements, 3-dimensional vector for the general case), while $\vec{\mu}$ is a multi-dimensional vector where each component corresponds to the activity of one single muscle. If we are interested in one particular muscle, we can write Eq.(1.2) for the corresponding component as:

$$\mu = \Gamma(\vec{F}) \qquad (1.3)$$

In the presence of a perturbing field, two forces are exerted upon the hand of the monkey: the force $\Phi(\vec{\mu})$ of the muscles and the perturbing force $\vec{f}$. Thus, we can re-write Eqs.(1.1) as follows:

$$\vec{F} = \Phi(\vec{\mu}) + \vec{f} \qquad (1.4)$$

The following question is of interest here. How does the muscle activity (μ) need to change so to maintain the same trajectory (and therefore the same total force $\vec{F}$) in the presence of the perturbing force $\vec{f}$? In other words, we search $\Delta\mu$ such that:

$$\mu + \Delta\mu = \Gamma(\vec{F} - \vec{f}) \qquad (1.5)$$

given that $\mu = \Gamma(\vec{F})$. In particular, we are interested in two types of perturbing forces: angular forces (curl force fields) and radial forces (assistive/resistive loads). Thus, polar coordinates are the most natural choice of coordinate system. We can express the vector $\vec{F}$ as $\vec{F} = (\rho, \vartheta)$, where ρ and θ are the radial and curl component of the force, respectively. The perturbing force $\vec{f}$ will then be written:

$$\vec{f} = (f_\rho, f_\vartheta) \qquad (1.6)$$

If the perturbing force $\vec{f}$ is small[5], we can compute $\Delta\mu$ in Eq.(1.5) by linearizing Γ close to $\vec{F}$ as follows:

$$\Delta\mu \equiv \Delta\Gamma \cong \frac{\partial\Gamma}{\partial\rho}\delta\rho + \frac{\partial\Gamma}{\partial\theta}\delta\theta \qquad (1.7)$$

where $\delta\rho$ and $\delta\vartheta$ are the radial and curl components of the change of force. According to Eqs.(1.5) and (1.6), we have $(\delta\rho, \delta\vartheta) = -(f_\rho, f_\vartheta)$

Now the advantage of using polar coordinates becomes clear. We will consider the following two cases.

Case 1: Angular force only (curl force field):

$$\vec{f} = (0, f_\vartheta) \Rightarrow (\delta\rho, \delta\vartheta) = (0, -f_\vartheta) \quad \Rightarrow \quad \Delta\mu = -\frac{\partial\Gamma}{\partial\theta} f_\vartheta \qquad (1.8)$$

Case 2: Radial force only (assistive/resistive load):

$$\vec{f} = (f_\rho, 0) \Rightarrow (\delta\rho, \delta\vartheta) = (-f_\rho, 0) \quad \Rightarrow \quad \Delta\mu = -\frac{\partial\Gamma}{\partial\rho} f_\rho \qquad (1.9)$$

Before going further, let us remind that in Eqs.(1.8)-(1.9) $\Delta\mu$ is the change of muscle activity (for a given movement), Γ is the non-perturbed muscle activity, and f_ϑ and f_ρ are the angular and radial components of the external force, respectively. Somewhat surprisingly, we derived precise predictions on $\Delta\mu$ with quite limited assumptions.

At this point we need to say something more about the function Γ. In the definition of Eq.(1.2), Γ is essentially a function expressing the inverse dynamics, a rather complicated and non single-valued function of the output force. At this time, however, we are only interested in how Γ depends on the radial and angular variables ρ and θ. Because Γ is the non-perturbed muscle activity (i.e., the non-perturbed EMG

[5] This is essentially the only assumption of the argument.

tuning curve), we can assume the most common tuning curve form, namely a cosine tuning. In this case, we have:

$$\Gamma(\rho,\vartheta) = A + B\rho\cos(\theta - \theta_0) \qquad (1.10)$$

where θ_0 is the preferred direction (Pd) of the muscle. Essentially, Eq.(1.10) expresses the fact that for a given direction θ the muscle activity μ is a linear function of the output force ρ, and that the activity of the muscle varies with θ like a cosine function[6]. We can then compute the derivatives of $\Gamma(\rho,\vartheta)$ with respect to ρ and θ. We obtain:

$$\frac{\partial\Gamma}{\partial\rho} = B\cos(\theta - \theta_0) \qquad (1.11)$$

$$\frac{\partial\Gamma}{\partial\theta} = -B\rho\sin(\theta - \theta_0) \qquad (1.12)$$

For simplicity, we shall consider here the case of constant forces (as opposed to the viscous forces actually used in our experiment. By plugging Eqs.(1.11) and (1.12) respectively into Eqs.(1.9) and (1.8), we obtain:

Case 1.1: Constant curl force $\vec{f} = (0,\phi)$: (1.13)

$\mu = A + B\rho\cos(\theta - \theta_0)$ non-perturbed tuning curve

$\Delta\mu = \phi B\rho\sin(\theta - \theta_0)$ effect of the perturbation

CK / CCK force for ϕ<0 / ϕ>0

Case 2.1: Constant radial force $\vec{f} = (-k,0)$ (1.14)

$\mu = A + B\rho\cos(\theta - \theta_0)$ non-perturbed tuning curve

$\Delta\mu = kB\cos(\theta - \theta_0)$ effect of the perturbation

Assistive / Resistive force for k<0 / k>0

The curves described in (1.13) and (1.14) can be plotted directly, as we did here in Figures 1a and 1b, using A=1.1, B=1, $\theta_0 = \pi/2$, $\phi = -\pi/6$, and k=-0.5.

In the case of the curl force (Figure 1a), it can be noticed that the Pd of the muscle shifts indeed in the direction of the external force (CK). Note that no assumption was made on the original Pd of the muscle. In other words, the *direction* of the shift is the same for any muscle considered (provided that the muscle is directionally tuned, i.e. that a Pd can be defined). In the case of the radial assistive force (Figure 1b), it can be noticed that the *modulation* of the muscle is reduced. The activity decreases for movement directions where the activity was originally high, and increases for directions where the activity was originally low. In the case of radial resistive force (not shown), we have the opposite effect (enhanced *modulation*). The activity of the muscle increases for directions where the activity was originally high, and decreases for directions where the activity was

[6] In fact, $\Gamma(\rho,\vartheta)$ is equal to the *max* between the right-hand-side of Eq.(1.10) and 0. By assuming A>0, we implicitly integrate over the entire movement. Thus, $\Gamma(\rho,\vartheta)$ in Eq.(1.10) expresses the EMG tuning curve as recorded during the experiments, as opposed to the "instantaneous" tuning curve.

originally low. These predictions are consistent with the results of numerous studies that recorded the activity of muscles and neurons with assistive/resistive loads (e.g., Evarts, 1968).

In conclusion, we presented a simple model to describe the changes of muscle EMG in presence of external force fields. For the cases of curl forces and radial assistive/resistive forces, the model qualitatively replicates the empirical results.

References

1. Li, C-S.R., Padoa-Schioppa, C. & Bizzi, E. Neural correlates of motor performance and motor learning in the primary motor cortex of monkeys adapting to an external force field. *Neuron* **30,** 593-607 (2001).
2. Evarts, E.V. Relation of pyramidal tract activity to force exerted during voluntary movement. *J. Neurophysiol.* **31,** 14-27 (1968).

Figure legend

Effects of the load onto the EMG activity of muscles. **A.** The EMG tuning curve is plotted in polar coordinates. Two tuning curves and their respective Pd are superimposed. In blue color, the tuning curve and Pd of non-perturbed movements. In red color, the tuning curve and Pd under the effect of a curl force field (CK force). The two tuning curves differ according to Eq.(1.13). The net effect is that the Pd shifts in the direction of the external force (CK direction). **B.** Here we plot the case of a radial assistive force. The non-perturbed tuning curve is the same as in the previous case. Under the effect of the assistive force, the tuning curve varies according to Eq.(1.14). The Pd remains unchanged, but the muscle activity decreases for movements in the upward hemifield and increases for movements in the downward hemifield.

Figure

Figure 1

A

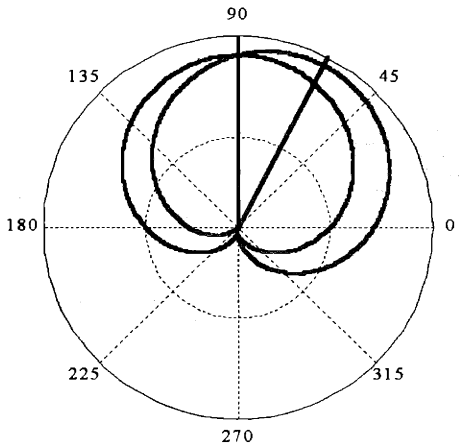

B